THE UNIVERSITY OF HULL

Development of Novel Colloidal Particles through Nanoimprinting Technology towards Nanoantibiotics

being a Thesis submitted for the Degree of Doctor of Philosophy

in the University of Hull

by

Josef Borovička, MChem (Hons)

September 2012

ACKNOWLEDGEMENTS

I would like to thank my supervisor Dr Vesselin Paunov who has provided me with support and encouragement throughout the four years of my PhD training. He has given me plenty of great ideas and guidance which were essential for my work, and helped me to become an independent researcher. I would also like to thank my industrial supervisor Prof. Simeon Stoyanov of Unilever R&D for his interest and fruitful discussions.

I would like to thank my wife, Naomi, who has always been there for me in times of self-doubt and worry. I know I can always rely on her. Without the support and care of my parents I would not have been able to be who I am. I owe my father the interest in Science as we have always had very interesting discussions. I have been blessed by the fact that my sister Marie, whom I am very close with, ended up reading for her medical degree in Hull and stayed with me for most of her studies. It is my family who gives me strength and encouragement in all decisions which I take.

I owe my colleagues and friends for helping me put problems into perspective. Mika has been an enormous source of support both with my academic work as well as personally. I would like to thank Marius for his friendship and facilitating the handing in of this thesis☺. I remember many interesting discussions about science which helped me better myself, and about life in general, which I had with Ben. I would like to thank Richard, Baghali, Andrew, Mathieu, Anais, Rawil and Tim for making the PhD training even more enjoyable. I would like to thank Martin, Heiko, Pete and Chris for their ongoing friendship. I have enjoyed the beers and films that I shared with them.

I would also like to thank Dr Leigh Madden, Dr Chris Walton and Mr John Metheringham for the fruitful collaboration. Finally, I would like to thank Mr Tony Sinclair for his help in producing very high quality SEM micrographs, without which this work would be much poorer.

PUBLICATIONS AND PRESENTATIONS

The work conducted throughout the PhD training period has given rise to the following publications and presentations:

Adsorption of Sterically Stabilized Latex Particles at Liquid Surfaces: Effects of Steric Stabilizer Surface Coverage, Particle Size, and Chain Length on Particle Wettability'. K. M. Reed, J. Borovicka, T. S. Horozov, and V. N. Paunov , K. L. Thompson, A. Walsh, and S. P. Armes. *Langmuir*, 2012, 28, pp 7291–7298

'**Development of Nanoantibiotics Based on Novel Nanoimprinting Technology'.** Fall MRS Meeting Proceedings, Boston, Massachusetts, November 2012

'Colloid Antibodies: Anisotropic particles for cell shape and size recognition. J. Borovicka, Simeon Stoyanov and V. N. Paunov, *Angewandte*, Submitted

'Borovicka et al - JACS 2013 - shape and size selective killing of microbes using photothermal colloid antibodies, Josef Borovička, William J. Metheringham, Leigh A. Madden, Christopher D. Walton, Simeon D. Stoyanov, and Vesselin N. Paunov, *Journal of American American Chemical Society*, Submitted

'The Theoretical Basis of the Cell Recognition by Nanoantibiotic Particles'. J. Borovicka, Simeon Stoyanov and V. N. Paunov – in preparation

'pH and Light Triggered Release of Active Compunds from Sporopollenin Capsules'. M. Lecouche, J. Borovicka, Simeon Stoyanov and V. N. Paunov – in preparation

Presentation '**Development of Nanoantibiotics Based on Novel Nanoimprinting Technology'** at Unilever Research, Vlaardingen, The Netherlands, June 2011

Presentation '**Development of Nanoantibiotics Based on Novel Nanoimprinting Technology'** at the Fall MRS Meeting, Boston, Massachusetts, November 2012

ABSTRACT

A novel class of physical anti-bacterial and potentially anti-viral agents has been proposed based on the shape and size recognition and specific binding to inorganic imprints produced by templating the chosen target pathogens with suitable inorganic material. The products of the templating process are partially fragmented nanoshells which are intended to selectively bind to their biological counterparts, therefore impairing microbial cell growth, replication and infection. Further combinations of the size- and shape-recognising particles with other toxins or conventional antibacterial agents could result in the delivery of high concentration of these agents onto the target cell surface. We have named this class of particles, which are capable of selectively recognising bacterial shape and size, "nanoantibiotics", due to the architecture of the nano-shells formed around the templated pathogen. The selective binding is driven by the increased area of contact upon recognition of the shape and size between the partial negative replicas of the pathogens and their templates. In this thesis we have tested this concept theoretically by calculating and assessing the DLVO interactions between the nanoantibiotic particles and spherical target cells, analysing the interaction energy between matching and mismatching nanoantibiotic-target particle pairs. The results of these calculations suggest that the binding energy can be orders of magnitude stronger in case of recognition.

We have also explored routes of fabrication of the nanoantibiotic particles using gold, zinc, and silica as shell forming materials. Additionally, we conducted a number of experiments which probed their shape and size selectivity using bacterial (*Bacillus subtilis*) and yeast (*Saccharomyces cerevisiae*) cells as test microorganisms as well as commercially available latex microspheres which have the advantage of fixed shape with variability in size. Latex particles were used only as a tool to study of the effect of the target particle size on the recognition events. Our experiments showed high levels of nanoantibiotic recognition selectivity which reinforced the concept of these novel antipathogenic agents.

Finally, we also developed gold nanoparticle-silica composite nanoantibiotic particles which showed the capability of selective killing of the target microbe when triggered by laser. We demonstrated this by selectively killing yeast in a mixture with other bacterial cells by triggered localised heating on the surface of the yeast cells through laser-

induced photothermal effect. Nanoantibiotic particles could be designed to bind and potentially deactivate strains of antibiotic resistant bacteria like MRSA, *E .coli* and many others where most conventional antibiotics are powerless. Nanoantibiotic particles can also find applications as non-toxic antibacterial agents, for example to prevent harmful bacterial strains of *E. coli* from growing on food and personal care formulations. They could be of great benefit to the pharmaceutical industry, and in applications in food and personal care sectors by acting as inorganic, long lasting and specific biocides.

CONTENTS

LIST OF ABBREVIATIONS

ABREVIATION	MEANING
APTES	3-aminopropyltriethoxysilane
AuNP	gold nanoparticle
CML	carboxylate modified latex
DLVO	Derjaguin-Landau-Vervey-Overbeek
DNA	deoxyribonucleic acid
eq(s)	equations (s)
FDA	fluorescein diacetate
g	gram
GaAs	gallium arsenide
GST	glass slide technique
Gtt	gel trapping technique
h	hour
HF	hydrofluoric acid
kg	kilogram
M	molar
mg	milligram
min	gram
mL	millilitre
mM	millimolar
NaCl	sodium chloride

PAH	poly(allylamine hydrochloride)
PDMS	polydimethylsiloxane
PEG	polyethylene glycol
Pss	poly(sodium styrene sulfonate)
RBITC	rhodamine B isothiocyanate
RMM	relative molecular mass
RNA	ribonucleic acid
rpm	revolutions per minute
S	second
SEI	surface element integration
SEM	scanning electron microscopy
Silar	successive ionic layer adsorption and reaction
TAA	thioacetamide
TEM	transmission electron microscopy
TEOS	tetraethoxy silane
$ZnAc_2$	zinc acetate
Zns	zinc sulfide

CHAPTER 1. INTRODUCTION

The aim of this research project is to develop techniques for the fabrication of negative inorganic replicas of micro- and nano-sized biological templates, which can be functionalised in order to recognise the templates not only geometrically but also to bind to them through specific surface interactions. Such techniques can subsequently be employed to produce particles which bind specifically to pathogenic bacteria and viruses of matching shape, size and surface properties. Such particles can be used as "nanoantibiotics". For example, viruses which have been bound specifically to their negative replicas would be unable to replicate due to the prevention of the disassembly of the viral capsid and the subsequent release of the viral DNA/RNA. In the case of bacteria this would impair mitosis. Such action is highly selective and does not pose toxic threat to the host or other non-target microorganisms unlike the conventional, chemical, antibiotics. See Section 1.4 for a discussion of the conventional antibiotics. For the purposes of this thesis we will referrer to these imprints as to nanoantibiotics or nanoantibiotic particles even though we might not have proven bactericidal or bacteriostatic effect of the particular type of particles. These particles could be of great benefit to the pharmaceutical industry, food and personal care sectors by acting as inorganic, long lasting biocides.

The methods for preparation of negative replicas of templates in micro- to nanoscopic dimensions can be fundamentally divided into two categories: (i) those which employ symmetric deposition of the shell material onto a template leading to the production of the so called core-shell particles, and (ii) those which employ asymmetric deposition by protecting parts of the templates (see Figure 1-1.). General core-shell particle production methods which use sacrificial cores produced from materials such as silica, polystyrene latexes or metal have been studied extensively over many years and there is an extensive literature covering this topic.[1-4]

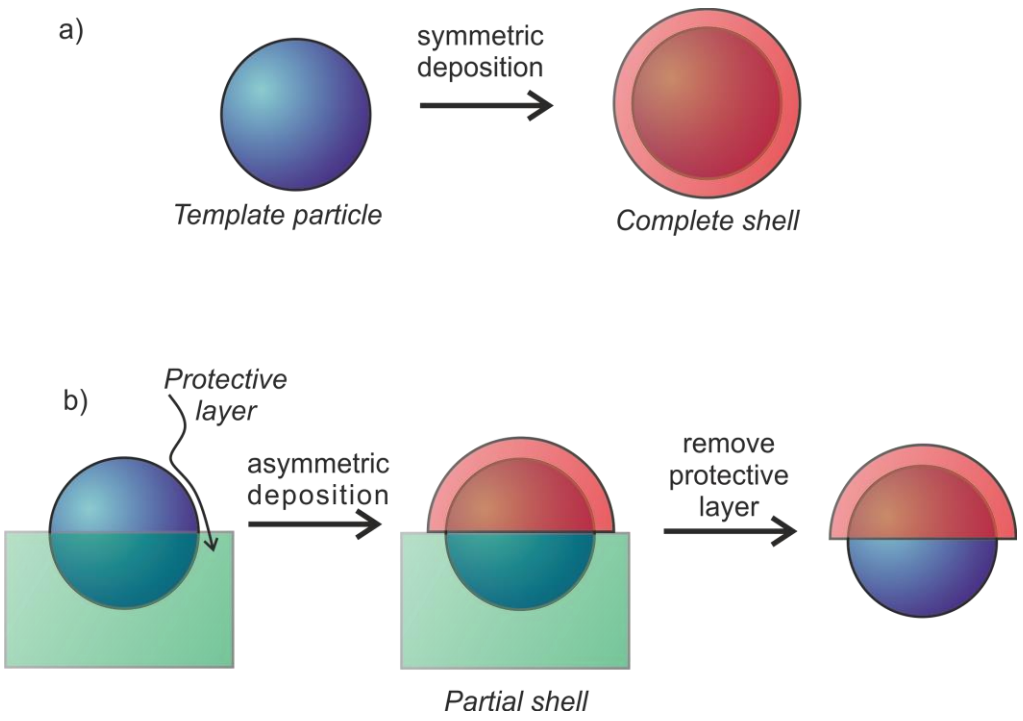

Figure 1-1. Symmetric and asymmetric deposition of a shell material onto a solid template. (a) Symmetric deposition leads to the coating of the template particles indiscriminately over the whole surface whereas (b) the asymmetric deposition gives the advantage of shielding portions of the particles surface and depositing shell material only over the available surface.

The suggested route of fabrication of the novel antiviral and anti-microbial agents (nanoantibiotics) developed in this thesis is achieved by the deposition of shell-forming material onto the targeted biological species, creating a "negative replica" of the target, which then may optionally be followed by the chemical passivation of the outer side of the negative replica. Such treatment of the "outer" surface of the nanoantibiotic "partial shell" particle renders it inactive with respect to the template target. We then release the nanoantibiotic particles from the original biological template to produce fragments of the nanoantibiotic particles; this can be achieved by, for instance, ultrasonic agitation. This process is to be followed by the subsequent removal of the template and the template-specific chemical functionalisation of the inner side of the shell in the case of symmetrical deposition. In the case of the asymmetrically deposited shell the same process is carried out with the omission of the shell fragmentation step. Figure 1-2. illustrates the process of the fabrication and the action of our nanoantibiotic particles.

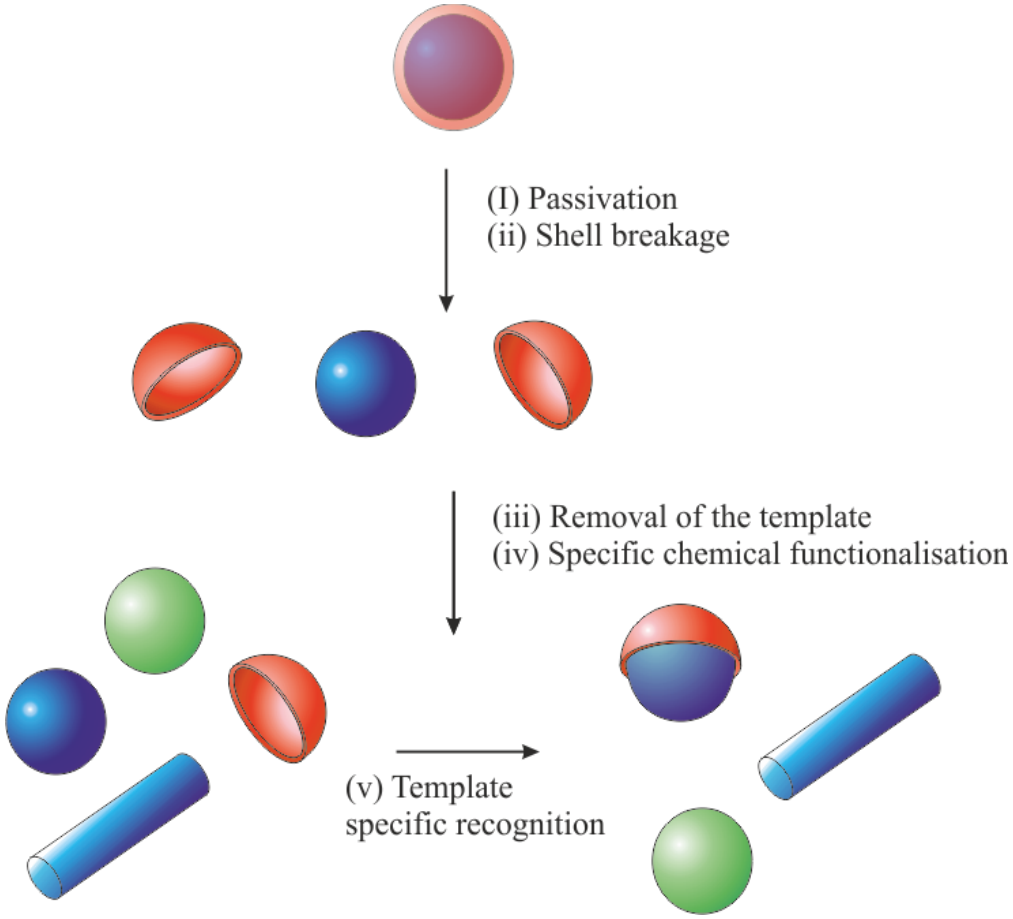

Figure 1-2. Proposed route of production and action of the novel class of antiviral and bactericidal agents shown on an example shell formed via the symmetric deposition process. The negative replica is separated from its template and chemically functionalised in order to secure a specific binding to of the biological target. The partial shell can be introduced into an environment containing the bacteria or the viruses which it can bind to specifically according to their surface chemistry, size and geometric shape. For the purposes of this diagram, the surface chemistry is represented by colour – blue signifies matching chemistry whereas green stands for a surface chemistry of the biological template which is not specific to the functionalisation of the anti-pathogenic agent.

1.1 The Lock and Key Interactions

The above described principle of physical nanoantibiotics, based on shape and size selectivity of their targets, is inspired by the Lock and Key model of the interactions between enzymes and their substrates as postulated by Emil Fischer in 1894. According to him, both the enzyme and the particular substrate are complementary

geometrically thus fitting exactly into one another (see Figure 1-3. for a schematic representation).[5] The non-covalent interactions, such as the van der Waals and electrostatic forces, hydrogen bonding, and hydrophobic interactions between the correctly-fitting enzyme-substrate species, are amplified in this specific configuration. In other words, such pairs that differ in shape or surface chemistry cannot productively bind. Such conformational specificity was also described to be present in the interactions between antigens and antibodies by Linus Pauling in 1940.[6]

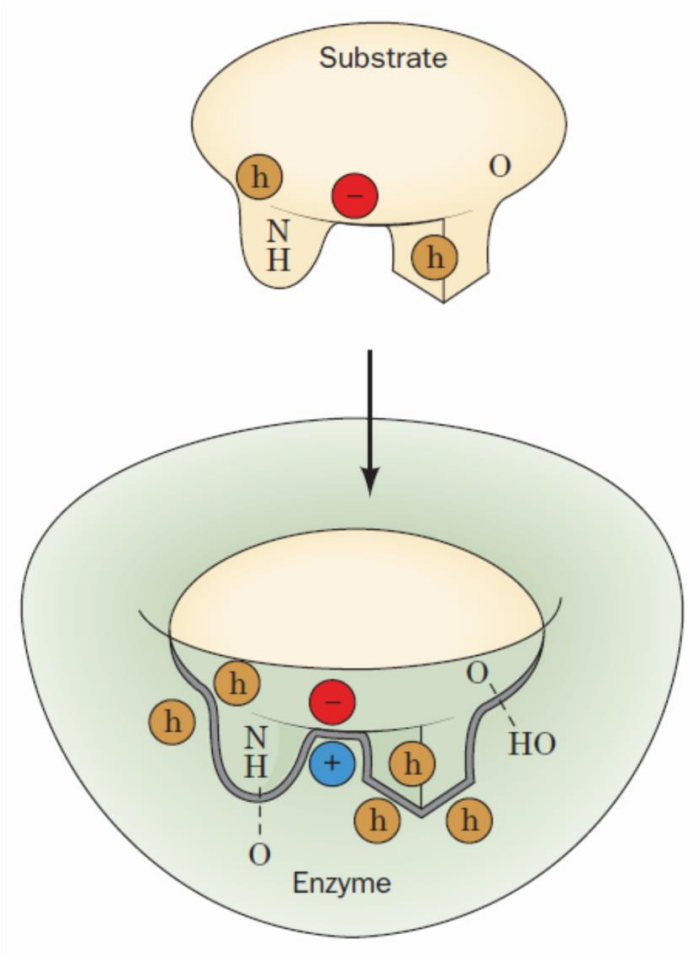

Figure 1-3. Specific enzyme-substrate complexation.[5] The geometric complementarity allows for effective non-covalent interactions. The brown circles with the letter "h" represent the hydrophobic groups and the dashed lines are the hydrogen bonds. Image reproduced from Reference 6.

Such geometric specificity in binding as found in the domain of natural macromolecules has been an inspiration for numerous scientists. The Lock and Key principle has been recently employed by Sacanna *et al*. to prepare colloidal systems which are capable of

programmed self-assembly into composite clusters.[7, 8] They fabricated polymeric spheroids with dimples which geometrically correspond to the curvature of other polymeric particles. They then introduced depletion attractions into the colloidal system containing the shape-conforming particles by adding a polymer of high molecular weight. As the depletion interactions increase with the displaced volume the colloids experienced highest depletion attraction forces when they were mutually oriented via their shape-complementary sites. This then lead to a reversible binding (see Figure 1-4. for a sample of their results).

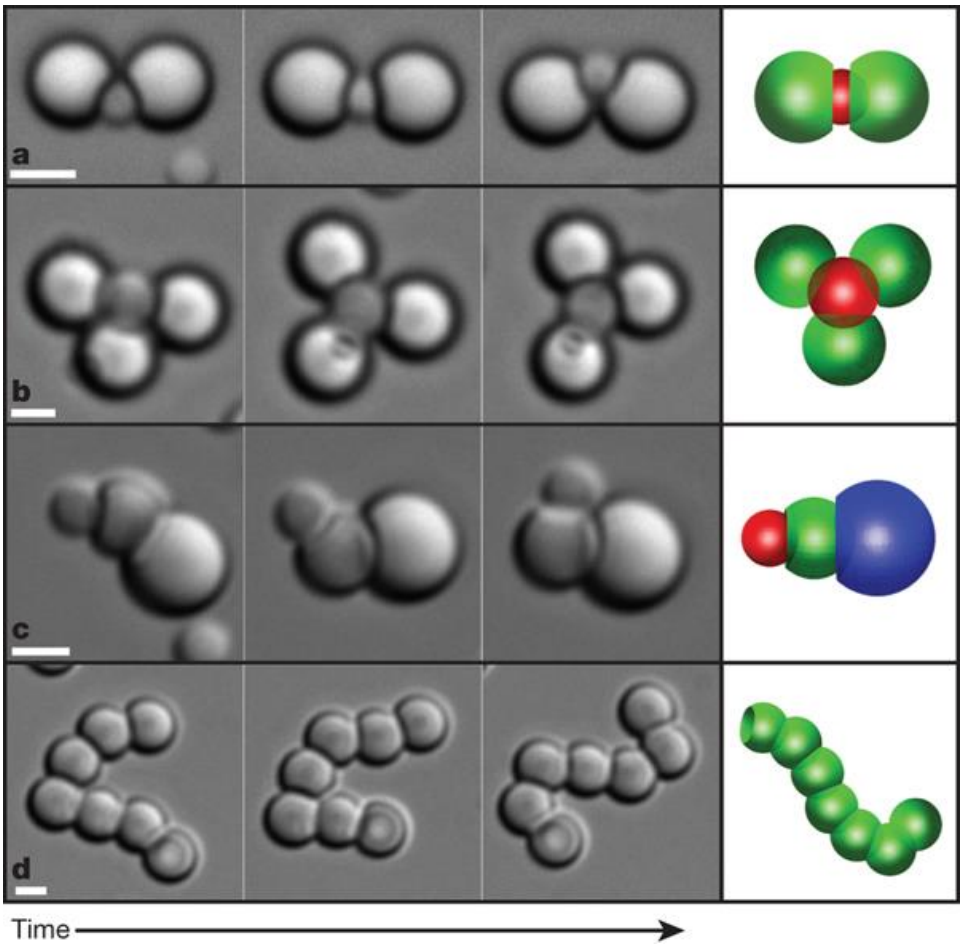

Figure 1-4. Optical micrographs of the programmed lock and key assemblies as fabricated by Sacanna *et al.*[7] The scale bars are 2 μm. Image reproduced from reference 8.

In more recent years, novel methods of biological recognition have been utilised for analytical applications by imprinting microorganisms onto a solid surface, thus allowing for the selective immobilisation of other microbes of the same species. In this way, Dickert and Hayden were able to establish the concentration of and distinguish

between three different genera of yeast after producing imprints of the respective species on polyurethane and sol-gel surfaces and obtaining feedback via a quartz crystal balance.[9] Again utilising sol-gel surfaces with microbial imprints, Cohen *et al*. were able to efficiently discriminate and selectively bind microbial organisms from their mixture in an aqueous medium.[10] The biological species included the bacterial cells of *Deinonococcus radiodurans, Escherichia coli, Bacillus subtilis* and *Sphaerotilus natans* as well as oocysts of the protozoan parasite *Cryptosporidium parvum*. In an interesting twist on the topic, Harvey *et al*. produced imprints on the surfaces of 100 – 200 μm polymer beads in order to detect bacterial spores.[11] The selectivity of binding based on the shape and size of the microorganisms was also demonstrated by Perez *et al.* who synthesized 100 μm beads with the imprints of rod–shaped *L. monocytogenes* and *S. aureus.*[12]

Although there are similarities in the above described examples of microbial immobilisation to the concept of nanoantibiotics, there are also important differences. Instead of a macro substrate of flat surfaces or beads, our system utilises fragments on the same scale as the target microorganisms, using matching pairs of the target microbe and a separate individual shell fragment which geometrically and chemically reflects the target. This novel approach leads to increased recognition rates due mainly to the mobility of both the microbial targets and their nanoshell imprints in the media.

1.2 DLVO Theory

The nanoantibiotic particles as presented in this work belong to the colloidal domain. The attraction and the consequent mutual binding or, by contrast, repulsion between the nanoantibiotics and their targets is dependent on colloidal interactions. The Derjaguin-Landau-Vervey-Overbeek (DLVO) theory quantitatively explains the stability of suspensions and emulsions by considering the effects of the attractive van der Waals forces and electrostatic forces stemming from the interaction of electrostatic double-layers around colloidal particles.[13, 14]

1.2.1 Van der Waals Forces

Van der Waals forces are a product of interactions between electric dipoles of molecules. The eponym of these attractive forces is Johannes Diderik van der Waals who was first to describe them when attempting to explain the non-ideal properties of gases and liquids. Molecules which have a permanent dipole will align with and attract to similar molecules. They will also attract neutral molecules and atoms in their vicinity by inducing an electric dipole. Instant induced dipoles can appear due to fluctuations in the electron density around atoms and molecules and their correlation leads to attractive London dispersion interactions. These interactions are considered non-directional and hence the differently oriented dipoles in large atom assemblies do not cancel each other. As colloidal particles can be considered as large assemblies of atoms, the van der Waals forces stemming from the London dispersion interaction are present between the colloid particles, causing attraction. These attractive forces are long-ranged when compared to the interactions of two isolated atoms. The van der Waals energy of interaction between two molecules 1 and 2 at a distance *r* is

$$U_{12}(r) = -\frac{C_{12}}{r^6} \tag{1-1}$$

where C_{12} is the van der Waals constant.

The attractive potential energy (U_{VW}) between two spherical particles of radius a of separation D ($D \ll 2a$) is expressed as:[14]

$$U_{VW} = \frac{A_H a}{12D} \tag{1-2}$$

where A_H is the Hamaker constant. A_H is a function of both electronic polarisability and the density of the material. In the presence of a liquid medium rather than a vacuum the van der Waals interaction energy between the two particles becomes notably lower as there is also an attraction with the medium.[14, 15] In this case, A_H must be replaced by the composite Hamaker constant. Let's consider the interaction between two particles, 1 and 2, across a medium 3 (Figure 1-5).

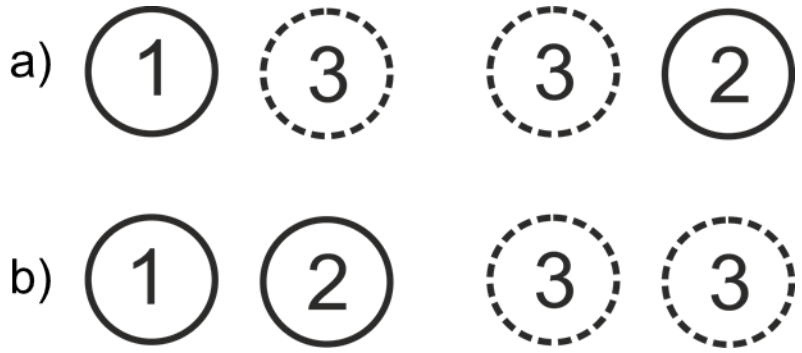

Figure 1-5. A schematic diagram of particle 1 and 2 in an interface 3. a) Particles 1 and are far apart. b) Particles 1 and 2 are brought close to each other. Redrawn from reference 15.

When the particles are separated by a long distance then the interactions which arise are the particle-dispersion medium interactions A_{13} and A_{23} (Figure 1-5. a). If the particle 2 is brought to the vicinity of particle 1 the dispersion medium must be displaced to the position originally occupied by the particle 2 and interactions which occur are those of particle-particle and dispersion medium-dispersion medium, A_{12} and A_{33} (Figure 1-5. b). The composite Hamaker constant is hence given by

$$A_H = A_{12}+A_{33}-A_{12}-A_{23} \quad (1\text{-}3)$$

Where

$$A_{ij} = A_{ii}A_{jj} \quad (1\text{-}4)$$

The composite Hamaker constant can be positive (interparticle attraction) where A_{11} and A_{22} are either both greater or less than A_{33}. The negative composite Hamaker, in the cases when A_{33} has an intermediate value compared to those of A_{11} and A_{22}, indicates repulsive van der Waals interaction.

1.2.2 Electrostatic Forces

Most colloidal particles acquire surface electric charge either from charged groups on their surfaces (e.g. OH, COOH, SO_4Na) or through adsorption of ions onto the surfaces from the solution they are suspended in. This results in formation of an electric double-layer around the particle. This so-called electrical double layer consists of the specifically adsorbed ions and diffusely distributed counter and co-ions which compensate the surface charge. The first layer of specifically adsorbed particles is

called the Stern plane. The rest of the electric double layer, which consists of counter and co-ions, is diffuse and extends over distances which are characterised by the Debye length κ^{-1} (see Figure 1-6 for a schematic representation). The Debye length is inversely proportional to the concentration of the electrolyte. The electrostatic interactions can hence be screened with increasing electrolyte concentration.

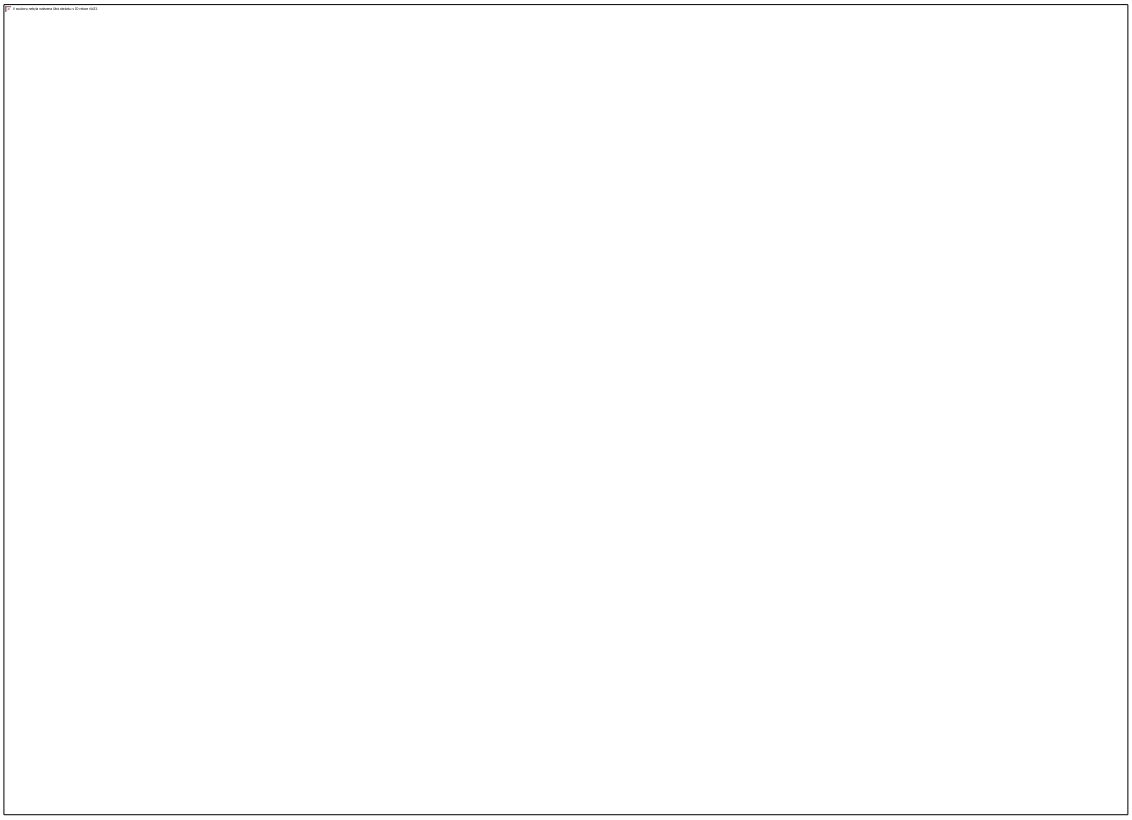

Figure 1-6. Schematics of the electrical double layer a charged colloid particle surface in contact with aqueous solution of electrolyte.

The electrostatic interaction of like-charged colloids is repulsive due to the increase of the osmotic pressure of the water in between the particles as their electric layers overlap leading to increased concentration of counterions. The electrostatic forces resulting from the overlapping of the electrical double layers of spheres of identical radii *a* can be calculated using the following expression:[16]

$$U_{EL} = \frac{B\pi a \exp(-\kappa D)}{\kappa} \tag{1-5}$$

where $B = 32\varepsilon_0\varepsilon_r\kappa\gamma_1\gamma_2\left(\frac{kT}{\nu e}\right)^2$

and ε_0 is the permeativity of vacuum, ε_r is the relative dielectric permeativity, κ is the inverse Debye screening length. In $\gamma_i = tanh(\Psi_i/4)$ and $\Psi_i = ve\psi_i/kT$, k is the Boltzman constant, v is the charge number, e is the electronic charge, T is the absolute temperature and ψ_i is the surface potential.

1.2.3 Total Interaction Energy

The total interaction energy, U_{total}, between two colloidal particles is a sum of the electrostatic forces and the van der Waals forces acting between them:

$$U_{total}=U_{EL}+U_{VW} \tag{1-6}$$

The total interaction energy can be represented as a function of the inter-particle separation D.

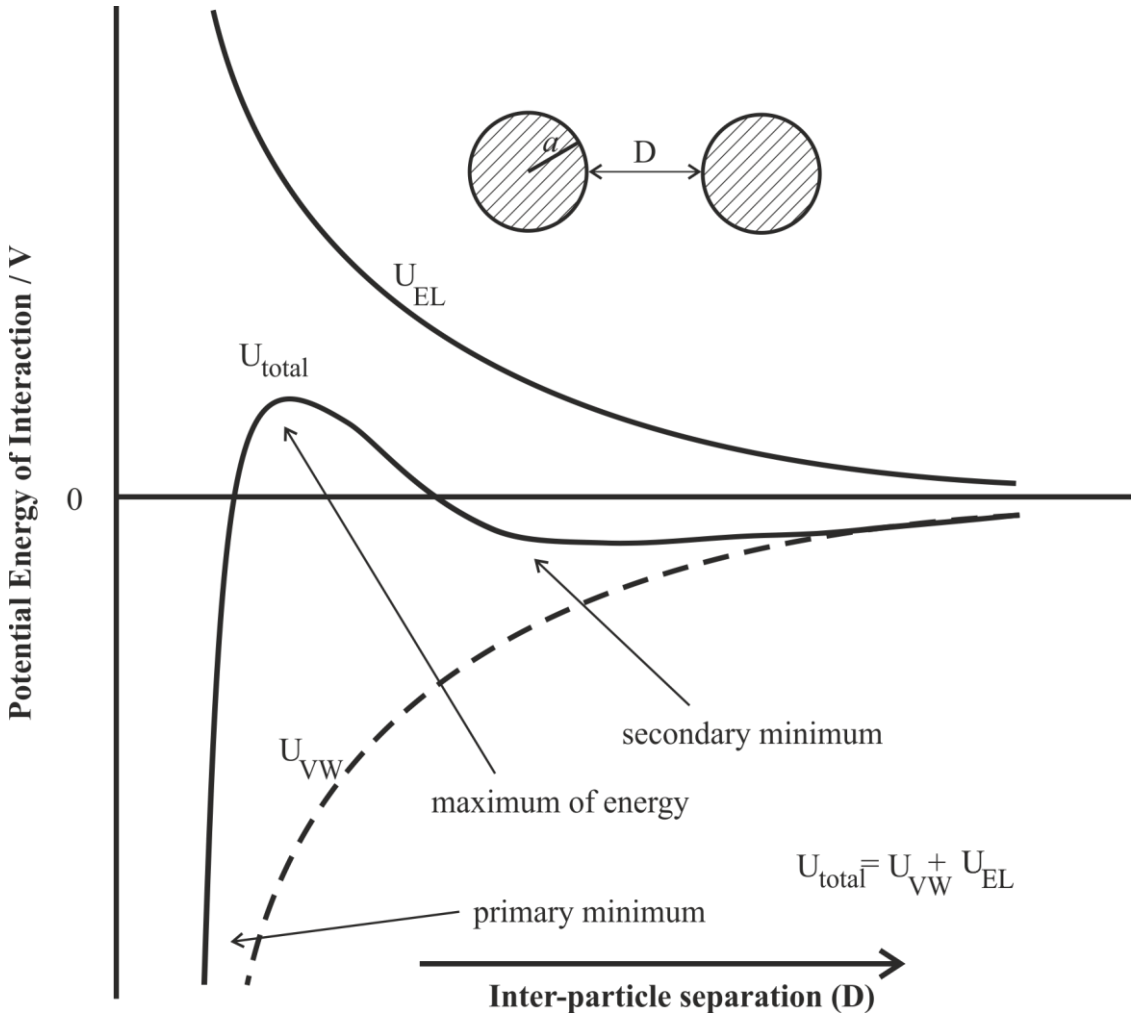

Figure 1-7. Interaction energy of colloidal particles of likely charged as a function of distance.

DLVO theory predicts an exponential decay of the electrostatic interaction energy whilst the van der Waals attraction forces decay with the inverse first power of the inter-particle separation. This means that the van der Waals interactions are far more long ranging than their electrostatic counterparts. The van der Waals forces also dominate at very small separations. However, at intermediate distances the electrostatic force has a strong effect and can give rise to an energy barrier rendering the colloidal system stable. This happens when the colloidal surfaces are of like charge which is sufficiently high and when the electrolyte concentration is sufficiently low and screening is not significant.

The DLVO theory can predict the stability of suspension and emulsion systems by calculating the total interaction energy. For example, the primary minimum, as shown in Figure 1-7, relates to the coalescence or coagulation events. Coalescence and coagulation are irreversible as the absolute value of the interaction energy at the primary minimum is much higher than thermal energy (kT). The secondary minimum relates to aggregation of particles or droplets which is reversible. The maximum energy point is the point of the energy barrier. If the energy barrier is lower than kT then the system is unstable to coalescence or coagulation.

1.3 Human Pathogens

There are a wide array of agents which may cause disease. These include viruses, bacteria, fungi, parasites such as various protozoa and worms, and prions. Prions are essentially protein folds and hence cannot be replicated and targeted using nanoantibiotics as they are proposed. The parasitic worms are also beyond the scope of the nanoantibiotics action as many of them are far larger than the constituents of the colloidal domain in which nanoantibiotics operate. For this reason we will only discuss the rest of the listed pathogens in greater detail. This section will be organised in line with their taxonomy. This will allow their general traits to be explored. The cellular prokaryotic pathogens with their eukaryotic counterparts will be discussed as well as the viruses which lack cellular structure and are often classed as non-living species. It is not intended that this section gives and exhaustive break down of this area. We want rather to present a general picture of the pathogens that can be a subject of nanoantibiotic action.

1.3.1 Viruses

Viruses are sub-micrometer infectious agents - generally about 20 – 300 nm in size, and are essentially fragments of genetic information protected by a protein capsule called a capsid, which is capable of infecting cells and biological organisms.[17] They are classified as non-living as they lack metabolic apparatus and cannot reproduce outside their host cells. Viruses can be divided into four basic categories based on the morphologies of the capsids: helical, which results in a filamentous or rod-like shape of the viruses; icosahedral, which form cage-like structures; enveloped; and complex.

In general, the infection/reproduction cycle can be divided into five steps.[18] The first step is the attachment of a virion, a single viral particle, onto the host cell. This binding is a specific property of the virus and is usually performed by specific attachment to a receptor on the target cell surface. This step is followed by the penetration, or endocytosis, at which the viral nucleic acid or the virus enters the host cell. Next, during the synthesis phase, the host cell metabolism starts producing the viral nucleic acid and protein as directed by the virus. During the maturation the proteins are self-assembled into a capsid around the viral genome to produce a new virion. The final step is the release of the mature virions from the cell. For a diagrammatic illustration of the viral life-cycle see Figure 1-8.

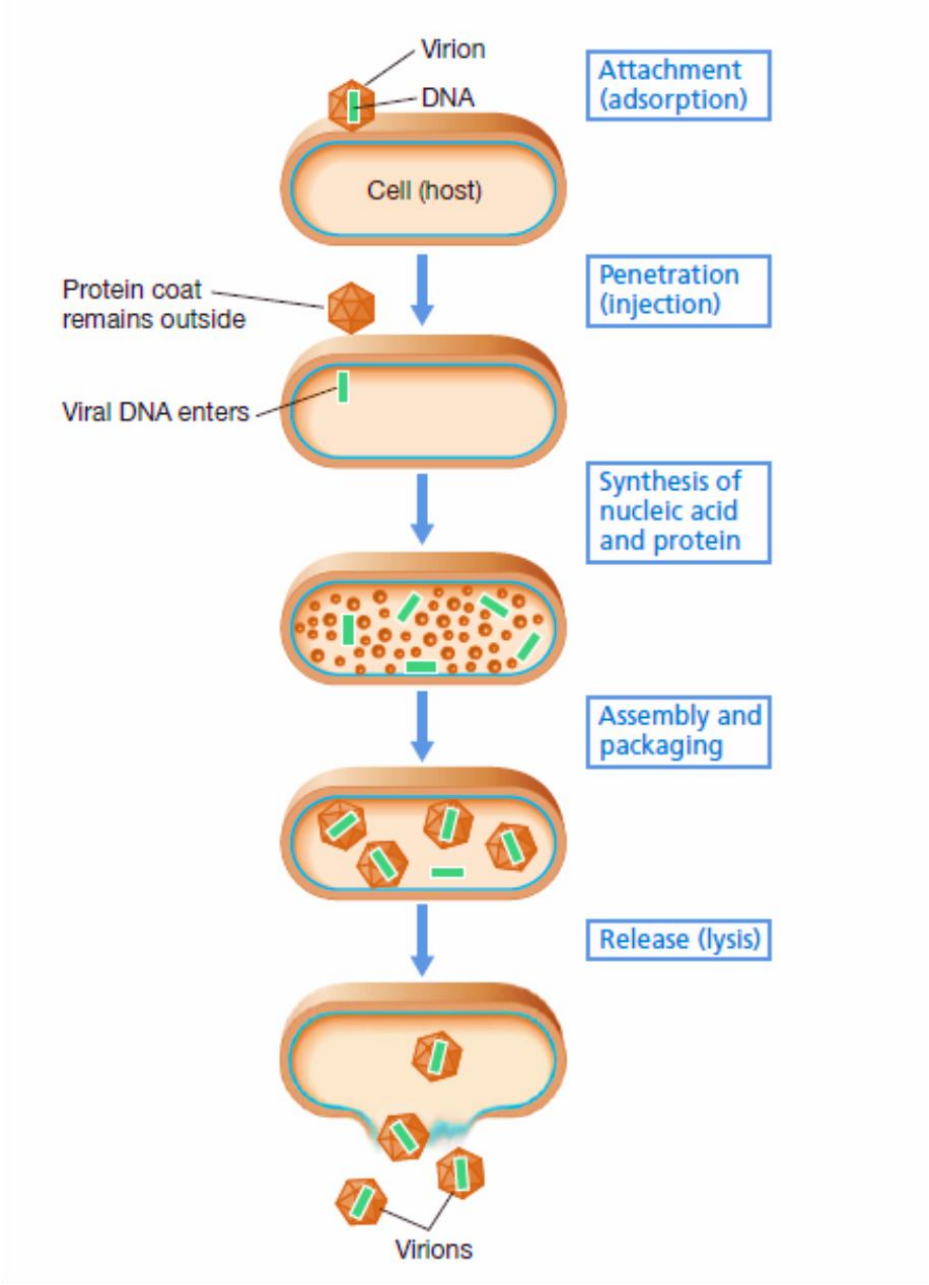

Figure 1-8. The viral life-cycle.[18] Image reproduced from Reference 18.

Many of the viral infections result in cell death or cell structure alterations. The causes of such events include cell lysis, cell membrane alterations and apoptosis. This is one of the causal mechanisms of viral diseases. Another mechanism of viral pathogenicity involves the effect of toxins which might be either products or by-products of the viral replication. Some viruses can also cause cancer by transforming the host cells via the integration of viral nucleic acid into the host chromosome and causing the cells to proliferate malignantly.[19, 20] Viral infections can also be responsible for the suppression of the host's immune mechanism by suppressing the synthesis of antibodies, destruction

of the antibody-producing cell and increasing the immunoglobulin catabolism. It is worthwhile noting that viruses can remain dormant for number of years showing no signs of infection. This is the case of the herpes viruses, for example.[21]

There are many diseases caused by viral infections, these include the common cold, influenza and cold sores as well as the very serious ones like ebola, AIDS and SARS. There are also a number of diseases which are under suspicion to be caused by viruses. Examples such illnesses include multiple sclerosis, chronic fatigue syndrome, and various psychiatric illnesses.[20]

1.3.2 Cellular Pathogens

The morphology of all of the living organisms has one common denominator, the cell.[18] Cells are the elemental building blocks of life. All cells have membranes which are made of a lipid bilayer and proteins. Their function is to isolate and protect the cellular interior from the environment. Within the cell membrane resides the cytoplasm which is a gel-like substance consisting of aqueous and internal cellular substructures, the organelles. The cytosol contains the necessary nutrients and electrolytes, assists in the waste product beak-down and the transport of material within the cell. Ribosomes, the organelles which contain RNA (ribonucleic acid) and are involved in proteins synthesis are also a common feature of all cells. There are two different kinds of genetic material: DNA (deoxyribonucleic acid) and the RNA.

1.3.2.1 Prokaryotes

Closer examination of the cellular structure however reveals two distinct patterns: the prokaryotes and the eukaryotes. The prokaryotes are structurally more simple and almost invariably unicellular organisms (see Figure 1-9. for an illustration).[18] They range in size typically between 1 and 10 μm. Their important feature is that their genome is held within a DNA/protein complex called the nucleoid which freely floats within the cytosol. They have a single outer membrane which is typically surrounded by a protective cell wall. The cell wall, which consists of polysaccharides, provides mechanical protection and holds the cell shape. The only prokaryotic organisms which do not have a cell wall are the mycoplasms which cause respiratory disease in humans. Prokaryotes reproduce asexually by binary fission.

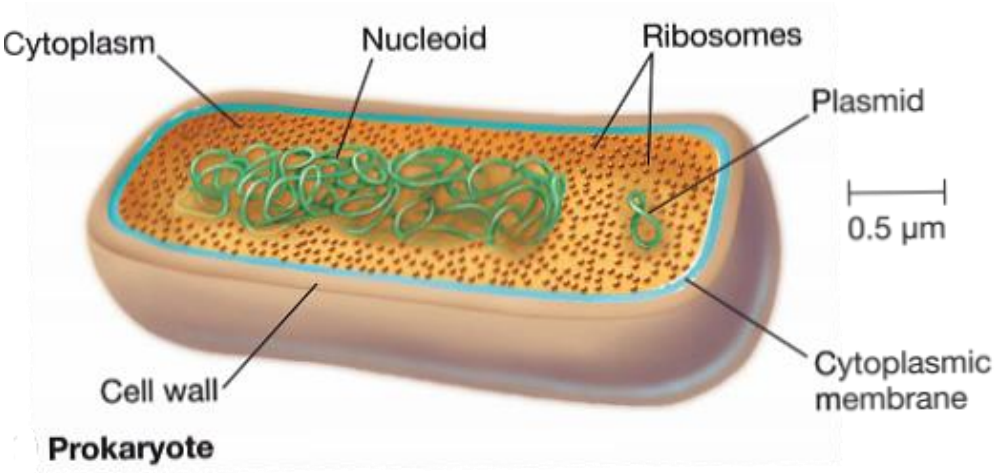

Figure 1-9. Schematic of a prokaryotic cell.[18] Image reproduced from Reference 18.

There are only two major classification domains: archaea and bacteria.[22] As all known disease-causing prokaryotes are bacteria we will only discuss this domain in further detail. Bacterial cells are varied in their morphology. Probably the simplest bacteria are the spherical cocci. There are also rod-shaped bacilli, spiral-shaped spirilla and many other shapes (see Figure 1-9 for examples of bacterial morphologies). Many bacterial cells also form clusters which are characteristic for the particular genera.

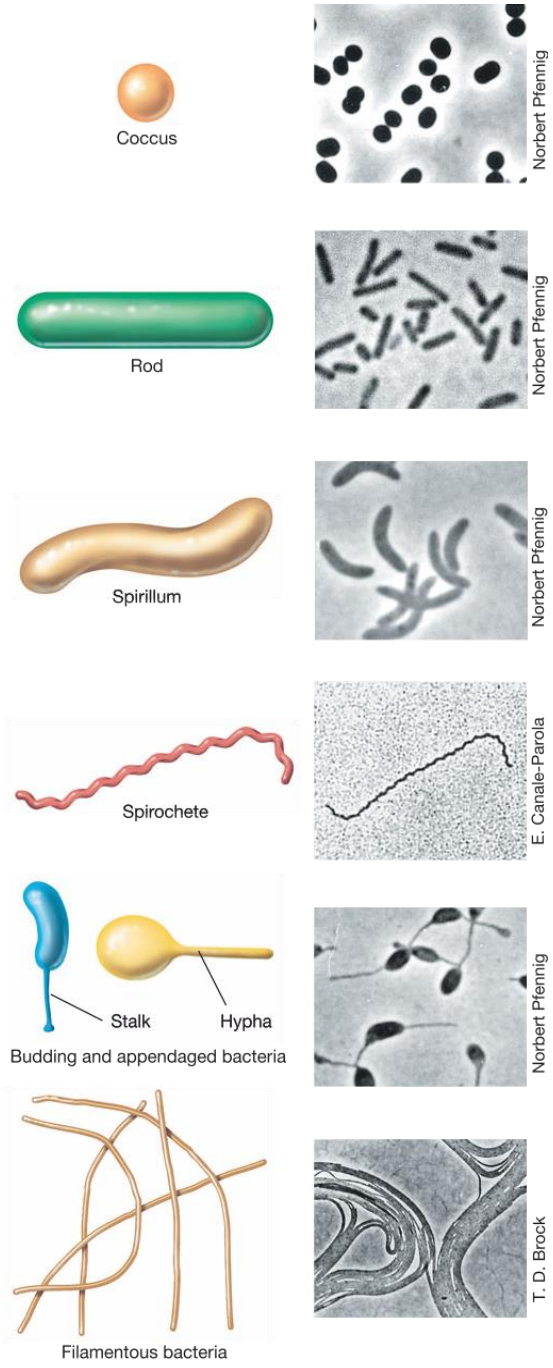

Figure 1-10. Common bacterial morphologies with corresponding optical micrographs of bacteria with various shapes and morphologies.[18] The examples of the coccus, rod-shaped bacillus, spirilium, spirochete, budding and appendaged bacteria and filamentous bacteria are *Thiocapsa roseopersicina* (diameter of a single cell 1.5 μm), *Desulfuromonas acetoxidans* (diameter 1 μm), *Rhodospirillum rubrum* (diameter 1 μm), *Spirochaeta stenostrepta* (diameter 0.25 μm), *Rhodomicrobium vannielii* (diameter 1.2 μm), *Chloroflexus aurantiacus* (diameter 0.8 μm), respectively. Image reproduced from Reference 18.

Beside the morphological categorization, bacteria are also divided into two large groups – Gram-positive and Gram-negative.[5] The Gram-positive bacteria generally have a single cellular membrane surrounded by a thick peptidoglycan layer which retains colouring acquired by the exposure to the Methyl violet stain (see Figure 1-11.). The Gram-negative bacteria on the other hand contain only a thin peptidoglycan layer which does not retain the colouring. This staining test which determines the nature of the bacterial cell protective layers is important as these layers determine the cell permeability to different types of chemical agents. For instance, in the case of antibiotics, which will be discussed in length in section 1.4, it was found that the cell walls of Gram-positive bacteria are more permeable and hence susceptible to wider range of therapeutic agents.

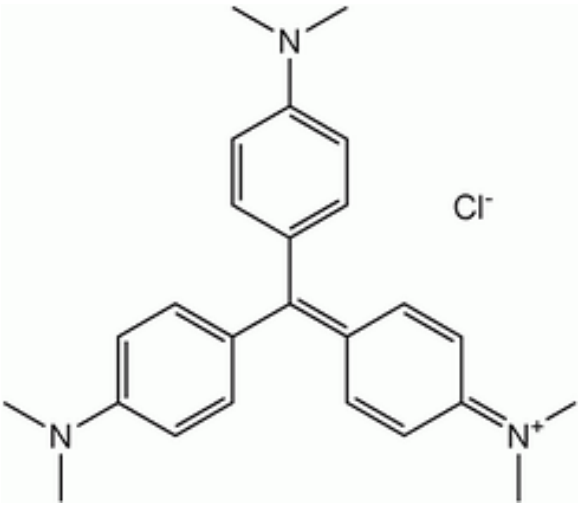

Figure 1-11. Structure of methyl violet stain.

The vast majority of bacteria are harmless and often even beneficial. More than 1000 bacterial species existing in the human gut flora strengthen our immunity via competitive exclusion and assist with the synthesis of vitamins such as folic acid, vitamin K and biotin.[23-26] They also help with the processing of sugars to lactic acid as well as with fermentation of the indigestible carbohydrates. However, they are also a major cause of diseases around the world. Tuberculosis is one of the most urgent public health threats worldwide. It is responsible for 1.5 million deaths per year and is caused most usually by the bacterium *Mycobacterium tuberculosis*.[27, 28] There are many other conditions that are caused by bacteria, these for instance include tetanus, typhoid fever, diphtheria, syphilis, cholera, foodborne illnesses, leprosy and tuberculosis.

As mentioned above, we are constantly infected by bacteria. They can be found on the human skin, in lungs as well as the gut. If the immune responses are weakened an illness caused by otherwise normally harmless bacteria can occur – these are the so-called opportunistic infections. There are number of mechanisms of bacterial pathogenesis.[29] The first step in pathogenesis is the adhesion. Having penetrated the innate barriers of the host which include for instance factors like low pH in the stomach, lysozymes in tears and leucocytes in the blood tissues, the bacteria must race against the host in order to dominate over the immune response. This is initially achieved by specific binding to the target host cells and surfaces. The factors used are called adhesins and can be made from polypeptides or polysaccharides. These factors also render the microbes more resistant to mechanical forces which are utilised by the host to "wash" the pathogens from their substrates. These mechanical forces include for instance coughing, sneezing and peristalsis. The adhesion step is crucial for the proliferation of the pathogens. This is then followed by secretion of polysaccharides which coat the pathogenic cells in order to protect them from the immune response. As a consequence of the apparent inefficiency the immune reaction is elevated causing tissue damage via an overactive inflammatory response.[22]

Bacteria often contain endotoxins which are incorporated within the cell wall.[22] Once the bacterial cells die and cell lysis occurs the toxins are released and can lead to a septic shock caused by overstimulation of the inflammatory response. Ironically, antibacterial drugs can therefore negatively impact on the patient's condition when used to treat microbial sepsis. Bacteria can also synthesise and excrete exo-toxins. These protein structures of enzymatic activity can transferred into the host cell or into the extracellular space. These toxins then disrupt the host cell signalling pathways, acting as a neurotoxin, or disrupt the structural integrity of the host cell or tissue.

The pathogenic cell proliferation is then mediated via intra- or extra-cellular replication. During the more common extracellular route the pathogenic cells break down the barriers with the host's tissue. This results in the creation of a niche in which the bacteria multiply and from which they invade the surrounding areas. The microbes which replicate extra-cellularly include for instance Staphylococcus *aureus* or *Pseudomonas aeruginosa.* The intracellular route is rarer. First, the pathogen must penetrate the host cell without killing it and survive and replicate within. Then, release and infection of further cells and tissues occurs. It can be extremely difficult to treat

intra-cellularly proliferating pathogens due to the circumvention of the standard immune response in the host and the shield which the host cell becomes. Mycobacterium tuberculosis or the chlamydias are classic examples of such pathogens.[21]

1.3.2.2 Eukaryotes

Eukaryotic cells are more much more compartmentalised than their prokaryotic counterparts (see Figure 1-12.).[18] They tend to contain more organelles and their size variation ranges from 0.8 μm to several hundreds of micrometres. The main aspect which segregates them from the prokaryotic cells is the nucleus. The nucleus is a membrane-delineated organelle attached to the cellular membrane which houses the cell's genome. Among the organelles which can be present in eukaryotic cells but are absent in the domain of prokaryotes are for instance the chloroplasts which are dedicated to photosynthesis.

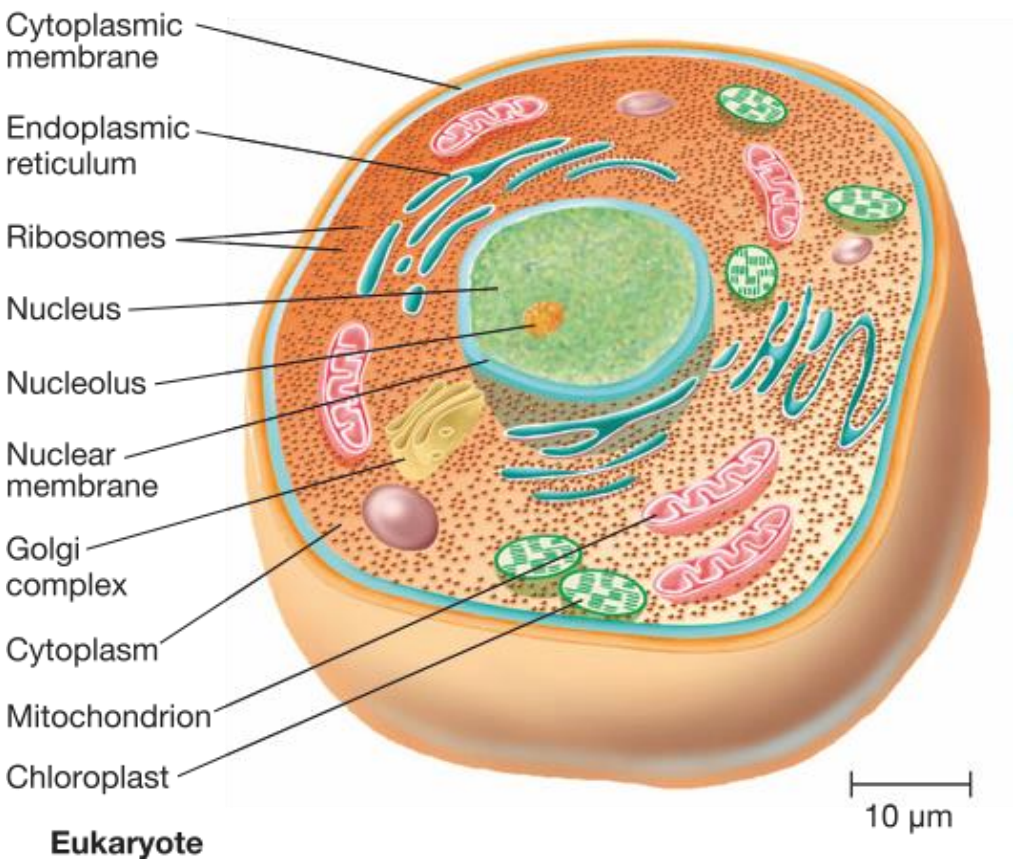

Figure 1-12. An example of the internal structure of an eukaryotic cell.[18] Image reproduced from Reference 18.

The eukaryotic pathogenic microorganisms include organisms in the kingdoms of protozoa and fungi. As protozoa lack the cell wall and hence do not have a single characteristic shape, nanoantibiotics as described in this thesis cannot be applied. Similarly, there are filamentous multicellular pathogenic fungi which, again, lack a single characteristic shape and cannot be targeted by nanoantibiotics. In the rest of this section we will therefore consider the unicellular pathogenic members of the Kingdom of fungi which have their shape fixed by a cell wall - the yeast cells. The ellipsoidal yeast cells size can vary in size depending on the species. The typical size is about 3-4 μm in diameter, some, however, can reach up to 40 μm.[30] They typically reproduce asexually via mitosis, and often in an asymmetric fashion called budding.

Fungal pathogenesis in general is much less well-understood compared to the bacterial one.[31] The disease-causing yeasts are opportunistic; they generally are part of the human flora acquired at the point of birth and cause infections in patients with supressed immunity. Similarly to bacteria they produce adhesins in order to avoid mechanical removal from the site of infection. Some yeasts are stable and capable of proliferation at elevated temperatures within the fever range, that is between 38 – 42 °C. This causes a major strain in the infected organism. The two most significant pathogenic yeasts are normally harmless commensals - *Candidas and Cryptococcus neoforman.*[21] The yeast cells from the genus of candida are universally found on human skin. Infections caused by *Candidas*, candidiasis, are generally localised and found on the skin, in the mouth or in the vagina. In patients with compromised immune system, or when introduced into the blood stream, they can cause a systemic disease producing abscess, inflammations of the veins, inner layer of the heart, eyes and other organs. Again, the infections caused by C. *neoforman*, cryptococci, are typically found in immunocompromised people. These yeast cells have an extra polysaccharide capsule which hinders recognition by the host's immune system.

1.4 Conventional Antibiotics

Antibiotics are chemical compounds that are capable of inhibition of the growth of or killing of microorganisms. Such chemical agents can be employed for therapeutical purposes in the case of an infection when the agent is sufficiently nontoxic to the host. This section will concentrate on the antibiotics which are more narrowly defined as drugs which affect bacteria. The modes of action will be briefly examined and antibiotic

resistance in pathogenic bacteria, which is a major concern in modern medicine, will be discussed.

When viewed from the point of view of their origin, there are two classes of antibiotics, synthetic and natural. The natural antibiotics are synthesized by various prokaryotes and microbial fungi for the sole purpose of killing other microbial organisms. Only about 1% of the known natural antibiotics can be used as antimicrobial drugs as most of them would be too toxic for the host. Natural antibiotics are often chemically altered in order to improve their efficacy – these are semi-synthetic antibiotics. The annual production of both synthetic and natural antimicrobials is about 10 tons worldwide.[22] Based on their biological activity they can be fundamentally divided into two categories – bactericidal and bacteriostatic. The deployment of bactericidals results in the killing of the pathogens whereas bacteriostatic antibiotics slow down or stall bacterial growth.

Antibacterial antibiotics are also commonly categorized according to their mechanism of action and target cellular structures (see Figure 1-13.) and according to their spectrum of activity. Antibiotics which affect the synthesis of the bacterial wall (β-lactams), cell membrane (polymixins) or interfere with essential bacterial enzymes (quinolones, sulfonamides) have bactericidal effects. Antibiotic agents which affect the protein synthesis (aminoglycosides, macrolides, and tetracyclines) are generally bacteriostatic.[32] The narrow-spectrum antibiotics target specific types of bacteria such Gram-positive or Gram-negative. The broad-range antibiotics, on the other hand, affect a wide spectrum of bacterial pathogens.

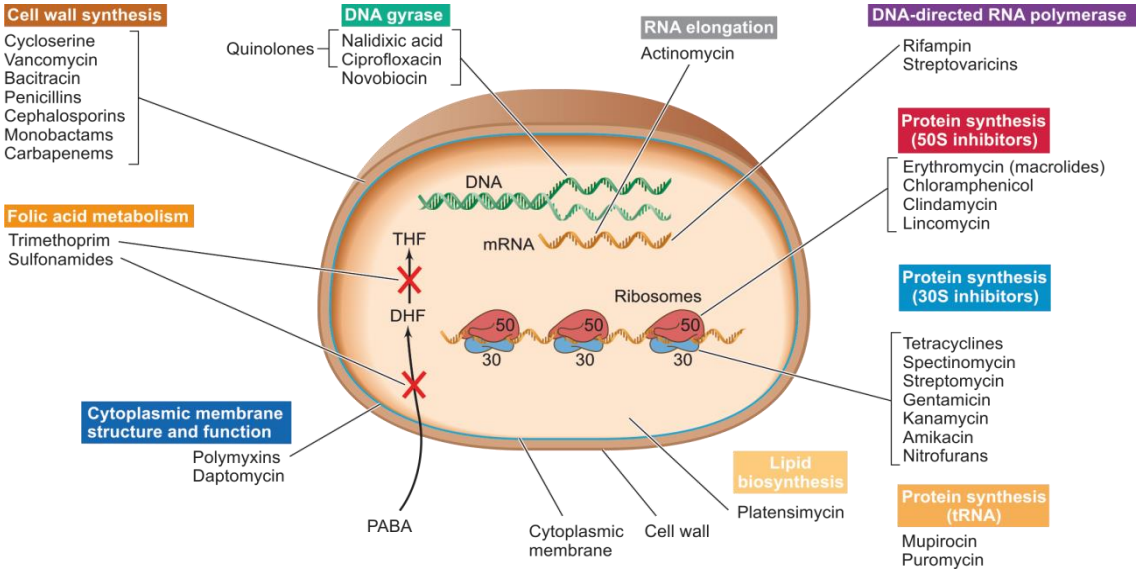

Figure 1-13. Mechanism of action of some major antibiotics. The drugs classified according to their target structures within the bacterial cell.[22] Image reproduced from Reference 22.

1.4.1 Synthetic antibiotics

Most of the synthetic antibiotics act as growth factor analogues. Growth factor is a specific chemical substance which is essential for the growth of a microbial organism. The growth factors must be acquired from the environment as the microbes are not capable of synthesising them on their own. Growth factor analogues are substances structurally similar to the growth factors but do not support the growth. The first commercially available antibiotics, sulphonamides, belong to the growth analogue category (see Figure 1-14. for the structure of the simplest sulphonamide). Sulphonamides were developed in 1930's by Gerhard Domagk who was awarded the Nobel Prize for medicine in 1939.[22] These chemical agents block the synthesis of folic acid leading to inhibition of nucleic acid synthesis. They used to be widely used to fight streptococcal infections. Resistance however emerged as the formerly susceptible microorganisms developed the ability to take up folic acid from the environment.

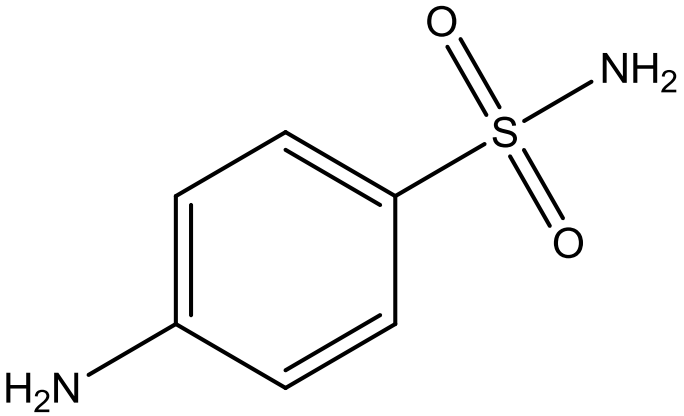

Figure 1-14. The structure of the simplest sulphonamide drug – sulphanilamide.[22]

Another type of growth factor analogues which target nucleic acid synthesis are the Nucleic Acid Base Analogues. These are formed by addition of a fluorine or bromine atom to the nucleic bases (see Figure 1-14). These alterations do not change how the compound is used by the bacteria, but change the chemical properties such that the compound cannot participate in the nucleic acid synthesis. This class of antibiotics can also be used as antiviral or antifungal agents.

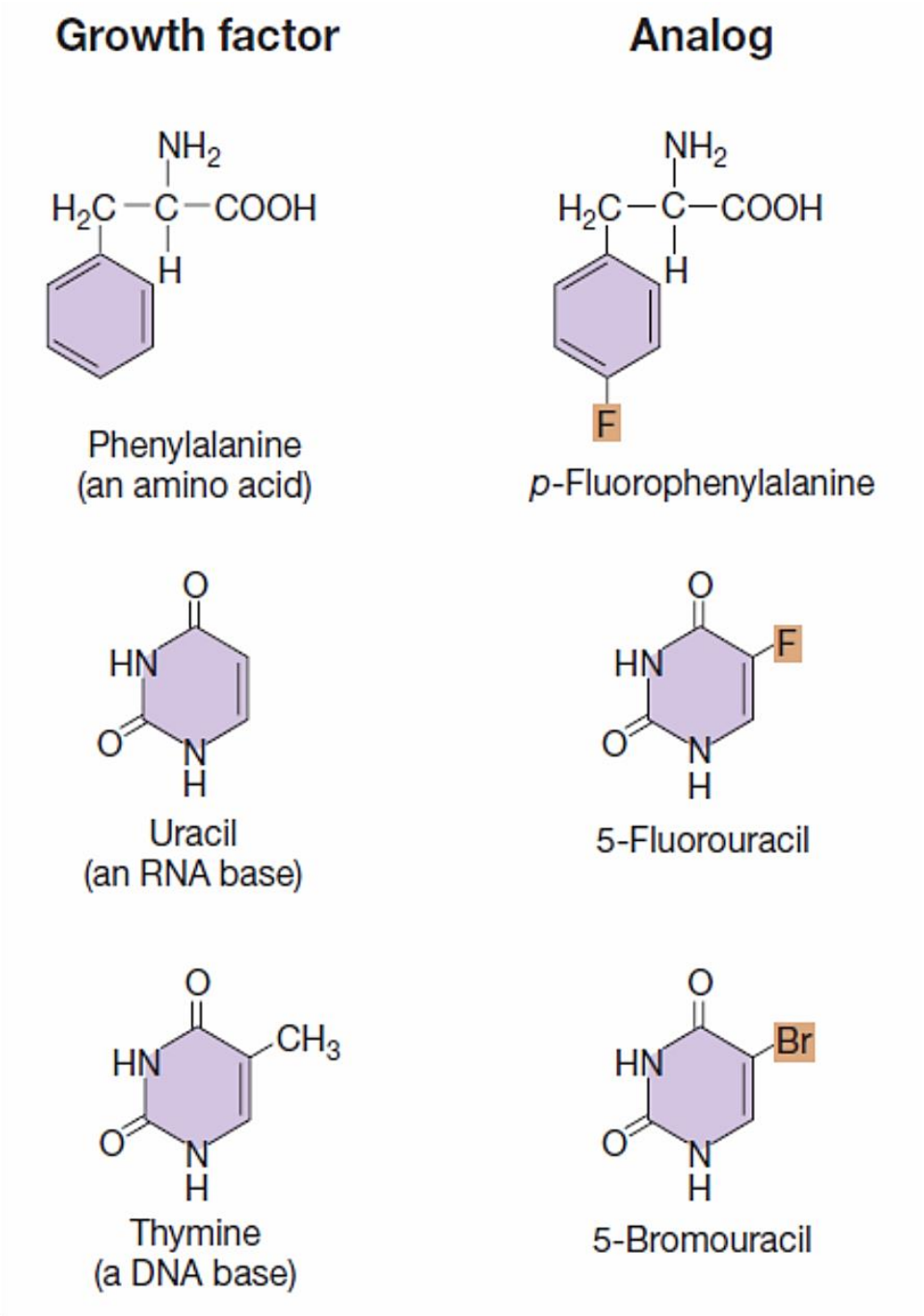

Figure 1-15. Growth factors and their microbial biologically active analogues.[22] Image reproduced from Reference 22.

Isoniazids are growth factor analogues which affect synthesis rendering it fragile.[22] The deployment of isoniazids is the most effective treatment of tuberculosis. Quinolones are growth factor analogues which interfere with the pathogenic DNA and are efficient in the treatment of urinary infections, anthrax and tuberculosis.

1.4.2 Natural Antibiotics

Here we will discuss the β-lactam group of antibiotics which are a fungal natural product and some of the most important classes of antibiotics of prokaryotic origin.

1.4.2.1 β-lactams

β-Lactam antibiotics are class of antibiotic agents which have a common structural characteristic – the presence of a β-lactam ring in their structure.[22] The first described and characterised β-lactam Penicillin was isolated from the fungus *Penicilliun chrysogenum* and described by Alexander Fleming in 1929. It can be said that this class of antibiotics is comprised from the derivatives of penicillin (See Figure 1-16. for structures of Penicillin and some of its derivatives). These include Methicillin, Oxacillin, Ampicillin, and Carbnicillin. Their mechanism of action involves the inhibition of cell wall synthesis resulting in structurally weak cell walls which are prone to autolysis which is followed by cell death. Many bacteria have developed resistance against the β-lactams by synthesising β-lactamase which is an enzyme that attacks the β-lactam ring.

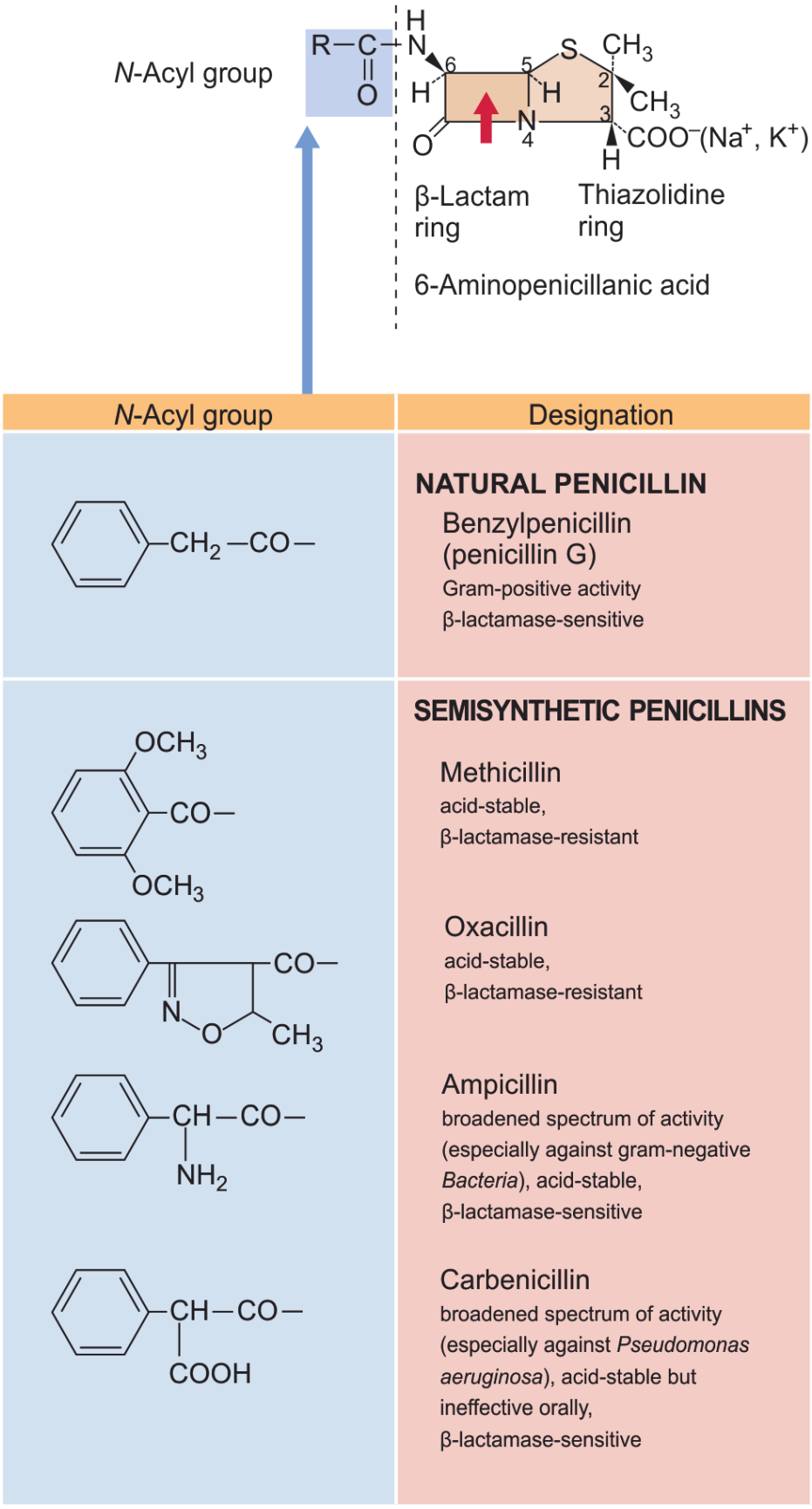

Figure 1-16. Penicillins. The red arrow indicates the site of the activity of β-lactamses. Image reproduced from Reference 22.

1.4.2.2 Antibiotics from Prokaryotes

About two-thirds of all natural clinically useful antibiotics are extracted from the bacteria which belong to the genus of Streptomyces.[22] Probably the best known antibiotic produced by this genus is Tetracyclin. Tetracyclines were the first broad-spectrum antibiotic which affected all gram-positive and negative bacteria. The mechanism of action of these antimicrobial agents involves the inhibition of protein synthesis. Tetracyclines together with the β-lactams are the two most important groups of antibiotics used in the medical field. Unfortunately, as a result of their use in dietary supplements for swine and poultry in some countries a wide-spread antibiotic resistance has emerged. Another class of protein inhibitors which are produced by the Streptomyces bacteria are Aminoglycosides. Aminoglycosides include for instance the streptomycin or neomycin which used to be very effective against Gram-positive bacteria and were used for instance in treatment of tuberculosis. Similarly to the Tetracyclines, the historically long use of these agents has led to bacterial resistance. Lincisamides, of which the most well-known representative is Clindamycin, are also starting to belong to the resistance-compromised protein inhibitors. Daptomycin, on the other hand, is a Streptomyces derived antibiotic of very rare bacterial resistance. This antibiotic binds to cellular membranes which are subsequently disturbed by the formation of pores. Another antibiotic of Streptomyces origin with a low resistance profile is Platensimycin which inhibits the biosynthesis of lipids and is used in treating infections caused by methicillin-resistant bacteria such as those caused by *Staphyloccocus aureus*.

The last prokaryote-sourced antibiotic to be mentioned in this overview is Vancomycin.[22] Vancomycin is isolated from bacteria from the genus of Actinobacteria. This has been a very powerful weapon in fighting β-lactam resistant bacteria such as *S. aureus*. The main reason for its historically long prominence, from its first isolation in 1953, is that it used to be administered intravenously in hospitals and was thus not abused widely. Unfortunately, Vancomycin-resistant bacteria are now becoming more and more common.

1.4.3 Antibiotic resistance

As it was noted in the overview of the most important antibacterial agents in the previous section many pathogens have developed resistance against the action of those drugs.[2, 22, 33-35] For instance, the broad-spectrum antibiotics such as Clindamycin, which is commonly used to treat infections of the respiratory tract, are known for also attacking the "good" commensal bacteria which reside in the guts, helping us digest food effectively and regulating the gut environment. The attack by such potent antibiotics may then lead to a imbalance of the intestinal flora giving rise to the possible overgrowth of harmful microorganisms such as *Clostridium difficile* which is associated with *Pseudomembranous colitis*.[2] Similar effects of antibiotics to this have also been observed in the vaginal flora.[34] However, probably the greatest challenge which has been encountered in the attempt to cure bacterial infections is the growing incidence of the evolution within the target bacteria of resistance to drugs. Probably the most commonly known microorganism which has developed such resistance is *Staphylococcus aureus*. The methicillin-resistant *S. aureus* (also known under the acronym MRSA) is frequently found in hospitals giving rise to complicated secondary infections and large increases in the rates of morbidity and mortality. In 2003, over 50% of the isolates of *S. aureus* in US hospitals were found to be MRSA.[33] This was complicated further by the discovery of MRSA populations that, in addition to resistance to methicillin and other antibiotics in the β-lactam family, had also evolved immunity to glycopeptide antibiotics such as vancomycin. *S. aureus* is not the only pathogen which is becoming increasingly immune to our current antibiotic arsenal; antibiotic-resistant strains of *Enterococcus faecium, Escherichia coli* and *Pseudomonas aeruginosa* are being encountered ever more regularly within the healthcare setting.[22] It is vital that new techniques to fight these aggressive strains of bacteria are discovered to ensure that the world does not return to a time when death from simple infections was commonplace.

1.4.3.1 Mechanisms of antibiotic resistance

There are six different mechanisms by which bacterial pathogens can resist antibiotic agents:[22]

1) Some microorganisms may lack the structure which the particular antibiotic targets. This is for instance the case in some bacteria, such as mycoplasms, which lack a cell wall and therefore cannot be attacked by β-lactams.
2) Some of the bacteria may be impermeable to the particular antibiotic. Most of the gram-negative bacteria are for instance resistant to Penicillin G or Plastensimycin.
3) The pathogens may be also able to inactivate the antibiotics. Many penicillin resistant staphylococci synthesise β-lacamases which cleave off the β-lactam ring.
4) The pathogens may evolve to alter the antibiotic target site. MRSA, for instance, has evolved an altered penicillin binding protein –the binding site of penicillins.
5) The organisms may develop an alternative biochemical pathway. The bacteria targeted by sulphonamides, for instance, have developed resistance by modifying their metabolism to take up folic acid from the environment.
6) The microorganism may pump out the antibiotics via a process called efflux.

The evolution of such protection mechanims represents a major challenge in the deployment of conventional antibiotics.

1.5 Photothermal Effect

The photothermal effect, in its broadest sense, is the term given to the process of using light to produce localised heating. It is widely employed within the experimental cancer therapy field to cause the selective death of tumours due to hyperthermia, with minimal damage to the surrounding healthy cells. This process takes advantage of the special properties of gold and other noble metal nanoparticles, utilising surface plasmon resonance (SPR) in the presence of irradiation laser to induce localised heating resulting in the killing of the target cells in a very selective manner.[36-38]

It was noticed as far back as the middle ages that gold, in small enough particles, changes colour from yellow to red. This property was harnessed by the medieval glass makers to produce ruby glass.[39] This phenomenon is due to the surface plasmon resonance effect.[40] At the interface between the metal and its surrounding, air or liquid, there is a layer of electrons balanced by positive charges. This layer of electrons can oscillate, forming a wave. When a light wave of the appropriate frequency interacts

with the wave, if the particle on which the wave is found is small enough, the wave is propagated around the particle, creating a standing wave of energy that can only be dissipated either by absorption into the particle, or by emission into the surroundings. In the case of colloidal gold in the stained glass, the wavelength is in the UV range, which causes the plasmon to resonate and the standing wave is emitted from the particles as red light. This effect is tuneable, depending on the size of the colloidal particles. The larger the colloidal particle size, the more red-shifted the absorbance maximum becomes. The more light energy absorbed by the particle, the shorter the wavelength of the light released. At sufficient energy input, the absorbance due to SPR results in the formation of a cloud of heated electron gas which cools rapidly by exchanging heat with the surrounding medium. Electron cloud temperatures in the thousands of Kelvin have been observed from very short periods of irradiation, leading to rapid localised heating which can thus lead to cell death.[41] Indeed, it has been observed that under the correct conditions, the localised heating has caused the vaporisation of a thin layer of fluid around the nanoparticles, leading to microscopic explosions and cavitation, which cause mechanical cell damage and death.[42-44]

This characteristic of gold nanoparticles has been widely utilised in so-called photothermal therapy to heat and consequently kill specifically cancer cells whilst leaving the surrounding tissues intact,[36, 37, 45-51] and has also been used to kill bacteria,[52-57] and damage viruses.[49-51] In all the cases mentioned above, the nanoparticles were guided to their cellular targets tissue via immunomodulation of the particles by tagging them with antibodies specific for the targeted cells. The particles are carried throughout the body and are taken up by the target tissues.

The excitation of the gold particles is routinely performed via irradiation by lasers. The efficiency of the light absorbance is very high, especially when compared to that of light-absorbing dyes. Additionally, as the wavelength at which the resonance occurs can be modulated by the size of the nanoparticles, an appropriate wavelength and particle pair can be selected which can most effectively be used in the target system, for example utilising a wavelength which is not absorbed by the body tissues, enabling the light source to remain outside the body, even when treating tissues deep within the body. It has been found that small nanoparticles with a large aspect ratio, for example

rod-like structures, absorb optimally in the NIR range, which is transmitted readily through the body.[58]

1.6 Shell Fabrication Techniques

Here, we will review the published methods of the replication of the size and shape of viral and microbial models. Model species are those which are extensively studied in order to understand biological phenomena typical for the class to which they belong.[59] Methods of deposition of the shells include using inorganic materials via the general symmetric deposition approach, and the generic colloidal approaches which lead to asymmetric shell deposition. Finally, strategies will be suggested for the production of this novel class of antibiotic agents.

1.6.1 Symmetrical Deposition of Shell Material

Here, we will consider methods of deposition of shell-forming materials over the whole surface of biological model systems which leads to the replication of the morphologies and structures on the templates; this process is often referred to as biomorphic mineralisation.[17] Viruses and microbial organisms such as yeast cells and bacteria possess different surface and morphological properties and will hence be considered separately.

1.6.1.1 Biomorphic Mineralisation of Viruses

Viruses can act as templates for material deposition in two ways: they can either facilitate the growth of species within themselves thus determining their shape and size,[60-65] or, they can act as cores in the core-shell deposition process.[66-75] Here, we will concentrate on the latter, shell-making, techniques which use non-bioengineered model organisms with the intention to produce negative replicas of naturally occurring organisms. Such imprints can be used for the recognition of the organisms based on their shape and size. It is, however, worth mentioning that the so called Phage Display technique, which alters the genetic information of bacteriophage viruses in order to produce new reactive amino acids and peptides, is widely used. For example, with the

help of this method the M13 bacteriophage was has been coated with zinc sulfide nanocrystals,[68, 69] cadmium sulfide nanocrystals,[76] and ferromagnetic iron-platinum alloy.[74]

Perhaps the most widely used model virus in the biomorphic mineralisation area is the rod-shaped Tobacco mosaic virus (TMV). This is probably as a consequence of the excellent robustness of the species which is about 300 nm long and about 4 nm wide, which implies a good versatility in terms of the deposition techniques used.[66] Its filamentous shape makes it an ideal candidate for preparation of nanowires and nanotubes. TMV is capable of withstanding biologically extreme conditions; it can survive treatments which involve temperatures reaching up to 60 °C and exposure to a range of pH between 2 and 10 without losing any of its structural features. The surface charge of the TMV is negative above its isoelectric point of pH 3.0 – 3.5 which makes it suitable for coating with materials which rely on electrostatic interactions in aqueous solvents by adjusting the polarity.[71] Furthermore, the presence of amino acid residues on the surfaces can be used in chemical modification geared to bind and nucleate specific mineral particles.[17]

Shenton and colleagues have demonstrated the versatility of the TMV templates by employing a wide range of synthetic routes in order to obtain shells (see Figure 1-17.).[75] They employed acid-catalysed sol-gel polycondensation of tetraethoxy silane (TEOS) at strong acidic conditions (below pH 2.5) in order to obtain a polymeric silica coating of the positively charged TMV (isoelectric point 3.0 -3.5). Lead sulfide and cadmium sulfide coatings were obtained at pH 5 and 7, respectively, by bubbling hydrogen sulfide gas through an aqueous solution containing the TMV particles and divalent lead and cadmium ions. They also deposited iron oxide shells onto the TMV cores at pH 9 by adding sodium hydroxide to a dispersion of the templates in a solution containing a mixture of divalent and trivalent iron ions. The last procedure has also been repeated at pH 6.5 and in anaerobic conditions yielding a better crystallinity of the coating.

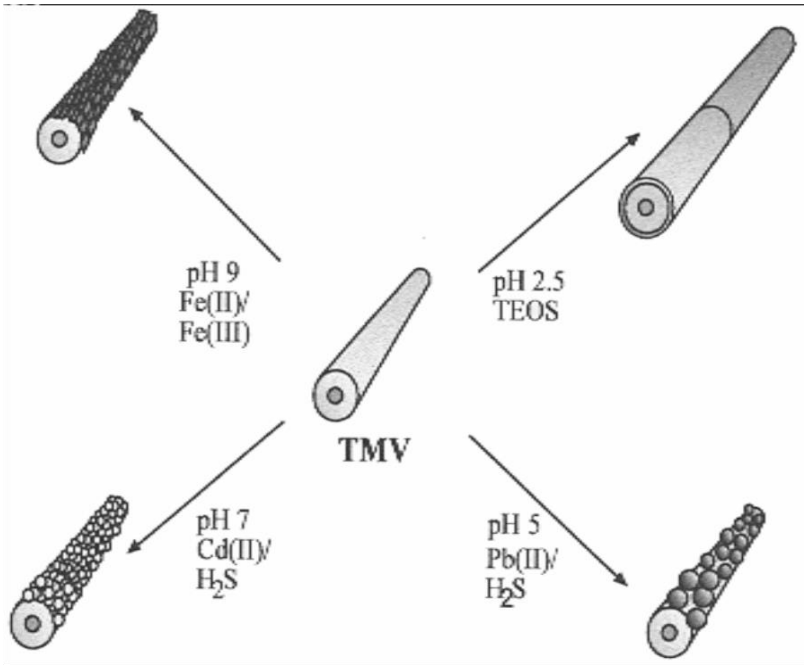

Figure 1-17. Biomorphic mineralisation routes of TMV as presented by Shenton *et al.*[75] Starting clockwise from the right: coating with polymeric silica by acid-catalysed polycondensation TEOS, coprecipitation of PbS and CdS and oxidative hydrolysis. Image reproduced from Reference 75.

Royston and co-workers came up with an improved route of further coating TMV particles with silica.[66, 71] A finer, more uniform coating was achieved by base-catalysed polycondensation of TEOS in 50-50 wt% mixture of methanol and water (TMV capsid proteins become denatured at concentrations below 40 %wt of water due to disruptions of intermolecular hydrogen binding) at pH 8.8 at the start of the polymerisation. The procedure was also performed with aniline-treated viruses, where the role of the aniline was to neutralize the surface charge and hydrophobic features present at the viral surface. The aniline-treated templates provided further improvements yielding thick (approx. 100 nm) robust shells resistant to sonication, organic solvents and drying effects (see Figure 1-18. for a sample picture). These shells were also functionalised with (3-mercaptopropyl)trimethysilane (MPS) and used for the deposition of silver (Ag), gold (Au), palladium (Pd) and platinum (Pt) shells by reduction of the metal salts. The mercapto groups ensured that the metals were deposited as the second layer.

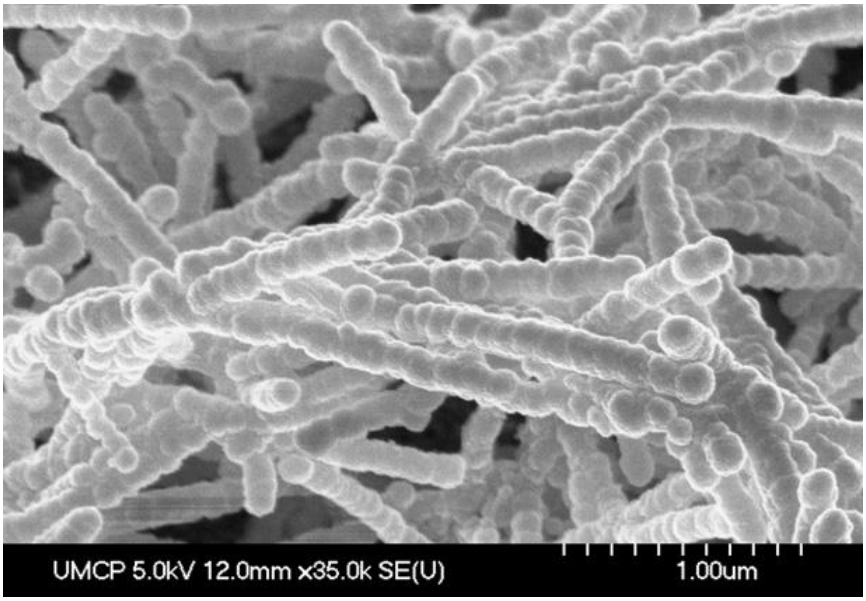

Figure 1-18. Core-shell particles produced by the deposition of silica onto the surface of TMV.[66] Image reproduced from Reference 66.

The presence of chemical groups with metal binding capabilities on the TMV templates facilitates the deposition of metal clusters, and this has been taken advantage of. Gold and platinum coatings of less than 10 nm in thickness have been produced by the *in situ* reduction of $[PtCl_6]^{2-}$ and $[AuCl_4]^-$ in acidic conditions by Dujardin *et al.*[62] Palladium, platinum, and gold clusters have also been deposited onto the TMV surface where the respective metal ions were bound via complexation or electrostatic interactions, notably to the carboxyl and hydroxyl amine groups of the capsid protein, this was followed by reduction with ascorbic acid.[61] In this work, Knez *et al.* also performed electroless plating by the selective reduction of nickel and cobalt ions, promoted by phosphate buffers, where the phosphate ions attached to the positively charged domains of the surface.

1.6.1.2 Biomorphic Mineralization of Bacteria and Yeast Cells

Both bacteria and yeast cells are microscopic single-cellular organisms which are typically 0.5-5μm and 3-4 μm in size, respectively.[17] Unlike the yeast cells which are spherical or ellipsoidal, bacteria give an additional motivation for the scientists to explore avenues of replicating their shapes: over time they have evolved a number of well-defined morphologies both on the micro- as well as nanoscopic level.[77] Both types of these microorganisms have been found to contain or even excrete a range of

inorganic materials which include pristine metals, metal alloys, sulfides and oxides.[17] These materials, produced by naturally occurring *biomineralisation*, are found both inside as well as on the exterior of the organisms and play several roles: they protect the cells from toxic environment, draw or release nutrients and provide or consume energy. It is therefore reasonable that researchers concentrate on these materials when using the organisms in question as templates.

The work of Zhou *et al.* has focused on producing hollow nanostructures produced by the one-pot sonochemical synthesis of hollow microstructures by taking advantage of readily available cells in the place of templates.[77-79] First, they successfully coated spherical *Streptococcus thermophilus* in zinc oxide via a two-step process.[79] In this process the functional groups on the cell walls covalently bond to triethanolamine (TEA), TEA then reacts with zinc acetate as a base producing zinc oxide coating. The cores were subsequently removed by calcination. Zhou and co-workers also developed a generic method for coating bacteria with sulfides, which was demonstrated by deposition of zinc sulfide and lead sulfide onto the cell walls of *Str. thermophilus* and *Lactobacillus bulgaricus* and achieved the formation of interesting hollow structures which resulted from ultrasound disruption (see Figure 1-19. for illustration of the proposed shell-making mechanisms and the structures obtained).[77, 78] This method, however, leads to disruption and removal of some of the cell templates in the process of the deposition. It is therefore believed that this technique might not completely copy the shape of the templates due to the removal of the templates before the deposition process is finished leading to further precipitation of the shell-forming material within the shell.

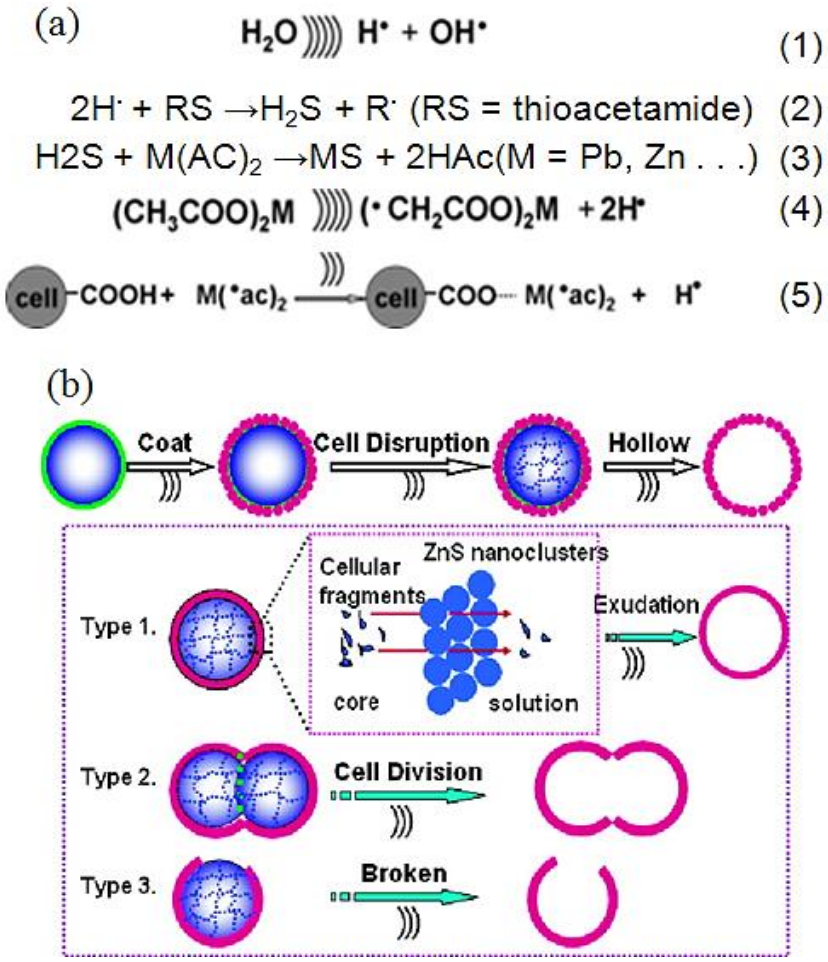

Figure 1-19. The proposed mechanism of the sonochemical one-step synthesis of metal chalcogenide coated bacteria and structures resulting from sonication of the products.[77, 78] (a) reaction mechanism of formation of metal sulfides: (1) primary radical produced by ultrasound-promoted dissociation of water; equations (2) and (3) represent the formation of chalcogenide nanoclusters which are deposited onto the cell walls, in theory because the acetate ligand could graft zinc onto the cell surfaces; equation (4) shows formation of solute radicals under sonochemical conditions; the metal acetates produced in this way can react (5) with carboxyl groups present at the surface of the cells, the metal acetate immobilised on the surface can then undergo ligand exchange as shown in equation (4). (b) Three types of structures were produced after ultrasound-promoted disruption of cell templates. Regular hollow spheres can be produced if the cell fragments are small enough to pass through the interstices of the hollow spheres. Similarly, hollow twin spheres are produced if the cells were coated at the point of division (mitosis). Finally, broken spheres can be formed if the sonication is vigorous or the cell coverage was incomplete in the first place. Image reproduced from Reference 78.

Berry and co-workers reported the successful deposition of a gold shell onto *B. cereus* rod-shaped bacteria by exploiting its high affinity to lysine.[80] They exposed the bacterial cells to a colloidal solution of 30 nm gold particles functionalised by lysine, this lead to the deposition of the particles onto the cell surface. Once the deposition was completed, the gold nano-particles were annealed by the application of an electric field. Kuo *et al.*, on the other hand, took advantage of the natural capability of some bacterial cells to reduce metal ions and their affinity to metal species by *in situ* reduction of trivalent gold ions resulting in self-encapsulation of *E. coli* cells in nanoshells.[81] The bacterial cells were simply dispersed in an aqueous solution of $AuCl_4^-$ ions and left to incubate for 32 h in order to obtain gold plated species. Similarly, Safarik and colleagues directly adsorbed iron oxide nanocrystals by mixing the same bacterial species with a ferrofluid.[82]

The final two examples of the encapsulation of microbial organisms covered in this review include the methods of layer-by-layer encapsulation of living fungi cells and using the same cells as templates for deposition of silica shells which has been employed in the current research. Fakhrullin *et al.* managed to incorporate gold and silver nanoparticles within oppositely charged polyelectrolyte layers which were deposited over the *S. Cerevisiae* and *T. Asperellum* cells (see Figure 1-20. for sample pictures and preparation scheme).[83] This method, which has been used before on non-living templates,[84] is very interesting because it involves no harsh treatments, in fact the whole encapsulation was carried out in physiological conditions, and it was proven that such a coating does not affect the viability of the encapsulated organisms. Weinzierl *et al.* used *S. Cerevisiae* yeast cells as biological templates for a precipitation reaction of silica via the hydrolysis of tetraethylorthosilicate (TEOS) in water-alcohol mixtures using ammonia as a catalyst according to the Stoeber process and subsequently removed the cores by calcination at 500 °C.[85]

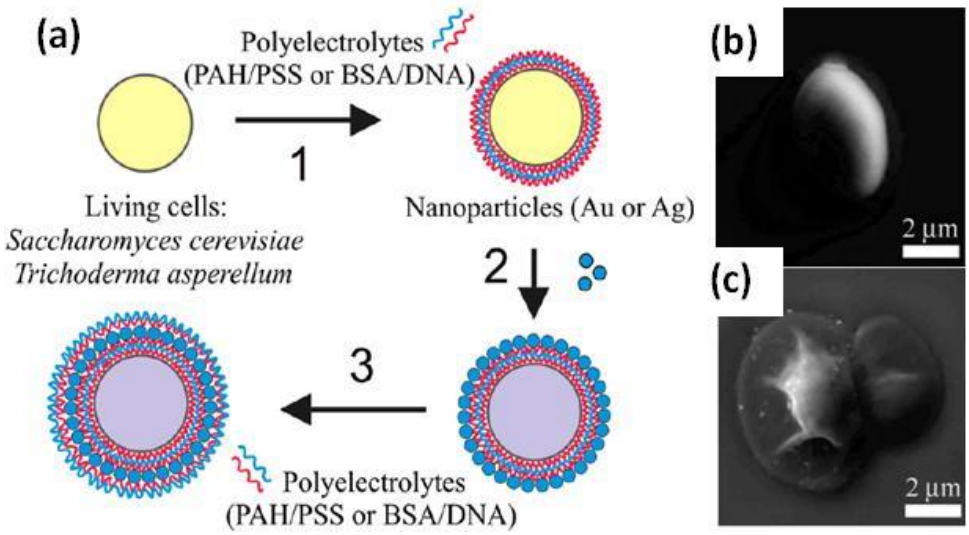

Figure 1-20. (a) Polyelectrolyte encapsulation of the living cells. (b) bare and (c) encapsulated yeast cells.[83] Images reproduced from Reference 83.

1.6.2 Asymmetric Deposition of Shell Material

The asymmetric deposition of shell making materials has been widely achieved via "Janus particle" preparation techniques. The term "Janus particle", named after the double faced Roman god of doors, Janus, was first used in 1991 on the occasion of the Nobel lecture by De Gennes who described spherical glass beads which consisted of distinct hemispheres of different chemical properties.[86] Since then, an entire new field of physical science focusing on preparation and study of such species has developed. There are four general routes of producing these particles: (i) toposelective surface modification, (ii) template-directed self-assembly, (iii) controlled self-assembly and (iv) controlled surface nucleation. Here, we will focus our attention onto the toposelective surface modification route which is based on a temporary partial shielding of the solid particles followed by a modification which, in one example, can be represented by a creation of a hemi-shell over the exposed particle surface. This most traditional and probably the simplest and fastest method of asymmetric deposition of material,[87] can be further subdivided into four categories (see Figure 1-21.): (i) temporary masking of one hemisphere during the surface modification of the other one, (ii) the use of directional fluxes or fields where the particle itself screens the face which is not to be modified, (iii) microcontact printing and (iv) partial contact of the particle with the reactive medium due to its arrangement at an interface supposing no rotation of the particle

occurs during the procedure. The above outlined subdivision of Janus particle preparation was adopted from Perro *et al.*[86]

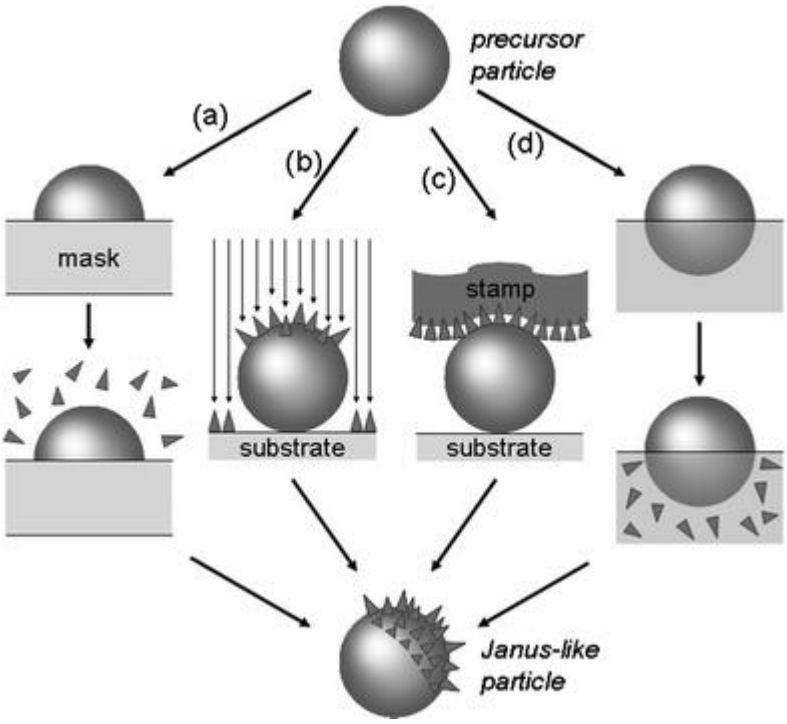

Figure 1-21. Schematic representation of the four toposelective surface modification methods as described by Perro *et al.*.[86] (a) masking/unmasking techniques, (b) techniques employing reactive directional fluxes and fields, (c) microcontact printing and (d) techniques which take advantage of partial contact with the reactive medium. Images reproduced from Reference 86.

1.6.2.1 Surface modification of partially masked particles

The first report of the masking/unmasking approach dates back to 1988. Casagrande and Veyssie produced amphiphilic glass microspheres (40 - 50 μm in diameter).[88] In their experiments, commercially purchased glass beads were deposited onto a solid substrate covered with a layer of cellulose varnish which partially protected the particles. The unprotected parts were then treated with octadecyltrichlorosilane in order to hydrophobize them. After this treatment, the varnish was dissolved and the particles washed and dried. The amphiphilic character of the treated breads was then proven using microscopy pictures which showed discriminatory formation of water droplets from vapour on the hydrophilic region which was protected from the hydrophobization treatment (see Figure 1-22.). Later, the behaviour of these particles at the oil-water

interface was studied and compared with their pristine hydrophilic precursors and fully hydrophobized counterparts. It was established that fully hydrophilic particles preferentially resided at the water phase near the interface and, inversely, the totally hydrophobised beads were immersed in the oil and the Janus particles were symmetrically positioned at the interface. This was rationalized by the consideration of the total energy of the system, which is comprised of the sum of interface energies of the particle and each liquid phase and between the liquids themselves. The major drawback of the cellulose varnish protection is that the minimum thickness of the varnish layer is above 1 μm, which limits this technique to particles with a diameter larger than the minimum thickness.

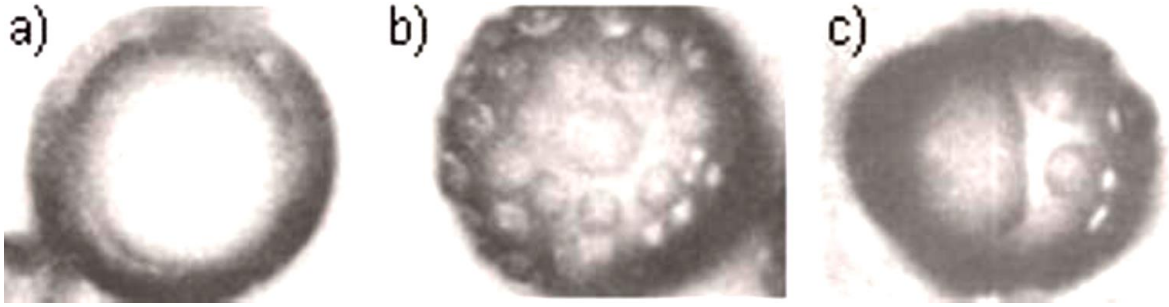

Figure 1-22. Optical microscopy images of (a) the hydrophobic face, (b) hydrophilic face and mixed face of 50 μm Janus beads prepared by Casagrande and Veyssie.[88] Images reproduced from Reference 88.

The particle size limitation of the varnish masking was successfully overcome by researchers at the Bell Laboratories (see Figure 1-23. for a schematic diagram).[89] They managed to selectively pattern silica spheres as small as 100 nm by protecting them with a photoresist layer. A silicon wafer was spin coated with non-contacting silica particles from a colloidal solution and treated at 250 °C to ensure good adhesion of the particles to the substrate. A photoresist was then spincast onto the wafer with the particles. Subsequently, the photoresist layer was then partially etched off using ion etching plasma in order to expose a portion of the silica spheres. This was followed by the deposition of various non-continuous layers of metals (Ti, Au, Ag, and Cu) or metal oxides (Al_2O_3, TiO_2) by e-beam sputtering. The particles were then released by dissolution of the photoresist.

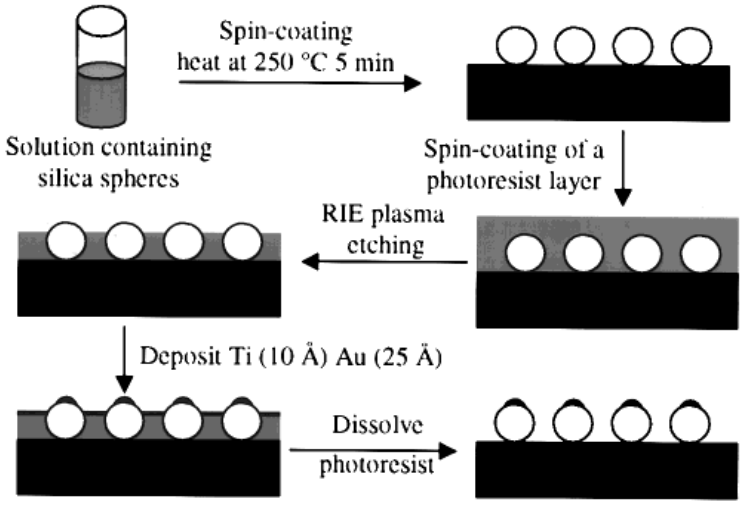

Figure 1-23. A schematic diagram depicting the procedure of masking silica spheres with a photoresist followed by its etching by O_2 plasma and deposition of a metal shell.[89] Image reproduced from Reference 89.

The last example of the masking/unmasking approach reviewed here is represented by the work of Paunov and Cayre, employing their gel trapping technique (GTT),[90] which has also been used for the determination of contact angles of individual colloidal particles at liquid-liquid as well as liquid-air interfaces, and for production of microlens arrays templated by colloidal particles.[91, 92] The Janus particles were prepared as follows (see Figure 1-24. for a schematic diagram and pictures of sample results). Sulphate latex particles (3.9 μm and 2.7 μm in diameter) were spread on the interface of a hot aqueous gellan solution (2 wt%) and pre-warmed decane, the system was left to cool until the aqueous phase gelled, the decane phase was then replaced by polydimethylsiloxane (PDMS) oil which was cured for 48 h. The solid elastomer, together with the trapped particles, was subsequently peeled off the gel, and a gold layer was then deposited via evaporation onto the PDMS surface. Removal of the particles was performed mechanically using a metal blade or using sticky tape. This technique allows for functionalisation of particles as small as 100 nm, and is very versatile in terms of adjusting the portion of the particle altered. This can be for instance achieved by the choice of particles themselves, by the choice of the oil, by addition of salts into the water phase or by introduction of surfactants.

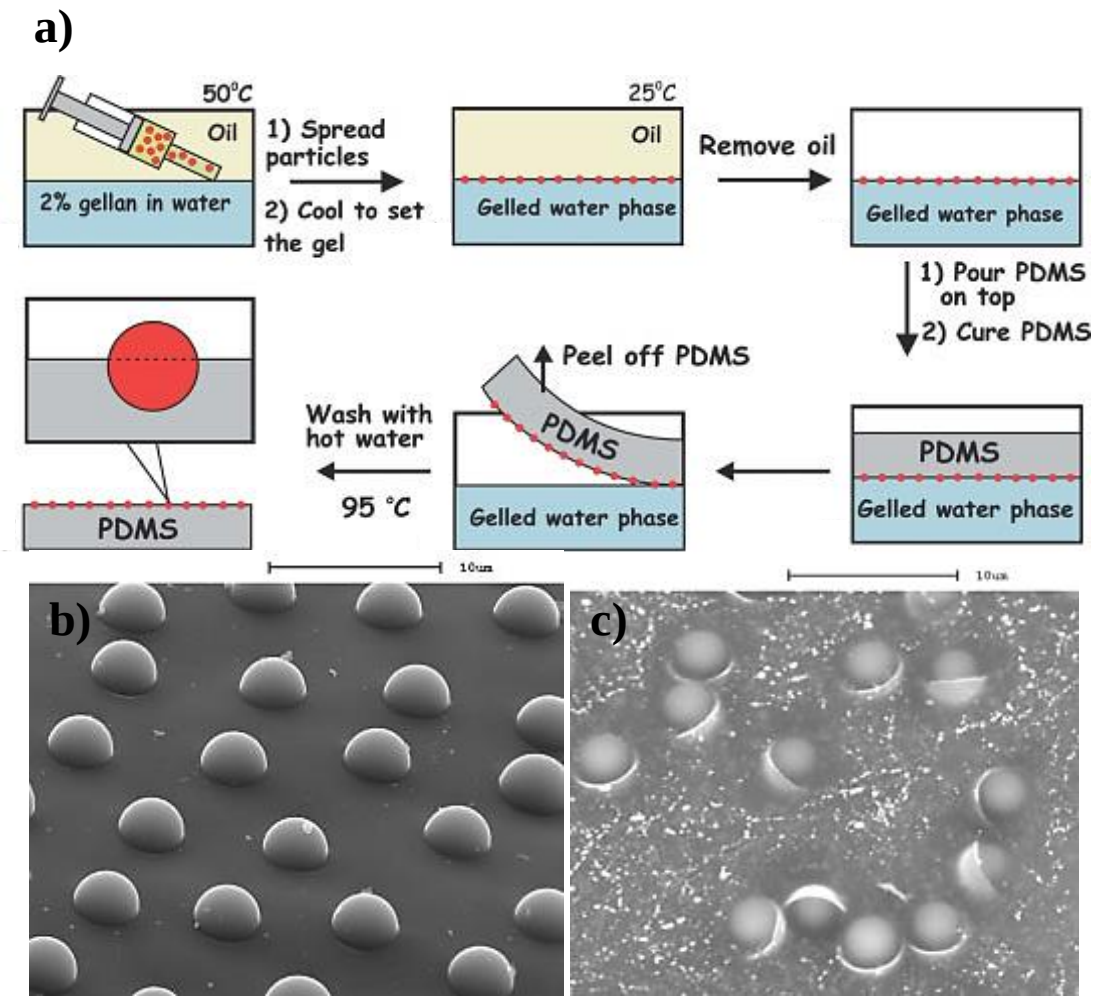

Figure 1-24. (a) A schematic of the GTT procedure, (b) SEM picture of 3.9 μm PS sulphate particles trapped in the PDMS surface, (c) the same particles treated by deposition of a gold layer which was followed by their removal using sticky tape.[90] Images reproduced from Reference 90.

1.6.2.2 Surface modification using directional fluxes and fields

Here we will outline what is probably the most rapid method of fabrication of Janus particles. This process involves the use of directional fluxes or fields aimed at a particle monolayer leading to a modification of the unshielded faces of the individual particles. This approach was probably first introduced by Takei and Shimizu in 1997 and was employed in partially coating 5 -50 μm fluorescent latex particles with a layer of gold via thermal evaporation.[93] The resulting partial coverage was demonstrated using fluorescence microscopy where the covered regions were quenched by the gold layer. Furthermore, the gold layer was functionalised by means of selective chemisorption

using thiolated reagents, thioglycolate (TG) and 2-aminoethanethiol bringing a positive charge onto the gold surface. The presence of a positive charge, and hence successful functionalisation, was then demonstrated by the electrophoretic rotation of the spheres (see Figure 1-25.).

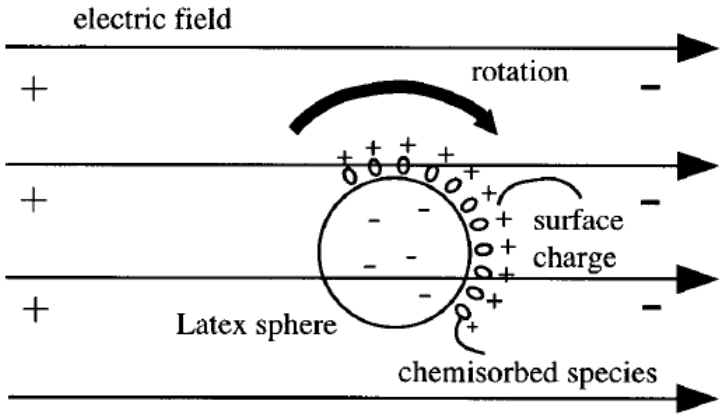

Figure 1-25. Electrophoretic rotation of a locally functionalised latex sphere.[93] Image reproduced from Reference 93.

In a very similar experiment, Himmelhaus and Takei thermally evaporated a gold layer over 110 nm latex spheres and functionalised the gold part with a biotin monolayer.[94] They then took advantage of the well-known specific binding of biotin to avidin and showed that even such small Janus particles can be specifically treated by chemisorption and found applications for instance as optical biosensors; the refractive index as well as the extinction coefficient shifted as avidin was bound to the biotin monolayer. Petit *et al.* have extended the technique of directional flux modification further by coating sub-100 nm silica beads via gold sputtering and suggested that particles of such small dimensions are likely to be coated unevenly; these particles even failed to self-screen and became fully covered after prolonged sputtering (over 1 min).[95]

Exactly the same approach has been routinely employed since the report by Takei and Shimizu. Howse *et al.*, for instance, partially coated 1.62 μm polystyrene spheres with platinum in order to produce self-propelled particles.[96] The platinum "cap" played the role of a catalyst in the reduction of a "fuel" of hydrogen peroxide into oxygen and water which created a hydrogen peroxide concentration gradient. Bajaj and Laibinis hydrophobized their silica particle templates before the deposition of a gold hemi-shell and hence obtained particles divided into hemispheres which displayed opposite wetting

properties.[97] These Janus species were then preferentially coated with different oligonucleotides and used for DNA-directed self-assembly. The last example of the production of Janus particles using this technique is the work of Love *et al.* They went one step further and used the Janus particles formed by metal thermal evaporation deposition as precursors for the creation of individual hemi-shells, i.e. negative replicas.[98] Layers of gold, platinum and palladium were deposited over monolayers of silica particles ranging from 100 to 500 nm in diameter. This procedure was followed by the dissolution of the silica spheres in aqueous hydrofluoric acid (HF). It was reported that the gold shells consisted of grains 40 - 50 nm in diameter and exhibited small pores near the boundaries when the shell thickness was below 15 nm. The shells constituted from palladium consisted of 15 – 20 nm grains and showed no signs of porosity. The finer texture of the grains enables these materials to replicate the templates in higher detail. These hemi-shells exhibited high structural robustness – only 5% of the particles 500 nm in diameter and as thin as 10 nm were distorted or damaged in the course of the fabrication process. It was concluded that hollow metallic hemispheres of well-defined shape and thickness were produced. However, the use of HF limits the shell-making materials to those which are inert to such treatment. As a consequence, materials which are susceptible to dissolution (e.g. nickel, titanium or sliver) have to bear a protective layer.

Bradley *et al.* produced Janus particles via electrodeposition of catalytically active metals (Pd, Au) onto 1-2 μm graphite spheres (see Figure 1-26. for a diagram depicting the procedure).[99] The spheres were spray deposited over cellulose paper sheets in order to form a monolayer. The sheets were then stacked in between two flat graphite electrodes and immersed in a solution of palladium chloride in toluene/acetonitrile. An electric field was then applied and consequently the conductive particles became polarised and the metallic Pd electrodeposited onto the cathodic region of the spheres. After the deposition of the palladium, a solution of gold bromide was introduced, the polarity of the electrodes reversed and a gold layer deposited onto the previously anodic parts of the graphite spheres. The resulting Janus particles were hence not consonant at any given region with their pristine precursors.

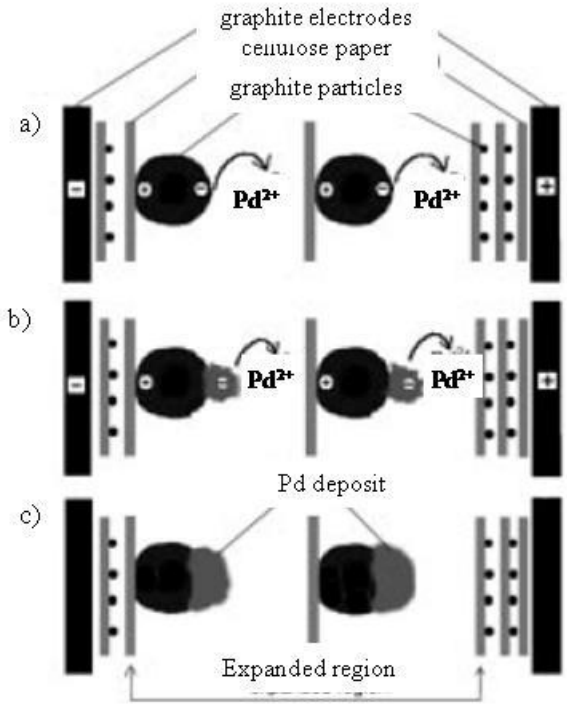

Figure 1-26. A representation of the contactless deposition of palladium metal onto graphite spheres.[99] (a) An electric field generated between the flat graphite electrodes polarizes the spherical graphite particles sandwiched between the electrodes. (b) Palladium metal is electrodeposited onto the cathodic regions of the spheres from the palladium salt solution. (c) Once the electric field is removed, the particles are washed and collected for further use. Image reproduced from Reference 99.

The final method presented in this section, which was developed by Hugonnot *et al.* (see Figure 1-27. for a schematic diagram and sample results), utilises a photochemical deposition process.[100] In this process, silica spheres (10 μm) were immobilized in an acidic hydroalcoholic solution containing $HCrO_4^-$ ions. An argon laser beam, tuned to the excitation wavelength of the hexavalent chromium, was then focused onto the regions of the particles where deposition of $Cr(OH)_3$ was desired. This technique, which can be controlled "in-time" using a microscope, is ideal for high precision coating. It is, however, limited to micron sized and larger objects because of the optical resolution, and allows for very limited yields as the Janus particles are prepared "one-by-one".

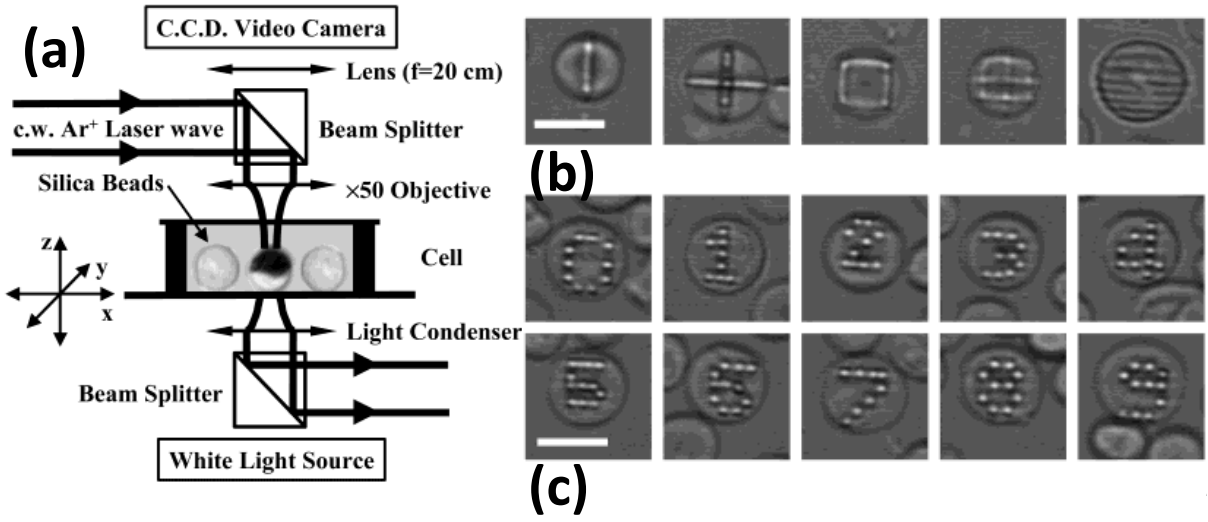

Figure 1-27. (a) Schematic diagram of the experimental setup used in laser-induced photochemical deposition.[100] (b) Pictures show patterns obtained by continuous moving of the laser beam over the silica templates whilst obtaining feedback via optical microscopy. (c) Pictures of the features obtained by computer matrix addressing of (x, y) translation stage, the dot size is approximately 1 μm. The scale bars represent 10 μm. Images reproduced from Reference 100.

1.6.2.3 Surface Modification of Microparticles Using Microcontact Printing

The fabrication of Janus particles produced via microcontact printing (μCP) was first reported by Cayre *et al.*[101] This technique is based on toposelective modification by pressing an elastomer "ink" bearing stamp over monolayers of particles which can be less than 1 μm in diameter (see Figure 1-28.). A monolayer of 9.6 μm negatively charged sulphate latex particles was first prepared by evaporating a latex suspension on a glass slide and a film of water-insoluble cationic octadecyltrimethylammonium bromide (ODTAB) surfactant was deposited over a hydrophilized PDMS stamp. The surfactant monolayer was then stamped over the monolayer and, subsequently, the anisotropically charged colloid particles were introduced into an aqueous dispersion. The Janus character of the particles produced using this technique was proven by using a fluorescent lipid lissamine-rhodamine in the place of ODTAB and visualized by means of fluorescent microscopy. The functionalised portion of the particles was adjusted by partial embedding the particles in a protective glucose film. Cayre *et al.* expanded on this method by printing colloids onto a colloidal monolayer (see Figure 1-28.).[102] The "inks" used in this case were fluorescent quantum dots and carboxyl latex

particles (2.5 μm) and the substrate was a monolayer of aliphatic amine latex particles (9.8 μm). It was rationalised that the interaction between the surfactant molecules as well as the quantum dots, which had a hydrophobic coating, and the latex particle substrate was based on hydrophobic interactions. It was further added that in the case of sulphate latex particles stamped onto the aliphatic amine latex spheres the electrostatic interaction was also aided by a hydrophobic component.

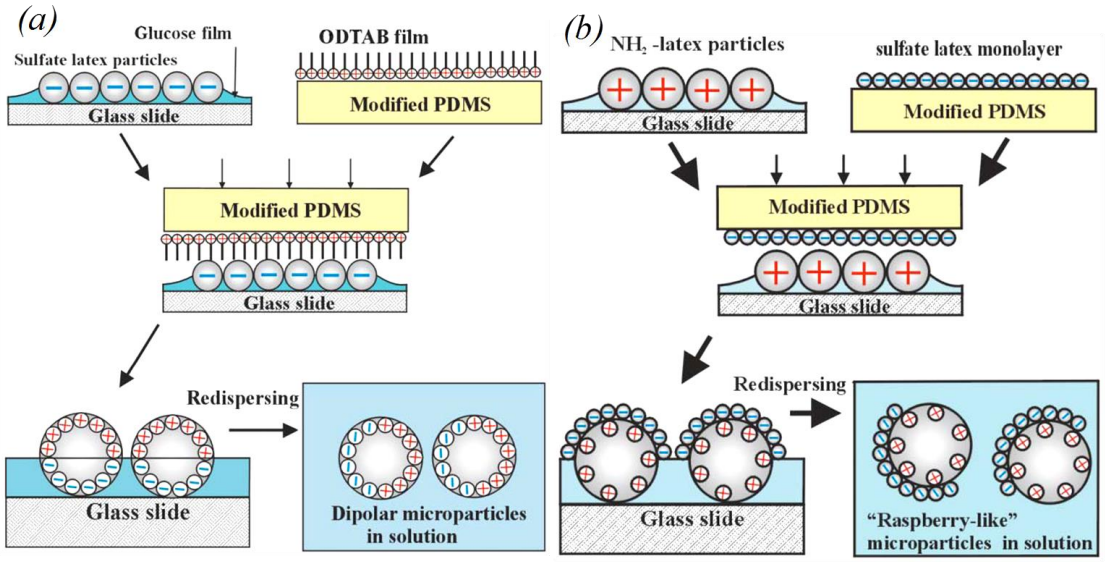

Figure 1-28. Microcontact printing technique as developed by Cayre *et al.*[101, 102] (a) Depicts deposition of the water insoluble ODTAB film over a layer of sulphate particles; (b) illustrates the use of the same process for deposition of "colloids on colloids", in this case sulphate particles over aliphatic amine particles. Images reproduced from Reference 102.

The following two examples of microcontact printing also resulted in colloidal particles stacked on top of each other. Both of them could be classed as indirect: in neither of the cases was the "ink" constituted of particles which would be imprinted onto the substrate particles. Antireflecting surfaces were produced by Koo *et al.* (see Figure 1-29. for a schematic diagram outlaying the procedure): snowman-like nano-structures were produced on a glass substrate and caused gradual variations of the refractive index between the air and the substrate which lead into a dramatic reduction in the light reflected at the glass surface.[103] The second example of stacking colloidal particles on top of each other by μCP was reported by Chen *et al.* who fabricated silver nanoparticle-doped polymer voids which replicated the size and the shape of the

template silica spheres onto which the silver nanoparticles were originally deposited (see Figure 1-28.).[104]

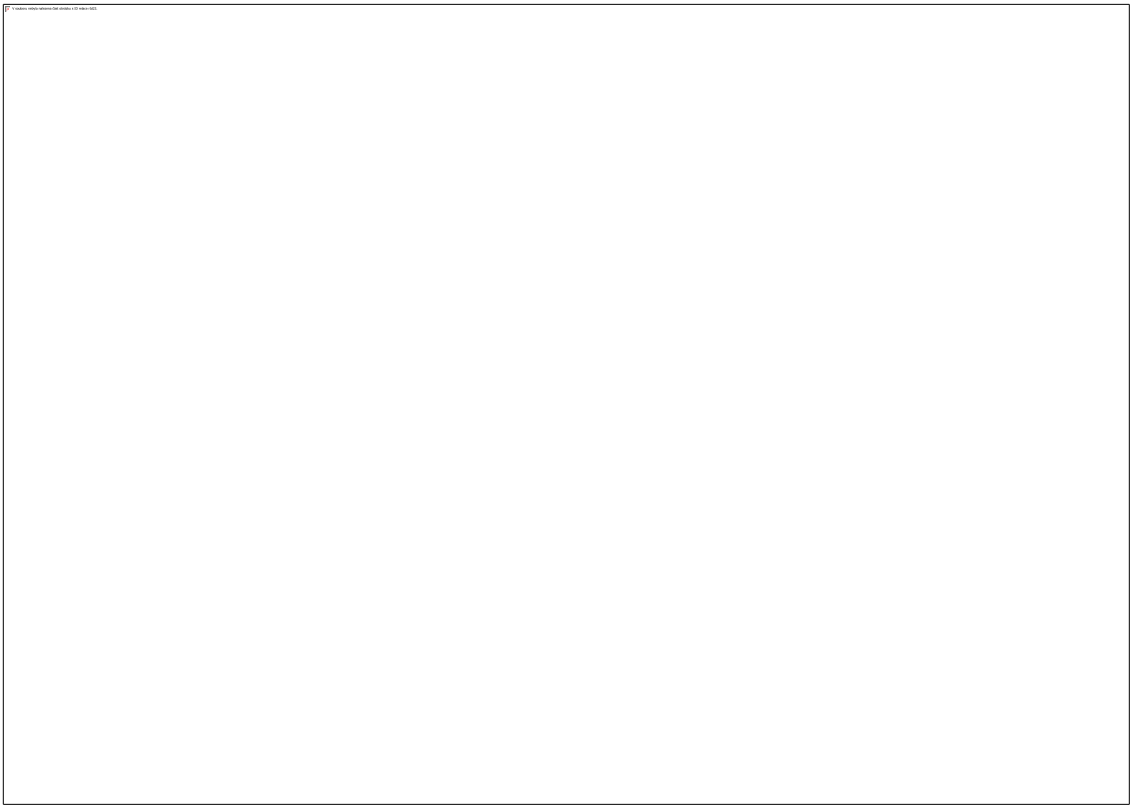

Figure 1-29. Two examples of the production of Janus particles via μCP which use colloidal particles in place of the "ink". (a) Snowman-like particles patterned on a glass surface were produced by the adsorption of negatively charged 100–nm PS latex spheres from a water dispersion onto a glass slide functionalised by a polyelectrolyte multilayer terminated by PAH.[103] The monolayer was then imprinted with a PDMS stamp containing a PAH "ink". A new layer of 50-nm PS latex particles was then allowed to adsorb onto the monolayer organised spheres. (b) Asymmetrically coated 520 nm silica spheres were ordered into a colloidal crystal from which a closely packed silica particle monolayer on a PDMS substrate was produced.[104] Immersion of the silica particles into a silver salt solution and its reduction which resulted in the deposition of silver nanoparticle layer on the exposed portions of the silica spheres followed. The PDMS stamp was then used to transfer the half-coated spheres onto poly(vinyl alcohol) which was heated in order to trap the Janus particles. The silica was then dissolved using aqueous HF thus leaving tightly packed negative replicas on the substrate. Images (a) and (b) are reproduced from Reference 103 and 104, respectively.

Another example of using PDMS stamps for printing with polyelectrolytes was described by Li *et al.*[105] who coated 5.6 μm amine-functionalised latex particles in neutral polymer (polyacrylamide) and a weak polyelectrolyte (poly(acrylic acid)). The particles were then deposited onto a glass slide and a layer of PAH "ink" was imprinted onto the top face of the spheres giving them a Janus character. The researchers subsequently dissolved the latex templates with tetrahydrofuran and produced hollow Janus particles.

1.6.2.4 Surface Modification via Partial Particle Contact with a Reactive Medium

In the last section of the review of fabrication of Janus particles we will consider techniques which involve the arrangement of the precursor particles at an interface between two media where one of the phases alters the surface of the templates and the other, inert in respect to the surface of the particles, effectively shields a portion of the templates. Here, we will also cover methods based on Janus template particles which can be used as superior emulsion stabilizers as described by Velev *et al.*.[106] These techniques were not formally included into the category of modification via partial contact with a reactive medium as described by Perro *et al.*.[86] However, the principle of the two approaches is the same.

Fujimoto *et al.* functionalised negatively charged particles (1.5 μm in diameter) by spreading them on an air/water interface, specifically hydrolyzing the immersed face and subsequently immobilizing human immunoglobulin G on the hydrolyzed face.[107] A variation of this procedure, where the water phase contained positively charged 200 nm particles, resulted in dipolar particles with a raspberry morphology of the functionalised face; the same morphology was also achieved by immobilizing the negatively charged spheres onto a glass substrate followed by immersion of the dispersion of 200 nm polystyrene particles (see Figure 1-30. for a schematic diagram of the method and sample results). Very similar results were reported by Petit *et al.* whereby positively charged amine functionalised silica nanospheres (90 – 120 nm) adsorbed along an air/water interface were functionalised by gold nanoclusters.[108]

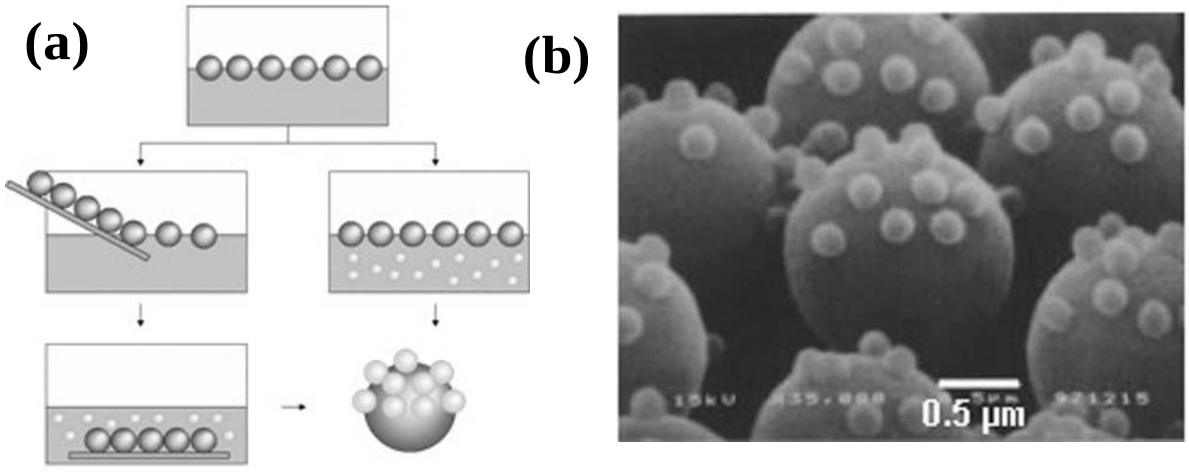

Figure 1-30. (a) A schematic diagram of the preparation of Janus particles by Fujimoto *et al.*[107] The left route depicts the functionalisation of particles arranged along a liquid/solid interface, and the right route show particles adsorbed at an air/water interface being functionalised from the liquid. (b) Raspberry architecture of the modified particles. Images reproduced from reference 107.

The Langmuir-Blodgett trough has also been used in the study of the modification of particle monolayers at air/water and water/solid interfaces. Nakahama *et al.* produced nonsymmetrical amphiphilic 200-nm spheres by depositing a monolayer of hydrophilic amine functionalised polymer particles onto a glass substrate and coating them with a hydrophobic film, made up from fluorine-containing terpolymer, which was produced by spreading and compressing at the air/water interface.[109] Petit *et al.* used the Langmuir-Blodgett trough for concentrating a monolayer of 100 nm silica particles along an air/water interface and functionalised them with 8 - 10 nm gold clusters taking advantage of the affinity of amine groups to colloidal gold.[95] In the same study, a monolayer of the silica particles was deposited onto a glass substrate which was subsequently followed by the immersion of the glass-supported monolayer into the gold nano-cluster dispersion. Both of the approaches employed by Petit *et al.* yielded asymmetrically coated Janus species exhibiting similar raspberry-like architecture as previously reported by Fujimoto *et al.*[107]

Lastly, we will cover a few examples of Janus particle fabrication via so called Pickering emulsions, i.e. emulsions stabilized by particles. Gu *et al.* used ferric oxide (8 nm), FePt (8 nm) and gold nanocrystals (5 nm) for stabilization of oil-in-water emulsions which was then followed by the reduction of silver nitrate dissolved in water

and consequent deposition of silver nuclei onto the stabilizers followed by the seeded growth of one silver particle.[110] Since the report of Gu *et al.* the production of asymmetric particles through Pickering emulsion templates has become increasingly popular as a method of toposelective surface modification because of its versatility in terms of size of the modified particles, superior yields and tunability of the portion of the particles to be functionalised.[111] Hong *et al.* improved this method even further, by using molten paraffin wax in the place of the oil: once the system is cooled and the drops are solidified it is possible to chemically functionalise the "locked" particles, which are incapable of rotation, from the water phase.[111] After the functionalisation, the drops can be dissolved in organic solvent and the untreated face of the particles altered (see Figure 1-31. for an illustrative scheme). The authors of this improvement demonstrated the viability of their suggestion by treating 0.8 and 1.5 μm fused silica with (aminopropyl)triethoxisilane (APS), which rendered the treated faces cationic in character, and/or with *n*-octadecanetrichlorosilane rendering the treated faces hydrophobic. Such "solidified" Pickering emulsions can also be produced by using water-in-oil systems where the aqueous cores can be gelled.[112]

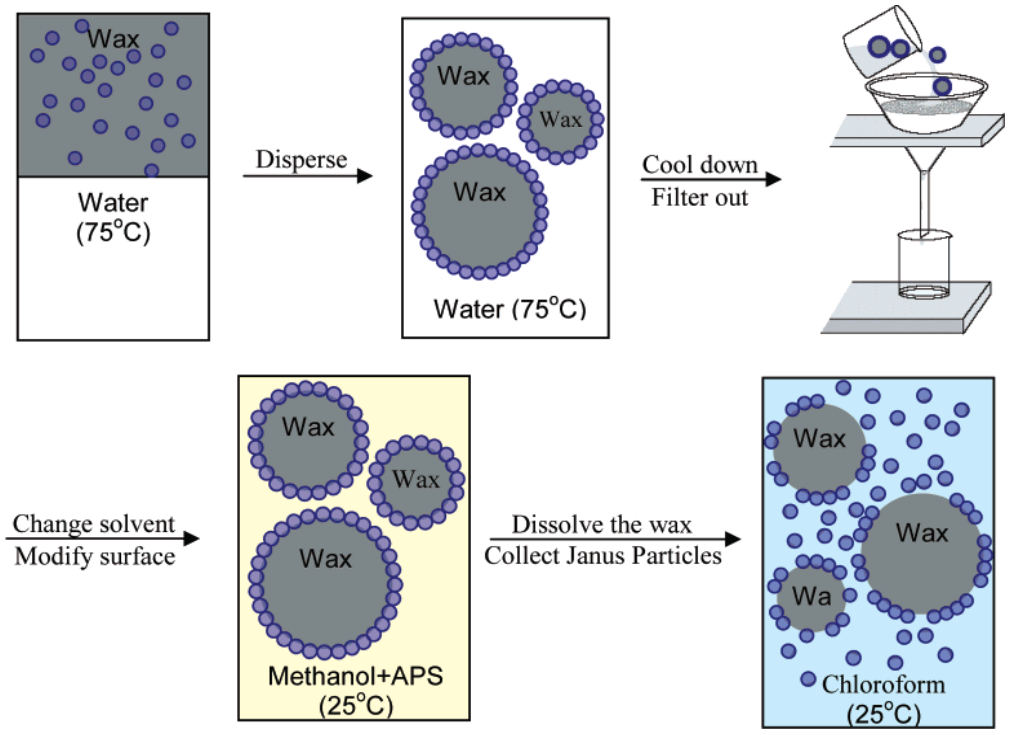

Figure 1-31. An improved method production of Janus particles utilizing colloidosomes formed in a Pickering emulsion as developed by Hong *et al.*[111] Image reproduced from reference 111.

Perro and coworkers used the hot Pickering emulsion of paraffin in water method for modifying silica particles as small as 100 nm.[113] The silica spheres were modified with organosilane-bearing amine groups which allowed for the adsorption of colloidal gold onto the unprotected parts of the spheres. The usefulness of this method in adjusting the penetration depth of the stabilizing particles was demonstrated by introducing various concentrations of sodium dodecyl sulfate (SDS) which acted as a surfactant; increasing the concentration of SDS led to the increasing hydrophobization of the particles and consequent deeper penetration into the wax spheres.

We will finish the review of the Pickering emulsion-assisted functionalisation of particles with an example of the templated production of hemi-shells. Fuchigami and co-workers used 8 μm spherical vaterite calcium carbonate particles to stabilize an emulsion of methyl methacrylate in water together with sodium dodecylbenzenesulfonate (SDBS).[114] Once the emulsion was formed, a catalytic amount of benzoyl peroxide was added to initiate the polymerisation of MMA. After the polymerisation finished a base-activated sol-gel polycondensation of tetraethoxysilane was initiated and the resulting polymeric silica shell was deposited solely on the exposed vaterite surface because of its hydrophilic character which contrasted with the hydrophobic polymethyl methacrylate (PMMA). The empty shells were then prepared by dissolution of the PMMA in acetone and of the template vaterite spheres in 1 N hydrochloric acid.

1.6.3 A Brief Summary of the Deposition Methods

The purpose of the literature review part of the Introduction section was by no means to provide an all-encompassing summary of all the research areas of biomorphic mineralisation and fabrication of Janus particles. In addition to giving a general background on the materials and techniques used in creating shells on model organism templates, here we summarized the methods for partial-surface modification of colloidal particles. However, there are several general points which relate to the overall research project which we can draw.

Viruses as well as bacteria and yeast cells are living organisms which require appropriate treatment – the chemical process to which they are exposed to have to be relatively mild and the conditions such that their integrity is not challenged

mechanically in order to sustain their viability and most importantly their shape.[17] The tobacco mosaic virus, the subject of much research activity, including all of the aforementioned cases on biotemplated core-shell particle fabrication, has been so widely studied because of its exceptional stability. Pristine metals like silver or gold together with metal alloys, metal sulfides and oxides are commonplace within the domain of microorganisms and as such they suggest themselves for being used in microorganism-templated core-shell production.

Whilst there are no reports about alteration of biological templates via the four discussed routes of the anisotropic functionalisation of colloidal particles, there is no reason to doubt that these methods would be suitable for use with microbiological organisms like bacteria or yeast cells as the lower limit of particles used is, in the case of the μCP, below 1 μm and about 100 nm in the case of the remaining three techniques. Each of the approaches has its advantages and disadvantages which have to be considered when making a selection. The oldest method of surface modification of partially masked particles provides very good control, especially the GTT,[90] over the functionalized surfaces but provides relatively low yields and is time consuming in terms of the template preparation (PDMS curing in the GTT takes 24 h). The methods which employ directional fluxes and fields are probably the most rapid but also provide the least control over the thickness and uniformity of the material, and in case of particles under 100 nm in diameter there is also poor control over the coated section, and in the case of the directional fluxes there is a limit of the possible coating materials to those which can undergo physical vapour deposition. The μCP techniques are useful because of the high reproducibility of the products, but are very time-demanding because of the time it takes to prepare the PDMS stamps. The last approach covered which includes techniques which employ partial immersion of the templates into a reactive medium provides probably the best yields whilst keeping a good control over the functionalised portions, however, these techniques are demanding on preparation. The production of negative replicas of viruses will have to be achieved via depositing a shell-making material isotropically over the whole viral template which would then be followed by breaking of the shell and removing the virus as outlined in Figures 1-2.

1.7 Objectives of This Thesis

The goals of this research project can be broken down into the following areas.

- The first goal was to find the appropriate shell-making techniques using model templates such as commercially available latex microspheres or test microorganisms which included common Baker's yeast cells and *Bacillus subtilis* bacterial cells.
- Following this, the next step was to create a model system for the demonstration of the action of the novel anti-pathogenic agents as proposed in the Introduction section. It was important to explore the role in the shape and size recognition in the nanoantibiotic action.
- Finally, we decided to explore the advantages of integration of gold nanoparticles within the structure of the nanonatibiotic particles in order to enhance their action with local heating, through the photothermal effect, and subsequent killing of the target pathogens.

1.8 Presentation of this Thesis

Our experimental work was supplemented by the theoretical examination of the DLVO interactions between the nanoantibiotic particles and the target pathogens. This was important as the DLVO forces were dominant in the model nanoantibiotic-pathoghen systems. The reader can find the results of this work in Chapter 3.

Chapter 4 is dedicated to the summary of the shell fabrication techniques employed. Some of these techniques were then used to fabricate model nanoantibiotics for the purpose of the study of the shape and size in the key-and-lock recognition with test microorganisms and nanoantibiotic systems. Our findings about the specificity of the novel antibiotic agents are presented in Chapter 5.

The experiments which involved the synergistic effects of the combination of the specific nanoantibiotic recognition and their bacteriostatic augmentation via their photothermal capability are summarised in Chapter 6.

The summary of the conclusions and suggestions for future work are described in Chapter 7.

1.9 References

1. S. Kalele, S. W. Gosavi, J. Urban and S. K. Kulkarni, *Current Science.*, 2006, **91**, 1038-1052.
2. F. Guarner and J.-R. Malagelada, *The Lancet*, 2003, **361**, 512-519.
3. Y. Piao, A. Burns, J. Kim, U. Wiesner and T. Hyeon, *Advanced Functional Materials*, 2008, **18**, 3745-3758.
4. F. Caruso, *Advanced Materials.*, 2001, **13**, 11-22.
5. D. Voet, J. G. Voet and C. W. Pratt, John Wiley & Sons, Hoboken, NJ, Editon edn., 2012.
6. L. Pauling, *Journal of the American Chemical Society*, 1940, **62**, 2643-2657.
7. S. Sacanna, W. T. M. Irvine, P. M. Chaikin and D. J. Pine, *Nature*, 2010, **464**, 575-578.
8. S. Sacanna, W. T. M. Irvine, L. Rossi and D. J. Pine, *Soft Matter*, 2011, **7**, 1631-1634.
9. F. L. Dickert and O. Hayden, *Analytical Chemistry*, 2002, **74**, 1302-1306.
10. T. Cohen, J. Starosvetsky, U. Cheruti and R. Armon, *International Journal of Molecular Sciences*, 2010, **11**, 1236-1252.
11. S. Harvey, G. Mong, R. Ozanich, J. McLean, S. Goodwin, N. Valentine and J. Fredrickson, *Analytical and Bioanalytical Chemistry*, 2006, **386**, 211-219.
12. N. Perez, C. Alexander and E. N. Vulfson, in *Techniques and Instrumentation in Analytical Chemistry*, ed. S. Börje, Elsevier, Editon edn., 2000, vol. Volume 23, pp. 295-304.
13. H. Ohshima and K. Furusawa, in *Surfactant science series*, Taylor and Francis, New York, Editon edn., 1998, pp. xiii, 628 p.
14. T. Cosgrove, *Colloid science : principles, methods and applications*, 2nd edn., Wiley, Chichester, West Sussex, 2010.
15. D. J. Shaw, *Introduction to colloid and surface chemistry*, 4th edn., Butterworth-Heinemann, Oxford ; Boston, 1992.
16. G. John, *Journal of Colloid and Interface Science*, 1975, **51**, 44-51.
17. T.-X. Fan, S.-K. Chow and D. Zhang, *Progress in Materials Science*, 2009, **54**, 542-659.
18. M. T. Madigan, J. M. Martinko and T. D. Brock, Pearson Prentice Hall, Upper Saddle River, NJ, Editon edn., 2006, p. p.

19. J. M. M. Walboomers, M. V. Jacobs, M. M. Manos, F. X. Bosch, J. A. Kummer, K. V. Shah, P. J. F. Snijders, J. Peto, C. J. L. M. Meijer and N. Muñoz, *Journal of Pathology*, 1999, **189**, 12-19.
20. R. Glaser, D. A. Padgett, M. L. Litsky, R. A. Baiocchi, E. V. Yang, M. Chen, P.-E. Yeh, N. G. Klimas, G. D. Marshall, T. Whiteside, R. Herberman, J. Kiecolt-Glaser and M. V. Williams, *Brain, Behavior, and Immunity*, 2005, **19**, 91-103.
21. G. F. Brooks, E. Jawetz, J. L. Melnick and E. A. Adelberg, *Jawetz, Melnick, & Adelberg's medical microbiology*, McGraw Hill Medical, New York, 2010.
22. M. T. Madigan, Benjamin Cummings, San Francisco, Editon edn., 2012, pp. xxviii, 1043, 1077 p.
23. A. M. O'Hara and F. Shanahan, *EMBO Rep*, 2006, **7**, 688-693.
24. E. G. Zoetendal, E. E. Vaughan and W. M. De Vos, *Molecular Microbiology*, 2006, **59**, 1639-1650.
25. S. L. Gorbach, *Annals of Medicine*, 1990, **22**, 37-41.
26. S. J. Salminen, M. Gueimonde and E. Isolauri, *The Journal of Nutrition*, 2005, **135**, 1294-1298.
27. S. T. Cole, R. Brosch, J. Parkhill, T. Garnier, C. Churcher, D. Harris, S. V. Gordon, K. Eiglmeier, S. Gas, C. E. Barry Iii, F. Tekaia, K. Badcock, D. Basham, D. Brown, T. Chillingworth, R. Connor, R. Davies, K. Devlin, T. Feltwell, S. Gentles, N. Hamlin, S. Holroyd, T. Hornsby, K. Jagels, A. Krogh, J. McLean, S. Moule, L. Murphy, K. Oliver, J. Osborne, M. A. Quail, M. A. Rajandream, J. Rogers, S. Rutter, K. Seeger, J. Skelton, R. Squares, S. Squares, J. E. Sulston, K. Taylor, S. Whitehead and B. G. Barrell, *Nature*, 1998, **393**, 537-544.
28. O. Lamrabet and M. Drancourt, *Tuberculosis*, 2012, **92**, 365-376.
29. J. W. Wilson, M. J. Schurr, C. L. LeBlanc, R. Ramamurthy, K. L. Buchanan and C. A. Nickerson, *Postgraduate Medical Journal*, 2002, **78**, 216-224.
30. K. Walker, H. Skelton and K. Smith, *Journal of Cutaneous Pathology*, 2002, **29**, 616-618.
31. J. A. Van Burik, *Annual Reviews of Microbiology*, 2001, **55**, 743-772.
32. R. W. Finberg, R. C. Moellering, F. P. Tally, W. A. Craig, G. A. Pankey, E. P. Dellinger, M. A. West, M. Joshi, P. K. Linden, K. V. Rolston, J. C. Rotschafer and M. J. Rybak, *Clinical Infectious Diseases*, 2004, **39**, 1314-1320.

33. C. A. Arias and B. E. Murray, *New England Journal of Medicine*, 2009, **360**, 439-443.
34. M. V. Pirotta and S. M. Garland, *Journal of Clinical Microbiology*, 2006, **44**, 3213-3217.
35. A. Koul, E. Arnoult, N. Lounis, J. Guillemont and K. Andries, *Nature*, 2011, **469**, 483-490.
36. L. C. Kennedy, L. R. Bickford, N. A. Lewinski, A. J. Coughlin, Y. Hu, E. S. Day, J. L. West and R. A. Drezek, *Small*, 2011, **7**, 169-183.
37. X. Huang, P. Jain, I. El-Sayed and M. El-Sayed, *Lasers in Medical Science*, 2008, **23**, 217-228.
38. V. P. Zharov, J.-W. Kim, D. T. Curiel and M. Everts, *Nanomedicine: Nanotechnology, Biology and Medicine*, 2005, **1**, 326-345.
39. L. Hunt, *Gold Bulletin*, 1976, **9**, 134-139.
40. S. Eustis and M. A. El-Sayed, *Chemical Society Reviews*, 2006, **35**, 209-217.
41. S. Link and M. A. El-Sayed, *International Reviews in Physical Chemistry*, 2000, **19**, 409-453.
42. C. M. Pitsillides, E. K. Joe, X. Wei, R. R. Anderson and C. P. Lin, *Biophysical Journal*, 2003, **84**, 4023-4032.
43. C. P. Lin and M. W. Kelly, *Applied Physics Letters*, 1998, **72**, 2800-2802.
44. C. P. Lin, M. W. Kelly, S. A. B. Sibayan, M. A. Latina and R. R. Anderson, *Selected Topics in Quantum Electronics, IEEE Journal of*, 1999, **5**, 963-968.
45. X. Huang, P. K. Jain, I. H. El-Sayed and M. A. El-Sayed, *Photochemistry and Photobiology*, 2006, **82**, 412-417.
46. R. R. Letfullin, C. Joenathan, T. F. George and V. P. Zharov, *Nanomedicine (London, England)*, 2006, **1**, 473-480.
47. D. P. O'Neal, L. R. Hirsch, N. J. Halas, J. D. Payne and J. L. West, *Cancer Letters*, 2004, **209**, 171-176.
48. V. P. Zharov, R. R. Letfullin and E. N. Galitovskaya, *Journal of Physics D: Applied Physics*, 2005, **38**, 2571-2581.
49. V. Saini, V. P. Zharov, C. S. Brazel, D. E. Nikles, D. T. Johnson and M. Everts, *Nanomedicine: Nanotechnology, Biology, and Medicine*, 2006, **2**, 200-206.
50. M. Everts, V. Saini, J. L. Leddon, R. J. Kok, M. Stoff-Khalili, M. A. Preuss, C. L. Millican, G. Perkins, J. M. Brown, H. Bagaria, D. E. Nikles, D. T. Johnson, V. P. Zharov and D. T. Curiel, *Nano Letters*, 2006, **6**, 587-591.

51. V. P. Zharov, J. W. Kim, D. T. Curiel and M. Everts, *Nanomedicine: Nanotechnology, Biology, and Medicine*, 2005, **1**, 326-345.
52. W. C. Huang, P. J. Tsai and Y. C. Chen, *Small*, 2009, **5**, 51-56.
53. S. A. Khan, A. K. Singh, D. Senapati, Z. Fan and P. C. Ray, *Journal of Materials Chemistry*, 2011, **21**, 17705-17709.
54. C. B. Kim, D. K. Yi, P. S. S. Kim, W. Lee and M. J. Kim, *Journal of Nanoscience and Nanotechnology*, 2009, **9**, 2841-2845.
55. R. Sean Norman, J. W. Stone, A. Gole, C. J. Murphy and T. L. Sabo-Attwood, *Nano Letters*, 2008, **8**, 302-306.
56. S. Wang, A. K. Singh, D. Senapati, A. Neely, H. Yu and P. C. Ray, *Chemistry - A European Journal*, 2010, **16**, 5600-5606.
57. V. P. Zharov, K. E. Mercer, E. N. Galitovskaya and M. S. Smeltzer, *Biophysical Journal*, 2006, **90**, 619-627.
58. R. Weissleder, *Nature Biotechnology*, 2001, **19**, 316-317.
59. S. Fields and M. Johnston, *Science*, 2005, **307**, 1885-1886.
60. S. Balci, A. M. Bittner, K. Hahn, C. Scheu, M. Knez, A. Kadri, C. Wege, H. Jeske and K. Kern, *Electrochimica Acta*, 2006, **51**, 6251-6257.
61. M. S. M. Knez, A. M. Bittner, C. Wege, H. Jeske, T. P. Martin, K. Kern,, *Adv. Funct. Mater.*, 2004, **14**, 116-124.
62. E. Dujardin, C. Peet, G. Stubbs, J. N. Culver and S. Mann, *Nano Letters*, 2003, **3**, 413-417.
63. T. Douglas and M. Young, *Nature*, 1998, **393**, 152-155.
64. M. Y. Trevor Douglas, *Advanced Materials*, 1999, **11**, 679-681.
65. E. S. T. Douglas, D. Willits, A. Aitouchen, M. Libera, M. Young,, *Adanced Mateials*, 2002, **14**, 415-418.
66. E. S. Royston, A. D. Brown, M. T. Harris and J. N. Culver, *Journal of Colloid and Interface Science*, 2009, **332**, 402-407.
67. R. R. Naik, S. J. Stringer, G. Agarwal, S. E. Jones and M. O. Stone, *Nature Materials*, 2002, **1**, 169-172.
68. C. E. Flynn, S.-W. Lee, B. R. Peelle and A. M. Belcher, *Acta Mateialia*, 2003, **51**, 5867-5880.
69. S. W. Lee, C. Mao, C. E. Flynn and A. M. Belcher, *Science*, 2002, **296**, 892-895.

70. W. S. C. E. Fowler, G. Stubbs, S. Mann,, *Advanced Materials*, 2001, **13**, 1266-1269.
71. E. Royston, S.-Y. Lee, J. N. Culver and M. T. Harris, *Journal of Colloid and Interface Science*, 2006, **298**, 706-712.
72. R. Y. Sweeney, C. Mao, X. Gao, J. L. Burt, A. M. Belcher, G. Georgiou and B. L. Iverson, *Chemistry & Biology*, 2004, **11**, 1553-1559.
73. S. R. Whaley, D. S. English, E. L. Hu, P. F. Barbara and A. M. Belcher, *Nature*, 2000, **405**, 665-668.
74. B. D. Reiss, C. Mao, D. J. Solis, K. S. Ryan, T. Thomson and A. M. Belcher, *Nano Letters*, 2004, **4**, 1127-1132.
75. T. D. W. Shenton, M. Young, G. Stubbs, S. Mann, *Advanced MAterials*, 999, **11**, 253-256.
76. C. E. Flynn, C. B. Mao, A. Hayhurst, J. L. Williams, G. Georgiou, B. Iverson and A. M. Belcher, *Journal of Materials Chemistry*, 2003, **13**, 2414-2421.
77. H. Zhou, T. Fan, D. Zhang, Q. Guo and H. Ogawa, *Chemistry of Materials*, 2007, **19**, 2144-2146.
78. H. Zhou, T. Fan, T. Han, X. Li, J. Ding, D. Zhang, Q. Guo and H. Ogawa, *Nanotechnology*, 2009, **20**, 085603.
79. H. Zhou, T. Fan and D. Zhang, *Microporous and Mesoporous Materials*, 2007, **100**, 322-327.
80. V. Berry, S. Rangaswamy and R. F. Saraf, *Nano Letters*, 2004, **4**, 939-942.
81. W. S. Kuo, C. M. Wu, Z. S. Yang, S. Y. Chen, C. Y. Chen, C. C. Huang, W. M. Li, C. K. Sun and C. S. Yeh, *Chemical Communications*, 2008, 4430-4432.
82. I. Safarik, L. F. T. Rego, M. Borovska, E. Mosiniewicz-Szablewska, F. Weyda and M. Safarikova, *Enzyme and Microbial Technology*, 2007, **40**, 1551-1556.
83. R. F. Fakhrullin, A. I. Zamaleeva, M. V. Morozov, D. I. Tazetdinova, F. K. Alimova, A. K. Hilmutdinov, R. I. Zhdanov, M. Kahraman and M. Culha, *Langmuir*, 2009, **25**, 4628-4634.
84. B. Holt, R. Lam, F. C. Meldrum, S. D. Stoyanov and V. N. Paunov, *Soft Matter*, 2007, **3**, 188-190.
85. D. Weinzierl, A. Lind and W. Kunz, *Crystal Growth & Design*, 2009, **9**, 2318-2323.
86. A. Perro, S. Reculusa, S. Ravaine, E. B. Bourgeat-Lami and E. Duguet, *Journal of Materials Chemistry*, 2005, **15**, 3745-3760.

87. A. Walther and A. H. E. Muller, *Soft Matter*, 2008, **4**, 663-668.
88. C. Casagrande and M. Veyssie, *Comptes Rendus De L Academie Des Sciences Serie Ii*, 1988, **306**, 1423-1425.
89. Z. N. Bao, L. Chen, M. Weldon, E. Chandross, O. Cherniavskaya, Y. Dai and J. B. H. Tok, *Chemistry of Materials*, 2002, **14**, 24-+.
90. V. N. Paunov and O. J. Cayre, *Adanced Materials*, 2004, **16**, 788-+.
91. V. N. Paunov and O. J. Cayre, in *Nontraditional Approaches to Patterning*, Boston, MA, Editon edn., 2004, pp. 149-151.
92. O. J. Cayre and V. N. Paunov, *Journal of Materials Chemistry*, 2004, **14**, 3300-3302.
93. H. Takei and N. Shimizu, *Langmuir*, 1997, **13**, 1865-1868.
94. M. Himmelhaus and H. Takei, *Sensors and Actuators B: Chemical*, 2000, **63**, 24-30.
95. L. Petit, J.-P. Manaud, C. Mingotaud, S. Ravaine and E. Duguet, *Materials Letters*, 2001, **51**, 478-484.
96. J. R. Howse, R. A. L. Jones, A. J. Ryan, T. Gough, R. Vafabakhsh and R. Golestanian, *Physical Review Letters*, 2007, **99**, 048102.
97. Bajaj Manish G. and Laibinis Paul E., *Molecular Engineering of Biological and Chemical Systems*, 2004.
98. J. C. Love, B. D. Gates, D. B. Wolfe, K. E. Paul and G. M. Whitesides, *Nano Letters*, 2002, **2**, 891-894.
99. Z. M. Jean-Claude Bradley, *Angewandte Chemie International Edition*, 1999, **38**, 1663-1666.
100. E. Hugonnot, A. Carles, M.-H. Delville, P. Panizza and J.-P. Delville, *Langmuir*, 2003, **19**, 226-229.
101. O. Cayre, V. N. Paunov and O. D. Velev, *Chemical Communications*, 2003, 2296-2297.
102. O. Cayre, V. N. Paunov and O. D. Velev, *Journal of Materials Chemistry*, 2003, **13**, 2445-2450.
103. H. Y. Koo, D. K. Yi, S. J. Yoo and D. Y. Kim, *Advanced Materials*, 2004, **16**, 274-+.
104. T. G. Z. M. Chen, X. Yan, X. Li, J. H. Zhang, Y. F. Wang, X. Chen, Z. Q. Sun, K. Zhang, B. Zhao, B. Yang,, *Adv. Mater.*, 2006, **18**, 924-929.

105. Z. Li, D. Lee, M. F. Rubner and R. E. Cohen, *Macromolecules*, 2005, **38**, 7876-7879.
106. O. D. Velev, K. Furusawa and K. Nagayama, *Langmuir*, 1996, **12**, 2385-2391.
107. K. Fujimoto, K. Nakahama, M. Shidara and H. Kawaguchi, *Langmuir*, 1999, **15**, 4630-4635.
108. L. Petit, E. Sellier, E. Duguet, S. Ravaine and C. Mingotaud, *Journal of Materials Chemistry*, 2000, **10**, 253-254.
109. K. Nakahama, H. Kawaguchi and K. Fujimoto, *Langmuir*, 2000, **16**, 7882-7886.
110. H. Gu, Z. Yang, J. Gao, C. K. Chang and B. Xu, *Journal of the American Chemical Society*, 2005, **127**, 34-35.
111. L. Hong, S. Jiang and S. Granick, *Langmuir*, 2006, **22**, 9495-9499.
112. O. J. Cayre, P. F. Noble and V. N. Paunov, *Journal of Materials Chemistry*, 2004, **14**, 3351-3355.
113. A. Perro, F. Meunier, V. Schmitt and S. Ravaine, *Colloids and Surfaces A: Physicochemical and Engineering Aspects*, 2009, **332**, 57-62.
114. Y. T. Kiyomi Fuchigami, Masato Tanaka,, *Polymers for Advanced Technologies*, 2007, **18**, 946-952.
115. M. C. Jamur and C. Oliver, *Immunocytochemical methods and protocols*, 3rd edn., Humana press, New York, 2009.
116. Y. Lu, J. McLellan and Y. Xia, *Langmuir*, 2004, **20**, 3464-3470.
117. M. P. Valkonen, S. Lindroos, T. Kanniainen, M. Leskelä, U. Tapper and E. Kauppinen, *Applied Surface Science*, 1997, **120**, 58-64.
118. S. Lindroos, T. Kanniainen and M. Leskelä, *Materials Research Bulletin*, 1997, **32**, 1631-1636.
119. S. Lindroos, Y. Charreire, D. Bonnin and M. Leskelä, *Materials Research Bulletin*, 1998, **33**, 453-459.
120. G. Laukaitis, S. Lindroos, S. Tamulevicius, M. Leskelä and M. Rackaitis, *Materials Science and Engineering A*, 2000, **288**, 223-230.
121. X. D. Gao, X. M. Li and W. D. Yu, *Thin Solid Films*, 2004, **468**, 43-47.
122. R. S. Mane, B. R. Sankapal and C. D. Lokhande, *Materials Chemistry and Physics*, 2000, **64**, 215-221.
123. V. N. Paunov and O. J. Cayre, Boston, MA, 2003.
124. C. J. van Oss, R. F. Giese, P. M. Bronson, A. Docoslis, P. Edwards and W. T. Ruyechan, *Colloids and Surfaces B: Biointerfaces*, 2003, **30**, 25-36.

125. L. Li, S. Chen, J. Zheng, B. D. Ratner and S. Jiang, *The Journal of Physical Chemistry B*, 2005, **109**, 2934-2941.
126. J. C. Love, L. A. Estroff, J. K. Kriebel, R. G. Nuzzo and G. M. Whitesides, *Chemical Reviews*, 2005, **105**, 1103-1170.
127. I. Inc, *Coupling of Proteins to IDC UltraClean Latex by Passive Adsorption*, http://www.idclatex.com/body_bgrounder_highactivity-protocol-1.asp, Accessed 17/05, 2009.
128. C.-M. Yam, C.-M. Pradier, M. Salmain, P. Marcus and G. Jaouen, *Journal of Colloid and Interface Science*, 2001, **235**, 183-189.
129. J. García-Alonso, R. F. Fakhrullin and V. N. Paunov, *Biosensors and Bioelectronics*, 2010, **25**, 1816-1819.

CHAPTER 2. EXPERIMENTAL

In accordance with the research objectives which are defined in Section 1.7, the research performed included:

- Fabrication of nanoantibiotic particles using commercially available latex microspheres and yeast and bacterial cells as templates as well as targets. The materials used for the imprinting included zinc sulfide (ZnS), gold and silica. Silica nanoshells with integrated gold nanoparticles (AuNP) for the purposes of localised heating via the photothermal effect were also fabricated.
- Fluorescent tagging of the nanoantibiotic particles and their cell targets for the purposes of improved visualization using optical microscopy.
- Functionalization of gold nanoantibiotics and their latex microsphere targets with biotin and streptavidin, respectively, to increase the specificity of the nanoantibiotic recognition.
- Performing various experiments which were designed to examine the role of the shape and size of the target cells in the nanoantibiotic recognition. The laser triggered targeted killing of yeast cells in a mixture of microbial cells via the photothermal effect combined with the cell recognition.

This section contains a description of all the methods and techniques which have been employed to perform the research as outlined above.

2.1 Materials

2.1.1 Solvents

The solvents used for washing the glass slides and other experimental surfaces as well all the other applications included toluene, acetone, isopropanol, ethanol, and methanol (all HPLC Grade, Fischer Scientific).

2.1.2 Water

All the water used was purified by passing through an Elgastat Prima reverse osmosis unit followed by a Millipore Milli-Q reagent water system.

2.1.3 Templates for Fabrication of Target-Cell Specific Nanoantibiotics

The yeast cells used as nanoshell templates were standard Baker's yeast (*S. cerevisiae*) purchased from Tesco in the form of dried cooking yeasts. Before the experimental use, the cells were redispersed in water, washed 3 times with Milli-Q water and separated by centrifugation.

The *Bacillus subtilis* cells were supplied by the teaching labs in the Department of Biology at the University of Hull. The bacteria were first grown in a 20 mL portion in a 150 mL Erlenmeyer flask in growth medium (Oxoid nutrient broth, 25 g; Oxoid yeast extract, 25 g; glucose (Bioreagent grade), 10 g; and dibasic potassium phosphate (ACS grade), 5 g in 1 L of Milli Q water) for 24 h at 30 °C by inoculation from an agar plate. This was followed by transferring 2 mL of the bacterial medium into a 1 L Erlenmeyer flask containing 200 mL of a fresh growth medium and growing only for 12 h in order to harvest the bacteria before they reach the stationary or sporulation phase. The cells were washed twice with Milli Q water by centrifugation (5000 rpm) at 0 °C. All the reagents except for the glucose were purchased from Fisher Scientific, UK. The glucose was purchased from Sigma-Aldrich, UK.

The latex template particles which were used in the directed silica deposition experiments included 3.2 μm aliphatic amine latex particles (4.1 % w/v) and 3, 6 and μm CML latex particles (4 % w/v) and were purchased from IDC Inc (Eugene, USA). The latex microspheres, which were used to prepare the monolayers used in the production the asymmetrically gold coated particles included 2.5 μm carboxyl, 2.9 μm sulphate and 4.1 μm aliphatic amine latex particles, all purchased from IDC Inc (Eugene, USA) (all particle size values are diameters).

2.1.4 Precursors for the Gold Nanoparticle Synthesis

The gold nanoparticles were synthesized from chloroauric acid (99.999% trace metals basis), trisodium citrate dihydrate (≥99%), tannic acid, (ACS reagent) and potassium carbonate (ACS reagent). These were all purchased from Sigma-Aldrich, UK.

2.1.5 Shell Fabrication Precursors

The low melting point agarose (Gelling Temperature 26-30°C, Melting Temperature <65°C for 1.5% solution) used in the gel matrix experiments was purchased from Melford Ltd. (Chelsworth, UK).

The zinc acetate dihydrate ($ZnAc_2$) (ACS reagent, ≥98%), zinc chloride (ACS reagent, ≥97%), sodium sulfide nonahydrate (ACS reagent, ≥98%) and thioacetamide (TAA) (reagent grade, 98%) used in the zinc sulfide deposition onto yeast cell templates were all purchased from Sigma-Aldrich , UK.

The tetraethoxysiliane (TEOS) (ReagentPlus, ≥99%) used in the production of silica coated yeast cells and latex particles was purchased from Sigma-Aldrich UK. The aqueous ammonium hydroxide solution (35%, AR) and the catalysis of the sol-gel process were purchased from Fisher Scientific, UK.

The Piranha solution used for the yeast cell template removal was prepared using sulfuric acid (AR grade, 98%) and hydrogen peroxide (BioReagent, 30%) both of which were purchased from Fisher Scientific, UK.

The PDMS polymer used in the gel trapping technique was prepared using the SYLGARD® 184 Silicone Elastomer Kit from Dow Corning Corporation (MI, USA). Dodecane (purity 99+ %) was purchased from Avocado Research Chemicals Ltd. (Heysham, UK). The aluminium oxide (activated, 0.063-0.200 mm, neutral) used for purification of the dodecane was purchased from Merck Chemicals Ltd. (Nottingham, UK). The urea (analytical reagent grade) used for washing the PDMS polymer was purchased from Fisher Scientific UK.

LUDOX TMA silica nanoparticles (22 nm nominal diameter, E.I. du Pont de Nemours & Co., Inc) were purchased from Sigma-Aldrich.

The gold wire (99.9% metals basis) used for the deposition onto the microsphere monolayers was purchased from Fisher Scientific.

2.1.6 Fluorescent Tagging, Polyelectrolyte Coating and Surface Functionalisation with Biotin and Streptavidin

The cationic polyelectrolyte poly(allylamine hydrochloride) (PAH) (average Mw ~56,000) and the anionic polyelectroyte poly(sodium styrene sulfonate) (PSS) (average Mw ~70,000) used for adjusting the surface charge of the cell templates in the nanoshell deposition experiments and in the silica nanoshell-yeast cell recognition experiments were purchased from Sigma-Aldrich UK. The sodium chloride (AnalaR) used in the polyelectrolyte solutions was purchased from VWR UK.

The 3-aminopropyltriethoxysilane (APTES) (≥99%) used for the amine functionalisation shells before the fluorescent tagging was purchased from Sigma-Aldrich UK. Rhodamine B isothiocyanate (RBITC) (mixed isomers) was purchased from Sigma-Aldrich, UK.

The gold caps were functionalised on the outer surface with thiolated polyethylene glycol (mPEG Thiol, CH_3-O-$(CH_2CH_2O)_6$-CH_2CH_2SH, Plasmachem, Berlin, Germany) and inside with biotin (Biotin-terminated tri(ethylene glycol)undecanethiol, Asemblon, Redmond, USA), used as received.

Streptavidin (affinity purified, lyophilized from 10 mM potassium phosphate, ≥13 units/mg protein) which was used for functionalising the sulphate latex particles was purchased from Sigma-Aldrich UK. The phosphate buffers – sodium phosphate dibasic heptahydrate (purity 98.0-102.0%) and sodium phosphate monobasic monohydrate (purity 98.0 - 102.0%) as well as sodium azide (purity 99%) were purchased from Sigma-Aldrich UK. Glycine (purity > 99%) was purchased from BDH Chemicals Ltd. (Lutterworth, Leicestershire).

2.1.7 Viability Assessment of the Test Microorganisms

The fluorescein diacetate (for cell viability staining) (FDA) used for the assessment of the viability of the test microbial organisms was purchased from Sigma-Aldrich, UK.

2.2 Microscopy Characterisation

2.2.1 Optical Microscopy

The bright field and fluorescence microscopy images were obtained using a BX-51 fluorescence microscope (Olympus, Japan). In the case of fluorescence microscopy, excitation occurred with light from an Hg-arc lamp housed in a U-RFL-T power supply (Olympus, Japan). All filter sets used were manufactured by Olympus. For visualisation of the cells or shells treated with RBITC the MW1BA2 filter set (460–490 nm excitation λ; 510–550 nm emission λ) was used, for the fluorescene-functionalised samples the MW1G2 filter set (520–550 nm excitation λ; 580 nm emission λ) was used; MNUA2 filters (360–370 nm excitation λ; 420–460 nm emission λ) were employed in the case of viewing the of the samples treated with perylene. The cross polar-polar microscopy images of the samples containing zinc sulfide deposits were taken using the same microscope. Digital images were taken using a DP70 camera (Olympus, Japan) and analysed using Image Pro Plus software.

2.2.2 Scanning Electron Microscopy (SEM)

Most of the SEM images were obtained using a Zeiss Evo 60 Scanning Electron Microscope (Zeiss, Germany) by Mr Tony Sinclair. A drop of the sample dispersion was placed onto a clean glass slide. The samples were left to dry at room temperature and stored in a sealed container. A 5 nm thick coating of electrically-conducting gold/palladium was applied onto the samples using an Edwards High Vacuum E12E2 vacuum deposition coating unit. This unit was also used for deposition of the gold and chromium layers in the fabrication of nanoshells which is further described in Section 2.3.5.

The SEM images of the silica shells deposited onto *B. subtilis* templates were taken using Hitachi TM-1000 bench top SEM (Hitachi, Japan).

2.2.3 Transmission Electron Microscopy (TEM)

TEM images contained in the thesis were obtained on a JEOL 2011 TEM (JEOL, Japan) by Mrs Ann Lowry, University of Hull.

2.3 Methods

2.3.1 Fabrication of Gold Nanoparticles

The gold nanoparticles (AuNP) were synthesized as follows.[1] A gold solution was made up from 79 mL of Milli-Q water and 100 μL of 10% chloroauric acid. A reducing solution was made up from 4 mL of 1% freshly prepared aqueous trisodium citrate, 100 μL 1% tannic acid, 0.5 mL 0.025 M potassium carbonate and 19.9 mL of Milli-Q water. These solutions were both heated to 60 °C at which point the reducing solution was added rapidly to the vigorously stirred gold solution. Once the solution turned red, the temperature was raised until boiling and subsequently cooled.

2.3.2 Fabrication of Fragmented Silica Nanoshells

Details of two methods of directed deposition of silica formed via base-catalysed polycondensation of TEOS which were utilised in the process of the research work will be covered in this section. The first technique was performed as described by Weinzierl *et al*., for the fabrication of negative replicas of yeast cells.[2] After examination of the products of this method using SEM (see results section), it was found that some of the silica shells produced using this procedure were disrupted in the process of their preparation, most probably during their washing and drying. This posed a challenge to our original idea of functionalising the outer part of the shell separately, then disrupting the shell and removing the original template and then functionalising the inside of the shells in order to allow for surface chemistry recognition as discussed in the beginning of the Introduction section. It was, however, hypothesised that by functionalising both the inner side and outer side of the shells in a manner which would allow for recognition of their cell targets, the predominant incidence of recognition will be mediated via the inner side of the silica replicas as this allows for maximum contact area of interaction and hence greater energy of interaction (for more details refer to section 2.4.1.2.3). The second technique, which was inspired by the method of Lu *et al.*,[3] opens the possibility of producing silica shells of various sizes using latex microsphere templates in order to study the role of the shape and size of the target particles as outlined in section 1.3.

As mentioned above, both of the experiments are variations of the base-catalyzed polycondensation of TEOS via the sol-gel method. The reaction was catalysed in both cases using ammonium hydroxide. The mechanism of the reaction can be divided into two stages (see Figure 2-1. for the reaction mechanism). The first stage of the sol-gel process involved the base-catalysed hydrolysis reaction of the TEOS, the hydrolysis is then followed by polycondensation which yields the silica polymer. The produced cells were characterised using optical and scanning electron microscopy.

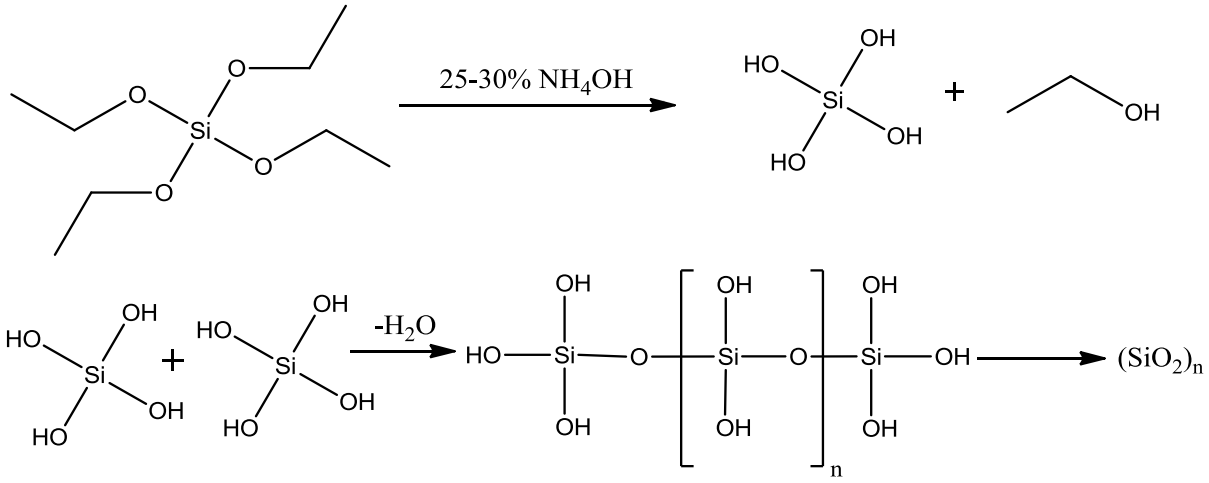

Figure 2-1.The sol – gel process used in our experiments. In the first stage the hydrolysis of TEOS occurs, this is then followed by polycondensation and formation of the silica polymer $(SiO_2)_n$.

2.3.2.1 Fabrication of Silica Nanoshells using Yeast Cells Cores, their Fragmentation and Removal of the Cell Templates

The experimental procedure for the fabrication of silica shells on yeast cells was performed as follows. Approximately 3 g of yeast cells were washed thrice with Milli-Q water by sequential centrifugation at 3000 RPM for 4 min and replacement of the supernatant water (using an Auto Bench Centrifuge Mark IV, Baird & Tatlock, Oldham, UK) then suspended in 6 mL 1:1 methanol:water mixture. This was followed by the addition of 0.5 mL of 25% ammonia as catalyst and 5 mL of TEOS. The suspension was then agitated at room temperature for 2 h. The product was recovered by centrifugation (5 min at 300 RPM) and washed thrice with methanol following two

washing steps with demineralized water. Afterwards, the precipitate was dried overnight at 105 °C. Then, 0.5 g of the core/shell particles were resuspended in water whilst being agitated with a magnetic stirrer. This was followed by agitation using an ultrasonic bath (Grant MXB, Grant Scientific, UK) for 6 min which was found to crack apart the majority of the nanoshells. The water was removed via 5 min centrifugation using the bench-top centrifuge at 3000 RPM and the sediment was exposed to 15 mL of Piranha solution (3:1 concentrated sulfuric acid and hydrogen peroxide) in order to remove the organic templates. The resulting silica nanoshells were washed thrice with water and characterised using optical and scanning electron microscopy.

2.3.2.2 Fabrication of Silica Nanoshells doped with AuNP using Yeast Cells Cores, their Fragmentation and Removal of the Cell Templates

The silica nanoshells with integrated AuNP which were used in the selective killing experiments were synthesized in the same way as the shells in Section 2.3.2.1 except that the yeast cells were precoated with the AuNP synthesized according to the method described in Section 2.3.1. The precoating was performed as follows, 25 mL of the AuNP solution was combined with 25 mL 10 mg mL^{-1} of aqueous poly(allylamine hydrochloride) (PAH), (MW = 1.5 104 Da) and agitated in an ultrasonic bath for 20 min. Next 1.5 g (wet weight) of yeast cells was added to the AuNP/PAH solution and left to incubate whilst shaking for 10 min. This was followed by triple washing through repeated gentle centrifugation and washing with Milli-Q water leaving a pink supernatant solution after the first centrifugation. A pink pellet of the AuNP covered yeast cells was then used for the yeast cell templated silica deposition. The fragmentation and Piranha solution bleaching then left the silica-based nanoantibiotics with AuNP on the inner side of the respective nanoshell.

2.3.2.3 Synthesis of Silica Nanoshells using Latex Microsphere Cores, Shell Fragmentation, and Removal of the Particle Templates

The silica shells on latex microsphere templates were fabricated using an adapted method by Lu *et al.* based on specifically templating aliphatic amine-terminated latex particles.[3] The researchers investigated the effect of the microsphere surface chemistry on the silica deposition, concluding that using aliphatic amine particles led to the synthesis of shells of good uniformity in thickness and coverage, which contrasted with

the results of sulfonate or carboxyl latex microspheres (see Figure 2-2.). It was deduced that this is an effect of the positive charge or neutral charge of these groups under the experimental conditions (pH 10-11.6) in contrast with the negative carboxyl or sulfonate groups which induced uneven coverage. The shells were characterised using optical and scanning electron microscopy.

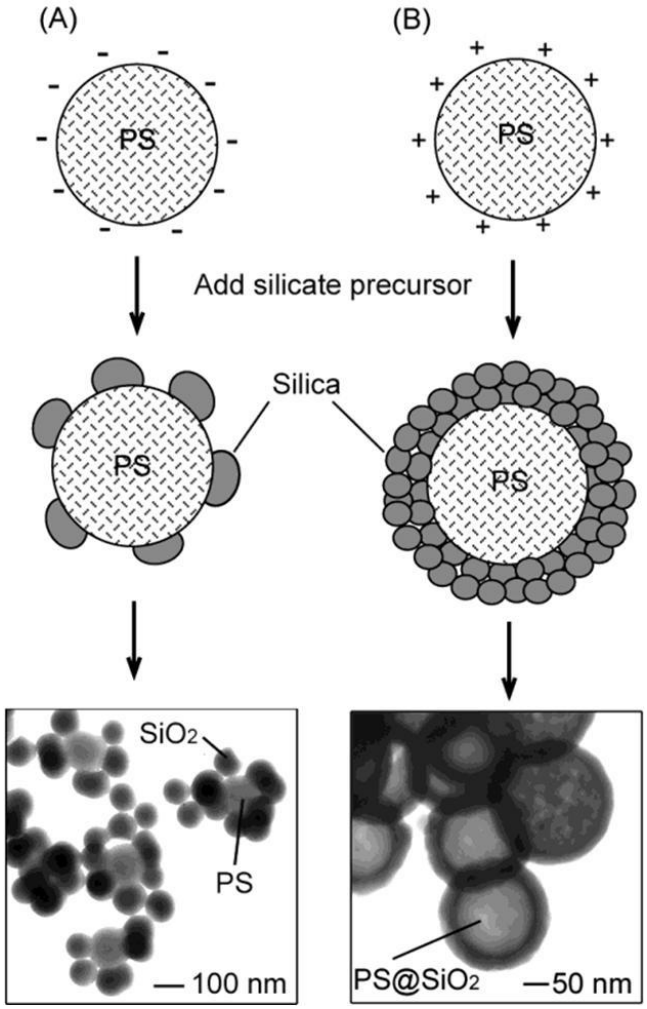

Figure 2-2. The two scenarios of silica deposition depending on the surface charge of the latex microparticle templates.[3] In scenario A sulfonate latex particles bearing negative charge were used and in scenario B positively charged aliphatic amine latex particles were utilized.

In our experiments, 3.2 μm aliphatic amine microspheres and 3, 6 and 10 μm CML-functionalized particles coated in a layer of PAH in the same way as the yeast cells in the previously described experiments, in order to reverse the native negative surface

charge, were used. The procedure was as follows: 0.5 mL of the latex particle dispersion was diluted with 3.5 mL of water and combined with 20 mL of propan-2-ol. The suspension was agitated under magnetic stirring and 0.5 mL of 30% ammonia was added. This was followed by addition of 0.345 mL of TEOS which resulted in a total TEOS concentration of 63 mM. The reaction was left to proceed at room temperature for 3 h. The suspension was centrifuged at 3000 RPM using a centifuge (Auto Bench Centrifuge Mark IV, Baird & Tatlock, Oldham, UK) for 3 min after which the latex particle composites were found to sediment leaving a milky supernatant liquid probably containing small silica particles which was decanted off. The core/shell particles were washed 4 times with isopropanol and 4 times with water. A portion of the resulting suspension was then taken and exposed to agitation in a sonic bath for 6 min. The suspension was centrifuged and washed twice with isopropanol then combined with toluene in order to dissolve the latex templates. This was followed by washing with isopropanol and resuspending in water. For removal of the templates, the silica nanoshells were disrupted via 10-min agitation in an ultrasonic bath (Grant MXB, Grant Scientific, UK) which was following by a double washing with isopropanol and exposure to toluene which dissolved the latex. Another double washing with isopropanol and resuspension in water then followed. The nanoshells were characterised using optical and scanning electron microscopy.

2.3.3 Fabrication of Zinc Sulfide Nanoshells

Here, the techniques which were performed in order to form zinc sulfide shells on yeast cell cores are described.

2.3.3.1 Silar Method

The successive ionic layer adsorption and reaction (Silar) method is a common technique of growing zinc sulphide on substrates such as glass, GaAs, polyester and silica,[4-8] and was therefore investigated for our templates. This approach led to the fabrication of ZnS encapsulated yeast cells. The technique is based on alternating incubations of the cell templates into the zinc cation and sulfide anion solutions interspersed by washing with water; the solutions were 1 – 2 M to 0.5 – 1 M, respectively. This technique allows for ZnS film growth of up to 22 nm per cycle. The

overall chemical reaction occurring in the course of the experiment can be written as follows:

$$ZnCl_2 + Na_2S \rightarrow ZnS\downarrow + 2\ NaCl$$

The yeast cells employed in the experiments were used either in their native state or were pre-treated with a layer of PAH, to render their surface positively charged, or a double layer of PAH and PSS, returning the surface to a negative charge. This was undertaken in order to study the effects of: (i) charge reversal, in the case of the originally slightly negatively charged yeast cells coated with PAH, and (ii) intercalation after both of the polyelectrolyte treatments. The experimental procedure was performed as follows. First, 500 mg of the yeast cells were washed 3 times in water by centrifuging at 2800 RPM for 5 min using a bench-top centrifuge (Auto Bench Centrifuge Mark IV, Baird & Tatlock, Oldham, UK) and replacing the supernatant water with pure Milli-Q water. In the case of using polyelectrolyte-coated cells, sequential 10 min incubation of 500 mg (wet weight) of the yeast cells in 4 mL of the respective polyelectrolyte solution (4 mg/mL dissolved in 0.5 M aqueous solution of sodium chloride), and triple washing with water followed. Special care was taken to ensure high levels of monodispersity of the cells by checking after each redispersion which followed the centrifugation washing steps using feedback from bright field microscopy. Then, 50 mg (wet weight) of the prepared yeast cells were placed into an Eppendorf tube and incubated for 20 s in 2M zinc chloride solution whilst shaking on IKA MS3 shaker. Subsequently, they were washed by centrifuging (15 s at 3300 rpm) using a microcentrifuge (MiniSpin plus, Eppendorf, Germany), redispersed in Milli-Q water using a minishaker (MS 3 digital orbital shaker, IKA, Germany), and centrifuged again. This was followed by incubation in 1M sodium sulfide and washing. This procedure was repeated for the total of up to 10 cycles. The obtained particles were characterised using optical and scanning electron microscopy.

2.3.3.2 Gel Matrix Method

In order to pursue methods which could result in thicker layers of zinc sulfide, resulting in more rigid shells, whilst avoiding aggregation we developed a method which allows for slow release of sulfide ions and hence controlled formation of the shells. The template deposition process of zinc sulfide described in this section utilizes TAA as a

source of sulfide ions which are introduced into the reaction mixture through the dissociation of the TAA, the dissociation is the rate determining step of the zinc sulfide deposition. The aggregation of the core/shell particles during the shell formation process was avoided by immobilising the cell templates in an agarose gel matrix. These experiments were performed without the exposure to sonication as in the work published by Zhou *et al.*,[9-11] which is discussed in Section 1.1.2, which led to disruption of the template cells and the possible formation of "inaccurate" negative replicas. The TAA was left to hydrolyse in water at a constant temperature of 25 °C. The sulphide-generating process can be described as follows.[12]

Thioacetamide can be written as:

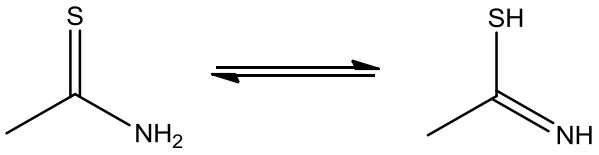

(2-1)

In acidic media, a protonation takes place:

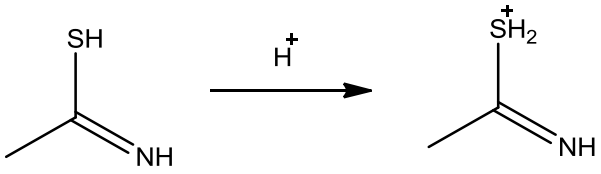

(2-2)

This intermediate compound dissociates to give H_2S as:

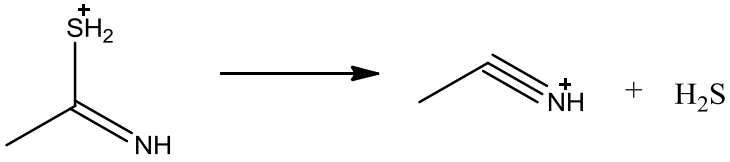

(2-3)

In the aqueous medium, H_2S dissociates as:

$$H_2S + H_2O \leftrightarrow HS^- + H_3O^+, K_1 = 10^{-7}$$

and

$$HS^- + H_2O \leftrightarrow S^{2-} + H_3O^+, K_2 = 10^{-17}$$

The predominant HS^- ions react with the zinc ions introduced into the reaction mixture in the form of zinc acetate to form zinc sulfide:

$$HS^- + Zn^{2+} \leftrightarrow ZnS + H^+$$

The amounts of reagents needed in the ZnS shell fabrication experiments were, unless exact literature methods were followed, always based on a projection of the thickness of the resulting shell. This was done by selecting the target shell thickness, calculating the total mass of the deposited material, number of moles of the deposited materials and from this the volume of the stock reagent solution of given molarity. The seven-step calculation will be demonstrated on the example of the 1 μm ZnS shells deposited onto 100 mg of yeast cell templates using 1 M stock solutions of TAA and $ZnAc_2$.

1. Calculation of the number of template particles. For the purpose of the calculations it was assumed that yeast cell density, $\rho_{\text{yeast cell}}$, is equal to 1050 kg m^{-3} and that the yeast cells can be approximated to a sphere with a radius, r, of 4 μm.

   Volume of one yeast cell: $\frac{4\pi r^3}{3} = \frac{4\pi \times (4 \times 10^{-6} m)^3}{3} = 2.6808 \times 10^{-16} m^3$

   Volume of 100 mg yeast cells:

   Total volume of the yeast cells: $\frac{m(total\ yeast\ cells)}{density\ of\ yeast} = \frac{1 \times 10^{-4} kg}{1050\ kg\ m^{-3}} =$

   $$= 9.5238 \times 10^{-8}\ m^3$$

Total number of the yeast cells: $\frac{Total\ volume}{volume\ of\ 1\ celle} = \frac{9.5238 \times 10^{-8}\ m^3}{2.6808 \times 10^{-16} m^3} =$

$$= 3.5543 \times 10^{8}$$

2. Calculation of the volume the ZnS shell per cell

Volume of a single ZnS shell:

$$\frac{4\pi(r+thickness\ of\ the\ shell)^3}{3} - \frac{4\pi r^3}{3} = 5.2330 \times 10^{-16} m^3 - 2.6808 \times 10^{-16} m^3$$

$$= 2.5552 \times 10^{-16}\ m^3$$

3. Calculation of the total volume of the shells (ZnS):

$$\text{Total number of yeast cells} \times \text{Volume of 1 shell} = 9.0774 \times 10^{-8}\ m^3$$

4. Calculation of the total mass of the shells (ZnS). Density of ZnS is 4090 kg m^3:

$$\text{Total volume of the shells} \times \text{Density (ZnS)} = 3.7126 \times 10^{-4}\ kg$$

$$\cong 0.3713\ g$$

5. Calculation of the number of moles in the shells (ZnS). RMM of ZnS is 97.474 g mol^{-1}:

$$\text{Total mass of the shells} \times \left(\text{RMM (ZnS)}\right)^{-1} = 3.8089 \times 10^{-3}\ moles$$

6. Volume of each 1 M solution (TAA and$ZnAc_2$) needed:

$$\text{Total mass of ZnS shells} \times (\text{Solution molarity})^{-1} = 3.8089 \times 10^{-3}\ L$$

$$\cong 3.81\ mL$$

The experiments were performed at constant concentrations of the reagents (zinc acetate and thioacetamide) at 0.25 M in the reaction mixture. For the gel matrix method, the volumes and amounts of cellular templates were therefore varied in order to obtain 1, 2 and 3 μm thick shells. Amounts of cellular templates had to be adjusted so that the whole reaction mixture fit into the reaction vessels (sample tubes) which had the

capacity of 30 mL and which were of complementary size to the custom-made water jackets. Tables 2-1 and 2-2. summarize the projected experimental conditions.

Table 2-1. Summary of the variables of the ZnS coating experiments. The concentrations of the stock solution of the reagents (zinc acetate and thioacetamide) were 1 M.

Thickness of Shell / μm	Mass of Yeast Cells / mg	Volume of each reagent / mL	Total volume / mL
1	100	3.81	15
2	40	3.80	15
3	40	6.97	28

Table 2-2. Summary of the ZnS shell coating experiments.

Experiment	Electrolyte Coating	Target Thickness / μm
1	PAH	1
2	PAH	2
3	PAH	3
4	PSS	1
5	PSS	2
6	PSS	3
7	Native	1
8	Native	2
9	Native	3

The experimental procedure was as follows. The yeast cells were washed 3 times with Milli-Q water by centrifugation at 3000 RPM for 4 min (Auto Bench Centrifuge Mark IV, Baird & Tatlock, Oldham, UK), then the supernatant water was replaced with pure Milli-Q water. The washing with Milli-Q water was then repeated. In the case of yeast cells coated with polylelectrolytes, incubation of 500 mg (wet weight) of the yeast cells in 5 mL of the respective polylectrolyte solution (4 mg/mL in 0.5 M aqueous NaCl solution) was followed by triple washing with Milli-Q water. Positively charged species were obtained by applying a single layer of PAH. In order to obtain yeast cells coated in an anionic polyelectrolyte, the PAH coated cells were further treated with PSS. Special care was taken to ensure high levels of monodispersity of the coated cells by checking after each redispersion, performed with a minishaker (MS 3 digital orbital shaker, IKA, Germany), using feedback from bright field microscopy.

At the same time, 1 M aqueous solutions of the reagents were prepared. These were divided into portions equal to a quarter of the total reaction mixture volume and placed into a water bath thermostated at 40 °C whilst a portion of 2% solution of low melting point agarose equal to half of the total volume of the reaction mixture was heated in a separate water bath to 80 °C until the agarose was dissolved. Appropriate amounts of the cells were then dispersed in the zinc acetate portions using an IKA Minishaker and added together with the thioacetamide portions to the molten agarose solutions whilst being stirred by a spatula. The reaction vessels were placed into a vacuum desiccator in order to remove air bubbles, cooled under a running water tap until the gel started to set (approximately 1 min), and placed into water jackets heated to 25 °C where the reaction was left to proceed for 24 h.

The yeast cells were then removed from their hydrocolloid matrix by placing portions of the gelled dispersion onto filter paper (Grade 6, pore size 3 μm, Whatman, UK), dissolving the matrix by pouring on boiling water, and simultaneously performing filtration under vacuum. The total volume of boiling water with which each sample was washed was about 0.5 L. The filtrates were white suggesting there was a lot of ZnS which did not precipitate onto the cell surfaces. This ZnS might have formed within the gel, or when the products were washed with the boiling water. The retained filtrands were then further washed with about 200 mL of Milli-Q water, dried under vacuum and redispersed in 15 mL of water by stirring on IKA multistirrer. The ZnS shells were characterised using optical and scanning electron microscopy.

2.3.4 Layer by Layer Encapsulation of Living Cells in Silica Nanoparticles

The cells coated in a multilayer of polyelectrolyte were produced using the protocol reported by Fakhrulin *et al.*[13] The yeast cells, *S. Cerevisiae*, were first washed thrice with milli-Q water by centrifugation at 2000 rpm using a Minispin Plus centrifuge (Eppendorf AG, Hamburg, Germany) in order to remove emulsifiers and nutrients which are present in the commercially available dried yeast, and the polyelectrolytes were dissolved in 0.5 M sodium chloride solution at the concentration of 2 mg/mL. Then, the initially negatively charged yeast cell surface was modified by incubating with the PAH for 10 min, then with PSS, and again by PAH. This procedure should lead to the formation of a uniformly spread positive charge on the yeast cells. Next the cells were stirred in a suspension of negatively charged LUDOX TMA silica particles

for 10 min and removed by sedimentation which was followed by incubation with PAH then PSS, respectively. The cells were washed three times with milli-Q water before each incubation step. The last two layers of polyelectrolyte were intended to prevent the silica particles from desorption. The resulting architecture of polyelectrolyte coating was as follows: PAH/PSS/PAH/LUDOX nanoparticles/PAH/PSS. The coated cells were then imaged using SEM.

2.3.5 Fabrication of Asymmetric Gold Nanoshells

The methods utilised in the production of asymmetrically coated particles involved the toposelective surface modification approach by physical vapour deposition of gold over a monolayer of templates. The coated monolayers were produced using the Gel Trapping Technique (GTT) and the Glass Slide Technique (GST) which were developed and extensively used by Paunov *et al.*[14-20]

The deposition of the gold layer over the monolayer of templates was always done after deposition of an underlayer of chromium. The chromium layer was employed for its comparative strength and also its brittleness which aids in the release and the separation of the individual gold nanoshells. Initially, when the method was tested, the metal capping consisted of a 10 nm layer of chromium and 50 nm of gold which was later reduced to 40 nm because the use of the thicker layer generated sheets of gold caps rather than separate negative replicas. The metal layer thickness was controlled by programming the sputterer. For the purposes of the production of caps which were to be functionalised an additional gold layer under the chromium coating was used. This sandwich-like triple coating was used in order to ensure the functionalisation of the gold on both sides via self-assembled monolayers of thiolates. The thickness of the chromium layer was kept constant at 20 nm whilst the gold layers were tested at thicknesses of 5 nm for both layers, then 10 nm for both layers. The particle monolayers produced by the two methods were characterized via both bright field optical microscopy and via scanning electron microscopy.

2.3.5.1 Preparation of a Particulate Monolayer via Gel Trapping Technique

The masking/unmasking approach of creating partially shelled particles represented by the Gel Trapping Technique (GTT) followed the procedures outlined by Paunov and Cayre (see Figure 1-27. in section 1.6.2.3 for a schematic diagram) with a small

modification.[19] First, the water phase was prepared by the dissolution of low melting point agarose in water heated above 50 °C followed by degassing via centrifugation at 3000 rpm for 1 min using a bench-top centrifuge (Auto Bench Centrifuge Mark IV, Baird & Tatlock, Oldham, UK). This was then poured into a plastic Petri dish. It should be noted that this step contains the only deviation from the reported method – agarose, a non-ionic gelling agent, was used in the place of the originally used gellan which is anionic and may interact with the positively charged amine particles. In a separate experiment we used an oil/water interface instead of air/water in order to produce trapped particles with a different contact angle and hence control the shape of the corresponding gold caps produced by the GTT. The oil/water interface was produced by the addition of dodecane which was purified on an alumina column, degassed via centrifugation, and preheated in order to avoid cooling of the water with the agarose solution. The monolayer was then gently deposited by spreading an isopropanoic dispersion of the template particles at the air-water or water-oil interface using a microsyringe. After approximately 1 h of cooling at room temperature the water-phase had gelled and the optional oil layer was removed. This was followed by spreading of the PDMS oil, mixed with the curing agent in 10:1 ratio, over the solid gelled surface. After 48 h of curing, the PDMS was peeled off and the PDMS surface with the embedded monolayer was washed in 8 M urea solution and rinsed with hot (90 °C) water in order to remove the agarose residues.

2.3.5.2 Preparation of a Particle Monolayer via the Glass Slide Technique

The Glass Slide Technique (GST) is a method for rapid preparation of very concentrated microparticle monolayers which can optionally incorporate a protective layer of glucose, the procedure was described by Cayre *et al.* (see Figure 2-3. for a schematic diagram).[14] First, a dispersion of microparticles in isopropanol (approximately 0.0006 wt%) was produced. In the following step, a few drops of the suspension were spread over a clean glass slide and the isopropanol left to evaporate. Finally, a drop of water was deposited onto one end of the glass slide and slid over the surface whilst raising the particles and carrying them over to the other end, in effect concentrating the monolayer. The glass slides were washed with toluene, acetone, Milli Q water and isopropanol, sequentially, before being dried by wiping with polyester/cellulose wipes. Rigorous care of manipulating the particles with nitrile

gloves was taken in order to prevent the detachment of the gold particles from the substrate during the washing steps.

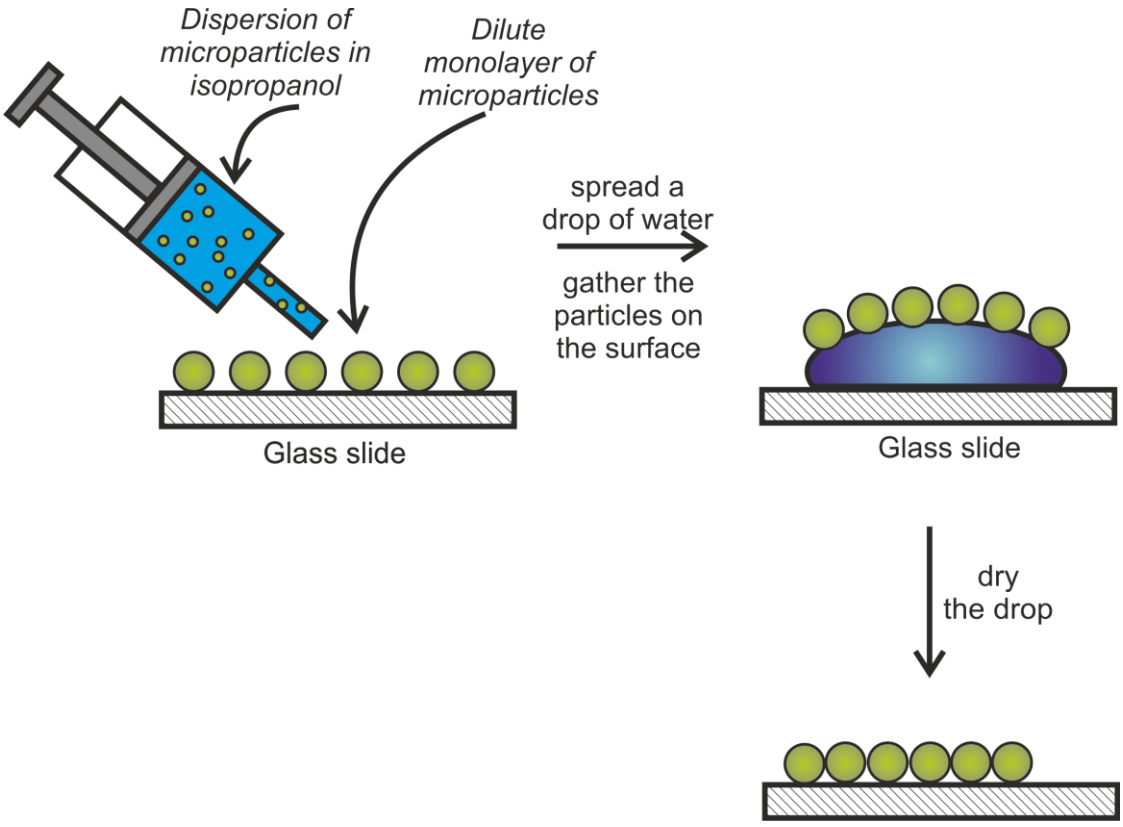

Figure 2-3 The principle of the GST. A microparticle dispersion in isopropanol is spread onto a glass slide After the evaporating of the solvent a concentrated particle monolayer is formed with a sliding water drop.

As mentioned above, the water drop may contain an added amount of glucose in order to create a protective layer.

2.3.5.3 Extraction of the Hemi-shells Produced via the Asymmetric Nanoshell Deposition

The metal coating deposited over the monolayers of particles produced via the GTT and GST was removed via either scraping using a scalpel blade which was wetted with a drop of ethanol or by applying a sticky tape onto the metal-coated PDMS or glass surface which was then lifted together with the tape (see Figure 2-4. for a diagram depicting the gold cap lifting procedure using a sticky tape). Then, either the scraped particles or the particles stuck on the sticky tape were immersed in toluene in order to dissolve the latex templates and the glue of the tape. Subsequently, in the case of the

sticky tape method, the tape was removed and the gold caps were further washed five times in toluene, then five times in ethanol and finally five times in Milli-Q water. These particles were collected from the washing liquid with a syringe filter (Anodisc 25, 1 μm, Whatman). The gold caps had to be gently redispersed by means of gentle sonication in the ultrasonic bath (F5300b, Decon Ltd., Hove, UK) for approximately 15 s because it was observed that they were aggregating in this solvent. The caps extracted by the above described methods were imaged by electron microscopy.

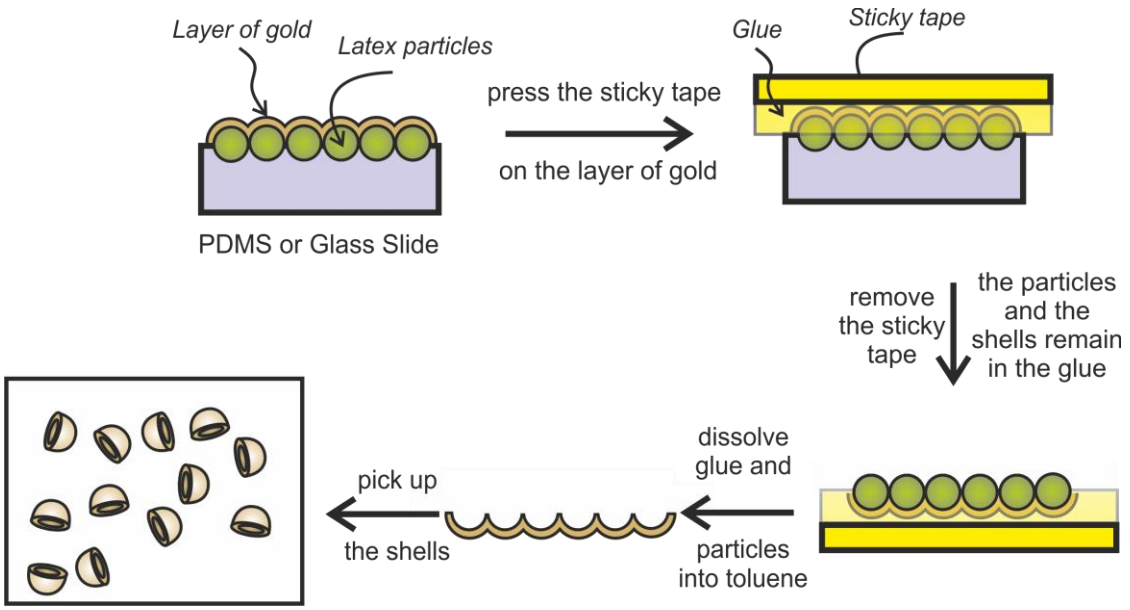

Figure 2-4. A diagram depicting the sticky tape procedure for gold cap removal. The sticky tape was first applied onto the metal film which was followed by the removal of the tape together with metal film and the dissolution of the tape glue and the latex particles in toluene.

2.3.6 Recognition Experiments of Silica Shell Nanoantibiotics and their Matching Yeast Cells

As mentioned previously in the thesis, some of the nanoshells produced using the technique of Weinzierl *et al.* had their integrity disturbed.[2] This circumstance did not allow us to separately functionalise the outer part and the inner part of the shells. It was therefore decided that the silica shells, after their further disruption via agitation in an ultrasonic bath and removal of the cellular templates using Piranha solution, will be treated identically on both the inner and outer sides in order to allow for recognition of

their yeast cell counterparts. The recognition interaction was based on a combination of electrostatic interactions and due to the shape of the shells it was expected that the interaction would occur predominantly via the inner side of the shells as a larger surface area would be in contact and hence the energy of interaction of the cell and the nanoantibiotic would be higher.

For the better evaluation of the results of recognition we decided to fluorescently tag the two counterparts. The cells were incubated in a 10^{-4} M ethanolic solution of perylene (about 0.5g of cells in 10 mL of the solution) for 10 min after being redispersed in water then used further. In the case of silica a slightly more complex method was selected. In order to tag the silica nanoshells with Rhodamine B isothiocyanate (RBITC) the shells were first functionalised with a monolayer of aminopropylsilane providing them with primary amine functionality which would then allow for the formation of a covalent bond with the isothiocyanate group on the fluorescent molecule (see Figure 2-5. for a reaction scheme). The fluorescent tagging of the silica shells was performed as follows. About 0.5 g of the nanoshell fragments were washed once in methanol and once in toluene before being resuspended in 10 mL of 10% APTES in toluene solution and incubated whilst being agitated by stirring on a magnetic stirrer plate for 1 h, this was followed by a triple washing with methanol and a 3 h incubation in 1 mM solution of RBITC in methanol, further triple washing with methanol, triple washing in water and redispersion in 20 mL of water. The polyelectrolyte coating of the negative silica replicas and the yeast cells was performed as in the previous experiments – that is, incubation in the respective polyelectrolyte solution (PAH or PSS, 4 mg/ml in 0.5 M NaCl solution) for 10 min followed by a triple washing with the water. The surface charge of the fluorescently tagged silica nanoshells was unclear – the surface might have consisted of a mixture of negatively charged silanol groups which are native to untreated silica and positively charged amine groups stemming from the treatment with APTES. The RBITC itself contains a positively charged quaternary amine and a zwitterionic pair of a tertiary amine and a carboxyl group. For this reason a set of 15 experiments were undertaken with all combination of yeast cells and silica nanoshell fragments treated in various ways. Yeast cells used were: (i) untreated with polyelectrolytes, (ii) treated with a monolayer of PAH, or (iii) with a double layer of PAH and PSS. The silica fragments were: (i) untreated, (ii) treated with monolayers of

either PAH or PSS, or (iii) treated with a double layer with the initial coating being either of PAH or PSS. Table 2-3. summarizes the experiments performed.

The recognition experiments themselves were performed in the following fashion. The silica nanoshell dispersion (0.025 g/mL) was added drop-wise to the dispersions of the yeast cells (0.1 g/ mL) whilst the latter was being agitated on an IKA minishaker in a 2:1 ratio (typically 0.2:0.1 mL), the combined dispersions were then left for 1 h whilst being agitated on an orbital shaker (Vibrax VXR basic, IKA, Germany) at a frequency of 1500 min^{-1}. The samples were then imaged by optical and fluorescence microscopy.

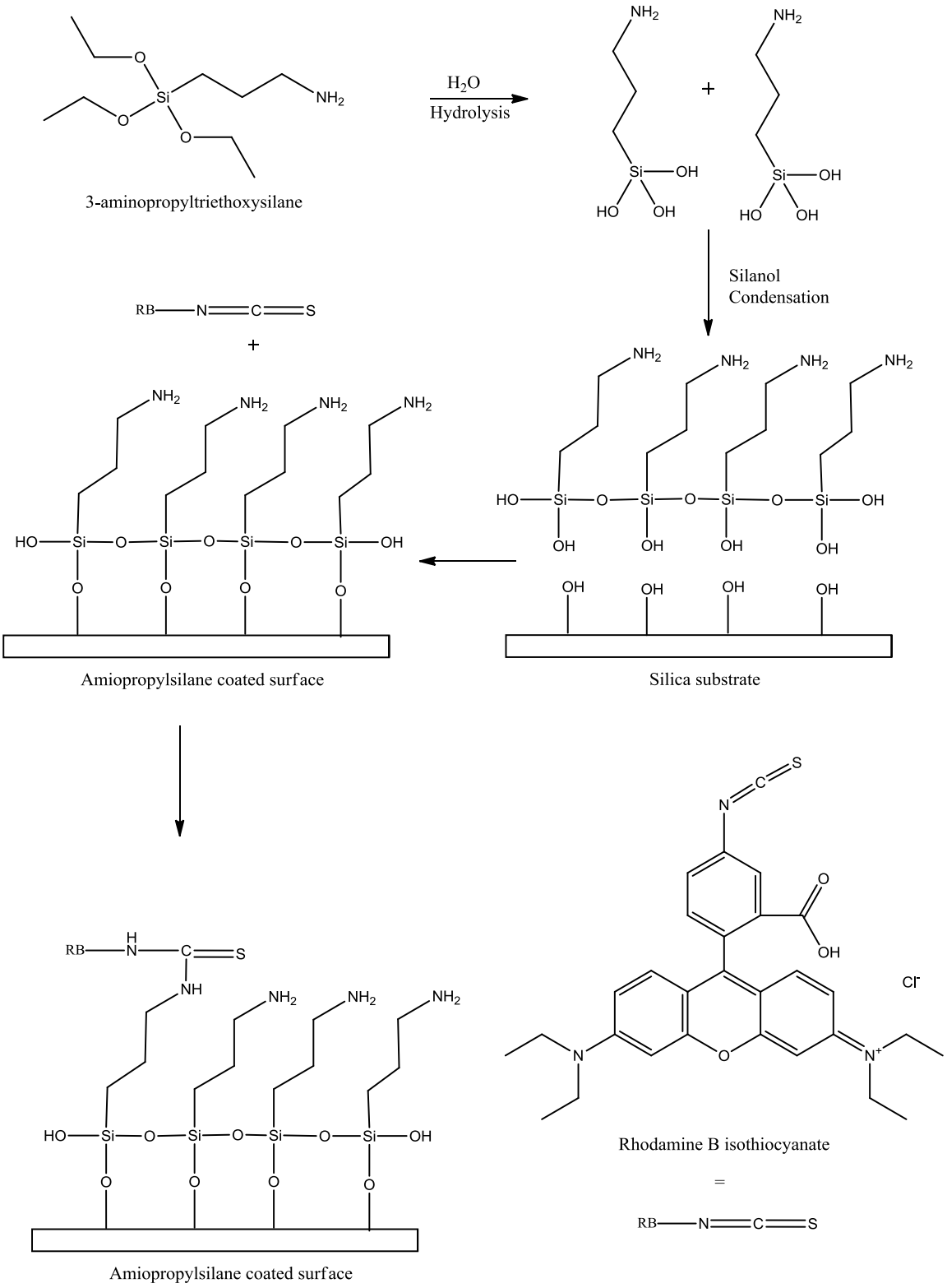

Figure 2-5. Reaction scheme depicting the tagging process of the silica shells with RBITC mediated via amine functionalisation of the shells with APTES. RB = Rhodamine B.

Table 2-3. Summary of the cell-shell recognition experiments.

Experiment	Cell treatment	Shell Treatment
1	-	-
2	PAH	-
3	PAH-PSS	-
4	-	PAH
5	PAH	PAH
6	PAH-PSS	PAH
7	-	PAH-PSS
8	PAH	PAH-PSS
9	PAH-PSS	PAH-PSS
10	-	PSS
11	PAH	PSS
12	PAH-PSS	PSS
13	-	PSS-PAH
14	PAH	PSS-PAH
15	PAH-PSS	PSS-PAH

2.3.7 Recognition Experiments of Silica Shell Nanoantibiotics and their Yeast Cells

The negative silica replicas which were fabricated according to the method in Section 2.3.2.3 were then fluorescently tagged with RBITC using the method in Section 2.3.6 prior to the experiments which were designed to evaluate the importance of size and shape in the nanoantibiotic-cell recognition as discussed in Chapter 5. The recognition experiments were performed as follows. The shells originating from 0.5 mL of the latex 6 μm microsphere templates were combined with 50 μl of the 6 μm CML latex particles and were left on bench top shaker at 1200 min^{-1} for 20 min. In the case of the recognition experiments involving the mixture of differently sized latex microspheres (see Section 2.3.1) and the 6 μm silica nanoshells , 1/3 of 50 μL of each latex suspension was used. The recognition was subsequently evaluated using bright field and fluoresce microscopy.

2.3.8 Recognition Experiments between Gold Nanoantibiotic Particles and Their Latex Microsphere Targets Functionalised by Biotin and Streptavidin

The principle of the antibody and antigen interaction was demonstrated using biotin-functionalised gold caps and streptavidin-functionalised latex particles matching the caps. Streptavidin is a protein which is used widely in molecular biology because of its very specific irreversible adsorption to biotin (also known as vitamin H or B_7).[21] In order to ensure that the particles will attach to the caps from the inside only, the outer cap site was treated with polyethylene glycol (PEG) before dissolving the latex particles. Grafting of PEGs to a surface is a common strategy of rendering those surfaces resistant to protein adsorption.[22] Both in the case of PEG as well as biotin, thiol derivatives were used as the grafting agents.

The gold caps employed were produced mostly via the glass slide method. The GTT technique was found to be much too time consuming (PDMS takes 48 h to cure). The overall process is described in Figure 2-6.

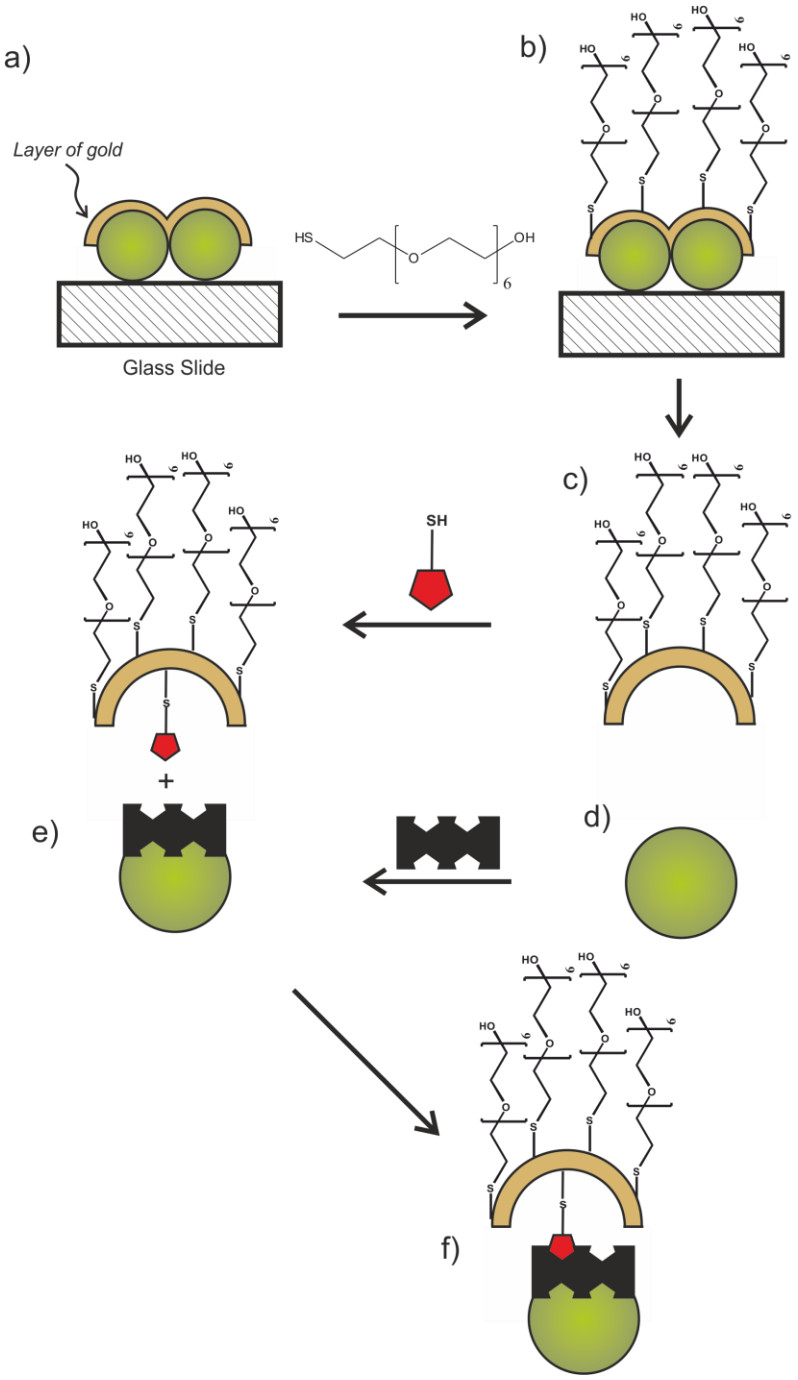

Figure 2-6. Model scheme for the novel class of nanoantibiotics. (a) The gold layer deposited onto a particle monolayer is treated with PEG-thiol in order to obtain (b) a self-assembled protective layer. The gold layer and the particles are then removed and the latex is dissolved into toluene in order to obtain (c) gold caps which can only bind to thiolated biotin from the inner side. (d) Streptavidin binds to the latex particles. (e) Specific binding of streptavidin to biotin demonstrates antigen-antibody interaction (f).

2.3.8.1 Functionalisation of Gold-Based Nanoshells

After the thermal evaporation deposition of the metal layers over the monolayer of 2.9 μm sulphate latex particles, the sample was placed into 1 mM solution of PEG-thiol in 95% ethanol/5% water solution and left to incubate for 24 h. Literature suggests that such a procedure allows for the formation of a dense protective monolayer of PEG.[22] It was followed by removal of the gold layer using either the sticky-tape method or scraping method followed by dissolution of the latex particles using toluene. After the particles had been dissolved, the gold caps were washed from the toluene using ethanol and milli-Q water, and separated by means of a gentle agitation. Thiolated biotin was bound to the inner side of the newly formed gold caps by placing the particles into 1 mM 95% ethanol/5% water solution of thiolated biotin for approximately 30 min. Such a short incubation time was used in order to prevent the displacement of some of the PEG molecules on the top side of the caps by the biotin as reported by Love *et al.*[23]

2.3.8.2 Functionalisation of Latex Particles with Streptavidin

Streptavidin was adsorbed to the surface of the "antigen" sulphate latex particles by the means of hydrophobic interactions according to the protocol published by the latex manufacturer, IDC Inc.[24] Briefly, 50 mg of the sulphate latex particles was stirred with 0.86 mg of streptavidin in a sodium phosphate buffer solution at a pH close to streptavidin's isoelectric point of pH 5-6 for two h in order to ensure hydrophobic adsorption.[25] The quantities were calculated using the following formula given in the IDC protocol:

$$\text{Weight of Ab} = \frac{\text{Weight of Ab for 1}\mu\text{m particle}}{\text{particle diameter in }\mu\text{m}}$$

where Ab is the antibody used, in this case streptavidin, and the weight of Ab for 1 μm particle is 5 mg. Using this relationship gives an amount corresponding to 200% of the protein required to form a monolayer on the latex particles. The particles were separated using centrifugation and washed with phosphate buffer solution adjusted to pH 7.2 in order to obtain dispersion without free streptavidin. The protein functionalised latex spheres were stored in a phosphate buffer adjusted to pH 7.2 which contained 0.1% w/v of glycine and 0.1% of sodium azide to keep the dispersion in sterile conditions. The only alteration to the IDC protocol was in the choice of the buffer solutions where it

was suggested to use phosphate buffered saline and 2-(*N*-morpholino)ethanesulfonic acid buffer for washing and storage. Instead phosphate buffers at the same pH were used.

2.3.8.3 Incubation of the Latex Microspheres and the Nanoantibiotics

The latex particle "antigens" were matched with the biotinylated cap "antibodies" by addition of the caps to the buffered latex dispersion whilst stirring. Testing for the specific "pathogen" – "nanoantibiotic" recognition was initially checked by the means of scanning electron microscopy and, also, by treating the latex particles with Nile Red fluorescent dye prior the attachment of streptavidin and checking the results via conventional bright field and fluorescent microscopy. The Nile Red treatment was performed by incubating of the latex spheres in 10^{-5} M ethanoic solution of Nile Red followed by washing with milli-Q water.

2.3.9 Selective Cell Killing with Photothermal Effect

The selective killing experiments which are discussed in Chapter 6 of this thesis were performed as follows. The silica nanoantibiotic particles doped with AuNP, which fabricated according to the method described in Section 2.3.2.2, were fluorescently tagged with Rhodamine B isothiocyanate (RBITC) in order to enable the convenient identification of the recognition events between the target test microorganisms and their negative replicas as described in Section 2.3.6.

Fresh yeast cells and living bacteria were each washed with water and gently centrifuged to produce a pellet. Then about 0.02 g wet weight of each of the microorganism pellets were redispersed in 5 mL water to which the sediment of 10 mL of the nanoantibiotic dispersion was added. The model multimicrobial – nanoantibiotic system was than agitated by shaking for about 10 min. The model system was placed in a cylindrical custom-made glass cuvette that has an internal diameter of 2 mm and a length of 2 cm. The sample was irradiated using a Nd:YVO4 micro-laser (Advanced Optical Technology) that emitting at a wavelength of 532 nm, pulse duration of 2 ns full width half maximum (FWHM) and a pulse energy of 10 mJ set at a pulse repetition frequency of 20 kHz. The experiments which involved only one of the test microorganisms were performed using half of the volume of nanoantibiotic suspension. The nanoantibiotic suspension was replaced with Milli-Q water in the control

experiments where no nanoantibiotics were required. The results were evaluated using optical and fluorescent microscopy.

2.3.10 Viability Assessment of the Test Microorganisms

The viability of the microorganisms was checked via FDA staining and subsequent fluorescence microscopy observations according to the protocol of Fakhrullin *et al*.[26] A stock solution of FDA in acetone at the concentration of 10 mg mL^{-1} was prepared and an aliquot (10 μL) of this solution added to 0.49 mL of water. The microbial cells were then suspended in the aqueous FDA solution and incubated for 20 min while shaking, triple washing with water assisted by centrifugation then followed. Next, the cells were examined by fluorescence microscopy.

2.4 References

1. M. C. Jamur and C. Oliver, *Immunocytochemical methods and protocols*, 3rd edn., Humana press, New York, 2009.
2. D. Weinzierl, A. Lind and W. Kunz, *Crystal Growth & Design*, 2009, **9**, 2318.
3. Y. Lu, J. McLellan and Y. Xia, *Langmuir*, 2004, **20**, 3464.
4. M. P. Valkonen, S. Lindroos, T. Kanniainen, M. Leskelä, U. Tapper and E. Kauppinen, *Applied Surface Science*, 1997, **120**, 58.
5. S. Lindroos, T. Kanniainen and M. Leskelä, *Materials Research Bulletin*, 1997, **32**, 1631.
6. S. Lindroos, Y. Charreire, D. Bonnin and M. Leskelä, *Materials Research Bulletin*, 1998, **33**, 453.
7. G. Laukaitis, S. Lindroos, S. Tamulevicius, M. Leskelä and M. Rackaitis, *Materials Science and Engineering A*, 2000, **288**, 223.
8. X. D. Gao, X. M. Li and W. D. Yu, *Thin Solid Films*, 2004, **468**, 43.
9. H. Zhou, T. Fan, T. Han, X. Li, J. Ding, D. Zhang, Q. Guo and H. Ogawa, *Nanotechnology*, 2009, **20**, 085603.
10. H. Zhou, T. Fan and D. Zhang, *Microporous and Mesoporous Materials*, 2007, **100**, 322.
11. H. Zhou, T. Fan, D. Zhang, Q. Guo and H. Ogawa, *Chemistry of Materials*, 2007, **19**, 2144.
12. R. S. Mane, B. R. Sankapal and C. D. Lokhande, *Materials Chemistry and Physics*, 2000, **64**, 215.
13. R. F. Fakhrullin, A. I. Zamaleeva, M. V. Morozov, D. I. Tazetdinova, F. K. Alimova, A. K. Hilmutdinov, R. I. Zhdanov, M. Kahraman and M. Culha, *Langmuir*, 2009, **25**, 4628.
14. O. Cayre, V. N. Paunov and O. D. Velev, *Journal of Materials Chemistry*, 2003, **13**, 2445.
15. O. Cayre, V. N. Paunov and O. D. Velev, *Chemical Communications*, 2003, 2296.
16. O. J. Cayre, P. F. Noble and V. N. Paunov, *Journal of Materials Chemistry*, 2004, **14**, 3351.

17. O. J. Cayre and V. N. Paunov, *Journal of Materials Chemistry*, 2004, **14**, 3300.
18. V. N. Paunov and O. J. Cayre, Boston, MA, 2003.
19. V. N. Paunov and O. J. Cayre, *Advanced Materials*, 2004, **16**, 788.
20. V. N. Paunov and O. J. Cayre, in *Nontraditional Approaches to Patterning*, Boston, MA, Editon edn., 2004, pp. 149.
21. C. J. van Oss, R. F. Giese, P. M. Bronson, A. Docoslis, P. Edwards and W. T. Ruyechan, *Colloids and Surfaces B: Biointerfaces*, 2003, **30**, 25.
22. L. Li, S. Chen, J. Zheng, B. D. Ratner and S. Jiang, *The Journal of Physical Chemistry B*, 2005, **109**, 2934.
23. J. C. Love, L. A. Estroff, J. K. Kriebel, R. G. Nuzzo and G. M. Whitesides, *Chemical Reviews*, 2005, **105**, 1103.
24. I. Inc, *Coupling of Proteins to IDC UltraClean Latex by Passive Adsorption*, http://www.idclatex.com/body_bgrounder_highactivity-protocol-1.asp, Accessed 17/05, 2009.
25. C.-M. Yam, C.-M. Pradier, M. Salmain, P. Marcus and G. Jaouen, *Journal of Colloid and Interface Science*, 2001, **235**, 183.
26. J. García-Alonso, R. F. Fakhrullin and V. N. Paunov, *Biosensors and Bioelectronics*, 2010, **25**, 1816.

CHAPTER 3. THE THEORETICAL BASIS OF THE CELL RECOGNITION BY NANOANTIBIOTIC PARTICLES

3.1 Introduction

In Chapter 2 of the present thesis we demonstrated methods by which nanoantibiotic particles may be produced as negative inorganic replicas of bacterial cells and how their surface chemistry can be modified in order to match explicitly their cell (or viral) targets, and in Chapter 4 we will present the results of the shell-forming experiments. In the present Chapter we propound the theoretical basis of the shape and size recognition of the nanoantibiotic particles and their matching target cells. Here we develop a theoretical analysis which represents an extension of the DLVO (Derjaguin-Landau-Verwey-Overbeek)[1, 2] interactions, which considers the van der Waals and the electric double layer interactions, adapted for the geometry of a spherical target particle (cell) interacting with its negative hemispherical-shell replica. We will examine the role of various factors, including the respective orientation of the two interacting species, their size ratio, along with the surface potentials of the spherical particle (cell) and the hemispherical shells (hemi-shells) and the ionic strength of the aqueous solution. There are many theoretical approaches which may be used to compute the colloidal interaction forces in such complex geometry via numerical methods, however approximate analytical formulas are available only in the limiting cases of interactions, such as those between two infinite plates, between two spherical colloid particles, and between a sphere and an infinite plane.[3-14] The Derjaguin approximation, which involves the calculation of colloidal interactions via the summation of the interactions of infinitesimal surface elements of planar geometry, can be extended and generalised for objects of non-spherical shapes such as cylinders.[1, 15-17] Bhattacharjee and Elimenech have developed the surface element integration (SEI) technique - a similar method whereby the integration domain does not only cover the opposing faces of the interacting species but also the retrograde interface.[18, 19] This technique has been employed for instance to estimate the interactions between spherical particles and cylindrical pores or spherical particles and rough surfaces.[20, 21] However, for the purposes of our calculation this technique[18,19] does not bring obvious advantage and allows only numerical estimation of the interaction. Given that our particles are of

micrometer size (e.g. cells) we found the SEI method does not help us to reveal clearly the physics of the interaction and the role of the geometrical factors. Here, we present an adaptation of the Derjaguin approximation for the estimation of the colloidal forces between a spherical target microparticle (cell) and a hemi-spherical shell which corresponds to our nanoantibiotic particle.

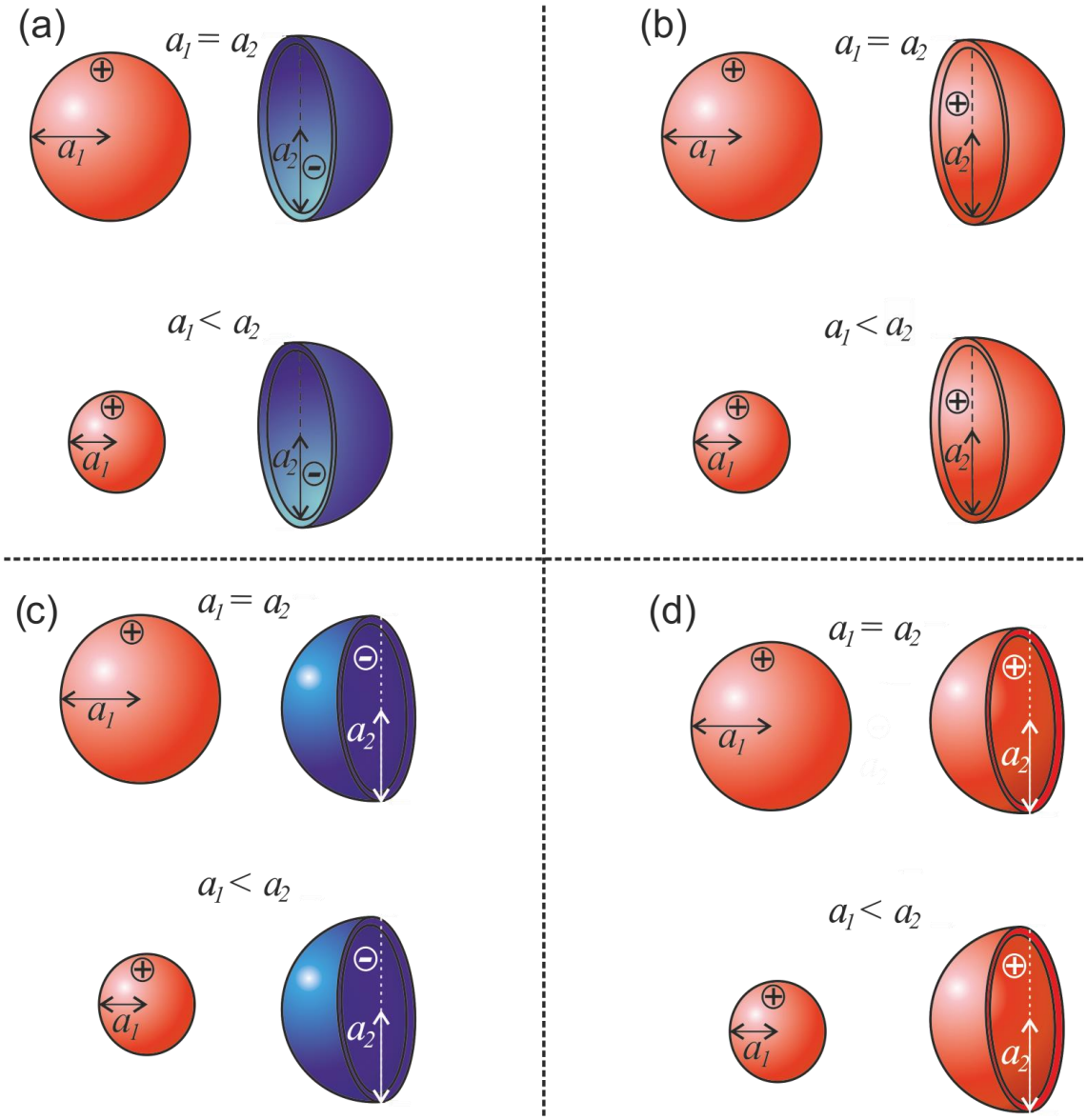

Figure 3-1. A scheme depicting the different scenarios of interactions between hemi-spherical shell of inner radius a_2 and a spherical particle (cell) of radius a_1. The red and blue colours signify positive and negative surface potentials, respectively. The scenario (a) involves the interaction of an oppositely charged sphere and its imprint arranged in a manner which leads to recognition, in (b) the surfaces geometrically match but have the same surface potential and situations (c) and (d) depict analogous interactions of species which are geometrically or orientation mismatched and hence shape recognition does not occur.

These calculations are done here for illustrative purposes which demonstrate the effect of the mismatch of the radius of curvature of the hemi-shell inner surface and the radius of curvature of the target particle. We also examine the interplay between the van der Waals forces and the electrostatic forces in the total interaction energy in this configuration. Here we derive simple and approximate analytical formulas for matching hemi-shells and spherical target particles which enable us to clarify the role of the surface charge (potential) for the interaction. We also derive analytical formulas for the interaction force and interaction energy between a hemi-shell and a target microsphere at different mismatches of their size and orientation.

3.2 Theoretical background

Let us consider the interaction between a spherical particle of radius a_1 and a hemispherical shell of silica of thickness δ and inner radius of curvature a_2. In order to explore the effect of surface forces on the hemi-shell – particle recognition we assume that their surface potentials in aqueous solution can be different due to their different material properties and different ionisable groups on their surfaces. For the sake of completeness, we will examine the influence of the size ratio between the spherical cell and the hemi-spherical shell both in the case when shape recognition occurs, that is when the spherical particle faces the interior of the hemispherical shell, as well as when the recognition does not occur (see Figure 3-1. for a scheme detailing the scenarios for which we have performed our calculations).

3.2.1 Interaction Energy between a Spherical Cell and the Facing Outer Surface of a Hemispherical Shell

The interaction between a sphere and the *outer* part of its silica hemispherical shell imprint was calculated in a similar way as interaction between two spherical colloid particles, as follows. The non-retarded van der Waals interaction energy E_{VW} between two semi-infinite phases is[22]

$$E_{VW}(h) = -\frac{A_H}{12\pi h^2} \tag{3-1}$$

where *h* is their separation. Here A_H is the compound Hamaker constant for the case of two semi-infinite phases interacting across aqueous film of thickness *h*. Obviously, this

is strictly correct only in the case of two uniform spherical particles. In the case of a hemispherical shell, oppositely orientated towards spherical particles, the formula will be similar but with a different, effective value of the Hamaker constant, taking into account the fact that the shell is hollow and there is an aqueous phase on the other side of the shell. However, the functional dependence of the van der Waals energy of interaction from the film thickness, *h*, will be the same. Using the Derjaguin approximation one can obtain the following expression for the van der Waals interaction energy:[19]

$$U_{VW} = -\frac{A_H a_1 a_2}{6(a_1 + a_2)D} \tag{3-2}$$

where *D* is the distance of closest approach between the two surfaces. When $a_1 = a_2 = a$, then

$$U_{VW} = -\frac{A_H a}{12D}. \tag{3-3}$$

The sphere-sphere electric double layer interaction energy can be estimated by using the linear superposition expression for an interaction between two planes per unit area:[23]

$$E_{EL}(h) = B\exp(-\kappa h), \qquad B = 32\varepsilon_0\varepsilon_r\kappa\gamma_1\gamma_2\left(\frac{kT}{ve}\right)^2. \tag{3-4}$$

Where ε_0 is the permittivity of vacuum, ε_r is the relative dielectric permittivity, κ is the inverse Debye screening length. γ_i=tanh$(\Psi_i/4)$ and $\Psi_i = ve\psi_i/kT$, (i=1,2) where *k* is the Boltzmann's constant, *v* is the valency of the electrolyte, *e* is the electronic charge, *T* is the absolute temperature and ψ_i are surface potentials. The total free energy of interaction between plane parallel surfaces, according to the DLVO theory, is a sum of the van der Waals and electrostatic contributions

$$E(h) = E_{VW}(h) + E_{EL}(h). \tag{3-5}$$

By applying the Derjaguin method to Eq. (3-4) one obtains the electrostatic energy of interaction in this geometric configuration[23]

$$U_{EL} = 2\pi B\left(\frac{a_1 a_2}{a_1 + a_2}\right)\frac{1}{\kappa}\exp(-\kappa D) \tag{3-6}$$

When the particle size and the hemispherical shell are equally sized, then $a = a_1 = a_2$, then:

$$U_{EL} = \frac{\pi a B}{\kappa} \exp(-\kappa D) \tag{3-7}$$

The total interaction energy U_{total} was then calculated by summing Eq. (3-2) and Eq. (3-6):

$$U_{total} = U_{VW} + U_{EL} \tag{3-8}$$

$$U_{total} = -\frac{A_H a_1 a_2}{6(a_1 + a_2)D} + 2\pi B \left(\frac{a_1 a_2}{a_1 + a_2} \right) \frac{1}{\kappa} \mathrm{e}^{-\kappa D}, \tag{3-9}$$

which for equal curvatures reduces to:

$$U_{total} = -\frac{A_H a}{12D} + \frac{\pi B a}{\kappa} \mathrm{e}^{-\kappa D}. \tag{3-10}$$

Please note that Eqs. (3-9) and (3-10) are approximate and are only valid within the framework of the Derjaguin approximation in colloid science for the DLVO interaction between two spherical particles in an aqueous solution, which requires that the radius of action of the colloid forces between the particle surfaces is much smaller than the radius of curvature of the particle surface. Geometrically, this situation corresponds to Figures 3-1 (c) and (d) in our diagram of interaction between a spherical particle and oppositely orientated hemispherical shell.

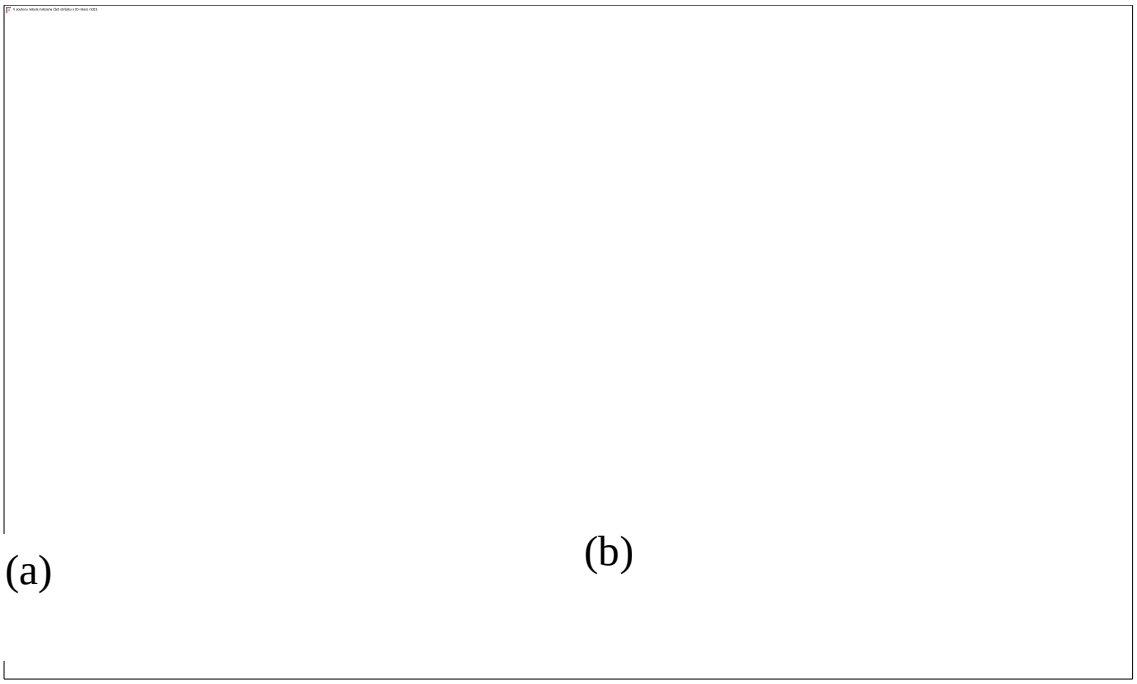

Figure 3-2. Schematics of the interaction between a spherical particle of radius a_1 and a hemispherical shell of inner radius of curvature a_2 at a distance *D* between their surfaces. (a) The particle radius of curvature is smaller than (or equal) to the inner radius of curvature of the hemispherical shell. (b) The particle radius of curvature is larger than the inner radius of curvature of the hemispherical shell. In this case the rim of the hemispherical-shell (of thickness δ) also contributes to the interaction.

3.2.2 Interaction Energy between Spherical Cell and Facing the Inner Surface of the Hemispherical Shell

We have adapted the Derjaguin method to our specific scenario of the interaction of a sphere and the inner part of the hollow hemispherical shell, corresponding to Figure 3-1. (a) and (b). First we consider the case where the hemispherical shell has larger or equal radius of curvature than the spherical particle, $a_1 \leq a_2$. The complimentary case of a hemispherical shell with smaller radius of curvature than the spherical particle ($a_1 \geq a_2$) is considered in the following sub-section.

3.2.2.1 *Interaction between a Spherical Target Particle and a Larger Hemispherical Shell*

Let us consider the interaction between a spherical particle of radius a_1 and a hemispherical shell of radius a_2, where $a_1 \le a_2$. The schematic diagram of this case is presented in Figure 3-2 (A). The surface of the spherical particle and the inner surface of the hemispherical shell can be described by the following equations:

$$z_1(r) = a_1^2\sqrt{1-\frac{r^2}{a_1^2}}, \qquad z_2(r) = a_2^2\sqrt{1-\frac{r^2}{a_2^2}}. \tag{3-11}$$

The running distance $H_s(r)$ between the two surfaces is:

$$H_s(r) = D + a_1 - a_2 - z_1(r) + z_2(r). \tag{3-12}$$

For a small degree of mismatch between the hemispherical shell and the target particle and a small radius of action of the surface forces compared to both a_1 and a_2 we can use the Derjaguin approach to expand Eq (3-12) in series:

$$H_s(r) = D + \frac{1}{2}\left(\frac{1}{a_1}-\frac{1}{a_2}\right)r^2 + O(r^4) \tag{3-13}$$

The latter is equivalent to approximating the spherical parts of both surfaces with paraboloid surfaces with the same radius of curvature. If E(*h*) is the free surface energy of interaction of two plane-parallel surfaces of the same properties as the target particle and the hemi-shell, then the Derjaguin approximation in this case should be written as follows:

$$U = \iint_A E(H_s(r))dxdy = \int_0^{2\pi} d\varphi \int_0^{a_1} dr\left[rE(H_s(r))\right]. \tag{3-14}$$

Here we have changed the Cartesian coordinates (*x*,*y*) to polar coordinates (*r*, φ), according to the transformation

$$x = r\cos\varphi,\ y = r\sin\varphi,\ r^2 = x^2 + y^2. \tag{3-15}$$

Note that due to this approximation the surface integration of the interaction energy cannot be done from $r=0$ to $r=\infty$ as in the original work of Derjaguin for two spheres as this would give a divergence due to the infinite parabolic surfaces. The integration of the surface elements of these two surfaces will be done in an approximate manner only up to the smaller radius of curvature, i.e. up to the radius of curvature of the particle in the case depicted in Figure 3-2 (A). Hence the integration in Eq. (16) can be done in a general form as follows:

$$U = 2\pi \int_D^{H_1} E(h(r))d\left(\frac{r^2}{2}\right) = \frac{2\pi}{\frac{1}{a_1}-\frac{1}{a_2}} \int_D^{H_1} E\left[D+\frac{r^2}{2}\left(\frac{1}{a_1}-\frac{1}{a_2}\right)\right] d\left[D+\frac{r^2}{2}\left(\frac{1}{a_1}-\frac{1}{a_2}\right)\right] = \tag{3-16}$$

$$= \frac{2\pi a_1 a_2}{a_2 - a_1} \int_D^{H_1} E(h)dh$$

Here $H_1 = H_s(r = a_1)$ for this particular case (Figure 3-2 (A)). Using Eq. (3-1) and Eq. (3-16) for the van der Waals energy in this configuration we obtain:

$$U_{VW} = \frac{a_1 a_2 A_H}{6(a_2 - a_1)}\left(\frac{2a_2 A_H}{\left(2Da_2 + a_1 a_2 - a_1^2\right)} - \frac{1}{D}\right). \tag{3-17}$$

$$U_{EL} = \frac{2\pi B a_1 a_2}{\kappa(a_2 - a_1)}\left(-e^{-\frac{(2Da_2 + a_1 a_2 - a_1^2)\kappa}{a_2}} + e^{(-\kappa D)}\right). \tag{3-18}$$

The total interaction energy is a sum of Eq. (3-17) and Eq. (3-18), $U_{total} = U_{VW} + U_{EL}$. Please note that although there is the term $(a_2 - a_1)$ in the denominators of both equations (3-17) and (3-18) they do not diverge at $a_1 = a_2$ which corresponds to equal (matching) radii of curvature. Thus for matching spherical target particle and hemispherical shell ($a_1 \to a$, $a_2 \to a$), the modified Derjaguin approximations give:

$$U_{VW} = -\frac{a^2 A_H}{12D^2} \tag{3-19}$$

$$U_{EL} = \pi a^2 B \mathrm{e}^{-\kappa D} \tag{3-20}$$

$$U_{total} = -\frac{a^2 A_H}{12D^2} + \pi a^2 B \mathrm{e}^{-\kappa D} \tag{3-21}$$

One can see that there is a profound difference between this formula, Eq. (3-21), and the case of interaction of two spherical particles of equal radius, Eq. (3-10) when it comes to the dependence from the distance between the particle surfaces and the particle radius. Since the latter case is also similar to the case of a mis-orientated hemi-shell and a spherical particle, the difference between Eq. (3-21) and Eq. (3-10) gives the difference between the interaction energies in the case of the favorable and unfavorable orientations of the hemispherical shell with respect to the matching target particle. These results call for some further analysis. The ratio of the van der Waals interaction energies for the case of favorable (recognition), Eq. (3-19) and unfavorable orientation, Eq. (3-3) gives

$$\frac{U_{VW}^{favourable}}{U_{VW}^{unfavorable}} = \frac{-\frac{a^2 A_H}{12D^2}}{-\frac{A_H a}{12D}} = \frac{a}{D} >> 1 \ . \tag{3-22}$$

Here it is assumed that the Hamaker constant, A_H is similar in both cases which may be justified for hemi-shell thickness larger than of several tens of nanometers. This means that for large enough hemispherical shell in unfavorable orientation (Figure 3-1. (c) and (d)) it will interact with the target spherical particle just like a large spherical silica particle. Similarly, for thick enough silica hemispherical shells in a favorable orientation (Figure 3-1. (a) and (b)), the Hamaker constant will have a very similar value which justifies the comparison in Eq. (3-22). Note that since $D << a$, the van der Waals interaction upon target recognition (in favorable orientation) is much stronger than those in unfavorable orientation where there is no recognition. Similar comparison of the electrostatic interaction energies, Eqs. (3-20) and (3-7) gives

$$\frac{U_{EL}^{favourable}}{U_{EL}^{unfavorable}} = \frac{\pi a^2 B \exp(-\kappa D)}{\frac{\pi a B}{\kappa}\exp(-\kappa D)} = \kappa a >> 1 \ . \tag{3-23}$$

For typical values of $a = 3\mu m$ for bacterial cells and salt concentration 0.1 *M*, $\kappa^{-1} \approx 3nm$ which gives $\kappa a = 1000$. This corresponds to an electrostatic interaction energy upon recognition (Figure 3-1. (a), (b)) of the target particle by the hemispherical shell 3 orders of magnitude larger compared to the same interaction in an unfavorable orientation (no recognition, Figure 3-1. (c), (d)). This means that if the electrostatic

interaction is attractive (e.g. for oppositely charged target particle and hemi-shell), the size-based recognition between the target particle and the hemi-shell would amplify the interaction, making it more attractive. However, if the electrostatic interaction is repulsive (e.g. for like charged target and hemi-shell) the favorable orientation will make it even more repulsive.

3.2.2.2 Interaction between a Spherical Target Particle and a Smaller Hemispherical Shell

Let us consider the complimentary case where the hemispherical shell has a smaller inner radius than the radius of the target spherical particle, $a_1 \geq a_2$, as presented in Figure 3-2. (B). In this case, we can also derive approximate formulas for the interaction energy using the Derjaguin approach, but the integration of the interacting surface elements between the two surfaces has two contributions:

$$U = U_s + U_r, \tag{3-24}$$

where

$$U_s = U_s = \iint_{A_s} E(H_s(r))dxdy = \int_0^{2\pi} d\varphi \int_0^{a_2} dr\left[rE(H_s(r))\right] \tag{3-25}$$

is the interaction between the inner surface A_s of the hemispherical shell and its vertical projection over the target particle surface. Note that here the upper boundary of the surface integral ends at $r = a_2$ instead of $r = a_1$ in the case sketched in Figure 3-2. (A). In addition to this contribution there is also a contribution from the rim of the hemispherical shell interacting with its projection onto the target particle's surface

$$U_r = \iint_{A_r} E(H_s(r))dxdy = \int_0^{2\pi} d\varphi \int_{a_2}^{a_2+\delta} dr\left[rE(H_s(r))\right] \tag{3-26}$$

Here A_r is the projection of the rim surface onto the target particle surface. In Eq. (3-25) and Eq. (3-26), $H_s(r)$ is the running distance between the two surfaces, defined by Eq. (3-12). By using the same level of approximation of the two interacting surfaces with paraboloids as in Eq. (3-13) and caring out the integration in Eq. (3-25) we obtain:

$$U_s = \frac{2\pi a_1 a_2}{a_2 - a_1} \int_D^{H_2} E(h) dh. \tag{3-27}$$

where $H_2 = H_s(a_2)$. Using Eq. (3-12) one can expand the integral in Eq. (3-26) in series for small values of the parameter $\delta / a_2 << 1$ to obtain

$$U_r = 2\pi\delta a_2 E(H_2) + O(\delta^2). \tag{3-28}$$

Equation (3-28) can be obtained in an approximate manner by simply multiplying the surface free energy $E(H_2)$, by the approximate area of the hemi-shell rim, $2\pi a_2 \delta$. Equation (3-28) is valid only when $\delta << a_2$. Substituting Eqs. (3-1), (3-4) and (3-5) into Eq. (3-27) and caring out the integration gives

$$U_s = \frac{2\pi a_1 a_2}{a_2 - a_1} \left[\frac{B}{\kappa} \left(e^{-\kappa D} - e^{-\kappa H_2} \right) + \frac{A_H}{12\pi} \left(\frac{1}{H_2} - \frac{1}{D} \right) \right]. \tag{3-30}$$

Similarly, the combination of Eqs. (3-1), (3-4) and (3-5) into Eq. (3-28) gives:

$$U_r \approx 2\pi a_2 \delta \left[B e^{-\kappa H_2} - \frac{A_H}{12\pi H_2^2} \right], \quad a_1 > a_2. \tag{3-31}$$

The total interaction energy in this case is given by Eq. (3-24) where $H_2 = H_s(a_2)$ is calculated from Eq. (3-13). Note that when the inner radius of the hemi-spherical shell gets very close to that of the target particle, $a_1 = a_2 = a$, Eq. (3-30) can be expanded in power series for small values of $(a_2 - a_1)$ to give:

$$U_s \approx -\frac{a^2 A_H}{12 D^2} + \pi a^2 B e^{-\kappa D}, \qquad (a_1 = a_2 = a) \tag{3-32}$$

The last equation coincides with Eq. (3-21) which shows that the matching sizes the hemi-shell and the target particle give the same asymptotic results for the interaction energy. In this case, however, $U_r = 0$, by definition as the area A_r of the projection of the rim onto the target particle surface, is zero for the matching hemispherical shell and target microsphere. The comparison between the contributions of the inner shell surface, Eq. (3-30) and the rim, Eq. (3-31) show that their ratio is proportional to

$\delta/\alpha_2 << 1$. Hence the contribution of the hemi-shell rim to the interaction with the target particle can be neglected within the accuracy of this model.

3.3 Results and Discussion

In this section we have used Eqs. (3-8)-(3-10), (3-17)-(3-18), (3-24) and (3-30)-(3-31) to model the interaction of the target particles with hemispherical shells. For the sake of simplicity, we have chosen the target particles to have the material parameters of spherical latex particles and the hemi-shells are made of silica. The Hamaker constants of polystyrene and silica A_{ii} of 1.15×10^{-19} J and 5×10^{-19} J, respectively,[24] result in the effective Hamaker constant A_H in an aqueous medium ($A_{ii}=4.85 \times 10^{-20}$ J) of 5.79×10^{-20} J. We examined the energy of interaction for the following ionic strengths of the aqueous medium, $I=1 \times 10^{-2}$ M, $I=5 \times 10^{-3}$ M and $I=1 \times 10^{-5}$ M. The calculations were done at several different values of the surface potentials (ψ_s = ± 25 mV, ± 35 mV and ± 45 mV) of the hemi-shells and the target particles. We explored the influence of the ionic strength of the aqueous medium in which the target particles are incubated with the hemi-shells; the role of their surface potentials and the separation between them, as well as the size ratio and the orientation of the hemi-shell and the target particle. The influence of the separation was studied on 1 μm polystyrene microspheres and a matching silica hemispherical shell replicas over distances 5-100 nm. We use separation larger than 5 nm as the silica imprints have some surface roughness and also may be coated with polyelectrolytes as in our experiments described in Chapters 2 and 4 of this thesis. The influence of the size ratio was studied at constant separation of 10 nm and constant diameter of the silica a_1 = 1 μm whilst varying the diameter of the spherical target particle for a_1/a_2 ratios from 0.05 to 1. The orientation factor was probed by assuming the target spherical particle faced either the interior of the hemi-shell (as in Figure 3-1 (a), (b)) or its outer, convex, spherical, side (as in Figure 3-1. (c), (d)).

We have found that the recognition between oppositely charged interacting species energetically favours the binding of the target particle to the inner surface of the matching silica hemi-shell imprint in comparison to the scenario where the binding occurs on the outer part of the hemi-shell surface. This strongly upholds the hypothesis of the nanoantibiotic mode of action mentioned earlier, which is demonstrated by our

experimental results presented in the following thesis chapters. Considering the scenario where the separation D was varied, it has been noted that the U_{VW} between the inner part of the silica hemi-shell and the target microsphere was about -4.8 x 10^4 kT at the distance of 5 nm and becomes much weaker when D is 100 nm, then the interaction energy is approximately 119 kT. At these values of the parameters, the van der Waals interaction energy, U_{VW} between a latex particle facing the convex side of its matching silica hemi-shell is -238 kT when they are separated by 5 nm and about 12 kT when their separation reaches 100 nm. This shows us that the matching geometry increases the van der Waals attraction approximately 10 fold in the case of the relatively long distance interactions and about 200 fold in the case of 5 nm separation. This explains the importance of the size recognition between the target microsphere and the matching hemi-shell. Furthermore, the interaction energy between the latex microsphere and the silica hemi-shell oriented so that they match their hemi-shell is of the order of 10^4 to 10^5 kT whilst the interaction energy between the mismatches is in the order of hundreds of kT. The screening effect which arises from the salt ions present in the medium has a pronounced effect in both geometries. The electrostatic contribution to the total interaction energy generally increases for all three values of the ionic strength of the medium in the case of the mismatch situations. It can also be seen that a larger increase of the electrostatic interactions contribution occurs at about D = 20 nm (see Figure 3-3.).

The results presented in Figure 3-4. show that at the relatively low ionic strength of the aqueous medium, I = 1x10^{-5} M, which corresponds to κ^{-1} = 100 nm, the electric double layer interactions, U_{EL}, weaken and at distances D smaller than 10 nm the attractive van der Waals interaction energy, U_{VW} becomes dominant even when the target microsphere and the hemi-shell carry the same surface potential. The size matching between the target microsphere and the silica hemi-spherical shell has also proven to be very important. Figure 3-5. demonstrates that when oppositely charged species are separated by 10 nm the difference between the U_{total} when a_1/a_2= 0.05 and a_1/a_2=1 is about three orders of magnitude and that there is a difference of two orders of magnitude in the interaction energy for orientation where the hemi-shell faces the microsphere via its concave side compared with the case when it faces the microsphere via its convex part.

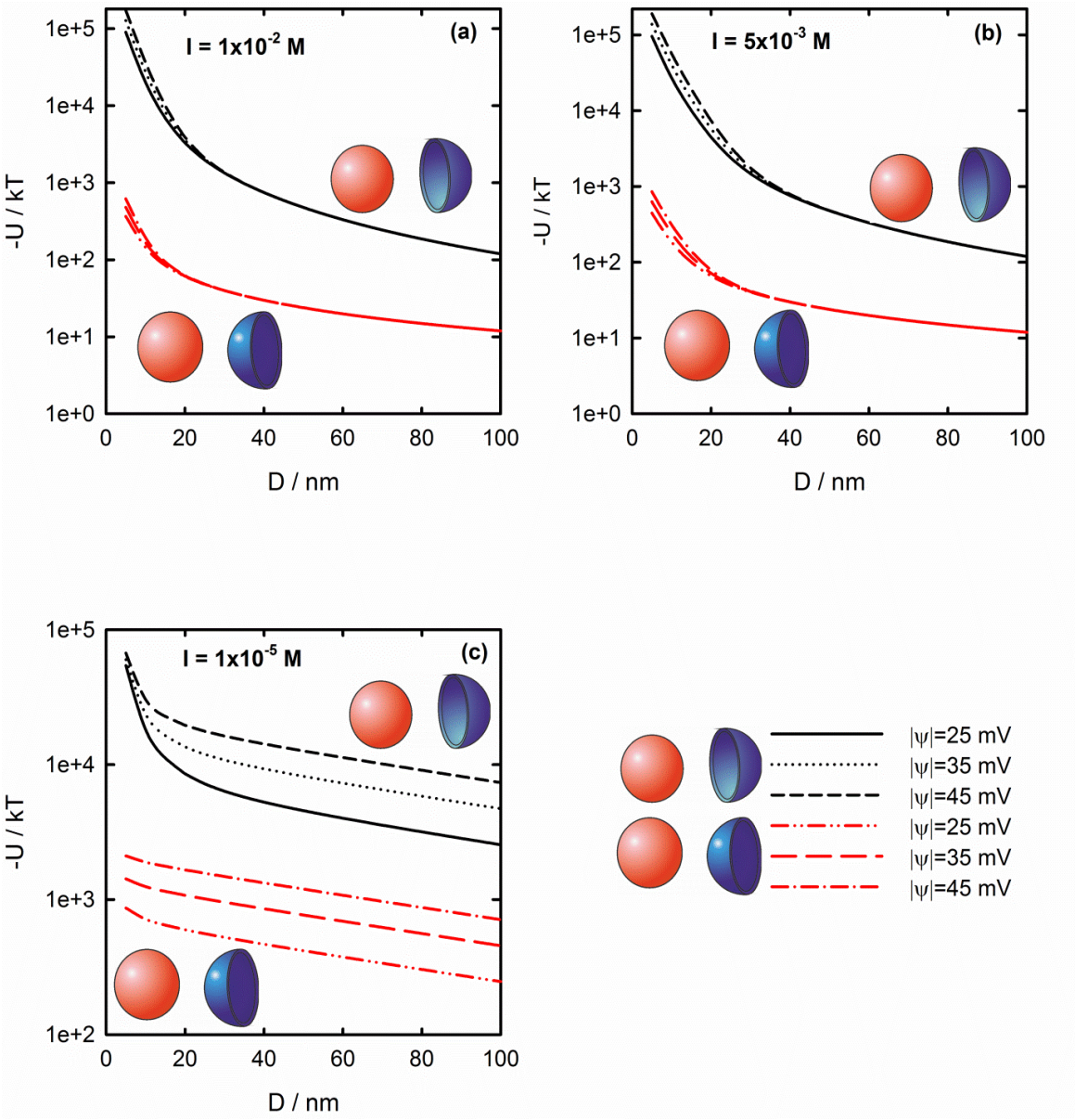

Figure 3-3. Total interaction energy between the spherical target microsphere of radius $a_1 = 1\mu m$ and its matching silica hemi-shell imprint ($a_2 = 1\mu m$) as a function of distance at various ionic strengths: (a) I = 1x10^{-2} M, (b) I = 5x10^{-3} M and (c) I = 1x10^{-5} M. The different curves correspond to different surface potentials and orientations of the hemi-shell and the target microsphere.

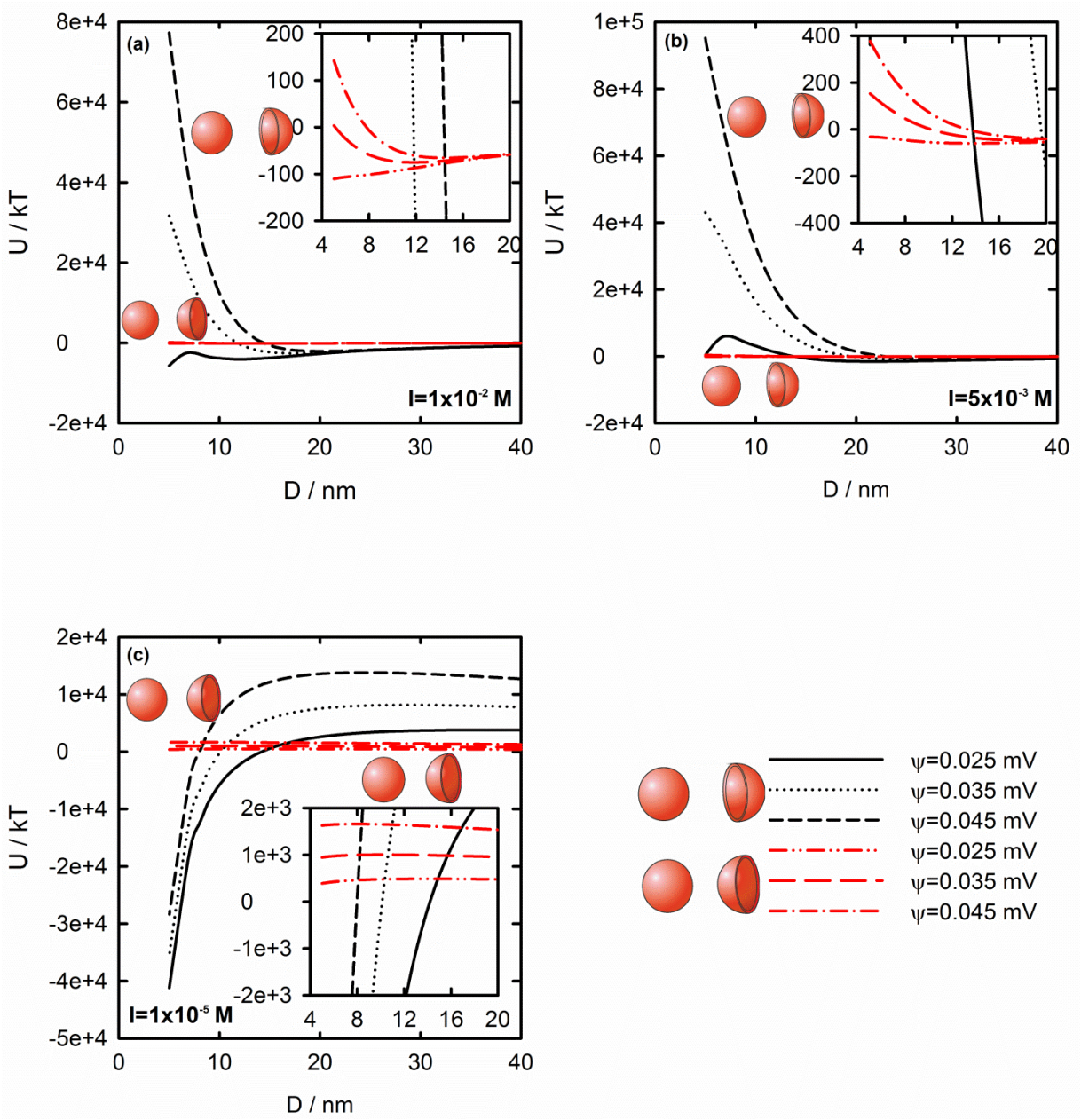

Figure 3-4. Total interaction energy between the target microsphere and its hemi-shell imprint as a function of distance at various levels of ionic strength, I, and equal surface potentials ψ (see legend). (a) I = 1x10^{-2} M, plot (b) I = 5x10^{-3} M and (c) I = 1x10^{-5} M.

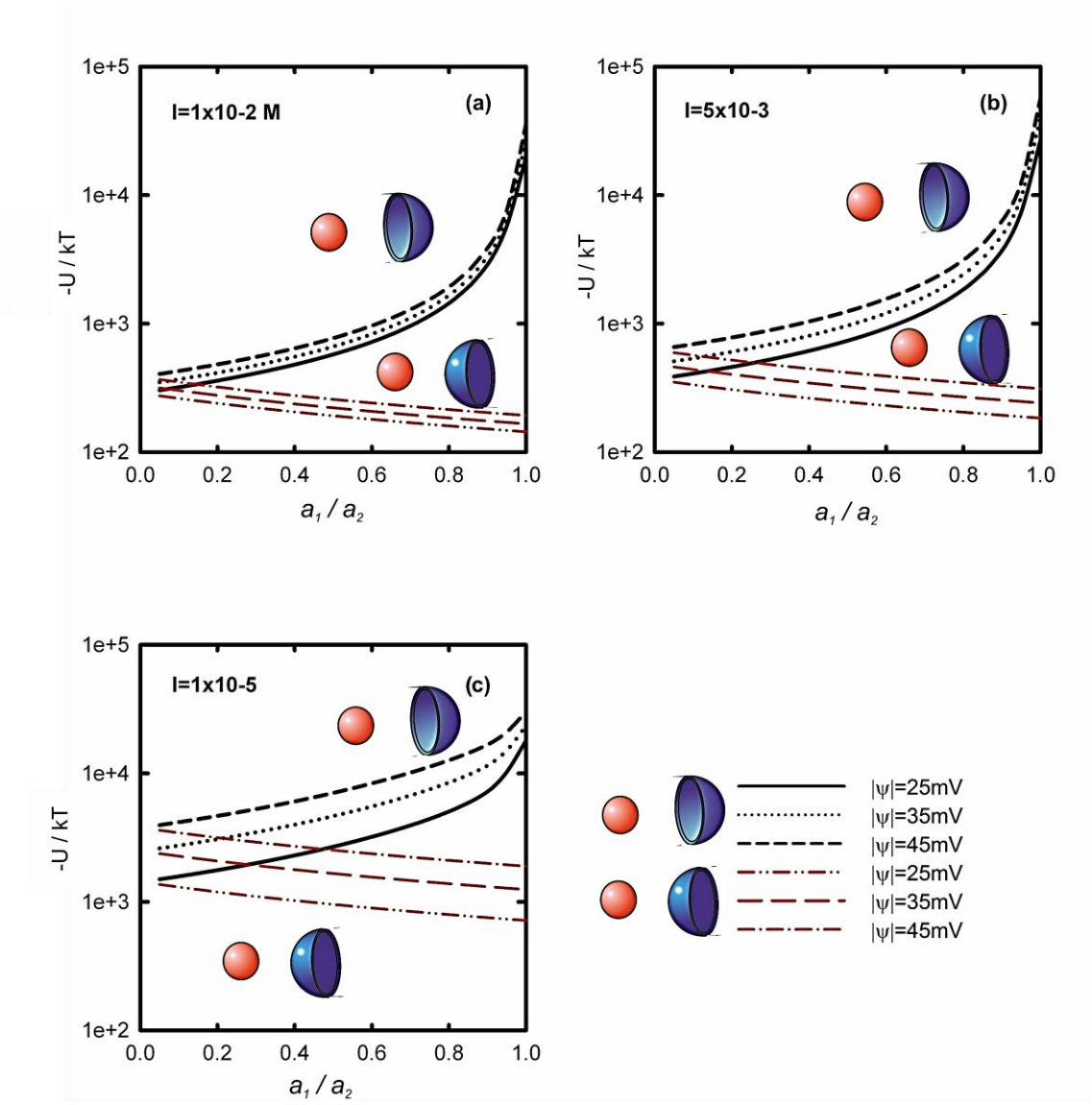

Figure 3-5. Total interaction energy between the target microsphere of radius $a_1 = 1\mu m$ and its silica hemi-shell imprint as a function *of* a_1/a_2 ratio at various ionic strengths, I, and surface potentials ψ. The target particle and the hemi-shell are oppositely charged. (a) I = 1x10^{-2} M, plot (b) I = 5x10^{-3} M and (c) I = 1x10^{-5} M. Here the separation is fixed to D=10 nm.

3.4 Conclusions

In this chapter we have used the Derjaguin approach to derive analytical formulas for the energy of interaction between a target microsphere and a hemispherical microparticle. The findings from this modelling clearly demonstrate that the size match between the target microsphere and the silica hemi-shells which represent the cell-nanoantibiotic interaction discussed in the previous chapter have a rigorous theoretical basis. In this chapter we have fixed the target particle shape to be spherical and only explored the role of the size mismatch and the particle materials parameters such as surface potentials and Hamaker constant as well as the ionic strength of the medium. We have demonstrated that the energy of interaction between the hemi-shell and the target particle is several orders of magnitude higher when the size recognition between them is achieved. We find that when the hemi-shell and the target microsphere are equally sized, the energy of interaction is larger in the case of favourable orientation of the microsphere towards the interior of the hemi-shell replica. The latter is stronger by the factor of a/D in the case of the van der Waals interactions compared to the unfavourable orientation when the microsphere approaches the outer part of the hemi-shell. In the case of electrostatic interactions, upon favourable approach of the microsphere towards the inner side of the hemi-shell we estimated levels of interaction energy which are κa times stronger in comparison to the unfavourable orientation.
Generally, the size recognition amplifies the magnitude of the interaction energy. If the interaction energy between the target particle and the hemi-shell is attractive, the size match amplifies the attraction. If the interaction is repulsive, the size and shape recognition amplifies the repulsion. For micrometer sized target particles (e.g. cells) and moderate ionic strength this can result in more than 3 orders of magnitude difference in the interaction energy.

Furthermore, we have shown a very strong effect on the interaction by the size mismatch between the target particle and the hemi-shell in both situations of favourable and unfavourable orientation. Since the interaction energy between the nanoantibiotic particle and its target cells is linked to their binding constant through an exponential dependence, even moderate increase of the energy of attraction leads to an exponential increase of their binding constant. This justifies the novel approach of nanoantibiotic

particles which can bind strongly to their target cells based on their shape and size recognition.

3.5 References

1. B. V. Derjaguin and L. Landau, *Acta Physisco-Chimica. URSS*, 1941, **14**, 633.
2. E. J. W. Verwey and J. T. G. Overbeek, *Theory of the Stability of Lyophobic Colloids*, Dover Publications, 1999.
3. S. L. Carnie, D. Y. C. Chan and J. Stankovich, *Journal of Colloid and Interface Science*, 1994, **165**, 116.
4. B. K. C. Chan and D. Y. C. Chan, *Journal of Colloid and Interface Science*, 1983, **92**, 281.
5. O. F. Devereux and P. L. D. Bruyn, *Interaction of plane-parallel double layers*, M. I. T. Press, 1963.
6. A. B. Glendinning and W. B. Russel, *Journal of Colloid and Interface Science*, 1983, **93**, 95.
7. M. L. Grant and D. A. Saville, *Journal of Colloid and Interface Science*, 1995, **171**, 35.
8. N. E. Hoskin, *Philosophical Transactions of the Royal Society of London. Series A, Mathematical and Physical Sciences*, 1956, **248**, 433.
9. N. E. Hoskin and S. Levine, *Philosophical Transactions of the Royal Society of London. Series A, Mathematical and Physical Sciences*, 1956, **248**, 449.
10. L. N. McCartney and S. Levine, *Journal of Colloid and Interface Science*, 1969, **30**, 345.
11. D. McCormack, S. L. Carnie and D. Y. C. Chan, *Journal of Colloid and Interface Science*, 1995, **169**, 177.
12. H. Ohshima, T. W. Healy and L. R. White, *Journal of Colloid and Interface Science*, 1982, **90**, 17.
13. H. Ohshima and T. Kondo, *Journal of Colloid and Interface Science*, 1988, **126**, 382.
14. J. Stankovich and S. L. Carnie, *Langmuir*, 1996, **12**, 1453.
15. B. V. Deriagin, *Surface forces / B.V. Derjaguin, N.V. Churaev and V.M. Muller ; translated from the Russian by V.I. Kisin ; translation edited by J.A. Kitchener*, Consultants Bureau, New York :, 1987.

16. Z. Adamczyk, P. Belouschek and D. Lorenz, *Berichte der Bunsengesellschaft für physikalische Chemie*, 1991, **95**, 566.
17. L. R. White, *Journal of Colloid and Interface Science*, 1983, **95**, 286.
18. S. Bhattacharjee and M. Elimelech, *Journal of Colloid and Interface Science*, 1997, **193**, 273.
19. S. Bhattacharjee, M. Elimelech and M. Borkovec, *Croatica Chemica Acta*, 1998, **71**, 883.
20. S. Bhattacharjee and A. Sharma, *Journal of Colloid and Interface Science*, 1997, **187**, 83.
21. X. Huang, S. Bhattacharjee and E. M. V. Hoek, *Langmuir*, 2010, **26**, 2528.
22. H. H.C, *Physica*, 1937, **4**, 1058.
23. G. John, *Journal of Colloid and Interface Science*, 1975, **51**, 44.
24. D. J. Shaw, *Introduction to colloid and surface chemistry*, Butterworths, 1966.

CHAPTER 4. FABRICATION OF NANOANTIBIOTIC PARTICLES

This Chapter presents and discusses the results of the methods of fabrication of negative replicas of yeast cells and latex particles as described in the Experimental chapter. Many of the resultant nanoshell replicas were used in further recognition experiments, the results of which will be discussed in further chapters of this thesis. As suggested in section 1.6 of , pristine metals such as gold as well as low solubility metal sulfides and oxides are biocompatible and should not harm the microorganisms which are not the targets of the nanoantibiotics. For this reason it was decided to experiment with the fabrication of silica-, zinc sulphide- and gold-based nanoantibiotic particles.

The pursued methods cover both symmetric as well as asymmetric deposition of nanoshell-forming material over the surface of latex microparticle and test microorganism templates. The first type, the simple symmetrical deposition, was pursued in order to fabricate silica, zinc sulfide and silica nanoparticle / polyelectrolyte composite nanoantibiotics. The silica nanoshells were fabricated following or adjusting the methods by Lu *et al*. and Weinzierl *et al*. who reported facile silica deposition methods over latex microsphere and yeast cell templates.[1, 2] Silica shells with integrated gold nanoparticles (AuNP) were also fabricated by modification of the technique reported by Weinzierl *et al*. The zinc sulfide deposition was performed onto yeast cell templates by utilizing the successive ionic layer adsorption and reaction (SILAR) method and by deposition of the zinc sulfide onto the cells which were immobilized in the agarose gel matrix whilst using thioacetamide as source of sulfide ions as described in Section 2.3.3.2 of the Experimental chapter.[3-11] The fabrication of the silica/polyelectrolyte composite shells was inspired by the work of Fakhrulin *et al.* who used gold and silver nanoparticles instead.[12] The gold cap fabrication via the metal sputtering method was done according to the report of Cayre *et al*.[13]

4.1 Fabrication of Silica Imprints of Latex Microspheres and Test Microorganisms

4.1.1 Synthesis of Silica Shells using Latex Microsphere Templates, their Fragmentation and Removal of the Latex Templates

Commercial latex microspheres were used initially as a template for the synthesis of shells due to their uniform spherical shape and uniform specific size availability, which is on a similar scale to that of the potential target microorganisms, and to their facile removal through their dissolution in toluene. The method based on the report by Lu *et al.* as described in Section 2.3.2.3 was followed.[1]

Good quality latex particle/silica core/shell particles were produced using both types of latex particles: aliphatic amine–functionalised as well as CML particles coated in a monolayer of PAH. Both particle types allowed for an even deposition of silica on their surfaces. The thickness of the silica nanoshells was measured in the case of aliphatic amine microspheres and was found to be ~ 90 nm at our experimental conditions. The size of the templated latex spheres had no detectable effect on the shell morphology. Figure 4-1. shows typical experimental results for silica nanoshells produced by templating latex microspheres.

Latex/silica core/shell particles

Silica shells

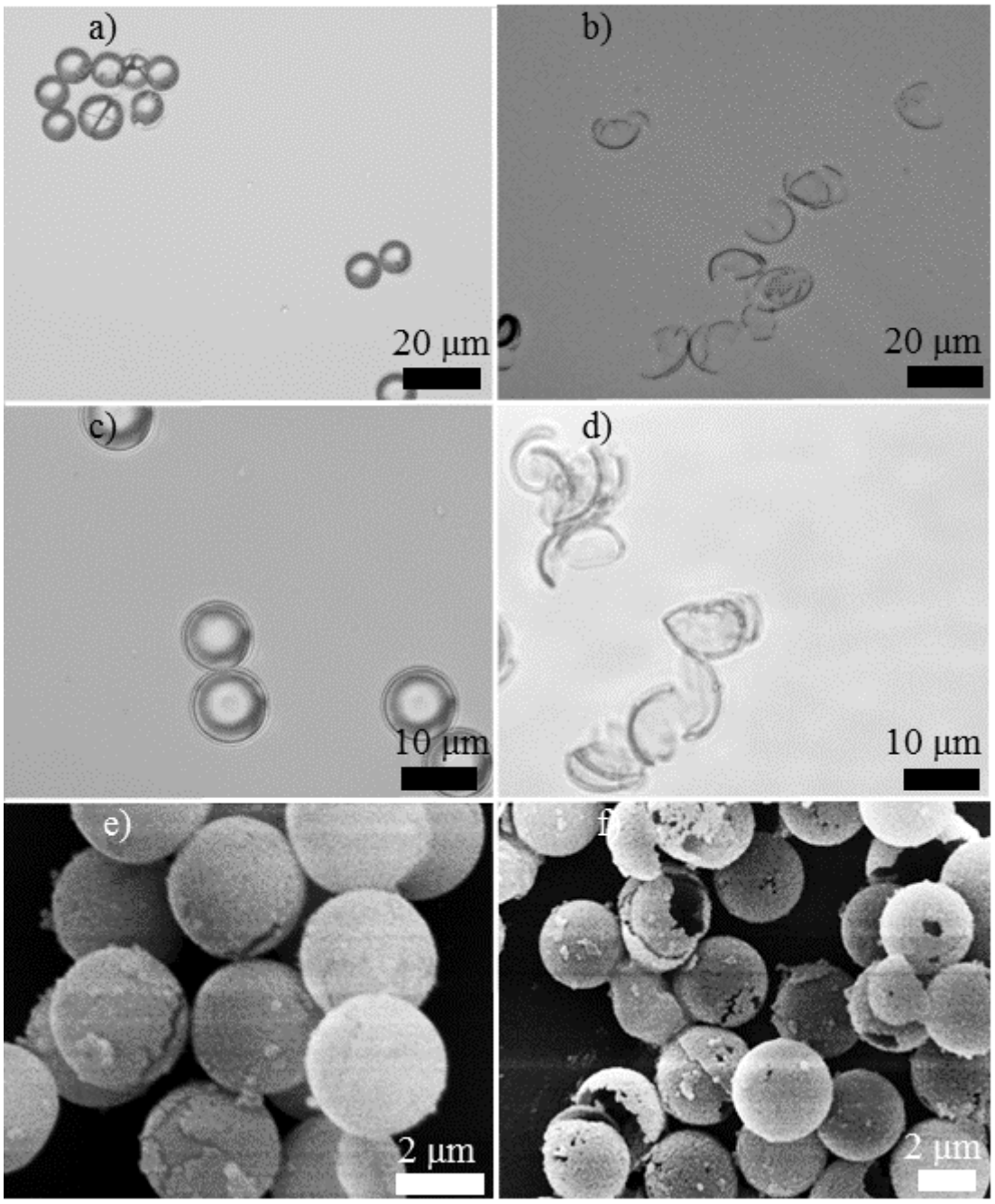

Figure 4-1. Micrographs of silica shells deposited onto latex microspheres and of the shells alone after the dissolution of their templates. The optical micrographs (a) – (d) display species fabricated using 10 µm CML latex particles coated with a layer of PAH and were taken under 50x magnification for (a) and (b) and 100x magnification for (c) and (d). The SEM images (e) and (f) show silica shells produced by templating of 3.2 µm aliphatic amine latex microspheres.

4.1.2 Synthesis of Silica Shells using Yeast Cell Templates, Shell Fragmentation and Removal of the Templates

As silica nanoshell production on latex particles was proved to be successful, the next step was to produce silica nanoshells on a model microorganism. We chose to use yeast cells as a test microorganism due to their robustness which arises from the relative rigidity of the cell wall.[14, 15] The method based on that of Weinzierl *et al.* as described in Section 2.3.2.1 was followed.[2] This technique was used for fabrication of the nanoantibiotics used for both the recognition experiments described in Chapter 5, and for the fabrication of AuNP integrated into silica nanoshells used for the selective cell killing experiments discussed in Chapter 6.

Figure 4-2. shows typical SEM images of the yeast cells with a layer of deposited silica. The SEM micrographs revealed that some of the produced shell species were already disrupted at the end of the procedure. This was probably caused by the centrifugation steps in the washing procedure. The disruption of the silica nanoshells using sonication in conjunction with the exposure to Piranha solution, however, led to the formation of very high quality fragments of negative replicas of the yeast cells which were then utilized in the recognition experiments (Figure 4-3). The shell thickness was estimated from the SEM images to be around ~ 220 nm.

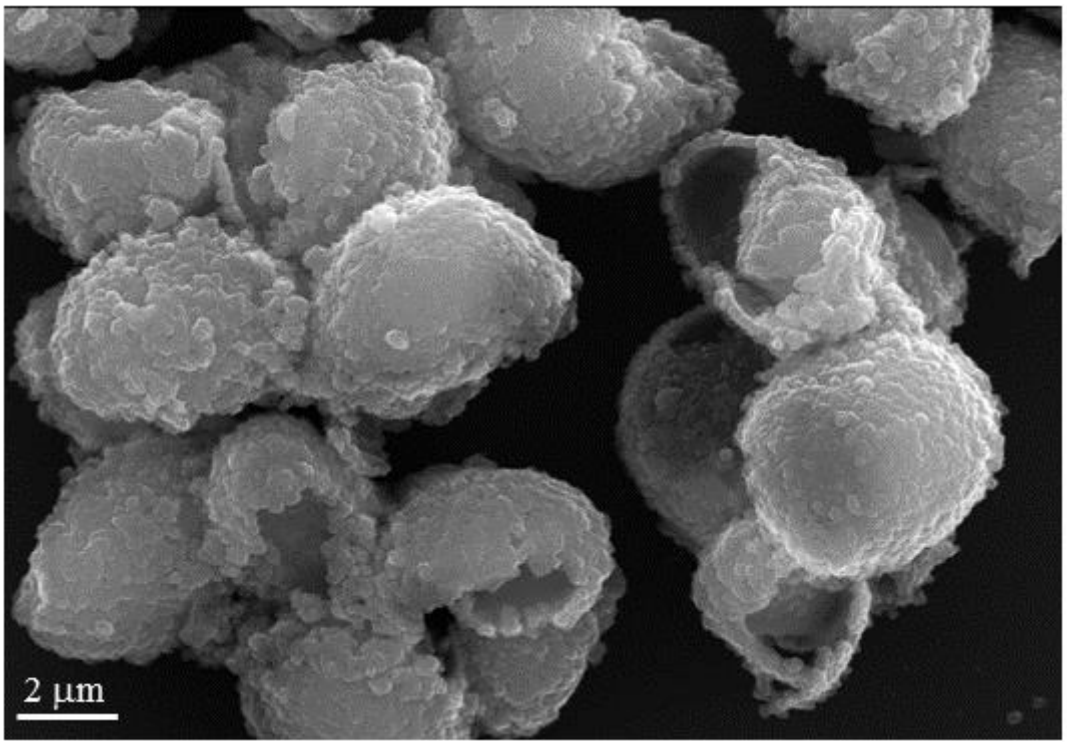

Figure 4-2. Yeast / silica core / shell particles before their fragmentation and template removal via sonication and exposure to the Piranha solution.

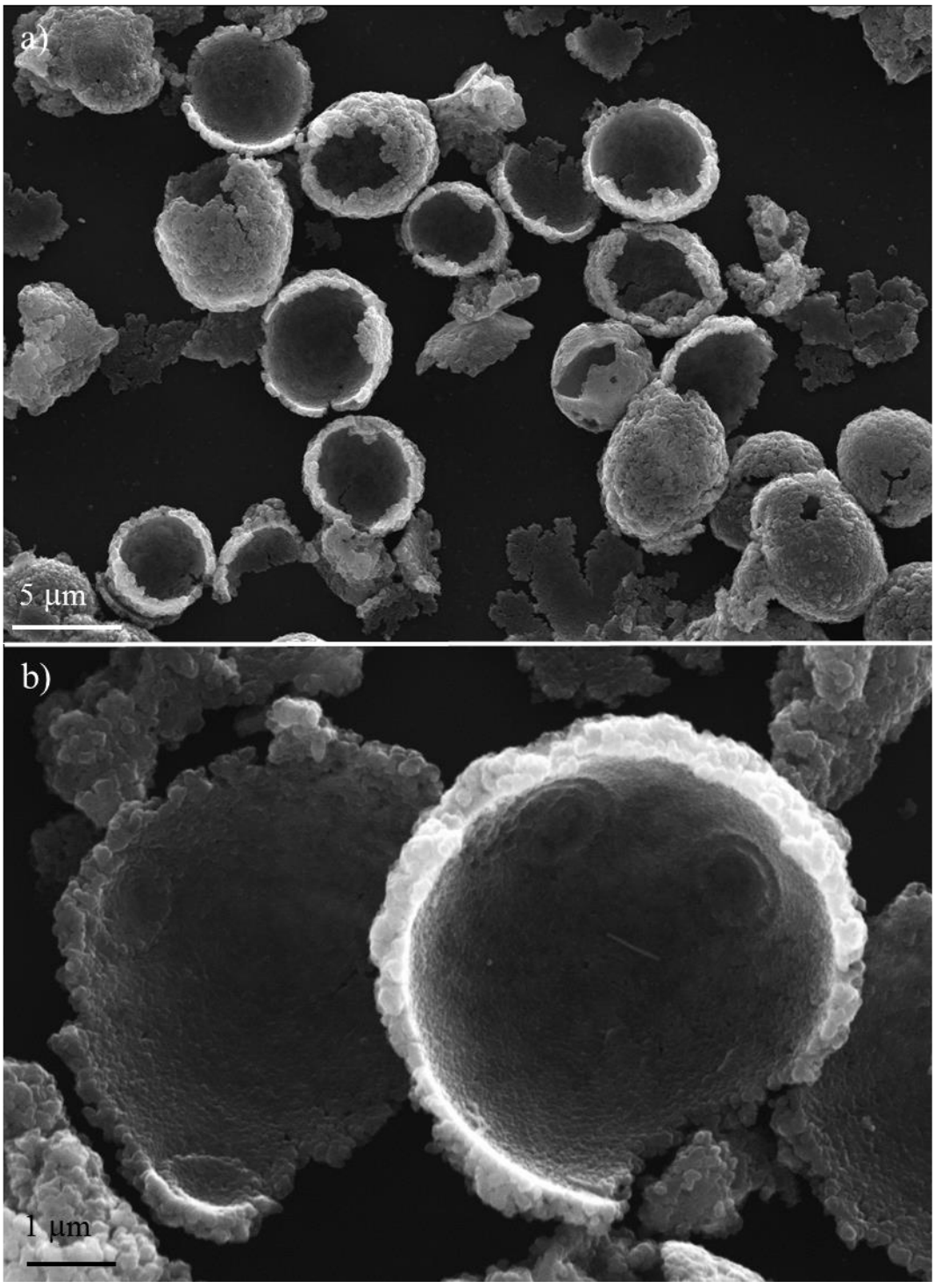

Figure 4-3 SEM images of negative replicas of a yeast cells after treatment with Piranha solution. Note detailed replication of the budding scar on the cell on the lower image.

4.1.3 Synthesis of Silica – Gold Nanoparticle Composite Nanoshells using Yeast Cell Templates, Shell Fragmentation and Removal of the Cell Templates

Gold nanoparticles were synthesised following the method in Section 2.3.5. The average size of the AuNP which were synthesized for the purpose of the pre-coating of the yeast cells was 10.38 ± 0.82 nm (see Figure 4-4). The AuNP coating of the yeast cells resulted in the formation of a dense layer with some nanoparticle aggregates which often reached the size of 30-40 nm. According to Khlebtsov *et al*. such sizes allow for the highest absorption in the visible spectrum in which the laser employed in the selective killing experiments operates.[16]

The synthesis of the silica negative replicas with integrated AuNP was performed in the same manner as the synthesis of negative silica replicas without the AuNP addition but with the additional initial AuNP-coating step onto the test cells and led to the formation of very similar nanoantibiotic fragments of equivalent wall thickness. In contrast to the usual colourless suspension of particles, the resultant AuNP-doped negative replica suspension displayed a characteristic purple-red colouration due to the colloidal scale of the embedded gold nanoparticles (Figure 4-5).

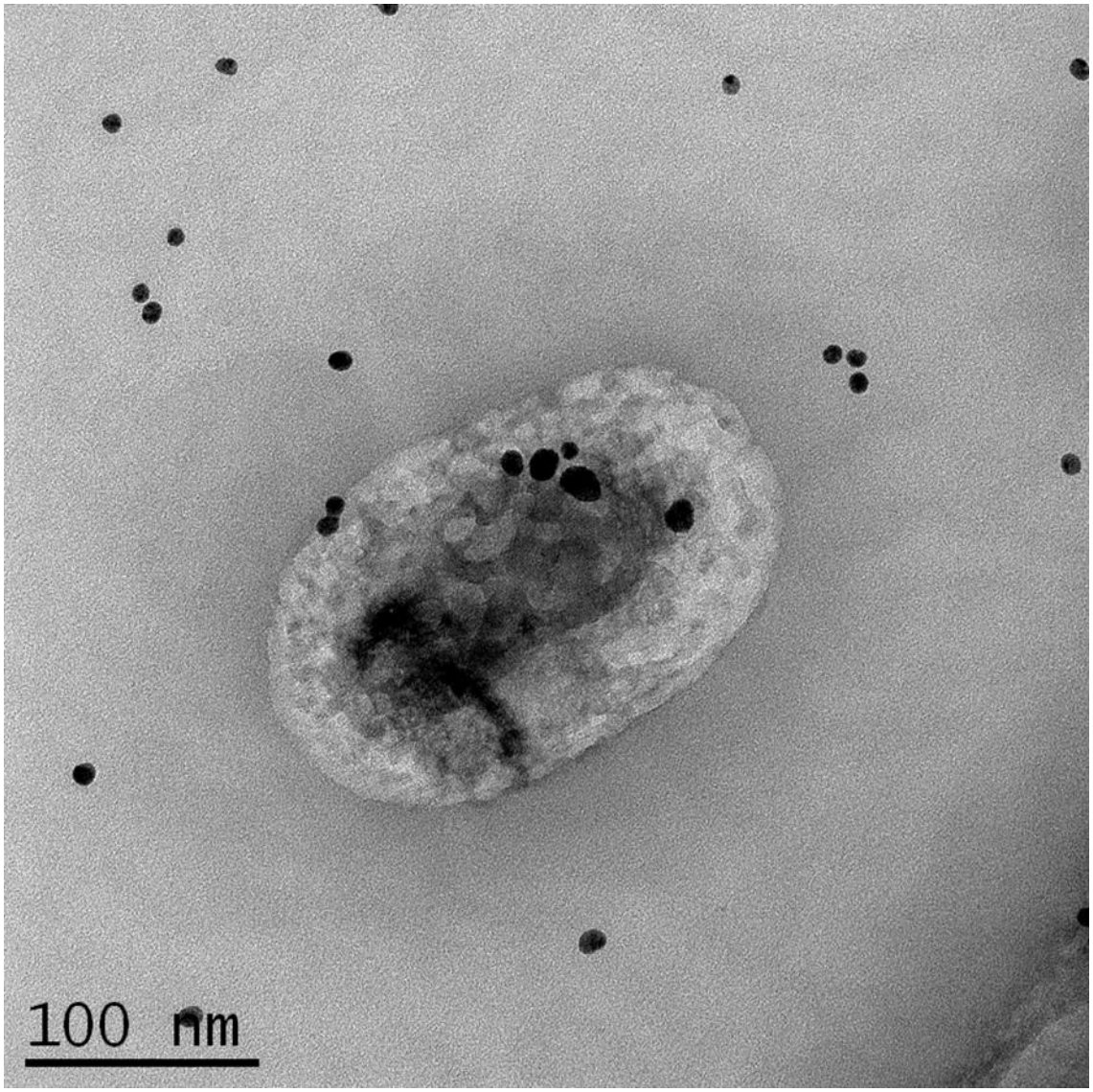

Figure 4-4. TEM image of AuNP synthesized for the purposes of fabrication of nanoantibiotics capable of killing their biological targets. The AuNP are the small black spheres – the large oval in the centre is an imaging artefact.

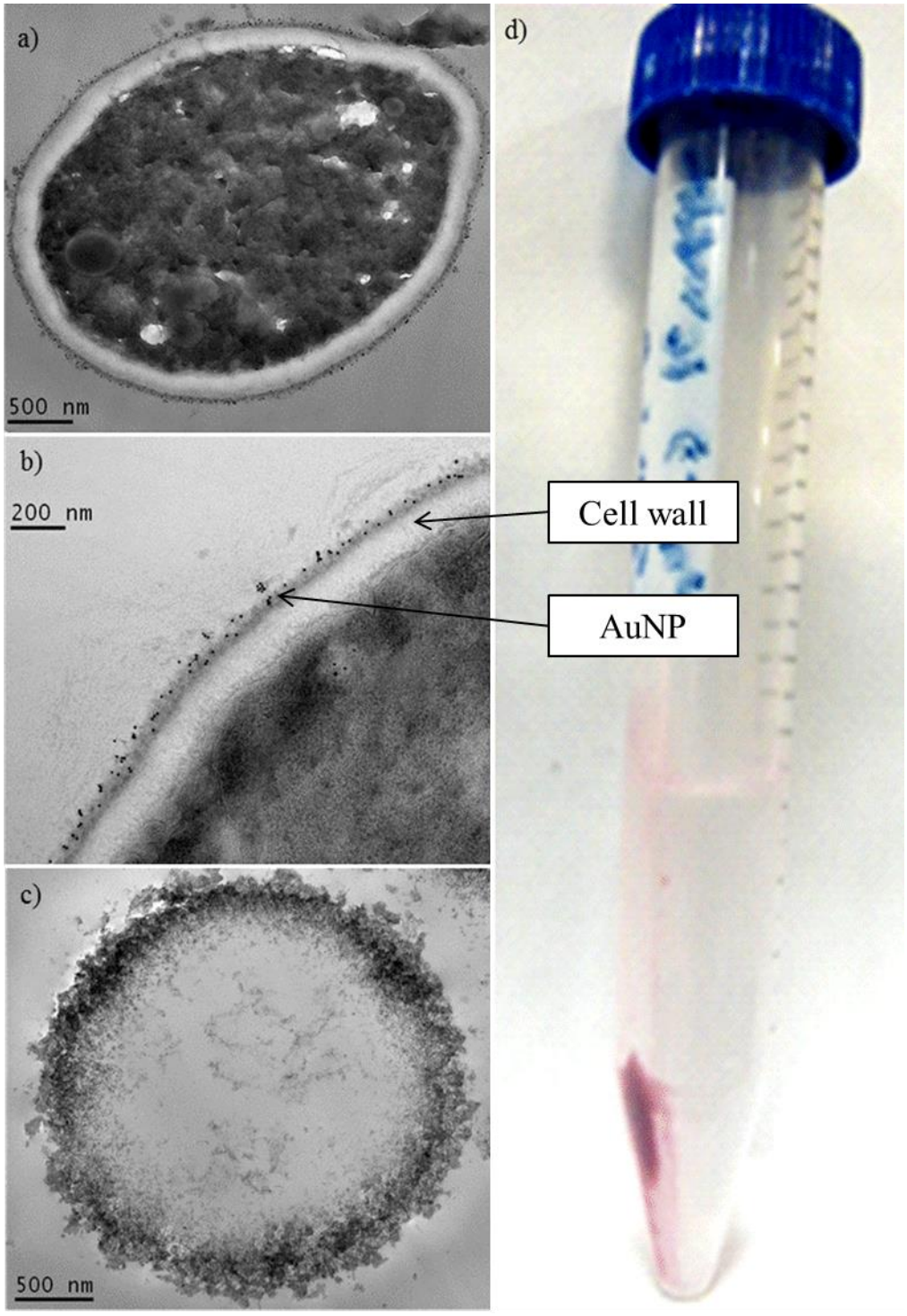

Figure 4-5. The fabrication of silica nanoantibiotics doped with AuNP. The TEM images (a) and (b) show the layer of the AuNP prior to the deposition of silica. The TEM image (c) shows a fragment of the silica shell with integrated AuNP after the bleaching of the yeast cell templates with Piranha solution. (d) A plastic vial with the purple sediment of AuNP doped partially fragmented silica nanoshells.

4.1.4 Synthesis of Silica Shells using Bacterial Templates, Shell Fragmentation and Removal of the Bacterial Templates

The method followed above for deposition of silica nanoshells onto yeast cells was followed again for the fabrication of silica nanoshells using *B. subtilis* templates. This resulted in the formation of core / shell particles with a shell thickness of ~ 70 nm. This relatively low shell thickness was probably responsible the low structural integrity of the imprints which manifested itself by the disintegration of the imprints into very small fragments after the application of the Piranha solution in order to bleach out the bacterial templates (see Figures 4-6. and 4-7.). These experiments have proved the applicability of the deposition method for the fabrication of bacterial imprints. Further optimization of the function of different concentrations of the silica precursors would be needed to address the shell thickness and achieve reducing of the brittleness necessary to produce larger fragments.

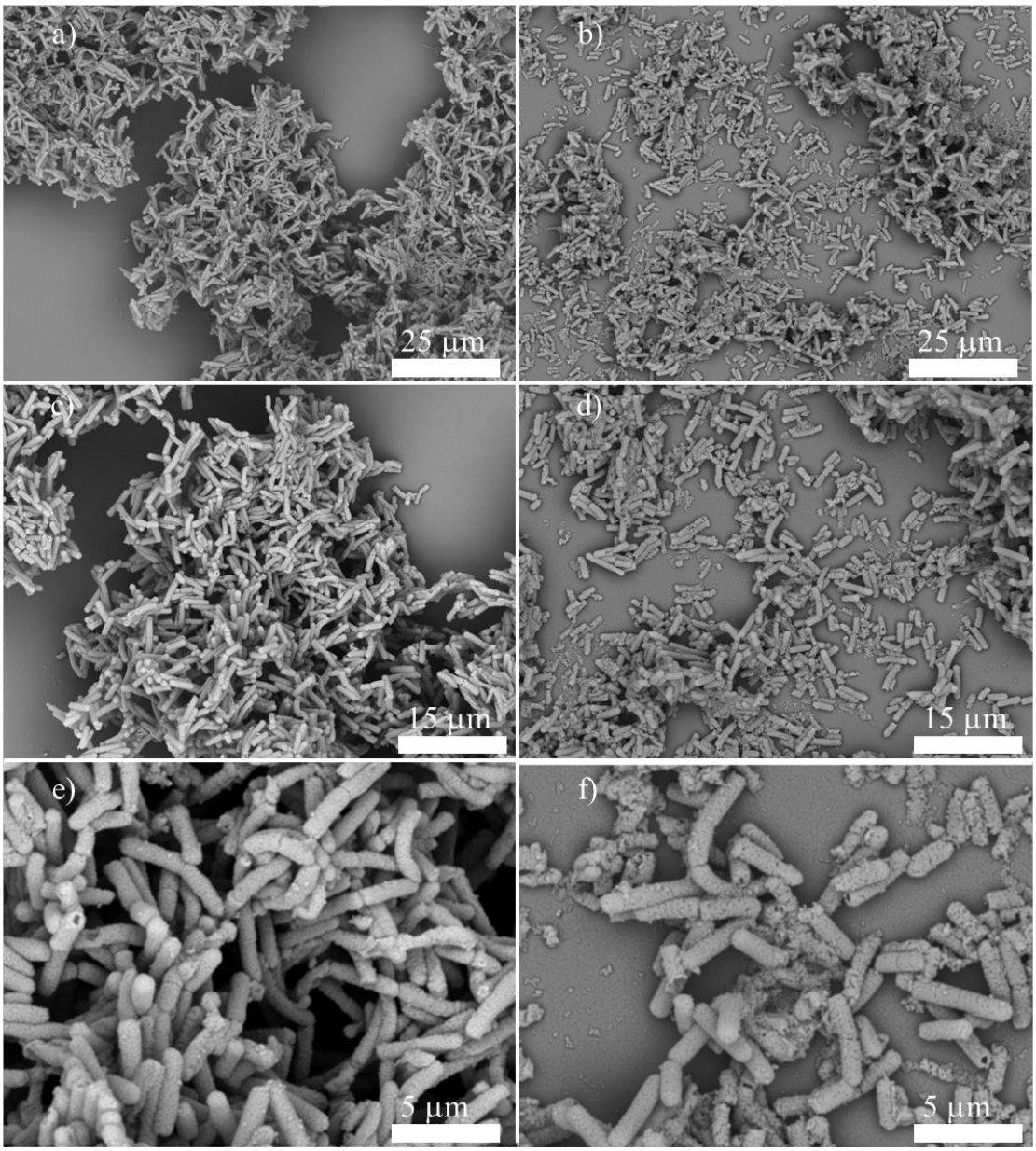

Figure 4-6. SEM micrographs of *B. subtilis* cells coated with silica. Images a), c) and e) show the core/shell particles before the exposure to Piranha solution whilst the images (b), (d) and (f) show the same sample after the bleaching of the bacterial cells with Piranha solution.

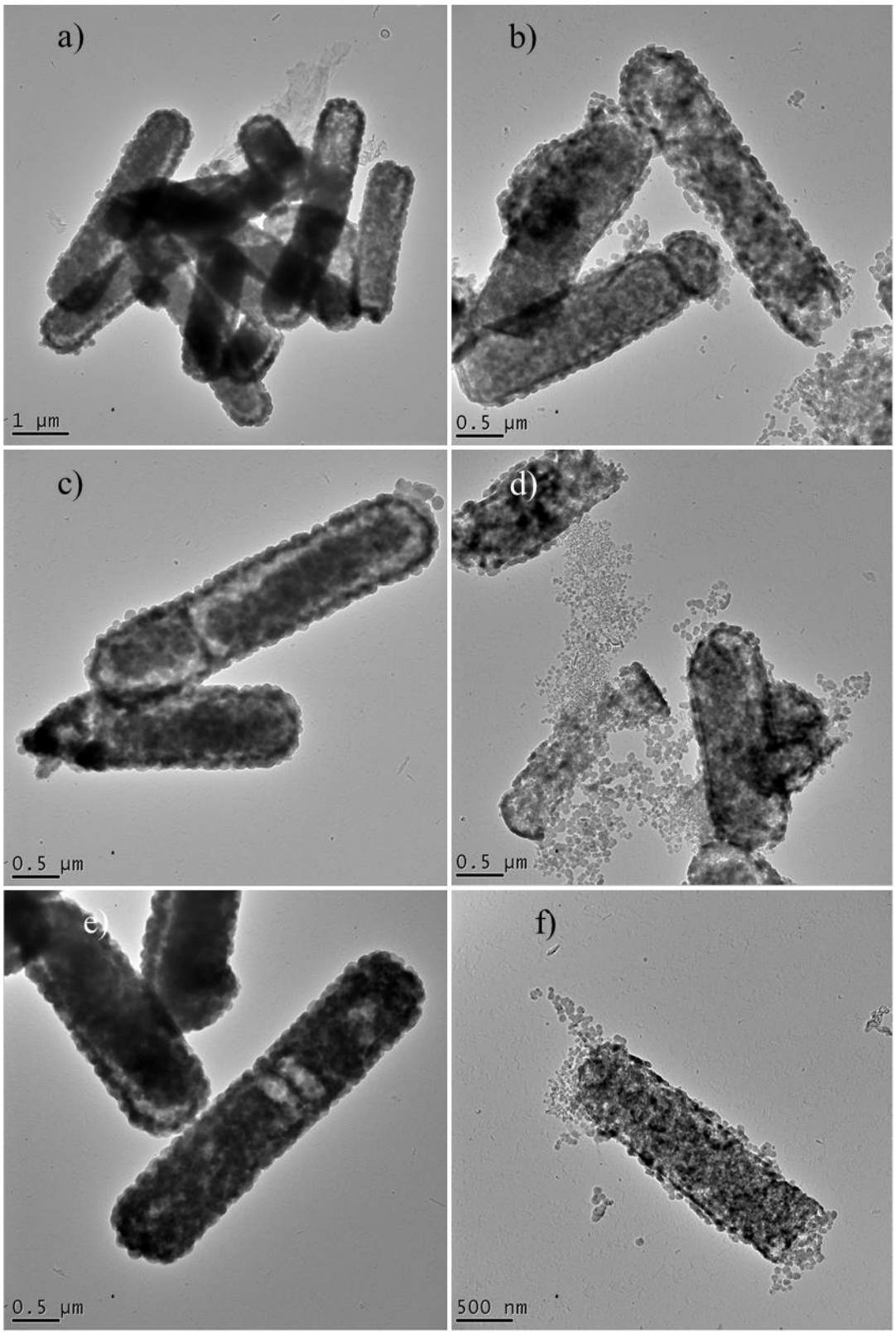

Figure 4-7. TEM micrographs of *B. subtilis* cells coated with silica. Images (a), (c) and (e) the core/shell particles before the exposure to Piranha solution whilst the images (b), (d) and (f) show the same sample after the bleaching of the bacterial cells with Piranha solution.

4.2 Fabrication of Zinc Sulfide Shells using Yeast Cell Templates

4.2.1 Silar Method

Zinc sulfide shells were fabricated on yeast cells using the methodology given in Section 2.3.3.1. The use of layering the yeast cells with different numbers and orders of polyelectrolyte layers prior to zinc sulfide deposition was investigated.

Yeast cell / ZnS core / shell particles were fabricated. No significant effect of the cell template pre-coating with polyelectrolyte layers on the final result was observed. In the course of the work it was established that the deposited ZnS was birefringent and cross-polar microscopy was hence used to reveal the deposition process. For an example of ZnS shell deposited onto native yeast cells see Figure 4-8. As described in the Experimental chapter, an increased aggregation of the core/shell particles was seen when the number of cycles involving the coating with ionic layers was higher than three. It is suggested that this was caused by a formation of an ion bilayer which screens the charge of the templates and renders the colloidal system unstable. The third cycle was probably critical as this was when a full encapsulation of the yeast cells was achieved. This challenge with the cell aggregation seemed to limit the thickness of the possible ZnS shells which lead to limited rigidity and ability of the shells to "remember" the shape of their cell templates. This was noticed by inspecting SEM images of the core/shell particles displaying a "wrinkled" morphology of the desiccated yeast cells.

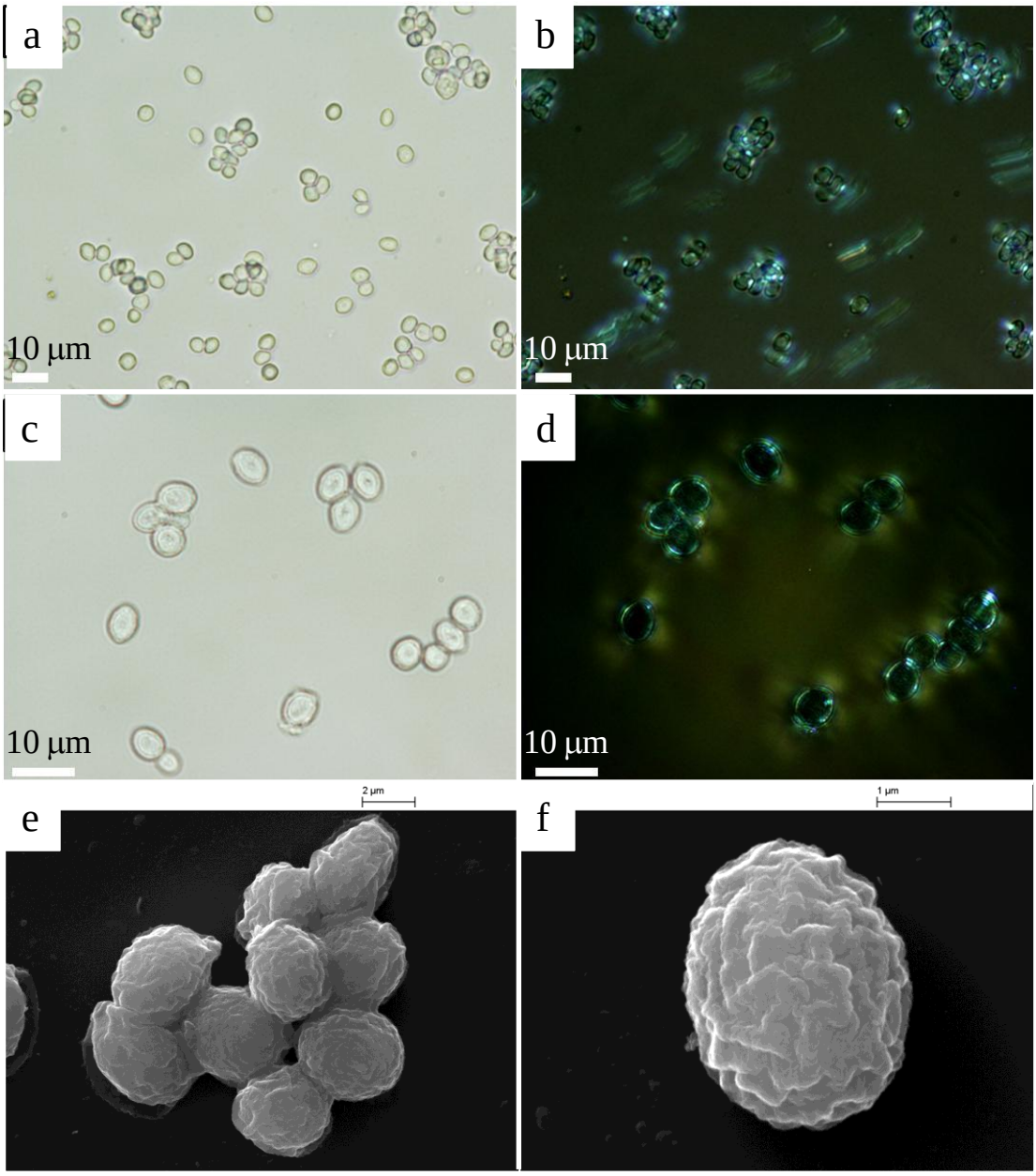

Figure 4-8. Native cells which were treated using the SILAR technique. Bright field image (a) and cross-polar image microscopy image (b) were taken under 50x magnification. Bright field image (c) and cross-polar image microscopy image (d) were taken under 100x magnification. Images (e) and (f) were taken using SEM.

4.2.2 Gel Matrix Method for Producing Zinc Sulfide Shells

Because of the challenges associated with the SILAR deposition it was decided to take a different approach to the ZnS shell deposition. The Gel matrix method as described in Section 2.3.3.2 was followed. High quality yeast cell/ZnS core/shell particles were obtained using the directed deposition of the shell-forming material in the gel matrix which was also responsible for the relatively high monodispersity of the resulting ZnS shell species. No relation between the polyelectrolyte functionalisation of the yeast cells and the quality of the coating was observed using optical microscopy and scanning electron microscopy. The SEM images of the core/shell particles showed no difference between the resultant shell thicknesses in the samples regardless of the different target thicknesses, with ZnS deposits being about 0.2 μm thick (see Section 2.3.3.2 for the layout of the experiments). The SEM micrographs also revealed "lumpy" morphology on the silica shells which was probably caused by secondary crystallization after insufficient washing of the core/shell particles. See Figure 4-9. for an example images of the formed ZnS shell species.

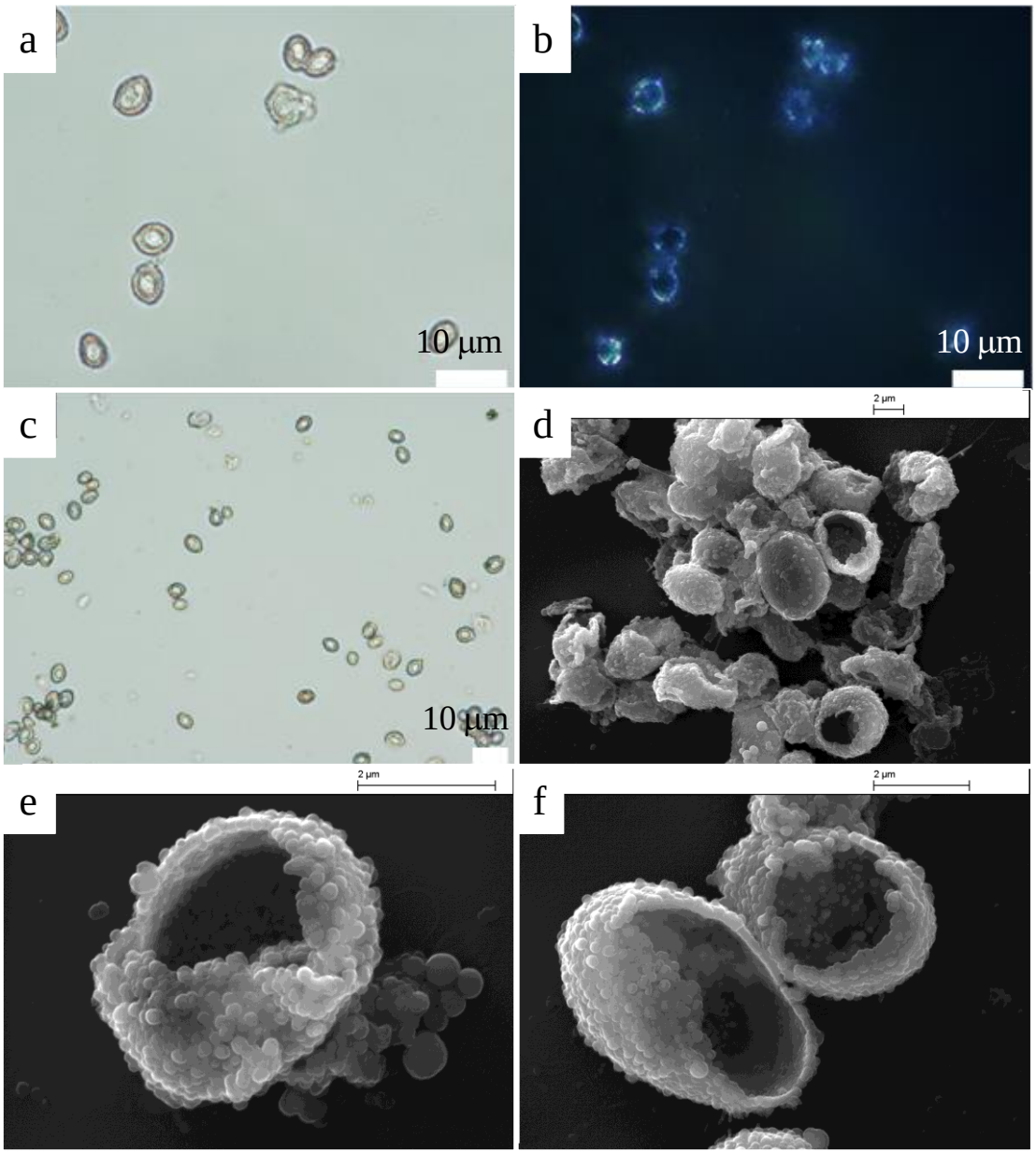

Figure 4-9. Native yeast cells in low melting point agarose matrix exposed to the reaction mixture of TAA and $ZnAc_2$ targeted to produce 2 µm thick ZnS shells. (a) and cross-polar (b) 100x, (c) 50x. Images (d)-(f) were taken using SEM.

4.3 Layer by Layer Encapsulation of Living Cells in Silica Nanoparticles

The yeast cells were successfully encapsulated in polyelectrolyte shells doped with silica nanoparticles. The capsules exhibited grainy features on their surface which were very similar to those reported by Fakhrullin *et al.* who encapsulated the cells in metal nanoparticles (Figure 4-10). Similarly to the results of Fakhrullin and co-workers, the capsules displayed relatively poor structural rigidity. The SEM pictures show the cells

which were desiccated as a result of the sample preparation for the SEM imaging in vacuum. These cells shrunk upon drying and their silica coating, relatively to the desiccated cells, collapsed. A similar occurrence has been reported by Holt and co-workers who used a similar encapsulation approach for treating calcium carbonate crystals with nano-cotton fibres.[17] It was reported that these polyelectrolyte / nano-cotton capsules did not retain the exact shape of the crystal templates after their dissolution. Holt *et al.* have however noticeably improved the firmness of the shells by repeating the encapsulation procedure three times. However, the limited capability of "remembering" the size and the shape of the templates indicates that the route of fabrication of nanoantibiotics based on nanoparticle and polyelectrolyte composites is probably not viable.

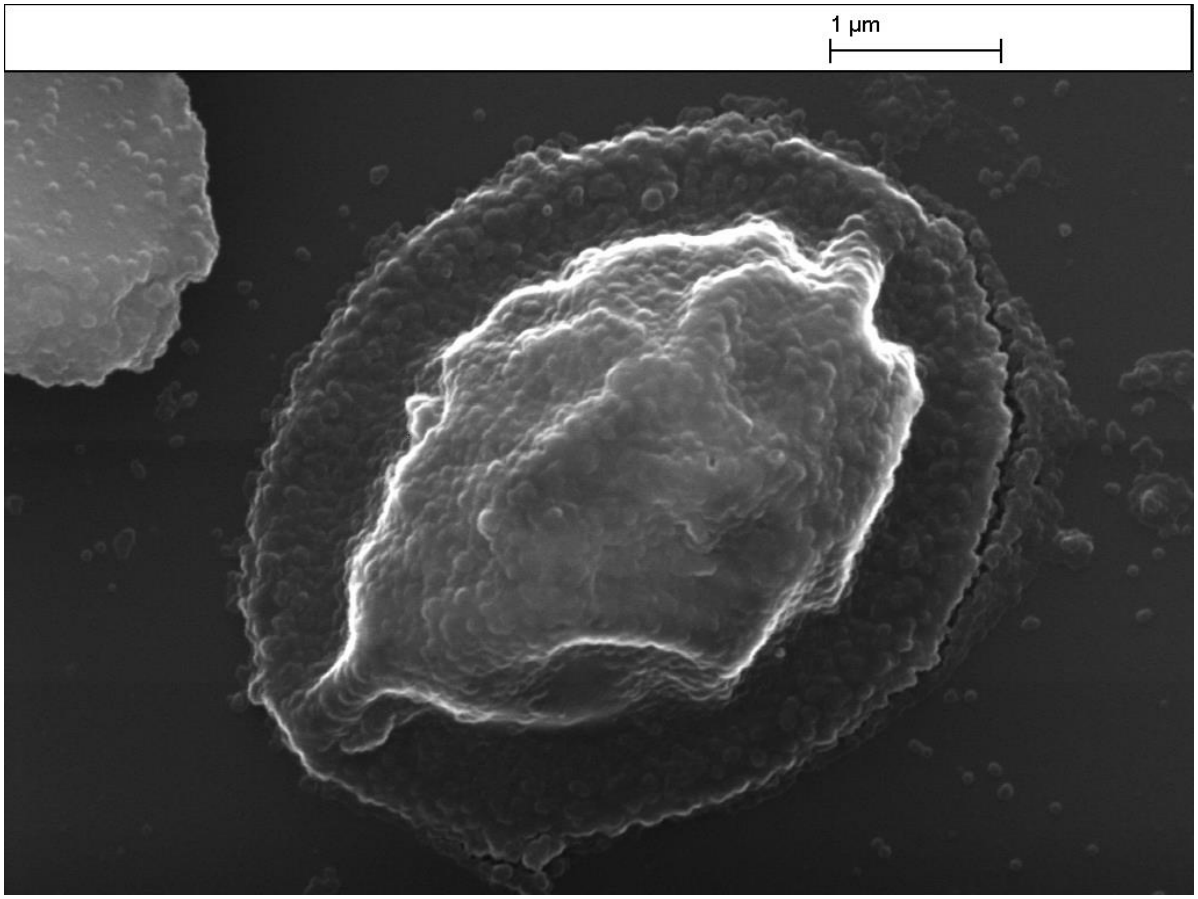

Figure 4-10. A SEM image of a yeast cell coated in silica nanoparticles using the layer-by-layer encapsulation method aided by polyelectrolytes.

4.4 Fabrication of Gold Nanocaps

Gold nanocaps were fabricated following the methods in Section 2.3.5. Deposition of the metal via physical vapour deposition over monolayers of latex particles produced via both GTT as well as GST resulted in the production of good quality gold nanocaps (see Figure 4-11. for examples of the produced monolayers and metal hemi-shells). It was found that removal of the gold-coated monolayer to harvest the gold caps using the sticky tape method was less destructive and yielded better quality gold caps than the scraping method as fewer apparent damaged gold nanocaps were observed.

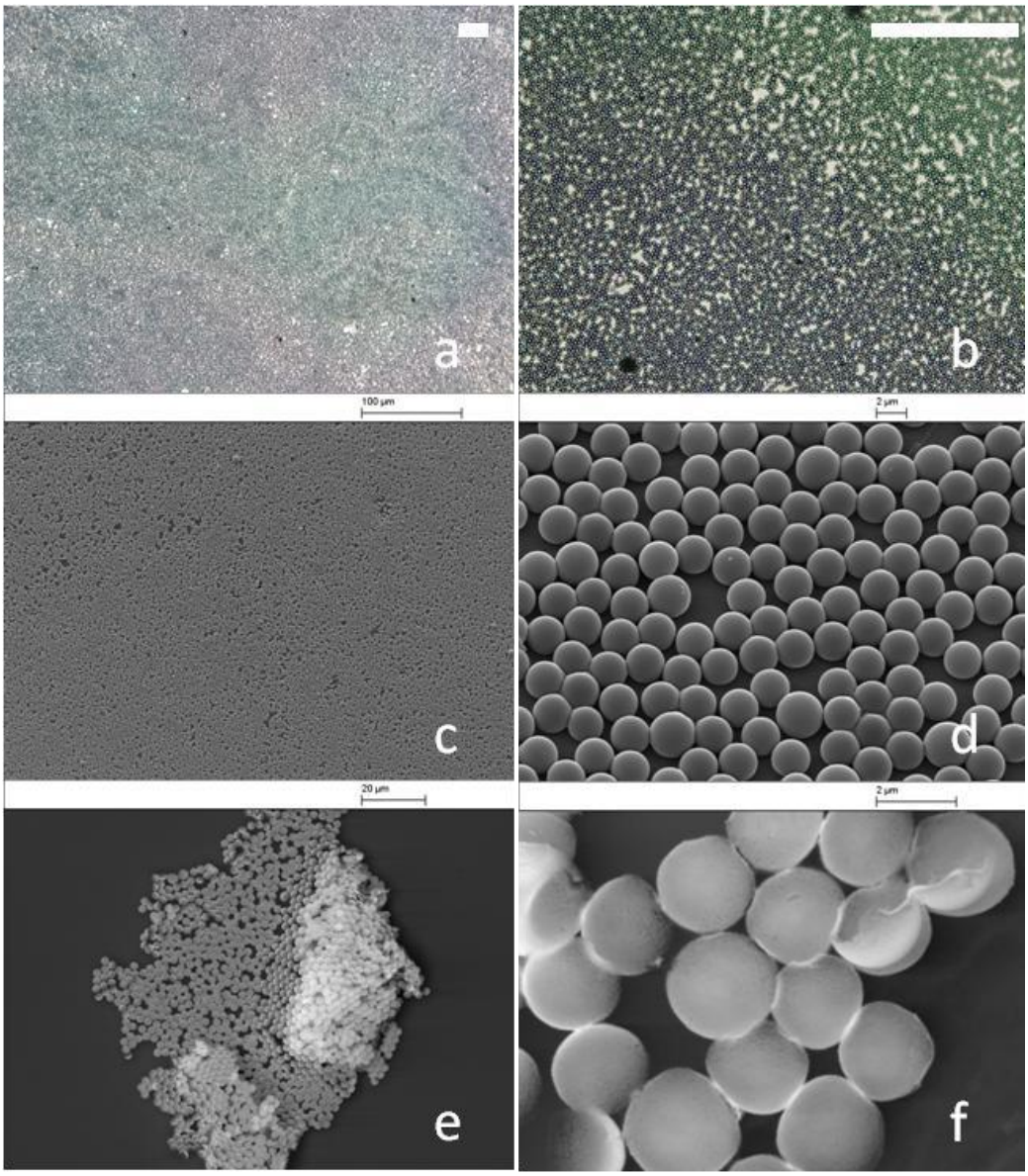

Figure 4-11. Some of the results obtained using the GTT and 2.5 μm carboxyl latex particles. Optical microscopy pictures (a) and (b) (10x and 50x magnification, respectively, the white bar is 10 μm) show a dense monolayer of latex particles formed on an air-water interface. Images (c) and (d), and, (e) and (f), obtained using SEM show the same monolayer and a pile of gold caps produced using the same latex particles.

4.5 Conclusions

The methods of fabrication of core / shell particles proved successful. The silica nanoshell fabrication using the latex microsphere and yeast templates yielded , and were used in further experiments, including the recognition experiments probing the nanoantibiotic recognition capability described in Chapter 5. The silica nanoshells with integrated AuNP were utilized in the experiments which were testing the selective cell killing capability of the nanoantibiotics with their action augmented by localized heating through the photothermal effect. The selective cell killing action of the AuNP-doped nanoantibiotics is discussed in Chapter 6.

The fabrication of the ZnS shell onto test microorganisms via their immobilisation in gel matrix coupled with the slow release of the sulfide ions was shown to be viable. However, this method was not continued for further investigation and research due to the non-uniformity of the ZnS nanoshells produced, and the time it takes to produce them. The fabrication of these shells took 24 h which is far longer than the 3 h procedure for the silica shell fabrication.

The gold hemishell experiments resulted in the fabrication of even nanoantibiotic particles with high resolution of their templates. These gold caps were utilised further in the recognition experiments enhanced by functionalization of their inner side with chemical species allowing for antibody-antigen recognition between the nanoantibiotic particles and their matching targets. These experiments are also discussed in Chapter 5.

Overall, deposition of silica nanoshells resulted in the most reliable, inexpensive, and easy-to-produce nanoantibiotic particles for recognition and binding to their target cells. This method was used in the production of the test cell negative replicas and the cell-recognition experiments.

4.6 References

1. Y. Lu, J. McLellan and Y. Xia, *Langmuir*, 2004, **20**, 3464.
2. D. Weinzierl, A. Lind and W. Kunz, *Crystal Growth & Design*, 2009, **9**, 2318.
3. M. P. Valkonen, S. Lindroos, T. Kanniainen, M. Leskelä, U. Tapper and E. Kauppinen, *Applied Surface Science*, 1997, **120**, 58.
4. S. Lindroos, T. Kanniainen and M. Leskelä, *Materials Research Bulletin*, 1997, **32**, 1631.
5. S. Lindroos, Y. Charreire, D. Bonnin and M. Leskelä, *Materials Research Bulletin*, 1998, **33**, 453.
6. G. Laukaitis, S. Lindroos, S. Tamulevicius, M. Leskelä and M. Rackaitis, *Materials Science and Engineering A*, 2000, **288**, 223.
7. X. D. Gao, X. M. Li and W. D. Yu, *Thin Solid Films*, 2004, **468**, 43.
8. H. Zhou, T. Fan, T. Han, X. Li, J. Ding, D. Zhang, Q. Guo and H. Ogawa, *Nanotechnology*, 2009, **20**, 085603.
9. H. Zhou, T. Fan and D. Zhang, *Microporous and Mesoporous Materials*, 2007, **100**, 322.
10. H. Zhou, T. Fan, D. Zhang, Q. Guo and H. Ogawa, *Chemistry of Materials*, 2007, **19**, 2144.
11. R. S. Mane, B. R. Sankapal and C. D. Lokhande, *Materials Chemistry and Physics*, 2000, **64**, 215.
12. R. F. Fakhrullin, A. I. Zamaleeva, M. V. Morozov, D. I. Tazetdinova, F. K. Alimova, A. K. Hilmutdinov, R. I. Zhdanov, M. Kahraman and M. Culha, *Langmuir*, 2009, **25**, 4628.
13. V. N. Paunov and O. J. Cayre, *Advanced Materials*, 2004, **16**, 788.
14. W. A. Linnemans, P. Boer and P. F. Elbers, *Journal of bacteriology*, 1977, **131**, 638.
15. C. K. Chow and S. P. Palecek, *Biotechnology progress*, 2004, **20**, 449.
16. K. Boris, Z. Vladimir, M. Andrei, T. Valery and K. Nikolai, *Nanotechnology*, 2006, **17**, 5167.
17. B. Holt, R. Lam, F. C. Meldrum, S. D. Stoyanov and V. N. Paunov, *Soft Matter*, 2007, **3**, 188.

CHAPTER 5. ROLE OF SHAPE AND SIZE IN THE NANOANTIBIOTIC-CELL RECOGNITION

In this chapter, we present and discuss the experiments which were designed to test the concept of fabrication of novel antibiotic particles based on shape and size recognition as presented in the Introduction section. Three separate model nanoantibiotic-pathogen systems have been prepared in order to verify the lock-and-key principle using silica nanoantibiotic particles which "remember" the shape and size of yeast cells (*Sacharomyces cerevisiae*) and latex microspheres. Additionally, recognition between gold-based nanoantibiotics and their latex templates was also studied.

The first system, which was designed to probe the importance of shape in the recognition between targets and their negative nanoshell replicas, was constructed from negative replicas of yeast cells and their biological counterparts. The negative replicas were fabricated from silica by producing yeast cell core / silica outer-shell particles which were disrupted via ultrasonic agitation and bleaching of the original cells. The interaction between the nanoantibiotic particles and their matching cells was further augmented by coating them and the cells with polyelectrolytes.

The second system was chosen to test if there is a preferential recognition of targets of matching size as well as shape. In order to ensure that the shape of the model targets was the same, three different sizes of the same type (CML) of latex microspheres were used and silica shells were made using the intermediately sized latex particles as templates. The silica nano-imprints were made via the preparation of latex / silica - core / shell particles, their fragmentation via ultrasonic agitation and dissolution of the latex cores in toluene, in a similar method used with the yeast cells. The three differently sized particles and the partially fragmented silica shells were then combined, first separately, that is by combining only one size of targets with shells, as well as secondly as a mixture of the three sets of latex particles with the silica imprints in order to simulate a real biological system.

Thirdly, the nanoantibiotic recognition action was assessed by examining the selectivity of the recognition of silica nanoantibiotic particles fabricated using ellipsoidal yeast cell templates and a mixture of complementary yeast cells and rod-shaped bacterial cells.

Finally, we also produced a system composed of gold negative replicas of latex microspheres which were functionalised with biotin and their latex microsphere targets which were functionalised with streptavidin. This was done in order to demonstrate the possibility of further increasing the nanoantibiotic-to-target specificity.

5.1 Recognition between Yeast Cell and Matching Nanoantibiotics

The experimental results summarized in this section are based on the simplest model of interaction of nanoantibiotics with test organisms as set out in the introduction. Yeast cells and the partially fragmented nanoshells were incubated together in milliQ water and the recognition incidents were then observed using optical microscopy and fluorescence (see Figure 5-1 for a pictorial representation of the experiments).

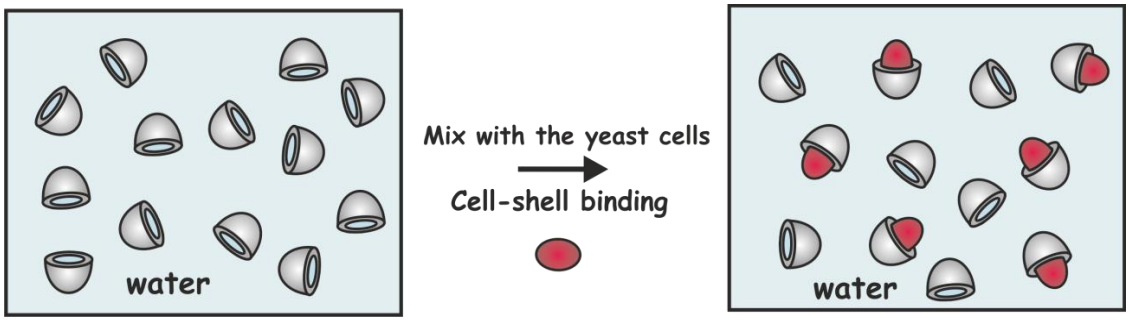

Figure 5-1. The first set of experiments involved the study of the interaction between yeast cell-templated silica nanoantibiotic particles and the yeast cells.

The recognition interaction was additionally augmented and probed by the introduction of different polyelectrolyte coatings to the matching species (see Figure 5-2).

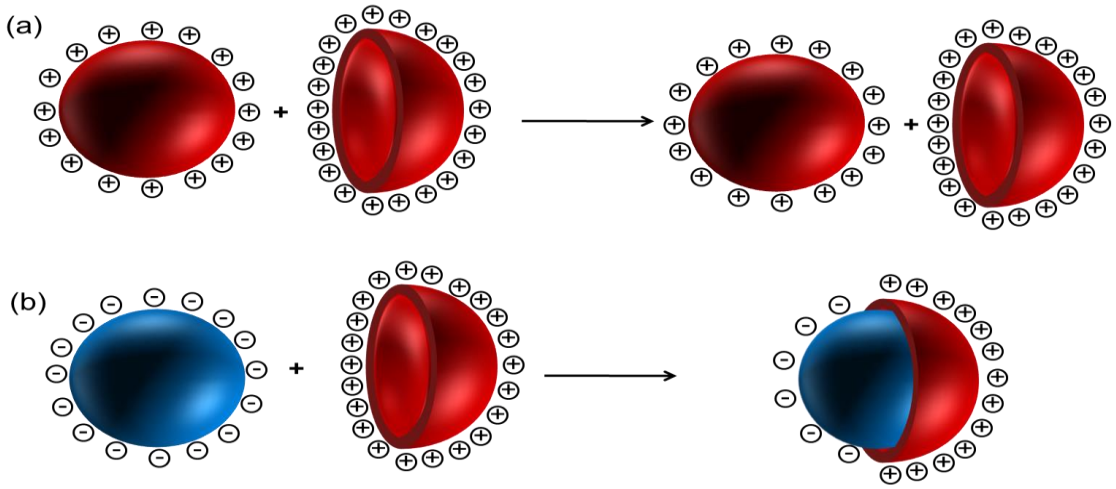

Figure 5-2. The electrostatic (and other) interactions between *S. cerevisiae* cells and their silica shell imprints can be amplified by cell shape recognition: (a) In the case of electrostatic repulsion between the nano-shell inner surface and the cell surface the repulsion is amplified and there is no binding as a result of the shape recognition. (b) The oppositely charged nano-shell and cell are attracted more strongly due to the electrostatic forces upon contact when there is shape recognition. The matching shapes in both cases (a) and (b) amplify the interaction due to the increased area of contact between the cells and the nanoshell fragments when they are favourably oriented to each other.

For the purposes of the study of interaction of the nanoshells and the yeast cell counterparts, the nanoshells were tagged with rhodamnine isothiocyanate (RBITC) while their yeast cell targets were stained with perylene. This was undertaken in order to visualise the recognition incidents as it was realised that the silica nanoshell fragments were often found on the retrograde side of the cell surface in relation the objective of the microscope used. This was probably caused by the shift of the centre of gravity of the cell-nanoshell complex species due to the denser silica, and led to a practical difficulty in registering the successful cell-nanoshell recognition events (see Figure 5-3. for an example of images with nanoshell fragments attached to the retrograde side of the yeast cells).

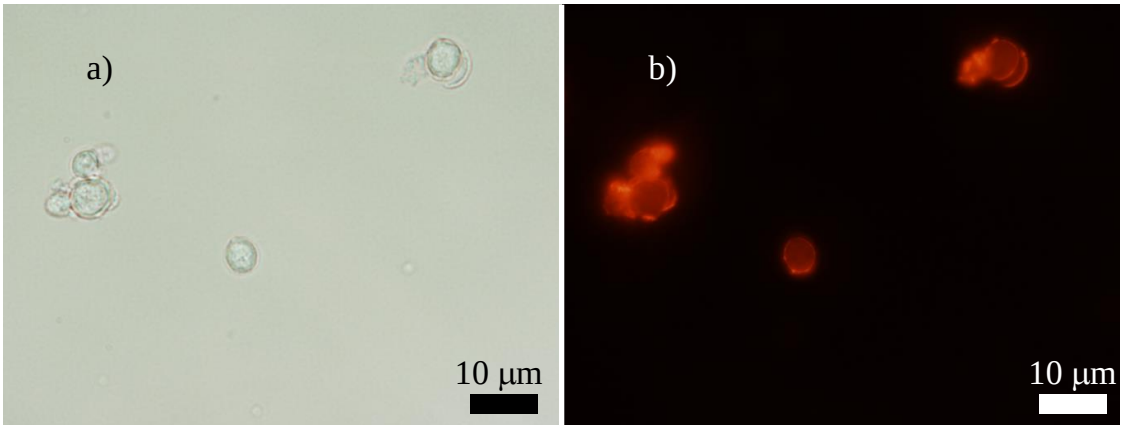

Figure 5-3. A recognition experiment involving PAH-PSS treated yeast cells and PSS-PAH treated nanoshells leading to a match of the nanoshell fragments and their cell targets. (a) The bright field image and (b) its corresponding fluorescence image taken with TRITC filter set which highlights the presence of the nanoshells portray the same situation. The shells cannot be visualised in the bright field image. The images were taken under 100x magnification.

The nanoshell fragments and the cells were coated with monolayers and bilayers of cationic and anionic polyelectrolytes in order to induce attractive and repulsive electrostatic forces between the matching species. We expected that this would enhance or deter the combination of the negative replicas and their targets. The positive surface charge was induced via the coating of the shells or the cells with polyelectrolytes using the layer-by-layer method, where the last coat was done with polyallylamine hydrochloride (PAH), while the negative surface charge was induced using polystyrene sulfonate (PSS) as a last coat. A set of 15 experiments was undertaken with all combinations of available treatments of the yeast cells and silica shell fragments. The yeast cells used: (i) were untreated with polyelectrolytes; (ii) treated with a monolayer of PAH; or (iii) treated with a double layer of PAH and PSS. The silica fragments were (iv) left untreated; (v) treated with a monolayer of either PAH or PSS; or (vi) treated with a double layer composed of each of those two polyelectrolytes in both possible orders. After examining the incubated samples by optical microscopy it was found that, as expected, the species which were coated with oppositely charged polyelectrolytes attracted each other and lead to recognition and vice versa. We also found that the fluorescently tagged nanoshells recognised the natively negatively charged yeast cells as well as the cells rendered positively charged through the modification using PAH.[1]

This is an indication that the RBITC treated shells are possibly zwitterionic due to the presence of both the negatively charged silanol groups, which are native to untreated silica and the anionic hydroxyl groups on the RBITC with which the silica shells had been stained, and the presence of the cationic amine groups from APTES and the quaternary amine and tertiary amine from the RBITC. As expected, there was no effect observed for the order of the coating of the nanoshells with polyelectrolyte layers (see Table 5-1 for a summary of the results).

Table 5-1. Summary of the results of the silica nanoshell-yeast cell recognition experiments. Ticks signify combinations of nanoshell fragments and their yeast cell targets where recognition was observed; the crosses signify no observable recognition.

Cell treatment	Shell treatment	Number of cells	Number of recognitions / mismatches	Mean percentage of recognition to cells ± standard deviation / %	Recognition observed?
-	-	45	40 / 3	89 ± 4	✓
PAH	-	69	68	99 ± 1	✓
PAH-PSS	-	29	26 / 1	72 ± 13	✓
-	PAH	35	28 / 2	80 ± 11	✓
PAH	PAH	-	-	0	×
PAH-PSS	PAH	26	20 / 2	77 ± 10	✓
-	PAH-PSS	-	-	0	×
PAH	PAH-PSS	62	40 / 1	76 ± 9	✓
PAH-PSS	PAH-PSS	-	-	0	×
-	PSS	-	-	0	×
PAH	PSS	33	25	64 ± 18	✓
PAH-PSS	PSS	-	-	0	×
-	PSS-PAH	40	27 / 2	68 ± 13	✓
PAH	PSS-PAH	-	-	0	×
PAH-PSS	PSS-PAH	26	15	58 ±17	✓

The samples were assessed for recognition by imaging with fluorescence microscopy with TRITC (green/red) and perylene (UV/blue) fluorescence filter sets and bright-field microscopy. The images acquired using fluorescence microscopy and their bright field counterparts were then superimposed in order to obtain one composite image and facilitate the analysis of the positions of the shell fragments and the cells. From these images, the total number of cells and the number of cells to which nanoshell fragments had attached were counted. From this the proportion of cell-nanoshell recognition compared to the number of visible cells could be calculated. The values given are estimates of the rate of recognition seen, however they are valid as a guide, whereby the closer the value is to 1, the higher the rate of recognition there is.

A graphical representation of the results is also included in Figure 5-3. It can be seen that the highest rate of recognition interactions between the nanoshell fragments and the yeast cell targets was observed for the untreated nanoshells, regardless of the surface coating of the cells. Note that the thickness of the polyelectrolyte coating may also play a certain role in the recognition events. Although a single layer of PAH or PSS is approximately 1.5 nm thick, a double layer on both PAH and PSS on the nanoshell and the cell has a combined thickness of 6 nm, which may cause a minor shape distortion between the nanoshell fragments and the cells, which are only 5 μm in diameter, thus resulting in less favourable interactions and a lower recognition rate.

We can also expect that other interactions, like van der Waals forces between the matching nanoshell fragments and the target cells, can be strong enough to bind the shells and targets together if their orientation is favourable regardless of their surface charge. We expect that this contribution will play the part of the major effect for untreated cells and or non-treated shells.

In the case of successful recognition, the shell fragments are attached to their cell counterparts via the concave side which corresponds to the largest achievable area of surface contact with the cell and maximal shell-cell adhesion. Our high-resolution microscope observations also revealed that in the experiments where recognition occurred most of the cells did have attached silica shell counterparts (Figure 5-6.).

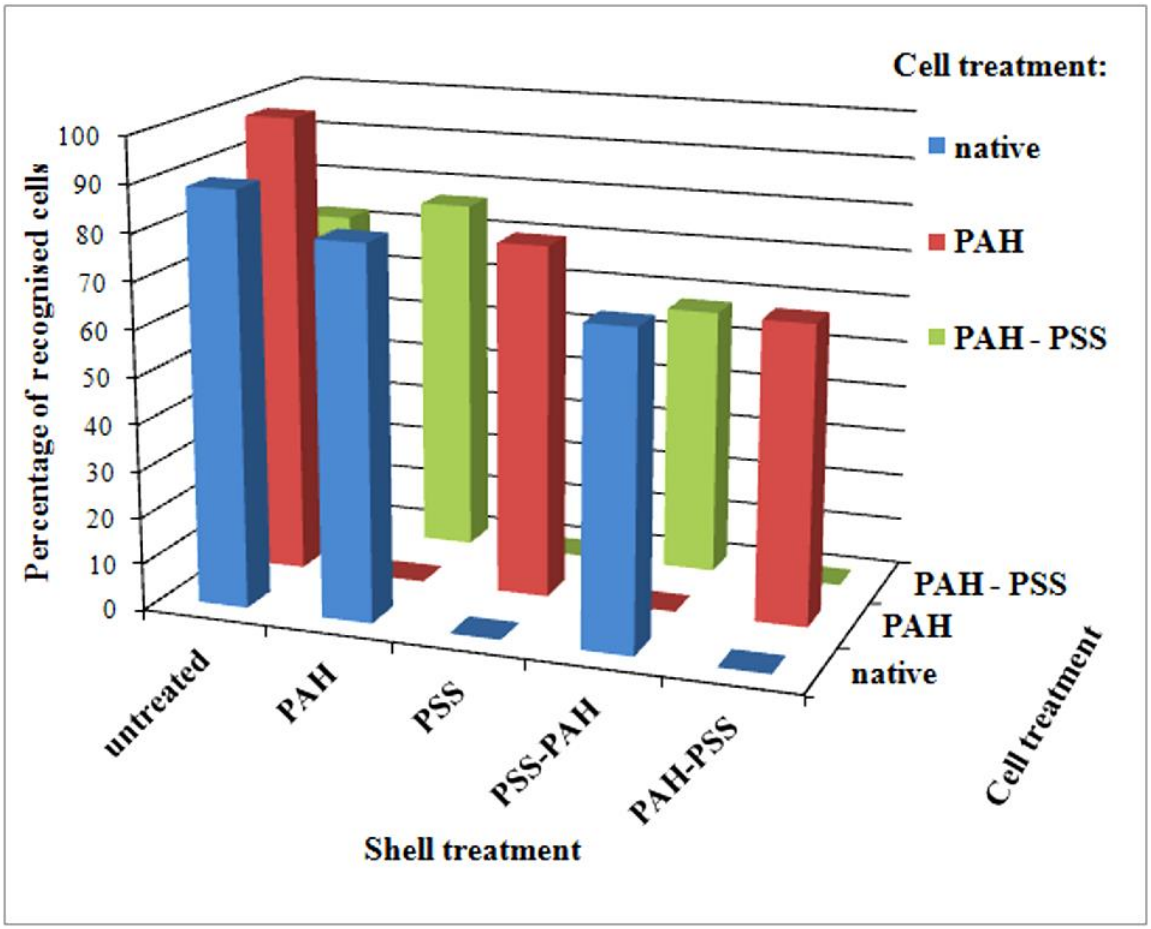

Figure 5-4. A graphical representation of the results of the silica nanoshell – yeast cell recognition experiments (as also presented in Table 1 and 2.).

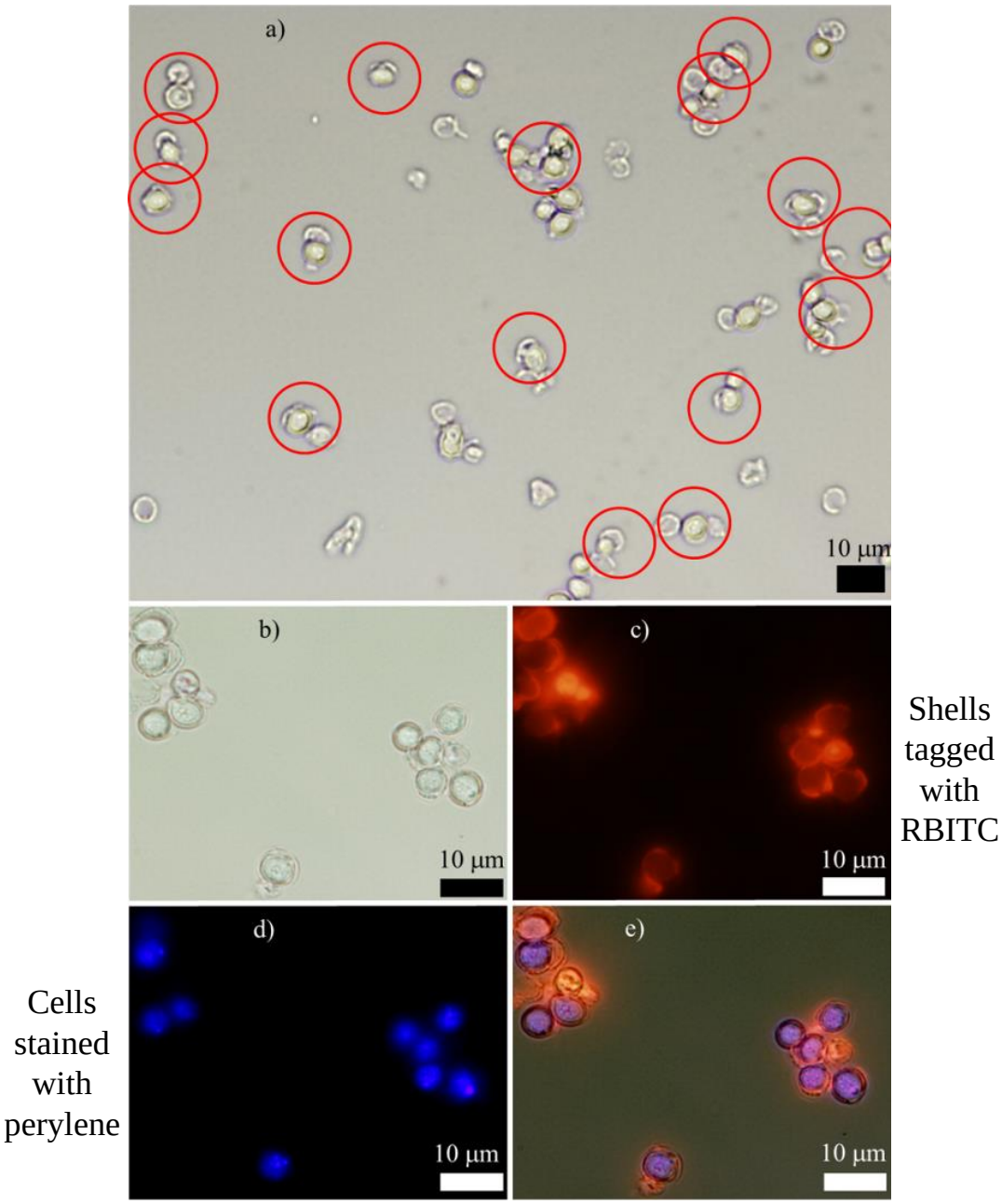

Figure 5-5. A recognition experiment which involved PAH-PSS treated yeast cells and PSS-PAH treated nanoshell fragments leading to a match of the nanoshells and their cell targets. The bright field image (a) was taken under 50x magnification. The bright field image (b), the fluorescence image (c) highlighting the RBITC tagged shells and the fluorescence microscopy image (d) which highlights the perylene treated yeast cells were taken under 100x magnification. The final image in (e) is a superposition of the three previous images, (b), (c) and (d).

It was noted that in all cases where recognition was observed between cells and nanoshell fragments, aggregation of the cell-nanoshell groups was observed, whereby all shelled cells were found aggregated together. This effect was seen to a much greater extent when the cells had a polyelectrolyte coating, presumably due to initial aggregation of cells formed during the coating process. The general effect will be due to the attraction between cell and shell also being present on the outer edge of the shells, therefore, after all of the interactions which are most energetically favourable have occurred, i.e. the binding of the cell to the inner surface of the nanoshell fragment, some of the less favourable but highly possible interactions between the unbound parts of the cell and the outside edges of the bound shells can occur.

After analysing a range of the available images, only a few instances of nanoshell interacting solely via the outer edge with cells were encountered, except in the cases of aggregation previously mentioned (see Table 1. for an overview of these mismatches). An example of a recognition investigation which did not lead to a match between the two experimental species can be seen in Figure 5-6.

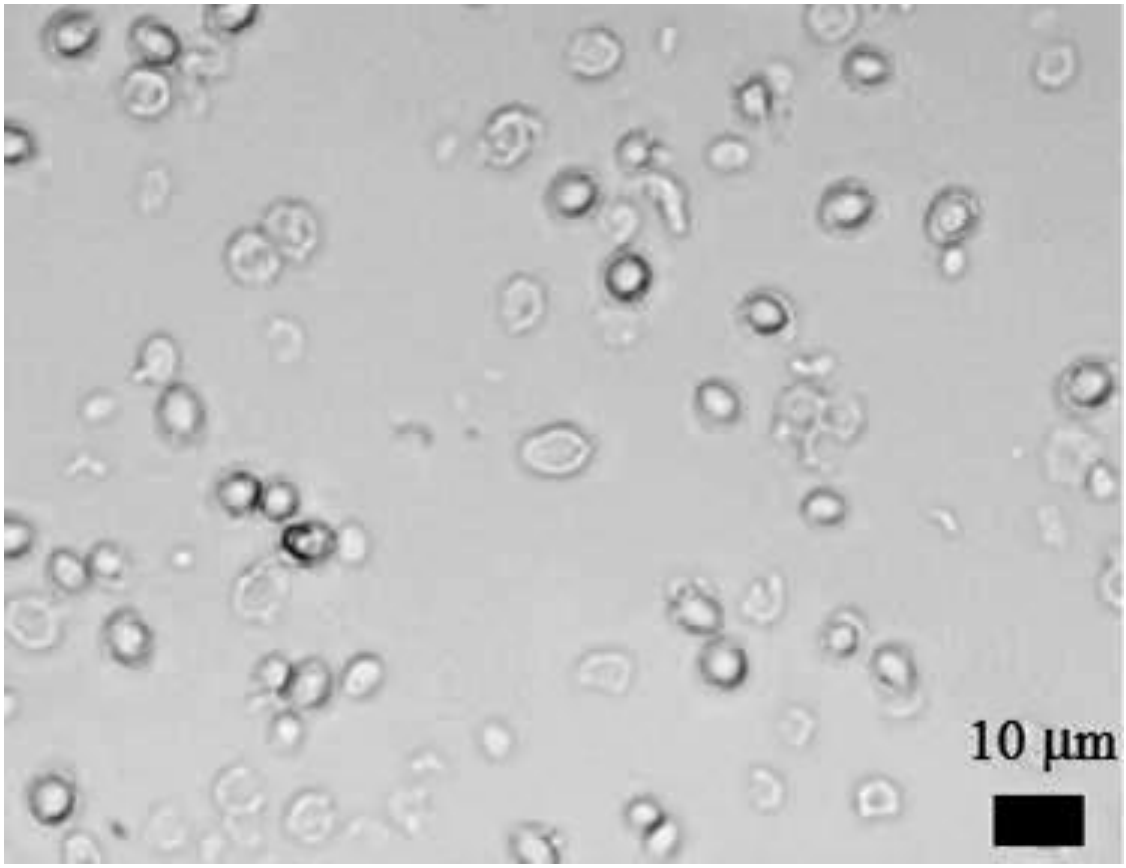

Figure 5-6. A recognition experiment performed using PAH treated cells and PSS-PAH treated nanoshells. Thes shells can be seen floating freely. The bright field microscopy images were taken under 50x magnification.

5.2 Investigation into the Role of the Target Size in the Nanoantibiotic Recognition

Following the successful demonstration of the recognition of the yeast cells by matching silica nanoshell fragments we probed the importance of the negative replica size on the recognition. To simplify the experiments and to exclude the effect of shape variation, we choose to use latex microspheres of three different diameters. We fabricated silica nanoshells using latex microsphere templates which were then incubated with latex microsphere targets that were smaller, larger and equal to the diameter of the original sacrificial latex templates all with identical surface chemistry. This allowed for the investigation role of the size of the targets of the nanoantibiotics in proportion to the nanoantibiotic particles themselves to be exclusively investigated (see Figure 5-7. for the outline of the experiments).

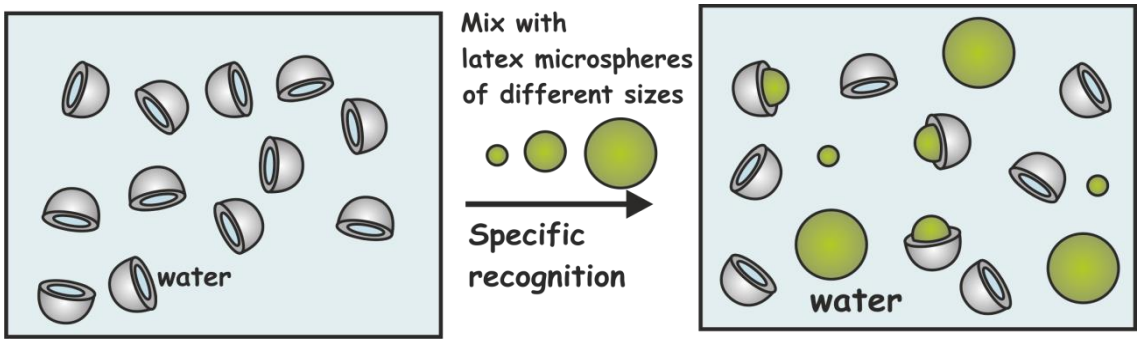

Figure 5-7. Schematics of our experiments probing the role of the target size in the nanoantibiotic - target recognition. The silica nanoshell fragments fabricated using 6 μm sacrificial latex particles were incubated with 3, 6 and 10 μm latex microspheres, respectively.

The silica shells were prepared according to the method of Lu *et al*. using 6 μm CML latex particles as templates which was followed by disruption of the nanoshells using ultrasonic agitation and dissolution of the particles in toluene.[2] Again, the nanoshell fragments were tagged with rhodamine dye in order to allow for their visualisation using fluorescent microscopy. The nanoshells were combined with CML latex microspheres firstly using a single size of particle, of 3, 6 and 10 μm diameter respectively, and then with a mixture of particles of all three sizes, in order to investigate the size recognition specificity of the nanoshell fragments. In the first series of experiments virtually no recognitions between the mismatching shell and microsphere pairs was observed. Very similar results were also noted in the experiments involving the mixture of latex particles of different size. It was seen that a large amount of interaction was observed between the nanoshells and the target latex particles of the matching size (6 μm) and very little was observed between either the smaller (3 μm) or the larger particles (10 μm). See Figure 5-6. for a typical micrograph depicting the scenario where the mixture of the differently sized latex particle sample was combined with the silica nanoshell fragments.

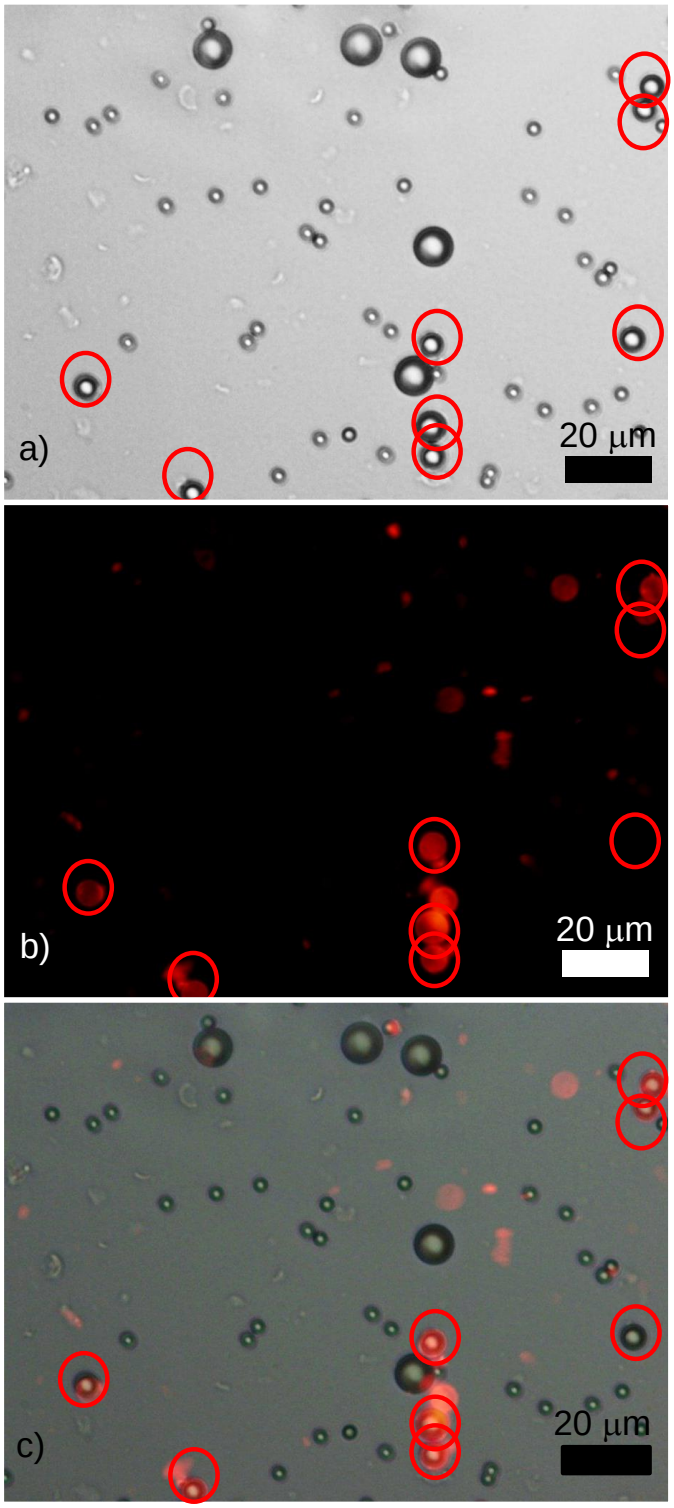

Figure 5-8. A typical result of an experiment where three sets of differently sized microspheres (3, 6, and 10 µm) were combined together with the matching negative replicas (stained with RBITC) of the intermediately sized particles. The optical micrograph (a), and the fluorescent image (b) were taken under 50x magnification, (c) is their overlay. The red circles indicate the location of the intermediately sized particles.

By analysing the images obtained from these experiments it were possible to put values to the frequency of the recognition events. As previously, the numbers only give a guideline to the rate of recognition seen; however the results are conclusive in showing the preferential recognition of the intermediate size particles by the nanoshells, despite the slightly elevated rate of recognitions observed in the other two sizes of latex particles. We analysed a number of images of the incubated silica nanoshell fragments produced by templating 6 μm latex particles with a separate sample of single size latexes. A recognition rate of 93% was found for the scenario where the nanoshell fragments matched the microspheres, whilst the number of mismatches, or "false recognitions" was very low and the recognitions in these cases were between "shapeless", very small fragments (not specific in shape). In order to assess the shape specificity of the recognition and thus simulate a real biological system, 24 images were analysed, each containing on average approximately 41, 9 and 5 of 3, 6, and 10 μm microspheres, respectively, which were dispersed in water together with an excess of 6 μm nanoshell fragments. As in the study of the interaction of yeast – templated nanoantibiotics and the yeast cells, the recognition rate as a percentage of recognition per average image was calculated. The percentage recognition between the shells and the 6 μm target microparticles was found to be 92%, whilst that of the mismatches was about 1% (see Table 5-2. and Figure 5-7. for the summary of the experimental results).

Table 5-2. Summary of the recognition experiments using a mixture of latex microparticles of three different sizes and nanoshell fragments matching the intermediate size particles.

Latex microsphere size / μm	Number of microspheres	Total number of recognitions / mismatches	Mean percentage of recognitions to particles ± standard deviation / %
3	1025	14 / 0	4 ± 2
6	214	193 / 16	92 ± 2
10	114	2 / 1	5 ± 4

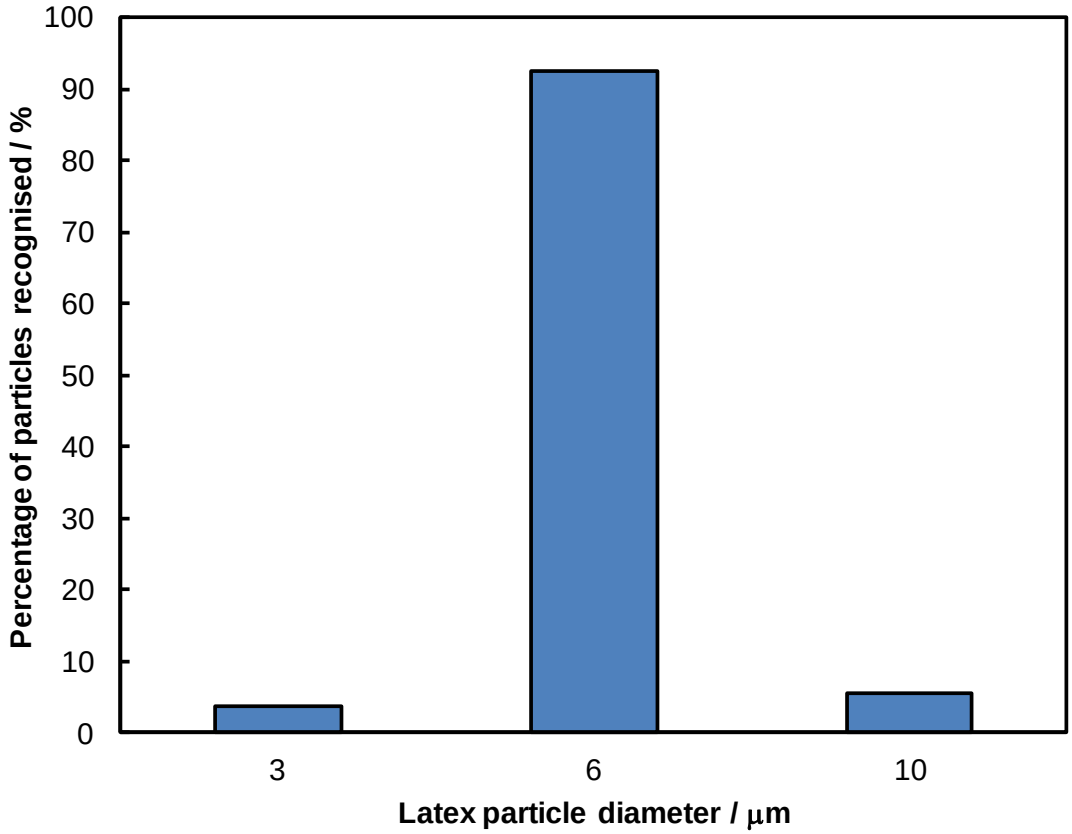

Figure 5-9. A graphical representation of the results from the experiments which investigated the role of the target particle (cell) size in the recognition with a nanoantibiotic system targeting only one specific size (see Table 5-2 for details).

5.3 Investigation of Recognition between Nanoantibiotics and their Targets in a System containing two Microbial Organisms

Following the successful demonstration of the specific recognition of nanoantibiotics and their targets using a simple *S. cerevisiae* – nanoantibiotic configuration and a system consisting the differently sized latex microspheres it was decided to investigate the nanoantibiotic selectivity in a mixture containing two microbial organisms. The role of the nanoantibiotic template / target test microorganism was, again, given to the yeast cells; whilst the part of the other non-matching test microorganism was played by the rod-shaped cells of *B. subtilis* (see Figure 5-10. for a pictorial summary of the experiment).

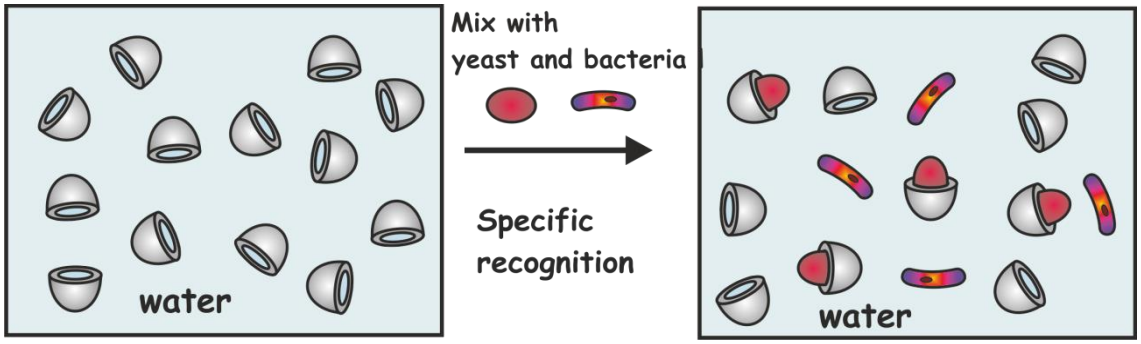

Figure 5-10. Experiments probing the selective action of nanoantibiotics in a mixture of test microbial organisms.

The yeast-templated silica nanoshells were treated with RBITC in the same way as in the experiments involving dual nanoantibiotic-yeast cell interaction. The recognition was, again, quantified in terms of the percentage of recognized cells and the mismatches. We examined fifteen sets of bright field and fluorescence micrographs and their overlays, with an average count of 14 yeast cells and 78 bacterial cells per image being established. An average 85 ± 11% recognition of yeast cells with no mismatches was observed. Apart from very small silica fragments with no specific shape, there was no evidence of yeast-templated nanoshell fragments coupling with *B. subtilis*.

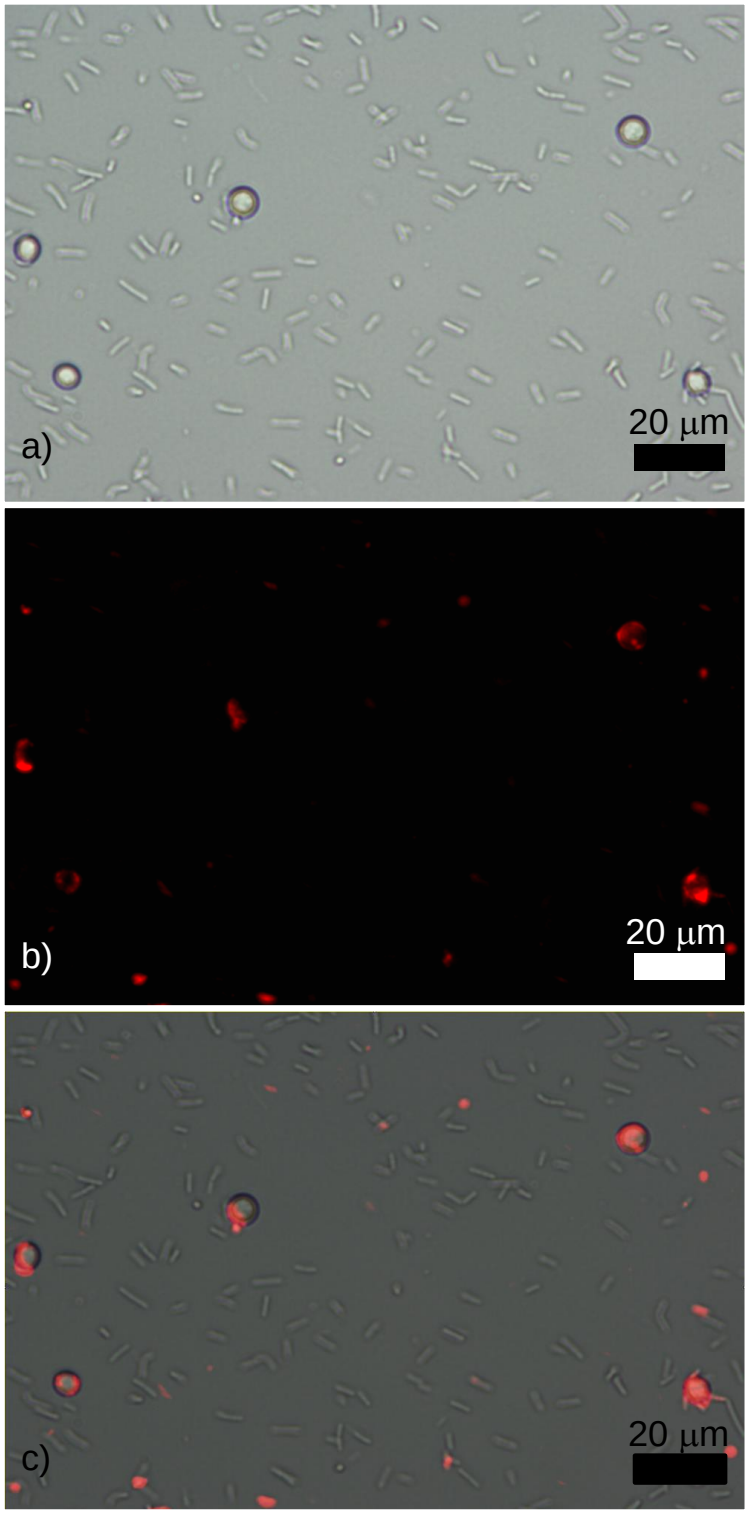

Figure 5-11. Sample results from the experiments involving the combination of bacterial and yeast cells together with the silica nanoshell fragments designed to match yeast cells. The bright field image (a) and fluorescent image(b) were taken under 50X magnification, (c) is the overlay of (a) and (b).

5.4 Specific Recognition between Gold-based Nanoantibiotics and their Latex Microsphere Templates

In real biological systems, pathogens contain antigens which are molecules capable of interacting with specific parts of the immune system called antibodies which, after detecting the specific antigen, trigger an immune reaction.[3] One of the most commonly used models of the antigen-antibody relationship is the interaction between streptavidin (antibody) and biotin (antigen).[4] Streptavidin is a protein which is used widely in molecular biology because of its very specific irreversible bonding to biotin (also known as vitamin H or B_7).

Because of this high binding specificity between streptavidin and biotin it was decided to test the action of the nanoantibiotics by functionalising the nanoantibiotic surface and our test microorganism particles with biotin and streptavidin respectively. We used 2.9 μm sulphate latex microspheres coated with a monolayer of streptavidin as test target particles. Using the GST method we produced gold caps and functionalised them with biotin (see Chapters 2 and 4 for the experimental details and the results of the fabrication of the gold nanoshells, respectively). The two species were then incubated and stirred together in order to examine the role of these specific interactions (see Figure 5-12 for a schematic representation of the experiment). Since gold has a high energy surface and in order to ensure that the particles would attach to the caps from the inside only, the outer side of the caps were treated with polyethylene glycol (PEG) before removing the latex particle templates and producing the gold caps. The grafting of PEGs to a surface is a common strategy of rendering those surfaces protein adsorption resistant.[5] Both in the case of PEG as well as biotin, thiol derivatives were used. The presence of the thiol group led to the construction of self-assembled monolayers of thiol-biotin on the gold surface. This process is driven by the formation of a relatively strong Au-S bond (about 50 kcal/mol).[6] See Section 2.3.8.1 for the functionalization procedure.

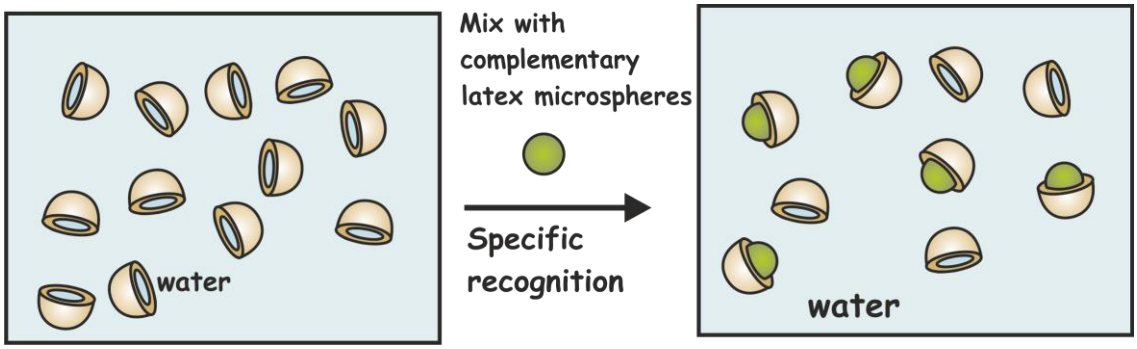

Figure 5-12. Recognition between gold cap nanoantibiotics and their original latex templates. The recognition was augmented by grafting a biotin monolayer onto the inner side of the gold shells and by functionalizing the latex microspheres with streptavidin.

The latex particles were stained with Nile Red fluorescent dye in order to produce contrasting images of the capped and uncapped regions of the spheres.

A number of images which show individual specific binding between the gold caps and the latex particles were produced (see Figure 5-13. for example). However, as the gold caps were not fluorescently tagged it was difficult to assess how many were on the retrograde side of the microspheres and hence rendered "invisible" As the numbers of visible gold cap – latex microsphere was very low, typically tens of the pairs among hundreds of microspheres, statistical analysis of the binding events was not performed. Empirically, however, it was established that relatively small number of gold caps were found unbound to the functionalised spheres but no mismatches were found.

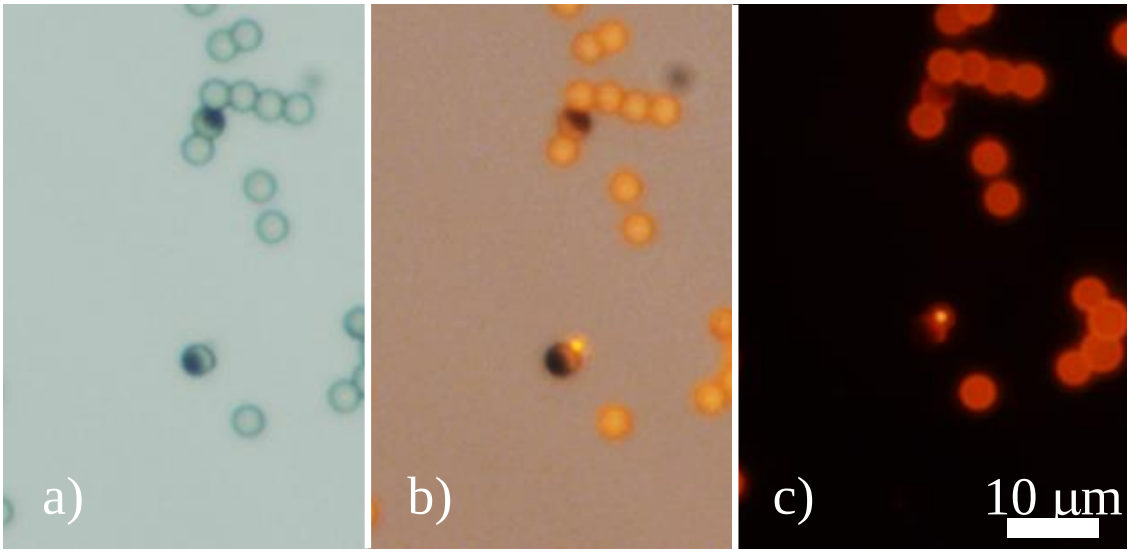

Figure 5-13. Typical results of the combination of the biotin functionalised gold shells which specifically attached to the 2.9 µm sulphate latex spheres covered with a layer of streptavidin. Images (a), (b) and (c) were taken using bright field, combination of bright field and fluorescent and fluorescent microscopy, respectively.

5.5 Conclusions

Silica shells fabricated using *S. cerevisiae* cells and the latex particles demonstrated successfully the concept of nanoantibiotics. These negative replicas were shown to selectively bind to the target particles when it was both electrostatically and geometrically favourable to occur so. An appropriate staining methodology enabled the imaging of these interactions in order to observe and quantify the test results. Observations such as the aggregation of cells and shells in the yeast experiments were successfully explained. We demonstrated the effect of the target particle size by conducting experiments with single size nanoshell fragments and a mixture of target latex particles of different sizes. The specificity of the shells in targeting the appropriately-sized latex particle was demonstrated, with a very strong set of results. We have also showed the specific yeast cells recognition by a matching nanoantibiotic system in a mixture of yeast and *B. subtilis* cells.

The very strong discriminatory behaviour between the nanoantibiotic particles and their targets presented in this chapter has to be, however, in the light of the fact that these experiments were designed as proof of principle. We have observed the interactions of very closely matching shells and their 6 µm latex microspheres and contrasted them

with the recognition events between the much smaller 3 and much larger 10 μm latex microspheres. Similarly, in the study of the recognition properties of the nanoantibiotics in a dual microbial system we have tested the interaction of the imprints of elipsoidal yeast cells, their biological counterparts, and the rod-shaped bacteria. From the perspective of the applicability of the nanoantibiotics in a real biological settings it would be interesting to study the recognition characteristics of the nanoantibiotic particles as a function of their size and shape closeness to the target particless.

Additionally, the results from the experiment which involved combining of biotinilated gold caps and streptavidin latex microspheres demonstrate a pathway towards nanoantibiotic selectivity which can be functionalised to bind more specifically than with polyelectrolyte coatings as in the first three sets of nanoantibiotic-target cell recognition experiments. The passivation of the outer side of the nanoantibiotic particles as demonstrated with the PEG is also a procedure which can be potentially very beneficial.

5.6 References

1. R. F. Fakhrullin, A. I. Zamaleeva, M. V. Morozov, D. I. Tazetdinova, F. K. Alimova, A. K. Hilmutdinov, R. I. Zhdanov, M. Kahraman and M. Culha, *Langmuir*, 2009, **25**, 4628.
2. Y. Lu, J. McLellan and Y. Xia, *Langmuir*, 2004, **20**, 3464.
3. M. T. Madigan, J. M. Martinko and T. D. Brock, *Brock biology of microorganisms*, 11th edn., Pearson Prentice Hall, Upper Saddle River, NJ, 2006.
4. C. J. van Oss, R. F. Giese, P. M. Bronson, A. Docoslis, P. Edwards and W. T. Ruyechan, *Colloids and Surfaces B: Biointerfaces*, 2003, **30**, 25.
5. L. Li, S. Chen, J. Zheng, B. D. Ratner and S. Jiang, *The Journal of Physical Chemistry B*, 2005, **109**, 2934.
6. J. C. Love, L. A. Estroff, J. K. Kriebel, R. G. Nuzzo and G. M. Whitesides, *Chemical Reviews*, 2005, **105**, 1103.

CHAPTER 6. SELECTIVE KILLING OF MICROBIAL CELLS WITH PHOTOTHERMAL EFFECT AUGMENTED NANOANTIBIOTICS

Following the demonstration of the ability of nanoantibiotics to recognize and bind to target cells as described in Chapter 5, here we explore the possibility of fabricating nanoantibiotic agents which would combine their lock-and-key selectivity with a controlled destruction of the target cells. The deployment of gold nanoparticles (AuNP) in the selective killing of cancer and pathogenic cells through photothermal therapy as described in the Introduction chapter was an inspiration in this pursuit. We designed a new type of nanoantibiotic particle based on the integration of gold nanoparticles into the silica nanoshell replicas of target cells. In a proof of principle study, we chose yeast cells as targets for selective killing with photothermal nanoantibiotic particles in a mixture with bacterial cells of the species *Bacillus subtilis*. This chapter demonstrates the feasibility of the concept of selective killing of microbial cells based on shape and size recognition combined with irradiation with laser to induce the photothermal effect.

6.1 Theory

The principle of the action of the gold nanoparticle-enhanced nanoantibiotic agents can be described as follows. The silica imprints with integrated gold nanoparticles specifically bind to the target cells, which is then followed by irradiation with a 532 nm laser giving rise to localized heating around the nanoparticles and thus the killing of the model pathogenic cells. The laser of this wavelength was selected because the gold nanoparticles of the size used in the following experiments absorb strongly at this wavelength and consequently heat up due to the photothermal effect.[1] See Figures 6-1. and 6-2. for schematic representations of the synthesis of these nanoantibiotics, which is described in detail in the part 2.3.2.2 of the Experimental chapter, and of their action.

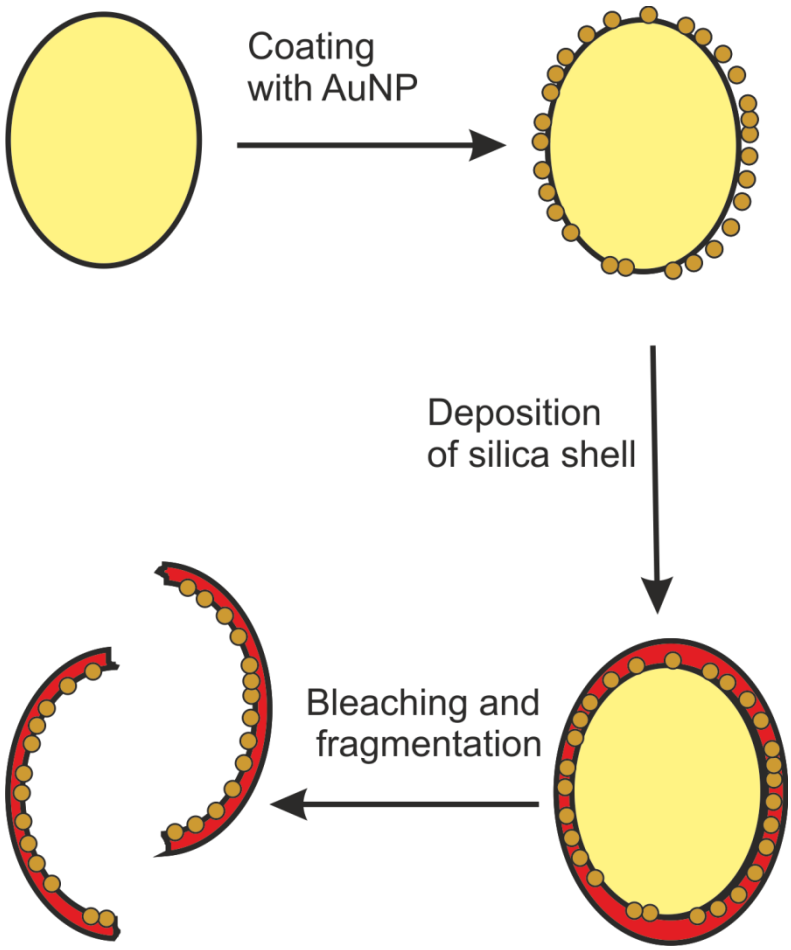

Figure 6-1. Scheme of the synthesis AuNP enhanced nanoantibiotics. The integration of the AuNP into the silica nanoshells is performed by the pre-coating of the template yeast cells with AuNP which is then followed by the deposition of silica and fragmentation of the resulting AuNP-nanoshells combined with the removal of the templates.

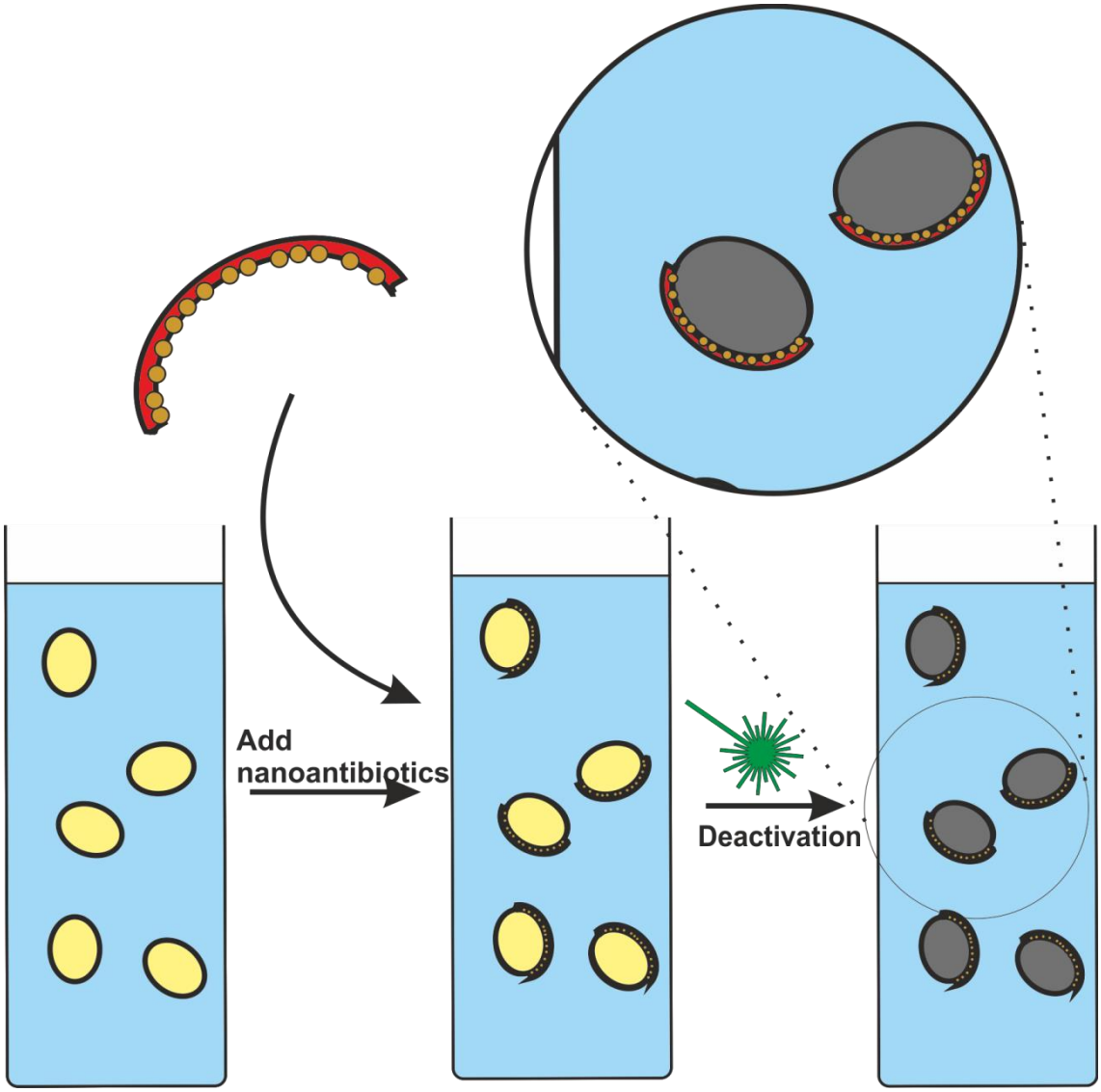

Figure 6-2. Scheme of the action of AuNP enhanced nanoantibiotics. The AuNP-silica nanoantibiotics are introduced into a suspension of their matching microbial cells. Following the selective binding the suspension is irradiated with laser. Deactivation of the matching microbial cells then follows (grey colour signifies dead cells).

6.2 Experimental protocol

Novel nanoantibiotics containing 10nm gold nanoparticles within the silica shell were synthesised using yeast cells as the template, following the method given in the Experimental chapter (section 2.3.2.2). We conducted a series of experiments which tested not only the killing capability of these AuNP enhanced nanoantibiotics but also their selectivity. The killing selectivity was verified by using a dual microbial system

composed of yeast as well as the rod-shaped *B. subtilis* cells. To facilitate the imaging of the recognised tagged yeast cells we tagged the yeast cell selective nanoantibiotics with RBITC in order to localise the individual nanoshell fragments. The viability of the microbial organisms was examined using the fluorescenin diacetate (FDA) protocol which is described together with all the other experimental details of the protocol in Section 2.3.10. FDA is normally a nonfluorescent, nonpolar molecule which is capable of penetrating eukaryotic and Gram-positive bacterial cell walls which is then followed by penetration though the cell membranes.[2] In living cells, the FDA is then hydrolysed by nonspecific esterases resulting in the formation of fluorescein (see Figure 6-3.). Contrary to FDA, fluorescein accumulates inside and renders the cells fluorescent in green when irradiated with blue light.

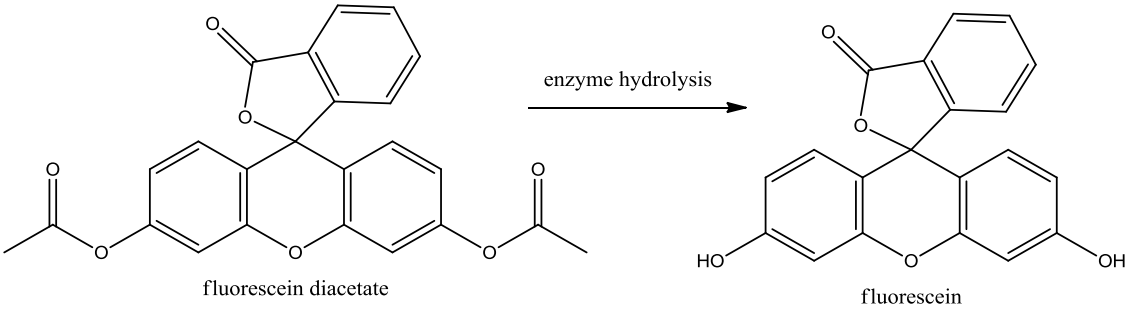

Figure 6-3. Hydrolysis of FDA by esterases results in the formation of fluorescein.

We examined the following effects: (i) the effect of laser irradiation on cells in solution without the novel nanoantibiotics; (ii) the effect of the nanoantibiotics on cells in solution without laser irradiation; (iii) the effect of laser irradiation on non-target cells incubated with the nanoantibiotics; (iv) the effect of laser irradiation on target cells incubated with the nanoantibiotics; and (v) finally the effect of laser irradiation on a mixture of target and non-target cells incubated together with the target-specific nanoantibiotics.

6.3 Viability of Cells upon Irradiation with Laser

The first set of experiments was designed to test the viability of the hydrated yeast cells and the freshly cultivated bacterial cells (*B. subtilis*) after the five minute irradiation with the laser (See Figure 6-4). Once the cell samples were irradiated they were treated with FDA and bright field and fluorescence micrographs of these samples were taken and analysed. See Figure 6-5. for the images of a bacterial and yeast cells where 89 ±

8% and 88 ± 4% of the cells were viable, respectively As expected no effect of combining the two microorganisms in one sample was noted with respect to their individual viability. Figure 6-6. shows a typical set of images of a sample containing a mixture of the two microbial organisms (*yeast cells and B. subtilis*). In this case, the percentage of the viable bacterial cells was 90 ± 4% compared with 92 ± 6% of the viable yeast cells.

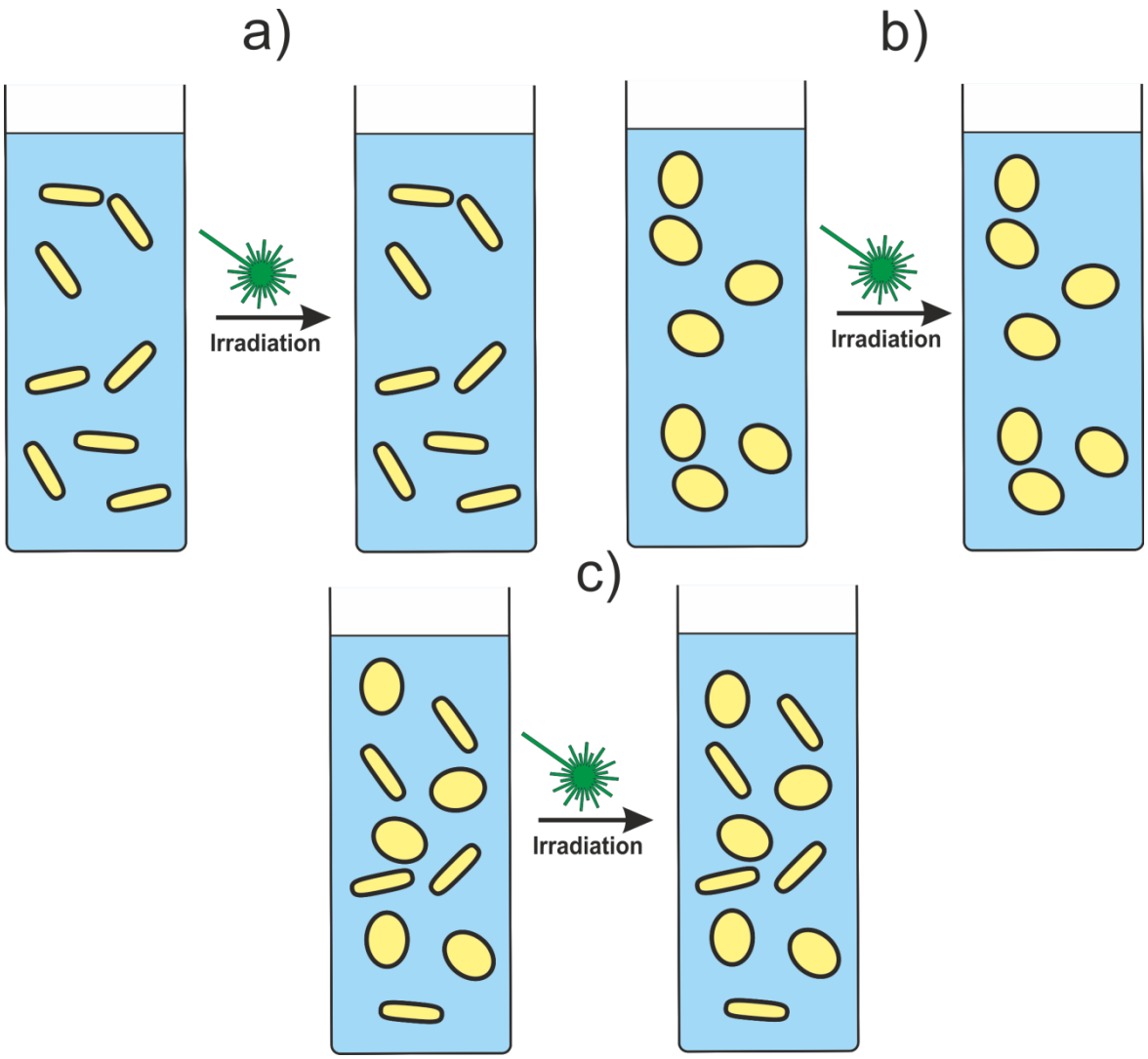

Figure 6-4. Schematics of the control experiments which were designed to probe the viability of the microorganisms before their incubation with the nanoantibiotics. (a) A sample of bacterial cells was irradiated and their viability checked. (b) In the same way the viability of the yeast cells and the viability of the mixture of yeast and bacterial cells (c) was tested.

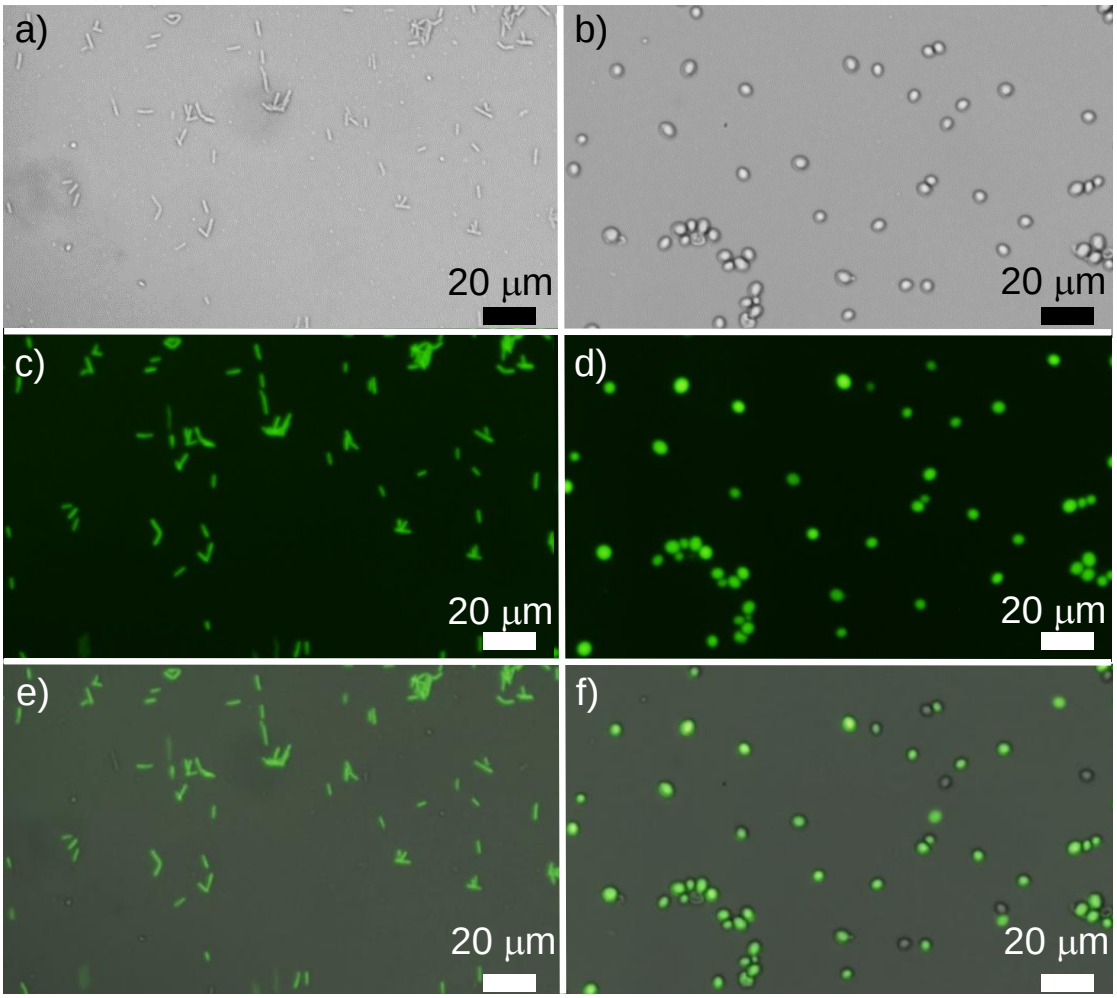

Figure 6-5. Images of the separate bacterial (*B. subtilis*) and yeast cell samples after being exposed to the laser irradiation and treated with FDA. The bright field image (a), the fluorescence microscopy image (c) and their composite image (e) show the bacterial sample. The images (b), (d) and (f) are of the counter parts of (a), (c) and (e) for the yeast cell sample, respectively.

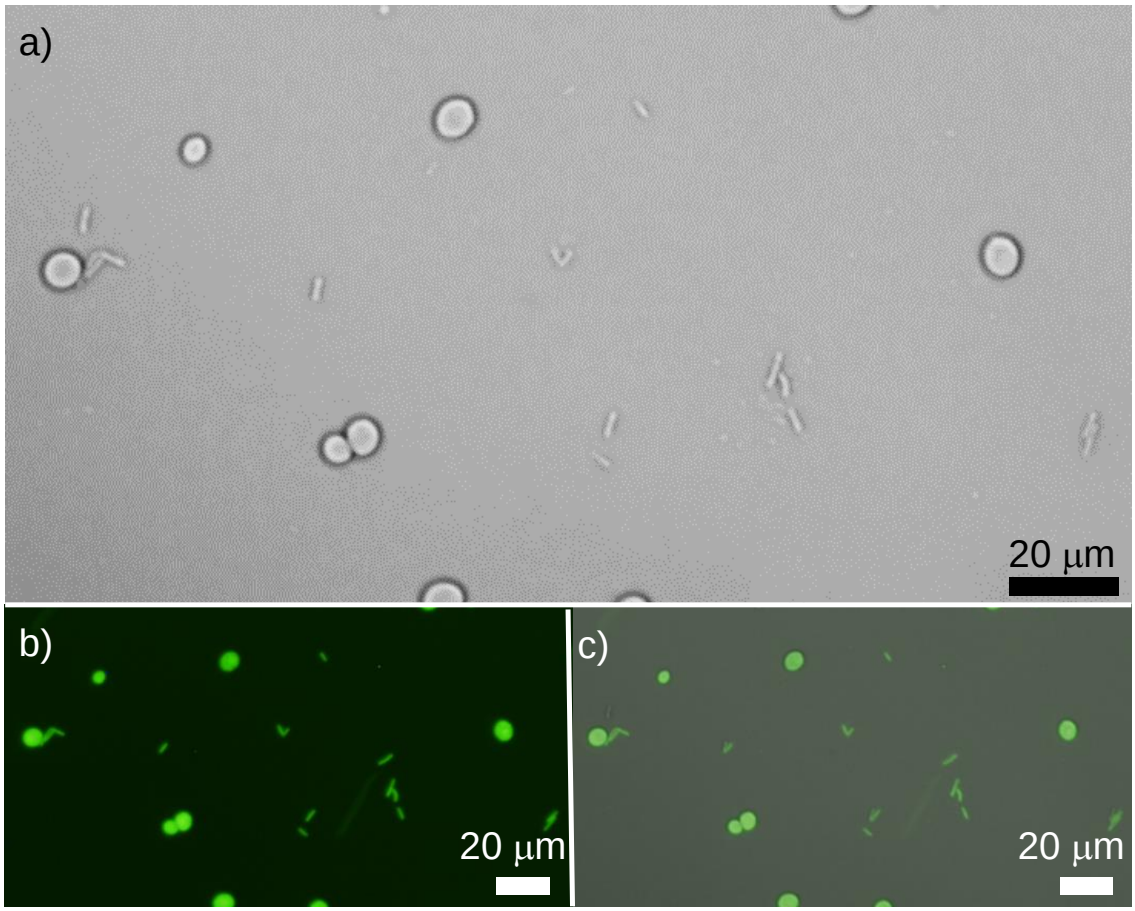

Figure 6-6. Images of the mixture of bacterial (*B. subtilis)* and yeast samples after being exposed to laser irradiation and treated with FDA. The bright field image (a) and the fluorescence microscopy image (b) were superimposed to produce the composite image (c).

6.4 Viability of Cells Incubated with Nanoantibiotics

The effect of exposure to the nanoantibiotic particles on the cell viability was also examined by incubating the nanoantibiotics with bacteria and yeast separately and conducting the FDA viability test after 10 minutes (see Figure 6-7. for schematics). No significant effect of a 10 minute exposure to the nanoantibiotic was found. The samples which were not irradiated exhibited 90 ± 3% and 81 ± 6% viability for the bacterial (*B. subtilis*) and yeast cells, respectively (see Figure 6-8. and Figure 6-9. for typical sets of images).

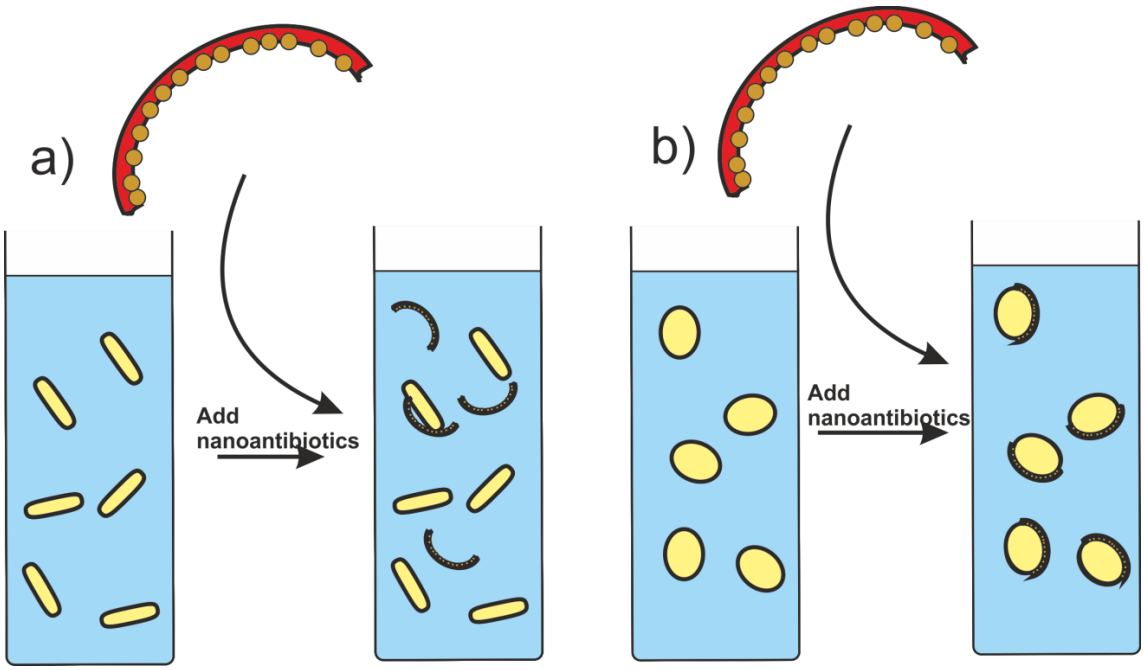

Figure 6-7. Schematics of the test of the effect of the nanoantibiotic particles on the viability of the microbial organisms. The experiment was done by incubating the nanoantibiotics with (a) a dispersion of bacteria and (b) with a dispersion of yeast cells, followed by FDA viability testing.

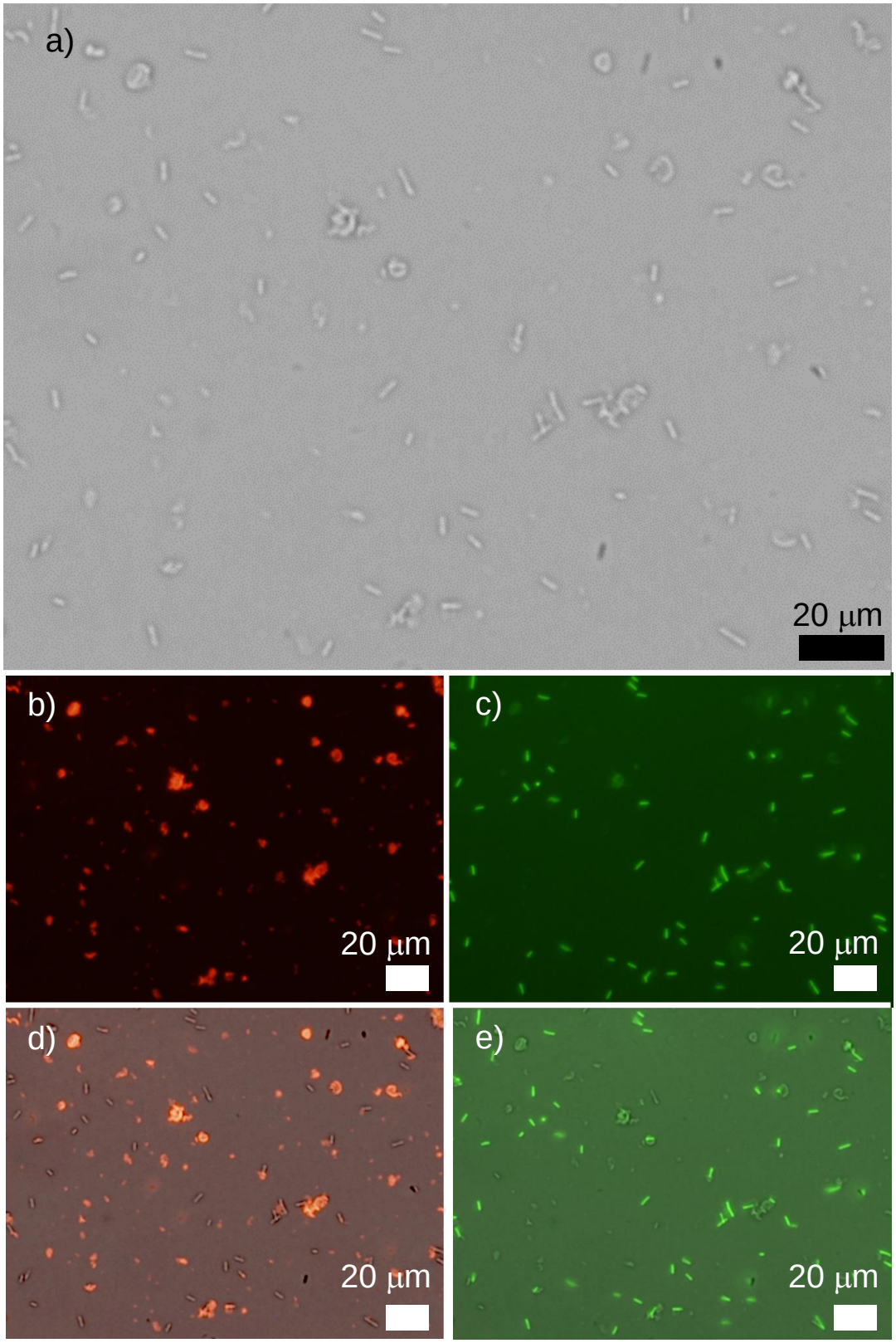

Figure 6-8. Images of a sample of bacterial cells (*B. subtilis*) which were incubated with the AuNP functionalised nanoantibiotics and subsequently treated with FDA. The bright field image (a) and the fluorescence image (b) highlighting the nanoantibiotics tagged with RBITC and the fluorescence microsscopy image (c) which shows the green fluorescing bacterial cells were taken to produce the composite image d) and e).

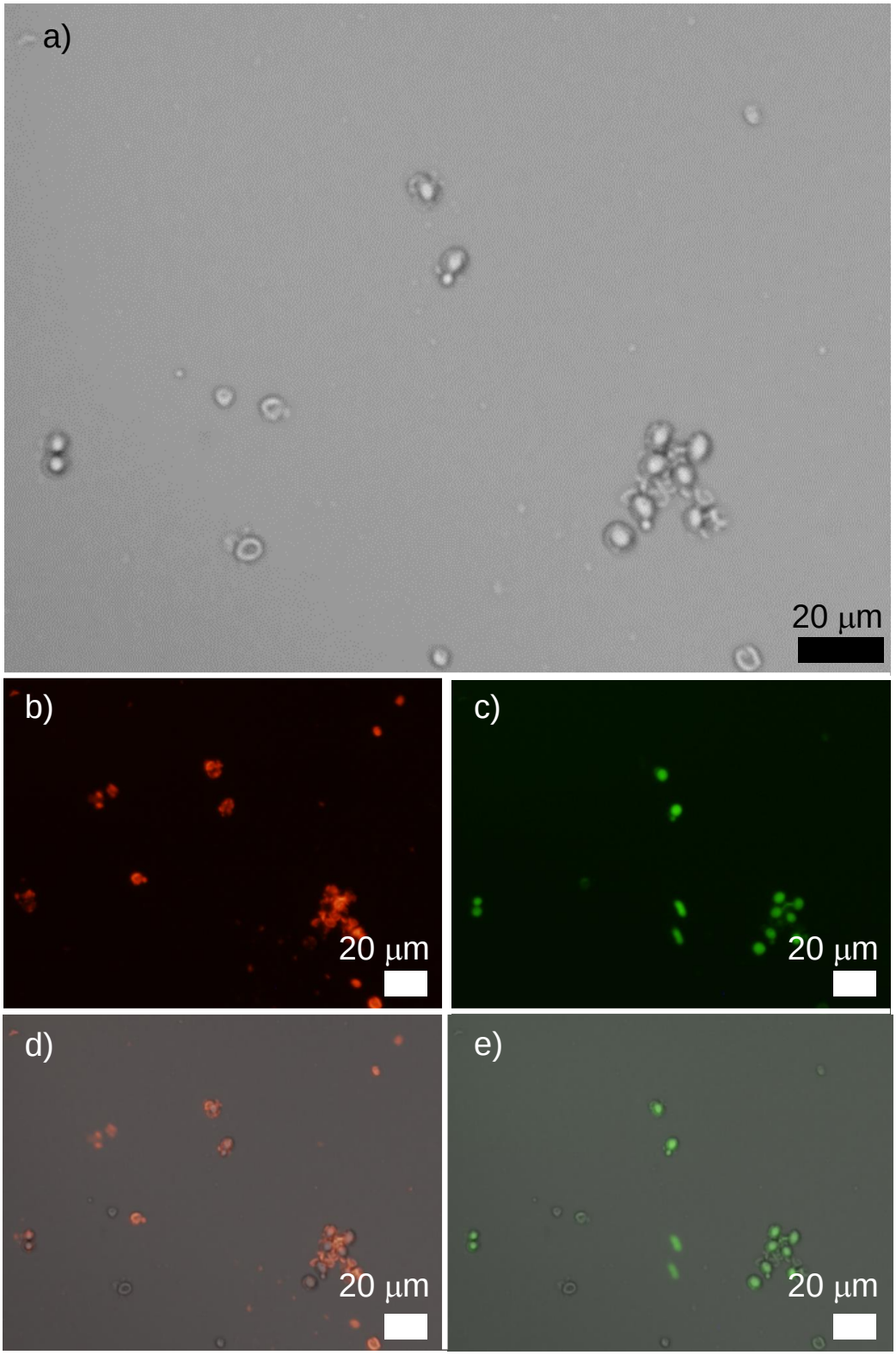

Figure 6-9. Images of a sample of bacterial cells (*B. subtilis*) which were incubated with the AuNP functionalised nanoantibiotics and subsequently treated with FDA. The bright field microscopy image (a) and the fluorescence microscopy image (b) highlight the position of the nanoantibiotics tagged with RBITC. The fluorescence microscopy image (c) shows the green fluorescing bacterial cells. The composite images (d) and (e) are produced by superimposing (a), and (b) and (c), respectively.

6.5 *Effects of Laser Irradiation on the Viability of the Cells in the Nanoantibiotic-cell Mixture*

Having established that the test microbial organisms maintain their viability when exposed to the presence of AuNP containing nanoantibiotic particles, we conducted three sets of experiments. The experiments utilised three sets of test cells: *B. subtilis*; yeast cells; and the mixture of yeast and *B. subtilis*. Each experiment included incubation of the cell set with the nanoantibiotics and irradiation of samples with laser (see Figures 6-1. and 6-10. for schematics). Microscopy analysis of the samples revealed very high rates of specific killing of the yeast cells: only 17 ± 5 and 13 ± 4% of the yeast cells remained viable after the laser treatment in the sample containing only yeast cells and a mixture of yeast and bacteria, respectively (See Figures 6-11. to 6-13 for micrographs). The average killing rate of the yeast cells with the shells attached was calculated to be 91 ± 3%. As expected, the *Bacillus subtilis* remained unaffected with the viability rates of 98 ± 4% in the single experiment with this test microorganism and 87± 4% in the mixture.

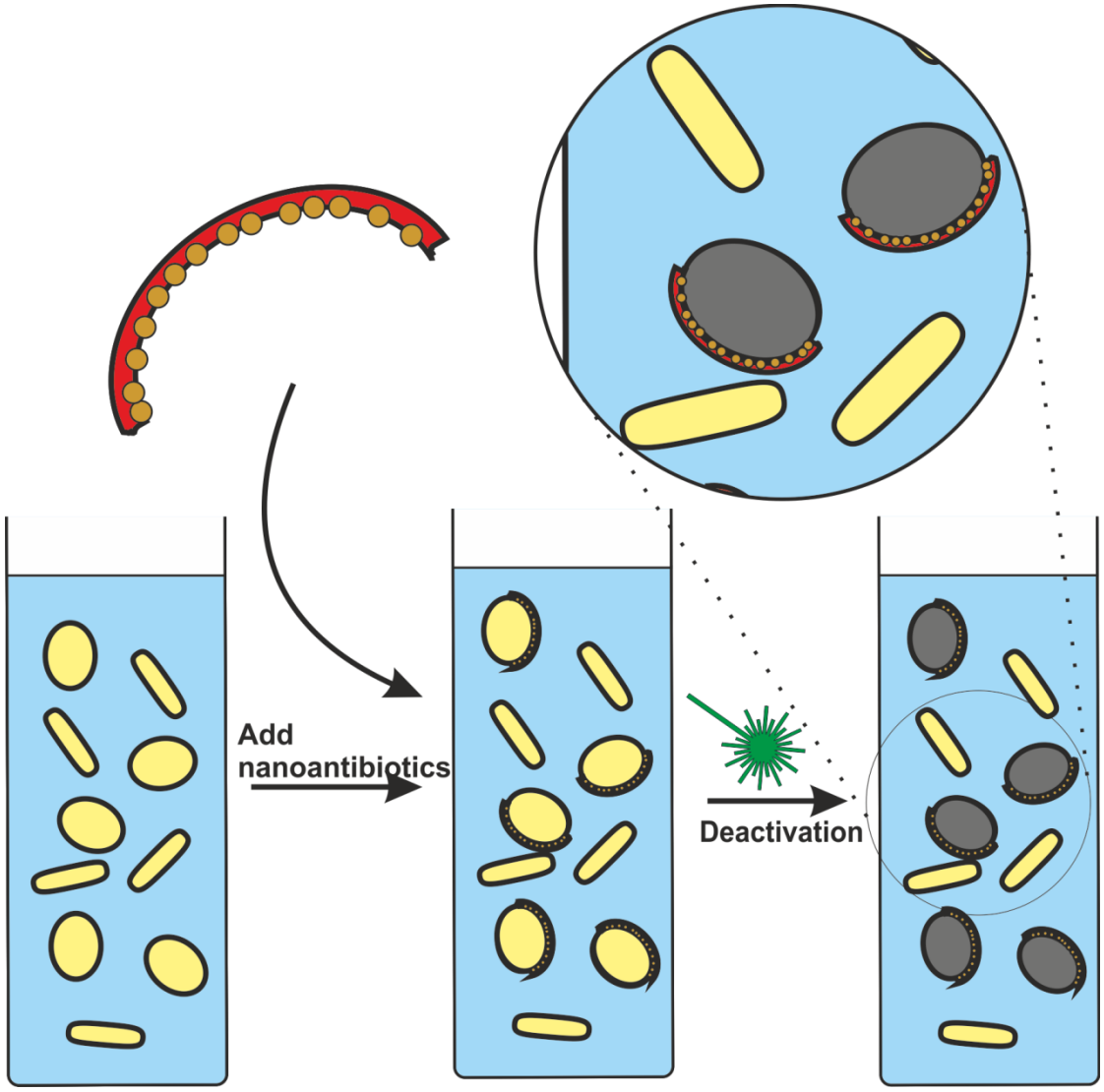

Figure 6-10. Schematics of the experiment on selective killing of one type of cell in a mixture of cells by using AuNP functionalized nanoantibiotics. The gold nanoparticle-functionalized nanoantibiotics were introduced into the suspension of ellipsoidal yeast and rod-like bacterial cells (*B. subtilis*). After 10 minute incubation with the yeast cell-templated AuNP-silica nanoantibiotics, the sample was irradiated with a laser at 532 nm, deactivating the target yeast cells (grey colour signifies dead cells).

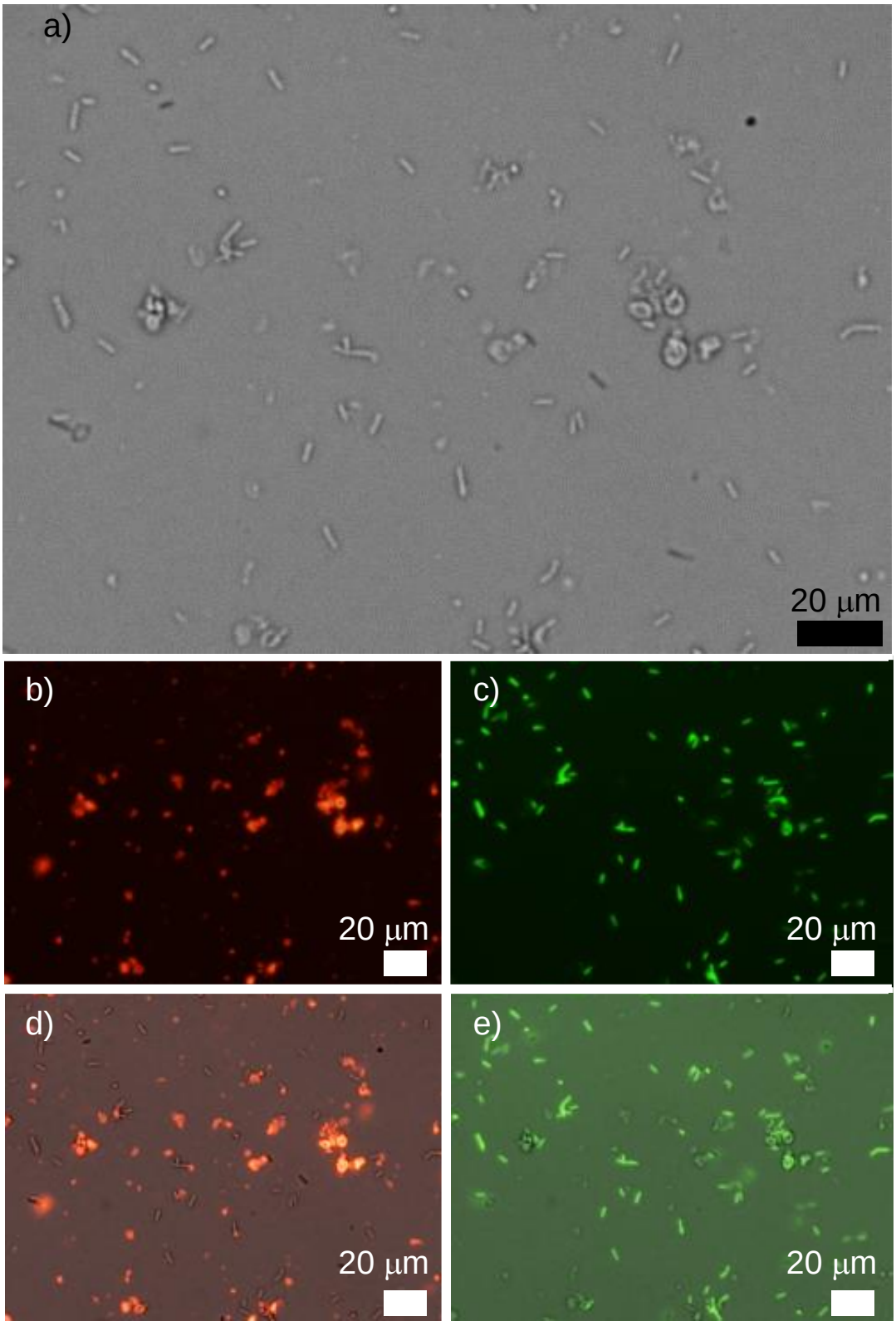

Figure 6-11. Images of a sample of bacterial cells after being incubated with the AuNP functionalised nanoantibiotics, irradiated with laser and subsequently treated with FDA. The bright field microscopy image (a) and the fluorescence microscopy image (b) highlighting the nanoantibiotics tagged with RBITC and the fluorescence image (c) which shows the green fluorescing bacterial cells were superimposed to produce the composite images (d) and (e).

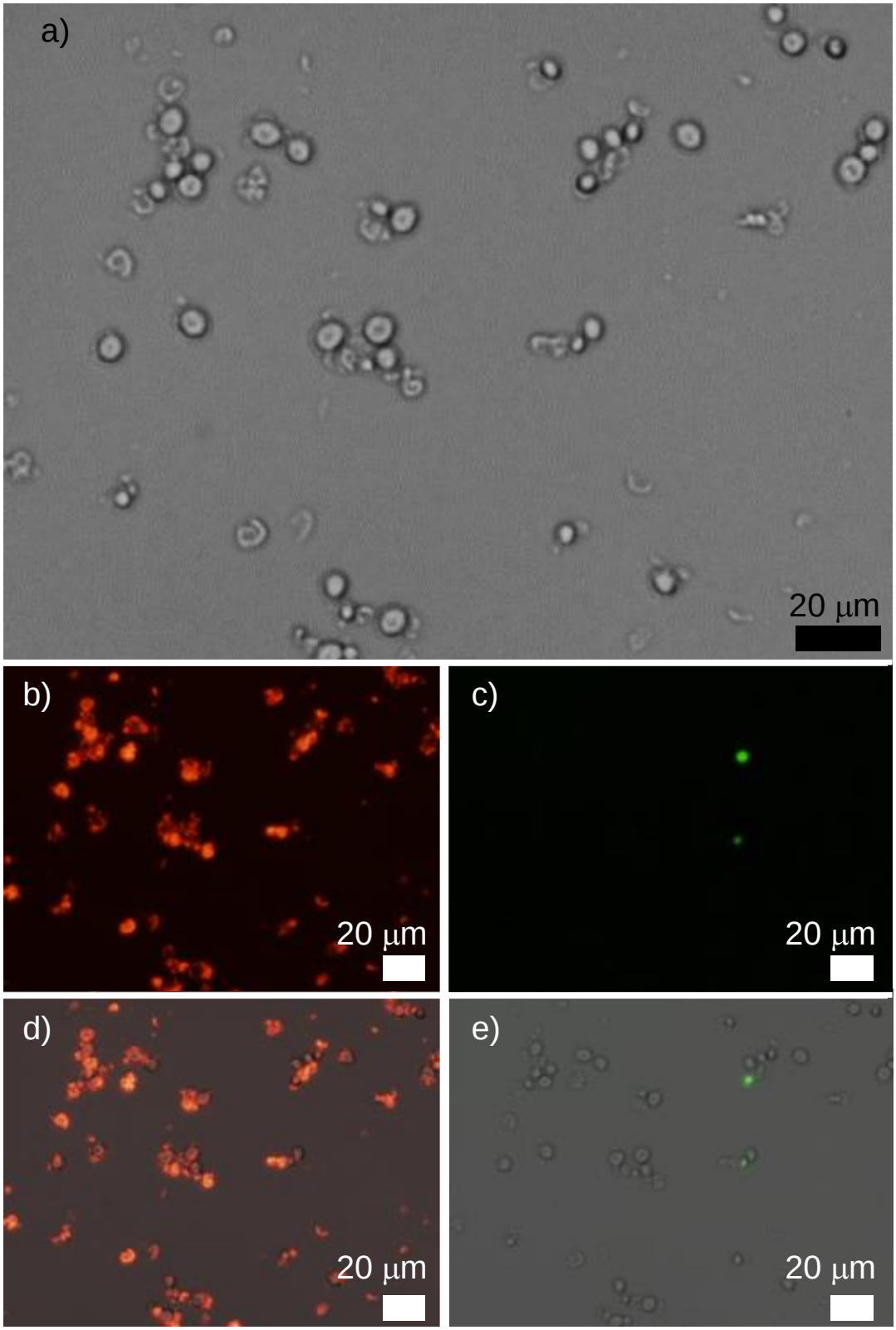

Figure 6-12. Images of a sample of yeast cells which were incubated with the AuNP functionalised nanoantibiotics, irradiated with laser and subsequently treated with FDA. The bright field microscopy image (a) and the fluorescence microscopy image (b) highlighting the nanoantibiotics tagged with RBITC and the fluorescence microscopy image (c) which shows the green fluorescing yeast cells were superimposed to produce the composite images (d) and (e).

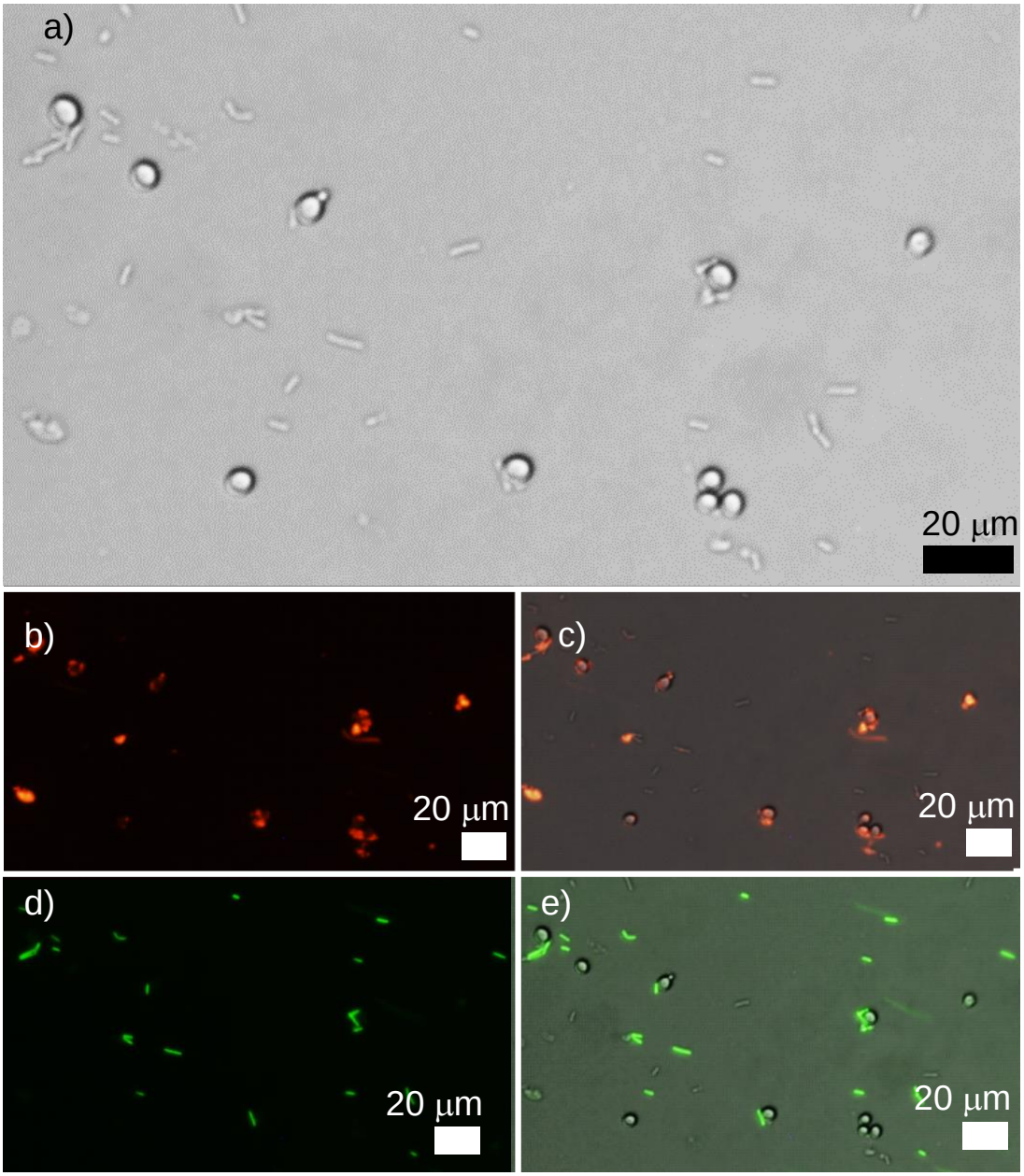

Figure 6-13. Images of a sample of a mixture of bacterial and yeast cells which were incubated with the AuNP functionalised nanoantibiotics, irradiated with laser and subsequently treated with FDA. The bright field microscopy image (a) and the fluorescence microscopy image (b) highlighting the nanoantibiotics tagged with RBITC and the fluorescence microscopy image (c) which shows the green fluorescing bacterial cells were superimposed to produce the composite images (d) and (e).

6.6 Conclusions

We have demonstrated high rates of specific recognition and selective phothermal killing in a system of two microorganisms and matching nanoantibiotics functionalized with gold nanoparticles. Yeast cells and *Bacillus subtillis* were used here as test microorganisms which mimic the role of pathogens. The control experiments which included viability testing of the microbial cells which were irradiated with laser did not reveal measurable influence on the microorganism viability. Secondly, the control experiments which examined the viability of the microorganisms which were exposed to the same nanoantibiotic particles but were not irradiated did not disclose the capability of the nanoantibiotics alone to affect the viability of the yeast or the bacteria within the 10 minute incubation period. The summary of the conducted experiments can be found in Figure 6-14. The specificity of recognition between our nanoantibiotics and the target (yeast cell) led to the desired selectivity in killing the target cells whilst leaving the differently shaped bacilli viable.

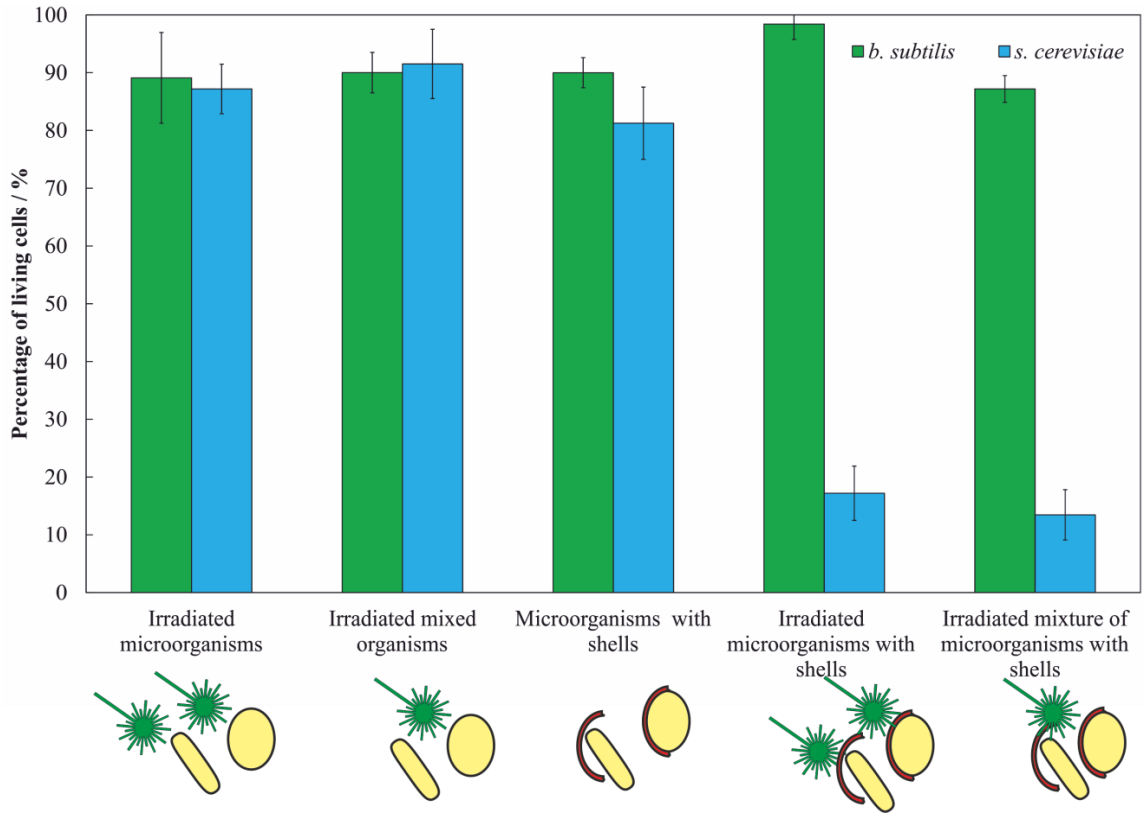

Figure 6-14. A graphical summary of the selective results of recognition and killing experiments of two different types of test microorganisms with AuNP functionalised nanoantibiotic particles. The error bars are the standard deviation of the mean.

To conclude, the action of "selective disinfection" with our newly proposed class of gold-functionalised nanoantibiotics based on the recognition of action of their shape has been demonstrated. It is anticipated that the novel non-molecular principle of the nanoantibiotics can potentially be a powerful weapon in the fight against antibiotic resistant bacteria as well as those against which current medicine is powerless. In future work on this topic, different mechanisms of killing of bacteria can be implemented together with the selective recognition of the nanoantibiotic particles. The non-toxic nature of these bactericidal agents can also be of advantage for the employment in food or personal care formulations to eliminate undesirable contaminations.

6.7 References

1. K. Boris, Z. Vladimir, M. Andrei, T. Valery and K. Nikolai, *Nanotechnology*, 2006, **17**, 5167.
2. T. H. Chrzanowski, R. D. Crotty, J. G. Hubbard and R. P. Welch, *Microbial Ecology*, 1984, **10**, 179.

CHAPTER 7. CONCLUSIONS AND OUTLOOK

Through this thesis we have introduced the concept of novel nanoantibiotic agents based on the shape and size recognition of microorganisms, which we explored from four different perspectives. These agents are fabricated by templating the original organism with inorganic materials which leads to the formation of nanoshells which match the shape and size of the biological template. After these inorganic nanoshells were fragmented and the microorganisms removed by bleaching out, the shell fragments retained their ability to bind preferentially to the original cells. Although in the thesis we worked only with bacterial cells to prove this concept, we envisage that this strategy should also work for some viruses. We suggested several strategies of selective killing of microorganisms by binding them to nanoantibiotic particles and implemented one of them based on the photothermal effect.

In Chapter 2 we described the materials and the methods used in several techniques which we explored for the preparation of nanoantibiotics based on shape and size recognition. We produced gold hemispherical caps by gold sputtering onto monolayers of our template particles, followed by removal of the templated shells by dissolution. Several strategies for the fabrication of zinc sulphide nanoshells on yeast and other templates were developed. However, our best results for fabrication of nanoantibiotics were based on producing silica nanoshells over our templates of interest by using our modification of the Stöber process. We developed and further refined a technique for the fragmentation of the nanoshells and the removal of the templated bacteria. The details of these preparations are given in Chapter 4. These nanoshell fragments were modified with polyelectrolytes further to control their surface charge and a range of experiments were conducted in which these materials were incubated in aqueous solution with cells or microparticles of different shape and size to test their ability to recognise the original target cells. We also conducted a small number of experiments where gold caps were functionalised with a ligand capable of binding to protein attached to the target particle surface. In both cases we found that the recognition of the target by the nanoshells fragments (or caps) is also very sensitive to their surface chemistry.

In Chapter 3 we have theoretically rationalised the interactions between the nanoantibiotic particles and their target cells by considering them in terms of the DLVO surface forces. We adapted the Derjaguin approximation to take into account the geometry factor in the colloidal interaction between a spherical target microorganism and a hemispherical shell at different orientations with respect to each other. For the sake of simplicity, we took into account only classical DLVO surface forces like the van der Waals and the electric double layer forces when we studied the interactions of spherical targets (microorganisms) and hemispherical shells as a function of their size ratio, mutual orientation, distance between their surfaces, their respective surface potentials and the ionic strength of the aqueous solution. We found that the calculated interaction energies between the matching target particles and hemispherical shells in terms of their orientation, shape and size are several orders higher than in the scenarios when match and recognition was not achieved. Our analysis revealed that the recognition effect of the hemispherical shell towards the target comes from the greatly increased surface contact area when a full match of the size and shape is produced. When the interaction between the surfaces of the shell and the target particles is attractive, the recognition greatly amplifies the attraction and this increases the likelihood of them to bind strongly. However, if the shell-target particle interaction is repulsive, the recognition makes this interaction even more repulsive and thus decreases the likelihood of binding. These results show that the surface chemistry of the shell and the target particles (cells) is very important in controlling the outcome of the interaction, while the recognition amplifies the interaction. In the case of non-monotonous interaction we discovered some interesting interplay between shape and surface chemistry which is discussed in the chapter.

Chapter 4 presents our results with nanoantibiotic particles synthesised by templating various model targets: latex microspheres; yeast (*S. Cerevisiae*) cells; and *Bacillus subtilis* bacterial cells. We explored the efficiency in "remembering" the shape of the target template by various shell-forming materials like gold; zinc sulphide; silica; and silica nanoparticles. Both symmetrical and asymmetrical shell deposition techniques onto the target particles were used. The silica and zinc sulphide shells were made using symmetrical deposition techniques, while the gold caps were fabricated using asymmetrical deposition. Our best and most robust results were produced with partially

fragmented silica nanoshells which were used in the bulk of the proof-of-principle work reported in the following chapters.

In Chapter 5 we have explored the interactions between the nanoantibiotic and their target particles by conducting experiments which were aimed at the assessment of the importance of shape and size, and chemically specific interactions in the nanoantibiotic action. By using yeast cells as test microorganisms we have demonstrated that the silica nanoshells, which retain the shape and the size of the yeast cells, are preferentially binding to their cell targets with an orientation of their inner side towards the cell. The target size specificity in the nanoantibiotic binding was also probed by investigating the binding events in a mixture of latex microspheres of different size (instead of cells) which were incubated together with nanoantibiotic fragments fabricated using the microspheres of intermediate size. The results have shown high levels of specificity of recognition of the geometrically and size matching targets with over 90 % specifically bound nanoantibiotics to the target particles. We also tested the binding of nanoantibiotic particles in a model test microorganism system containing two microbial species of distinct in shape and size – the rod shaped *B. subtilis* and the yeast cells. After incubation of the mixture of the two test microbes with yeast-specific nano-shell fragments we observed exclusive binding of this nanoantibiotic to the yeast cells. We also used the gold caps fabricated by asymmetric deposition of gold onto a monolayer of latex microspheres to demonstrate the possibility of introducing nanoantibiotic selectivity based on specific biomolecular interactions in addition to the shape and size. We passivated the outer shell surface with a monolayer of polyethylene glycol whilst introducing highly specific, antibody-antigen-like, functionalization with biotin and streptavidin onto the inner part of the nanoantibiotic particles and the latex microspheres, respectively. Incubation of the biotin-functionalised nanoantibiotics with their streptavidin-coated targets lead to their specific recognition by the caps with no mismatched binding observed.

In Chapter 6 we have focused our efforts onto the fabrication of nanoantibiotic particles which not only specifically bind to their targets but also have the capability of controllable and selective killing of the target microbial organisms. We have adopted the dual microorganism-nanoantibiotic system from Chapter 5, however, instead of using simple partially fragmented silica replicas of the yeast cells, we fabricated gold nanoparticle-silica nanoantibiotic composites which are capable of triggered localised

heating upon illumination with a laser as they are specifically bound to the test cell interface. This localised heating was triggered by irradiating the microorganism – nanoantibiotic mixture with a green 532 nm laser which induced a photothermal effect. These experiments lead to high selective killing rates of yeast with the viability of the *B. subtilis* remaining unaffected despite the laser illumination.

In summary, throughout this thesis, we have achieved a proof of principle that nanoantibiotics, produced by templating target microorganisms with a variety of synthetic nanoshells which then selectively bind to other organisms of the target species. We believe that shape and size recognition action of the nanoantibiotics has three major advantages compared to the conventional antibiotics. These are:

- They gives an important new route for the circumvention of natural microbial defences leading to antibiotic resistance;
- Many inorganic material-based nanoshells are chemically inert and would have no apparent toxicity, depending on the shell-forming material, which distinguishes them from molecular antibiotics which are based on the balance of the toxicity to the microbial organisms and their host;
- New nanoantibiotics allow rapid fabrication through a standard technique, while the development of new molecular antibiotics is dependent on gaining an understanding of the biochemical processes linked to action of the pathogenic microbe. This information is then used to synthesise chemical species which counter these mechanisms whereas nanoantibiotic fabrication, on the other hand, is essentially only dependent on the development of a robust nanoimprinting technique and the availability of the target microorganisms for templating.

There is a large scope for the further development of the idea of nanoantibiotics. Probably the most immediate task for further investigation would be to test the sensitivity of the nanoantibiotic particles in recognising their targets. This would be done by verifying their capability of discriminating between similar shapes and sizes of the targets. A new avenue of killing the target organisms could for instance involve integration of magnetic nanoparticles into the nanoshell fragments instead of the gold nanoparticles which allow for the utilisation of the photothermal effect as demonstrated in this thesis. Magnetic nanoparticles, when subjected to alternating magnetic fields, also can generate heat in a phenomenon is called magnetic hyperthermia.[1, 2] Magnetic

hyperthermia, similarly to photothermal effect, has been experimentally used for a long time as a cancer treatment. The introduction of the magnetic nanoparticles into the nanoantibiotic fragments could not only allow for targeted killing of microbes but also for their magnetic extraction from the solution and selective manipulation. The bacteriostatic effect of the nanoantibiotics has not been studied in the work connected to this thesis. It would be therefore beneficial to develop an understanding of the effect of the selectively bound nanoshells fragments onto the long-term viability and life-cycle of the target microorganisms. Future research could also include the development of methods which would allow for scaling down of the nanoimprint fabrication to virus level and the study of their effect on the virions and viral infections.

7.1 References

1. S.-H. Huang and R.-S. Juang, *Journal of Nanoparticle Research*, 2011, **13**, 4411.
2. L. M. Armijo, Y. I. Brandt, D. Mathew, S. Yadav, S. Maestas, A. C. Rivera, N. C. Cook, N. J. Withers, G. A. Smolyakov, N. L. Adolphi, T. C. Monson, D. L. Huber, H. D. C. Smyth and M. Osiński, *Nanomaterials*, 2012, **2**, 134.